Spring 2011

Postcyclic behavior of low-plasticity silt

Shuying Wang

Department: Civil, Architectural and Environmental Engineering

POSTCYCLIC BEHAVIOR OF LOW-PLASTICITY SILT

by

SHUYING WANG

A DISSERTATION

Presented to the Faculty of the Graduate School of the

MISSOURI UNIVERSITY OF SCIENCE AND TECHNOLOGY

In Partial Fulfillment of the Requirements for the Degree

DOCTOR OF PHILOSOPHY

in

CIVIL ENGINEERING

2011

Approved by

Ronaldo Luna, Advisor

Richard W. Stephenson

Louis Ge

Oh-Sung Kwon

David J. Rogers

ABSTRACT

Liquefaction of low-plasticity silt has been reported during earthquakes in the recent past. Excess pore pressure builds up due to the dynamic loading and then dissipates. The postcyclic behavior of low-plasticity silt was investigated in this research for materials obtained from the Mississippi River Valley. The experimental program involved specimen preparation using a slurry consolidation approach. A special technique was developed for specimen movement, reducing the testing program time by half. Both static and cyclic triaxial tests were conducted to confirm the ability to prepare replica specimens. In order to characterize the monotonic behavior, triaxial tests were conducted to determine the effective friction angle, critical state line, and normalized behavior. Then specimens were subjected to cyclic loading to develop the liquefaction curve. After full liquefaction, excess pore pressure was dissipated until various reconsolidation levels. The effect of full liquefaction on the permeability and compressibility was studied. The variation in postcyclic shear strength and stiffness with reconsolidation level and the effect of apparent consolidation on shear behavior were also discussed. The critical state lines for the pre- and postliquefaction conditions were compared and found to be not parallel. After limited liquefaction, two unique conditions were tested, at no reconsolidation and at full reconsolidation. The shear strength and stiffness changed significantly at an excess pore pressure ratio greater than 0.70. The experimental program culminated with the study of the effect of plasticity on the pre- and postcyclic shear behavior. Silt-bentonite mixtures resulted in modified plasticity and the transformation from a dilative to a plastic behavior were captured at relatively low plasticity ($PI > 6$).

ACKNOWLEDGEMENTS

I appreciate China Scholarship Council, who provided financial support and sent me here to pursue my study for Ph.D. degree. I thank Department of Civil, Architectural, and Environmental Engineering, MST, for giving me such an invaluable opportunity to conduct my research. I wish to express my sincere gratitude to my advisor, Dr. Ronaldo Luna, for his invaluable support, encouragement, and advice throughout my doctoral study program. Dr. Luna always showed great passion and interest in my research. I am also grateful for the comments and suggestions of Dr. Richard Stephenson, Dr. Louis Ge, Dr. Oh-sung Kwon, and Dr. David Rogers; and I thank them for their great interest and encouragement throughout this project. I wish to acknowledge the help and encouragement of the graduate students in geotechnical engineering, including Site Onyejekwe, Domenica Cambio, Xin Kang, Kermit N. Applegate, Kyle A. Kershaw, Nicholas T. Rocco, Abdalmajeed Ali, Mingyan Deng, and Betty T. Hailemariam. They provided invaluable help to support me throughout my research. I especially wish to express my gratitude to my wife, Ke Zhang, for her enormous contribution to my doctoral study. Her invaluable encouragement and support reduced my stress level and gave me more time to be involved in my research. Finally, I thank my parents, sister, and brother, whose endless encouragement gave me the passion to pursue my degree.

TABLE OF CONTENTS

Page

ABSTRACT iii

ACKNOWLEDGEMENTS iv

LIST OF ILLUSTRATIONS xii

LIST OF TABLES xviii

NOMENCLATURE xx

SECTION

1. INTRODUCTION 1

    1.1. GENERAL 1

    1.2. RESEARCH SIGNIFICANCE 4

    1.3. RESEARCH OBJECTIVES 5

    1.4. DISSERTATION ORGANIZATION 6

2. BACKGROUND AND LITERATURE REVIEW 9

    2.1. UNDRAINED SHEAR STRENGTH OF LIQUEFIED SOIL 9

    2.2. SPECIMEN PREPARATION 14

    2.3. MONOTONIC SHEAR BEHAVIOR OF LOW-PLASTICITY SILT 18

2.4. POSTCYCLIC BEHAVIOR OF SOIL WITH FULL LIQUEFACTION 22

2.5. POSTCYCLIC BEHAVIOR OF SOIL WITH LIMITED LIQUEFACTION....24

2.6. EFFECT OF PLASTICITY ON POSTCYCLIC SHEAR BEHAVIOR.....31

2.7. SUMMARY 33

3. EXPERIMENTAL PROGRAM.....34

3.1. SUBJECT SOIL 34

3.1.1 Material Description.....34

3.1.2 Particle Morphology.....38

3.1.3 Liquefaction Potential. 46

3.2. TRIAXIAL TESTING EQUIPMENT 48

3.3. TRIAXIAL TESTING PROCEDURES 52

3.3.1 Saturation.....52

3.3.2 Consolidation.....55

3.3.3 Static Triaxial Testing. 57

3.3.4 Cyclic Triaxial Testing.....57

3.3.5 Postcyclic Monotonic Triaxial Testing. 58

3.4. SUMMARY 61

4. SPECIMEN PREPARATION.....66

4.1. SPECIMEN RECONSTITUTION.....67

4.1.1 Reconstitution Procedures.....67

4.1.2 Specimen Uniformity. 70

4.2. SPECIMEN PREPARATION FOR TESTING 72

4.2.1 Movement Procedures.....72

4.2.2 Disturbance during Handling and Moving of Specimens. 76

4.3. TESTING REPLICAS 77

4.3.1 Static Triaxial Tests.....77

4.3.2 Cyclic Triaxial Tests. 79

4.4. SUMMARY 82

5. MONOTONIC AND CYCLIC SHEAR BEHAVIOR OF LOW-PLASTICITY SILT.....83

5.1. MONOTONIC SHEAR BEHAVIOR.....83

5.1.1 Undrained Shear Behavior. 83

5.1.2 Effective Friction Angle.....86

5.1.3 Critical State Line. 90

5.1.4 Normalized Behavior. 93

5.2. CYCLIC SHEAR BEHAVIOR 101

5.3. SUMMARY 102

6. POSTCYCLIC BEHAVIOR OF LOW-PLASTICITY SILT WITH FULL LIQUEFACTION 104

6.1. EXPERIMENTAL PROGRAM: FULL LIQUEFACTION 104

6.2. VOLUME CHANGE DUE TO FULL RECONSOLIDATION 105

6.2.1 Permeability. 106

6.2.2 Compression and Recompression Indices. 109

6.3. EFFECT OF CSR ON POSTLIQUEFACTION MONOTONIC BEHAVIOR 112

6.4. EFFECT OF RECONSOLIDATION LEVEL ON POSTLIQUEFACTION MONOTONIC SHEAR BEHAVIOR 115

6.4.1 Undrained Shear Behavior. 116

6.4.2 Shear Strength and Stiffness at Small Deformation. 118

6.4.3 Shear Strength and Stiffness at Large Deformation. 121

6.4.4 Apparent OCR. 124

6.5. COMPARISON WITH MONOTONIC SHEAR BEHAVIOR 127

6.5.1 Undrained Stress-strain Behavior. 127

6.5.2 Critical State Line. 129

6.6. DISCUSSION 131

6.6.1 Void Ratio Change and its Role. 131

6.6.2 Critical State Line. 132

6.6.3 Drainage for Reconsolidation. 133

6.7. SUMMARY 134

7. POSTCYCLIC BEHAVIOR OF LOW-PLASTICITY SILT WITH LIMITED LIQUEFACTION 136

7.1. EXPERIMENTAL PROGRAM: LIMITED LIQUEFACTION 136

7.2. POSTCYCLIC SHEAR BEHAVIOR WITH FULL RECONSOLIDATION. 138

7.2.1 Undrained Shear Behavior. 138

7.2.2 Shear Strength and Stiffness at Small Deformation. 140

7.2.3 Shear Strength and Stiffness at Large Deformation. 142

7.3. POSTCYCLIC SHEAR BEHAVIOR WITHOUT RECONSOLIDATION 145

7.3.1 Undrained Shear Behavior. 145

7.3.2 Shear Strength and Stiffness at Small Deformation. 147

7.3.3 Shear Strength and Stiffness at Large Deformation. 150

7.4. DISCUSSION 152

7.4.1 No Reconsolidation and Full Reconsolidation. 152

7.4.2 Comparisons with Other Available Laboratory Data. 156

7.5. SUMMARY 158

8. EFFECT OF PLASTICITY ON PRECYCLIC AND POSTCYCLIC BEHAVIOR OF LOW-PLASTICITY SILT 160

8.1. INDEX PROPERTIES OF SOIL MIXTURES.....160

8.2. EFFECT OF PLASTICITY ON MONOTONIC SHEAR BEHAVIOR.....165

8.2.1 Undrained Shear Behavior: Normally Consolidated. 166

8.2.2 Undrained Shear Behavior: Overconsolidated. 169

8.2.3 Effective Friction Angle. 173

8.2.4 Critical State Line. 175

8.3 EFFECT OF PLASTICITY ON CYCLIC SHEAR BEHAVIOR 177

8.3.1 Excess Pore Pressure Response. 177

8.3.2 Liquefaction Resistance. 183

8.4. EFFECT OF PLASTICITY ON POSTCYCLIC BEHAVIOR.....184

8.4.1 Variation in Consolidation Parameters.....185

8.4.2 Undrained Shear Behavior. 189

8.4.3 Shear Strength and Stiffness.....191

8.5. DISCUSSION 196

8.5.1 Failure Criteria. 196

8.5.2 Interpretation. 198

8.6. SUMMARY 200

9. CONCLUSIONS AND RECOMMENDATIONS FOR FUTURE RESEARCH ...202

9.1. CONCLUSIONS 202

9.2. RECOMMENDATIONS FOR FUTURE RESEARCH 208

APPENDIX RESULTS OF CYCLIC TRIAIXAL TESTS 211

BIBLIOGRAPHY 223

VITA 232

LIST OF ILLUSTRATIONS

Figure Page

2.1. Estimation of undrained shear strength of liquefied soil using steady-state strength approach 11

2.2. Relationship between corrected "clean sand" blowcount $(N_1)_{60\text{-}cs}$ and undrained shear strength (S_r) based on case studies 12

2.3. Comparison of steady-state strength (S_{us}) based on laboratory data with undrained shear strength (S_r) band determined from back-analysis of case histories for clean sands, silty sands, and silts 13

2.4. Comparison of static and postliquefaction response 23

2.5. Relationship between postcyclic consolidation volumetric strain of sand and the residual pore pressure ratio 25

2.6. Postcyclic monotonic responses at various levels of liquefaction 27

2.7. Stiffness-decreasing characteristics with normalized pore pressure 29

2.8. Comparison of deviator stress ratio at failure for samples with and without postcyclic recompression 30

2.9. Comparison of cyclic shear strength for first loading and postdrainage second loading 30

2.10. Relationship between shear modulus ratio and normalized pore pressure 32

3.1. Silt source location 34

3.2. Grain size distribution of MRV silt 36

3.3. Relationship between liquid limits determined by Casagrande and Fall Cone approaches 37

3.4. Modified Proctor compaction curve of MRV silt 39

3.5. Preparation of MRV silt samples for particle morphology 40

3.6. Image acquisition for MRV silt particle 41

3.7. Images of soil particles 43

3.8. Images of particle #1 from different directions 44

3.9. Images of particle #3 from different directions 45

3.10. Recommendations of Seed et al. for assessment of liquefiable soil types 47

3.11. Humboldt triaxial testing system 49

3.12. GCTS triaxial testing system 50

3.13. Modified tubing connection system in the GCTS equipment 52

3.14. Measurement of soil specimen height 54

3.15. Consolidation time of MRV silt specimen 56

3.16. Sliding of triaxial chamber from the GCTS to the Humboldt load frame 61

4.1. Experimental setup used to reconstitute silt specimens 68

4.2. Variation in water content from top to bottom of specimen 71

4.3. Variation in grain size distribution for seven (7) slices of silt specimen reconstituted by slurry deposition 72

4.4. Specimen movement from preparation location to triaxial base platen on load frame pedestal 74

4.5. Repeatability of Static Testing 78

4.6. Repeatability of cyclic testing with a CSR of 0.18 80

4.7. Repeatability of cyclic testing with a CSR of 0.35 81

5.1. Static testing results of MRV silt 85

5.2. Effective friction angle based on various failure criteria 88

5.3. Variation in effective friction angle based on various failure criteria 90

5.4. Stress paths in Cambridge space 91

5.5. Critical state diagram obtained from consolidated undrained tests 94

5.6. Normalized behaviors of the silt 96

5.7. Effect of OCR on normalized shear strength 99

5.8. Principal stress ratio versus axial strain of MRV silt 100

5.9. Liquefaction resistance of MRV silt normally consolidated to effective confining pressure of about 90 kPa 102

6.1 Time required to reach various reconsolidation levels after liquefaction 105

6.2. Testing procedures via stress paths to study postliquefaction behavior of MRV silt with various reconsolidation levels 106

6.3. Comparison of the permeability of MRV silt before and after liquefaction 108

6.4. Reconsolidation curves of MRV silt after full liquefaction 110

6.5. Comparison of compression and recompression indices before and after liquefaction of MRV silt 112

6.6. Postliquefaction monotonic shear behavior of MRV silt with full reconsolidation with various CSRs 114

6.7. Postliquefaction undrained shear behavior of MRV silt under various reconsolidation levels after full liquefaction 117

6.8. Determination of yield shear strength and initial stiffness 119

6.9. Variation in yield shear strength and initial stiffness with reconsolidation level 120

6.10. Recovery of yield shear strength and initial stiffness with reconsolidation 121

6.11. Illustration of determination of undrained shear strength and secant modulus 122

6.12. Variation in undrained shear strength and secant modulus with reconsolidation level 123

6.13. Recovery of undrained shear strength and secant modulus with reconsolidation 124

6.14. Variation in apparent overconsolidation ratio with reconsolidation level 125

6.15. Effect of OCR or OCR_{app} on the normalized undrained shear strength 126

6.16. Comparison of undrained stress-strain behavior of MRV silt with and without liquefaction 128

6.17. Critical state lines of MRV silt prior to and after liquefaction 130

6.18. Variation in undrained shear strength of MRV silt with void ratio prior to and after liquefaction 131

7.1. Testing procedures via stress paths to study postcyclic behavior of MRV silt with limited liquefaction 137

7.2. Postcyclic shear behavior of MRV silt with full reconsolidation after various liquefaction levels 139

7.3. Variation in yield shear strength and initial modulus with liquefaction level of MRV silt after full reconsolidation 141

7.4. Variation in yield shear strength and initial stiffness of MRV silt with increased liquefaction level 141

7.5. Effect of liquefaction level on undrained shear strength of MRV silt with full reconsolidation 142

7.6. Volumetric strain of MRV silt due to reconsolidation after various liquefaction levels 143

7.7. Effect of liquefaction level on secant modulus of fully reconsolidated MRV silt... 144

7.8. Determination of secant modulus for specimens with two liquefaction levels 144

7.9. Postcyclic behavior of MRV silt without reconsolidation after various liquefaction levels 146

7.10. Principal stress ratio versus axial strain of MRV silt without reconsolidation after limited liquefaction 148

7.11. Postcyclic behavior of MRV silt without reconsolidation after limited liquefaction at small deformation 148

7.12. Reductions in yield shear strength and initial stiffness of MRV silt with no reconsolidation after limited liquefaction 149

7.13. Effect of liquefaction level on normalized yield shear strength and initial stiffness of MRV silt without reconsolidation 150

7.14. Effect of liquefaction level on undrained shear strength of unreconsolidated MRV silt 151

7.15. Effect of liquefaction level on secant modulus of unreconsolidated MRV silt 151

7.16. Effect of reconsolidation on yield shear strength and initial stiffness of MRV silt after limited liquefaction 153

7.17. Effect of reconsolidation on undrained shear strength and secant modulus after limited liquefaction 154

7.18. Variation in volumetric strain with liquefaction level in MRV silt and clean and silty sand 156

7.19. Relationship between undrained shear strength and relative density 158

8.1. Variation in Atterberg limits with added bentonite content 161

8.2. Variation in permeability and related parameters of MRV silt-bentonite mixtures with added bentonite content 163

8.3. Variation in consolidation parameters related to compressibility of MRV silt-bentonite mixtures with added bentonite content 164

8.4. Monotonic shear behavior of MRV silt-bentonite mixtures consolidated normally to an effective consolidation pressure of 50 kPa 167

8.5. Monotonic shear behavior of MRV silt-bentonite mixtures consolidated normally to an effective consolidation pressure of 90 kPa 168

8.6. Monotonic shear behavior of MRV silt-bentonite mixtures at effective consolidation pressure of 90 kPa and OCRs of 1 and 8 170

8.7. Excess pore pressure responses of MRV-bentonite mixtures at effective consolidation pressure of 90 kPa and OCR of 8 171

8.8. Normalized deviator stress of the MRV silt and its mixtures with bentonite at an effective consolidation pressure of 90 kPa and OCRs of 1 and 8 172

8.9. Effective friction angles of MRV silt and its mixtures with bentonite using failure criterion of 15% axial strain 174

8.10. Critical state lines of MRV silt-bentonite mixtures 176

8.11. Cyclic shear behavior of MRV silt with a PI of 5.8 178

8.12. Cyclic shear behavior of MRV silt-bentonite mixture with a PI of 6.2 179

8.13. Cyclic shear behavior of MRV silt-bentonite mixture with a PI of 9.4 180

8.14. Cyclic shear behavior of MRV silt and its mixtures with various PIs at a CSR of 0.18 182

8.15. Variation in liquefaction resistance with PI of MRV silt-bentonite mixtures 184

8.16. Reconsolidation curves of MRV silt with added bentonite 186

8.17. Variation of normalized permeability and compression index with PI of MRV silt-bentonite mixtures 188

8.18. Postcyclic shear behavior of MRV silt-bentonite mixture with a PI of 6.2 190

8.19. Postcyclic behavior of the MRV silt-bentonite mixture with a PI of 9.4 192

8.20. Variations in undrained shear strength and initial stiffness of the MRV silt-bentonite mixtures with plasticity index 193

8.21. Variations in undrained shear strength and initial stiffness ratios of MRV silt-bentonite mixtures with PI 195

8.22. Variation in volumetric strain with PI due to full reconsolidation after nearly identical axial strain (9%) induced by cyclic loading 196

8.23. Soil types of MRV silt and its mixtures with bentonite plotted on 199

LIST OF TABLES

Table Page

2.1. Summary of static shear behavior of low-plasticity silt 20

3.1. Index properties of the MRV silt 35

3.2. List of MRV silt particles investigated using FEGSEM 42

3.3. Liquefaction susceptibility criteria proposed by Andrews and Martin (2000) 47

3.4. Humboldt and GCTS triaxial equipment specifications 51

3.5. Time required for various levels of reconsolidation 59

3.6. Summary of all triaxial tests 63

4.1. Change in diameter (mm) of specimen due to movement and handling 76

4.2. Statistics on number of loading cycles required to liquefy specimens with a CSR of 0.18 82

5.1. Static triaxial compression tests on MRV silt 84

5.2. Variation in normalized shear strength with OCR 98

5.3. Summary of cyclic triaxial tests on MRV silt normally consolidated to an effective consolidation pressure of about 90 kPa 101

6.1. Summary of postliquefaction triaxial compression tests to investigate the effect of CSR on postliquefaction shear behavior 113

6.2. Postliquefaction triaxial compression tests at various reconsolidation levels 116

7.1. Summary of triaxial tests of MRV silt with full reconsolidation after various liquefaction levels 138

7.2. Summary of triaxial tests of MRV silt with no reconsolidation after various liquefaction levels 145

8.1. Index properties of the silt-bentonite mixtures 161

8.2. Consolidation parameters of MRV silt-bentonite mixtures 162

8.3. Static triaxial compression tests on the MRV silt-bentonite mixtures..... 165

8.4. Cyclic triaxial tests on the MRV silt-bentonite mixtures..... 177

8.5. Postcyclic monotonic tests on MRV silt-bentonite mixtures..... 185

8.6. Postcyclic consolidation parameters of MRV silt-bentonite mixtures 187

NOMENCLATURE

Symbol	Description
σ'_c	isotropic effective consolidation pressure
σ'_{v0}	initial vertical effective stress
σ'_{vc}	vertical effective consolidation pressure
σ'_3	effective confining pressure
p'_c	mean effective consolidation pressure
p'	mean principal effective stress
σ'_p	preconsolidation pressure
σ_{BP}	back pressure
CSR	cyclic stress ratio
CSL	critical state line
NCL	normal consolidation line
PTL	phase transformation line
OCR	overconsolidation ratio
OCR_{app}	apparent overconsolidation ratio
S_{us}	undrained shear strength
S_r	residual undrained shear strength
$S_{u(PC)}$	postcyclic undrained shear strength
$S_{u(M)}$	initial undrained shear strength
$(N_1)_{60\text{-}cs}$	corrected standard penetration test blowcount for clean sand

D_r	relative density
q_{c1}	normalized tip resistance in cone penetration test
$Q_{tn,sc}$	equivalent clean sand value
PI	plasticity index
LL	liquid limit
PL	plastic limit
ε_v	volumetric strain
$E_{50(PC)}$	postcyclic secant deformation modulus
$E_{50(M)}$	initial secant deformation modulus
$G_{max,cy}$	postcyclic maximum shear modulus
$G_{max,\ NCi}$	precyclic maximum shear modulus
τ_s	initial shear stress
Δu	excess pore pressure
q_s	initial sustained deviator stress
G_s	specific gravity
e_{max}	maximum void ratio
e_{min}	minimum void ratio
C_c	compression index
C_r	recompression index
γ_{dry}	dry unit weight
w	water content
$w_{optimum}$	optimum water content
Δw	maximum difference in water content throughout specimen

H_0	initial specimen height
ΔH_s	change in specimen height during saturation
H	updated height of the specimen after consolidation
ΔV_{sat}	volume change during saturation
d'	deformation rate
ε'	strain rate
t_{50}	time of 50% primary consolidation (or reconsolidation)
$\Delta\sigma$	deviator stress
$A_{corrected}$	corrected cross area
A_0	initial cross area
ε_1	axial strain
ε_{cyc}	cyclic strain
u_e	excess pore pressure
$\Delta\sigma_{cyc}$	peak cyclic deviator stress
R_u	excess pore pressure ratio or liquefaction level
N_{cyc}	number of loading cycles
U_r	reconsolidation level
e	void ratio after consolidation
e'	void ratio after reconsolidation
Δe	change of void ratio due to reconsolidation
A_f	pore pressure coefficient A at critical state
ϕ'	effective friction angle
τ	shear stress

σ'	effective normal stress
M	slope of failure line in the stress space
ISP	initial state point
PTP	phase transformation point
CSP	critical state point
σ'_1	maximum effective principal stress
σ'_3	minimum effective principal stress
k	precyclic permeability
k'	postcyclic permeability
a_v	coefficient of compressibility
ρ	density of water
g	gravity acceleration
c_v	coefficient of consolidation
H_{dr}	drainage distance
T	time factor for consolidation
S_y	yield shear strength
E_i	initial stiffness
E_{sec}	secant modulus when deviator stress was half of that at critical state

1. INTRODUCTION

1.1. GENERAL

Low-plasticity silt is widespread throughout many countries, especially in countries located in large continents, such as the United States, China, and India. As noted by Puri (1984), one type of low-plasticity silt, loess, occupies the uppermost stratigraphic layer over extensive areas of the central United States; it is found in other parts of the country as well. Usually, the thickest deposits occur adjacent to the Missouri and Mississippi Rivers to the leeward side of the prevailing westerly winds. Low-plasticity silt is a difficult material to characterize. Its particle size lies between those of sand and clay, and its unique composition determines its behavior, which is different from that of sand and clay. These factors have two consequences: First, specimens for laboratory tests are difficult to prepare and handle. On one hand, because of its apparent lack of cohesion compared to clay, low-plasticity silt is very friable, so its fabric tends to break during sampling, trimming and preparation (Izadi, 2008). Undisturbed sampling of saturated silt is practically impossible with thin-walled tubes. On the other hand, vibration does not make silt as dense as it does sand, so the common moist tamping and water pluviation methods used for sand are not effective to prepare silt specimens. Second, because air is easily trapped among silt particles as it is among fine sand particles and cavitation easily occur due to negative excess pore pressure produced during shearing, saturation of specimens is more difficult than saturation of clay and coarse sand (Duncan and Wright, 2005; Izadi, 2008). These difficulties have discouraged research on the behavior of low-plasticity silt.

Silt liquefaction is a common phenomenon observed during earthquakes, such as, the 1976 Tangshan earthquake, the 1989 Loma Prieta earthquake, the 1994 Northridge earthquake, the 1999 Chi-Chi earthquake, the 1999 Kocaeli earthquake, and the 2010 Chile Earthquake, among others (e.g., Boulanger et al., 1998; Bray and Sancio, 2006; Boulanger and Idriss, 2006; Bray and Frost, 2010). However, the damage to property and potentially loss of life does not occur only during earthquakes. Some dams or slopes have failed not only due to cyclic loading during an earthquake, but also due to reduced shear strength or stiffness after an earthquake. Most failures of earth dams have occurred from just a few hours to up to 24 hours after an earthquake (Soroush and Soltani-Jigheh, 2009). This phenomenon, called delayed failure or delayed response, has demonstrated the need to study the postliquefaction characteristics of soils.

Some researchers have studied the postliquefaction behavior of sand (Chern and Lin, 1994; Vaid and Thomas, 1995; Porcino and Caridi, 2007; Amini and Trandafir, 2008; Alba and Ballestero, 2008; Ashour et al., 2009). In particular, a National Science Foundation workshop held in April, 1997, addressed the postliquefaction shear strength of granular soils (Stark et al., 1997). Byrne and Beaty's keynote paper in this report articulated the requirement that direct tests should be carried out to determine postliquefaction strength under consolidated undrained conditions. This requirement may be reasonable for sand due to its high permeability; however, low-plasticity silt is less permeable than sand. Additionally, the reconsolidation rate depends on drainage boundary conditions in the field. If low-permeability layers are present above or below in the liquefied zone, reconsolidation may take a long time. The 2000 Tottoriken-Seibu earthquake in Japan experienced high levels of pore water pressure a long time after the

earthquake. In the Takenouchi Industrial Park, the sand boiled for 7.5 hours, much longer than previously observed in sandy deposit in Niigata, Japan. The ground at the industrial park consists of no-plastic silt (Towhata, 2008). Before the ground can recover its stiffness and shear strength due to liquefaction, the soil must reconsolidate, it is during this period of instability that structures can undergo further damage. Therefore, one of the focuses in this research is the postliquefaction behavior of low-plasticity silt at various levels of reconsolidation after full liquefaction.

Full liquefaction does not necessarily occur during an earthquake. Its likelihood depends on the duration and magnitude of the earthquake and the resistance to liquefaction of the soil. During a short-duration or low-magnitude of earthquake, liquefaction does not occur; however, soil properties are affected. Typically, shear strength and stiffness of soil are reduced without reconsolidation and increased after full reconsolidation. This dissertation refers to the effect of limited cycles of dynamic loading on soil behavior as *limited liquefaction* (Ashour et al., 2009). This research also focuses on the postcyclic behavior of low-plasticity silt at various levels of liquefaction (i.e., excess pore pressure ratios) and further with full and no reconsolidation. Additionally, it investigates the effect of the plasticity on the postcyclic behavior of silt, by investigating the variations in shear strength and stiffness at different levels of PI.

The low-plasticity silt tested here was taken from the Mississippi River Valley (MRV) in the New Madrid seismic zone (NMSZ), a seismically prone area in the central United States. This research was a comprehensive experimental program limited to unit element tests in the laboratory. The understanding of postcyclic monotonic shear

behavior requires a reference for such behavior; therefore, the monotonic shear behavior of the MRV silt in triaxial compression was studied including the effect of PI.

Thus, this research project mainly addresses four issues: monotonic shear behavior, postliquefaction behavior at various levels of reconsolidation, postcyclic behavior with full and no reconsolidation at various levels of liquefaction, and the effect of PI on silt behavior.

1.2. RESEARCH SIGNIFICANCE

Silt liquefaction is a common phenomenon during earthquakes, as mentioned previously. The United States has experienced many earthquakes in recorded history. Puri's work points out that the NMSZ may have as high as a 98% probability of experiencing a magnitude 6.0 or greater earthquake between 2000 and 2050. According to the 2007 update to the National Inventory of Dams, approximately one third of the 80,000+ dams in the United States pose a high or significant hazard to life and property if failure occurs (FEMA, 2009). Additionally, about 70% of the 600,000 bridges in the United States were built prior to 1971 with little or no seismic design considerations (Anderson et al., 2001). Unless mitigation measures are taken, an earthquake would likely cause significant damage to many dams or bridges due to the liquefaction of the silty ground.

Study of the postcyclic behavior of low-plasticity silt under full and limited liquefaction is important to ensure the safety of infrastructure after an earthquake because shear strength and stiffness of the soil are usually reduced if the soil is not reconsolidated in a timely fashion (Porcino and Caridi, 2007; Yasuhara, 2003; Vaid and Thomas, 1995;

Ashour et al., 2009; Soroush and Soltani-Jigheh, 2009). Since low-plasticity silt does not drain as well as sand, it takes much more time to dissipate excess pore pressure. This explains why some dams have failed several hours after an earthquake. Thus, this work examines the postliquefaction behavior at various levels of reconsolidation. With lower cycles of loading or lower cyclic shear stress induced by an earthquake, the induced pore water pressure is insufficient to liquefy silt ground. The study of the postcyclic behavior of low-plasticity silt under limited liquefaction will clarify the effect of variation in level of cyclic loading on monotonic behavior. Little work has addressed the effect of PI on the reduction of precyclic and postcyclic behavior. This research will aid filling that gap in knowledge.

1.3. RESEARCH OBJECTIVES

The goal of this research is to advance the understanding of the behavior of low-plasticity silt under specific postcyclic conditions, including full and limited liquefaction. Given the particle size of silt, which exhibits frictional behavior at lower permeability than sand, postcyclic shear strength and stiffness are important. Specifically, the objectives of this experimental study are to:

a. examine the unique monotonic shear behavior of low-plasticity silt;
b. investigate the postliquefaction behavior at various levels of reconsolidation;
c. investigate the postcyclic behavior at various levels of liquefaction with full and no reconsolidation; and
d. assess the effect of PI on precyclic and postcyclic behavior of low-plasticity silt.

Accomplishment of these objectives will constitute a significant contribution to the published literature on soil mechanics and will advance the understanding of this challenging soil material. Experimental results and data are always welcome by the research community to improve the understanding of soil mechanics at specific initial state conditions and to verify numerical models. The results of this research will allow the development of mitigation measures to reduce the impact of liquefaction to civil infrastructure founded on or built with these silt materials.

1.4. DISSERTATION ORGANIZATION

This dissertation is organized in the same chronological order of the tasks presented in the work plan submitted to the faculty thesis committee. The following nine (9) Sections are described below:

Section 1 – Introduction: The significance, objectives and organization of the research activities are stated.

Section 2 – Literature Review: The state-of-the-art in postcyclic behavior of soil is reviewed as reported in the literature. Additionally, the laboratory specimen preparation techniques and the monotonic shear behavior of low-plasticity silt published by other researchers are also examined.

Section 3 – Experimental Program: The MRV silt was initially characterized by conducting multiple index property tests and using the aid of a scanning electron microscope. Then the different triaxial testing devices are briefly explained. The testing procedures for triaixal testing are described in detail to show how the static, cyclic, and

postcyclic shear tests were conducted. Finally, a summary of the tests conducted are presented in tabular form.

Section 4 – Specimen Preparation: The slurry consolidation approach to reconstitute silt specimens in a split vacuum mold are presented in detail. A special specimen movement technique to expedite testing is described. The replication of static and cyclic tests was reported to verify the validity of the specimen preparation approach used for triaxial tests.

Section 5 – Monotonic and Cyclic Shear Behavior: The monotonic shear behavior of the MRV silt using triaxial compression tests with various effective consolidation pressures (σ'_c) and overconsolidation ratios (OCRs) is presented. The effective friction angles of the MRV silt are determined using various failure criteria, and the best criterion to compute the effective friction angle for the MRV silt is determined. The critical state line (CSL) and the normalized behavior of the MRV silt are investigated. Cyclic shear behavior is investigated using cyclic triaxial tests, and the relationship of cyclic stress ratio (CSR) versus number of loading cycles is reported.

Section 6 – Postcyclic Behavior with Full Liquefaction: This section studies the postliquefaction behavior with various levels of reconsolidation after full liquefaction. The reconsolidation characteristics after cyclic loading are examined. The effect of the CSR on postcyclic shear behavior is investigated. The effect of reconsolidation level on postliquefaction shear strength and stiffness are presented. Additionally, the variation in normalized shear strength ratio with respect to apparent overconsolidation ratio (OCR_{app}) is evaluated. The CSL of the MRV silt after cyclic loading is compared to that of the MRV silt without previous cyclic loading.

Section 7 – Postcyclic Behavior with Limited Liquefaction: Here the condition of limited liquefaction is created by controlling the number of cycles to produce an excess pore pressure ratio less that the unity. The postcyclic shear tests are conducted after full and no reconsolidation of the MRV silt; the results are presented separately. Variations in postcyclic shear strength and stiffness with level of liquefaction are evaluated.

Section 8 – Effect of Plasticity on Precyclic and Postcyclic Behavior: Triaxial tests on normally consolidated specimens with varying plasticity (by adding bentonite to the MRV silt) determined the effect of PI on monotonic and cyclic shear behavior. Triaxial compression tests after cyclic loading evaluated the effect of PI on the changes in shear strength and stiffness of the MRV silt-bentonite mixture with full or no reconsolidation due to cyclic loading.

Section 9 – Conclusions and Recommendations: After the above sections, the findings for this research are summarized. In addition, some recommendations are made for future research.

2. BACKGROUND AND LITERATURE REVIEW

Compared to sand and clay, low-plasticity silt is a difficult soil material to test in the laboratory. It is usually thought to behave like clay or sand; however, Fleming and Duncan (1990) pointed out that the empirical correlations for strength and compressibility of clays may be inapplicable to silt. The same study also noted that failure to recognize the difference between the shear characteristics of silts and clays on one hand and sands on the other hand could lead to over-conservative designs of offshore structures. Research on the behavior of silt is still limited. For completeness, a summary of the key points related to the shear behavior of sands and clays will be presented herein, mainly reference material. The postcyclic monotonic behavior of the soil can be investigated using laboratory or field tests, and known liquefaction case studies. This section explains how to estimate undrained shear strength (S_{us}) of liquefied soil. The present work relies on an experimental approach to the study of the postcyclic shear behavior of low-plasticity silt; therefore, the findings in postcyclic shear behavior by other researchers were reported. This section reviews undrained shear strength of liquefied soil, specimen preparations, monotonic shear behavior of low-plasticity silt, postcyclic monotonic behavior, and the effect of plasticity on postcyclic monotonic behavior.

2.1. UNDRAINED SHEAR STRENGTH OF LIQUEFIED SOIL

Poulos et al. (1985) have labeled the undrained shear strength of liquefied soil as undrained steady-state shear strength. Others have called it residual undrained shear

strength (Seed, 1987), undrained critical shear strength (Stark and Mesri, 1992), and liquefied shear strength (Olson and Stark, 2002). All of these terms refer to shear strength mobilized at large deformation in the undrained condition after liquefaction.

Early studies of soil liquefaction assumed that soil liquefied at an excess pore pressure ratio equal to unity and resulted in zero undrained shear strength (Poulos et al., 1985; Marcuson et al., 1990). Poulos et al. (1985) stated that some undrained shear strength remains after 100% pore pressure buildup, and this remaining strength is the undrained steady-state strength, which is solely a function of void ratio. They presented a chart (reported in Figure 2.1) to estimate the undrained shear strength of liquefied soil. Determination of the in situ void ratio, however, is difficult. Small changes in the void ratio result in large changes in undrained shear strength because the small slope of the steady-state line makes postliquefaction undrained shear strength sensitive to the void ratio. Kramer (1989) quantified the uncertainties of in situ void ratio and steady-state line through a statistical analysis of previously reported data. He created a chart of the reduction factor to estimate the in situ steady-state shear strength with a specific probability overestimated by the deterministic steady-state procedure (Kramer, 1989).

The previous undrained steady-state strength based on laboratory testing follows three assumptions: (1) There is a unique relationship between steady-state strength and void ratio; (2) the slope of the steady-state line is the same for reconstituted and undisturbed sand samples; and (3) the slope of the steady-state line is independent of the method by which samples are reconstituted in the laboratory (Seed, 1987). However, other researchers have claimed that these assumptions were invalid because the slope of the steady-state line may depend on the method of sample preparation (Vaid and Chern,

1985; Seed, 1987; Stark and Mesri, 1992; Nocilla et al., 2006). Nocilla et al. (2006) observed that there are no unique normal consolidation lines (NCLs) and CSLs for Italian silts with PIs of 11 and 13. They concluded that specimens prepared with slurries of different water content generate different fabrics.

Figure 2.1. Estimation of undrained shear strength of liquefied soil using steady-state strength approach (Poulos et al., 1985)

Given the difficulty of undisturbed sampling to measure the in-situ void ratio, Seed (1987) presented a chart showing the relationship between residual undrained shear strength and the standard penetration test blowcount (SPT N) for sands. With an increased number of case studies, Seed and Harder (1990) updated the chart (reported in Figure 2.2) to estimate the residual shear strength based on a corrected clean sand

blowcount ($(N_1)_{60\text{-}cs}$). Thevanayagam et al. (1996) studied the relationship between residual undrained shear strength determined though back-analysis of case histories and the steady-state strength of liquefied soil obtained from laboratory tests studies. They related relative density (D_r) for laboratory data to the $(N_1)_{60\text{-}cs}$ using the equation $(N_1)_{60\text{-}cs}=0.0043D_r^3$ and developed a chart to compare residual undrained shear strength and steady-state strength of liquefied soil (Figure 2.3). Thevanayagam et al. (1996) found that the corresponding back-calculated data for undrained shear strength were similar in magnitude with the data on the steady-state strength of silty sands at comparable relative densities.

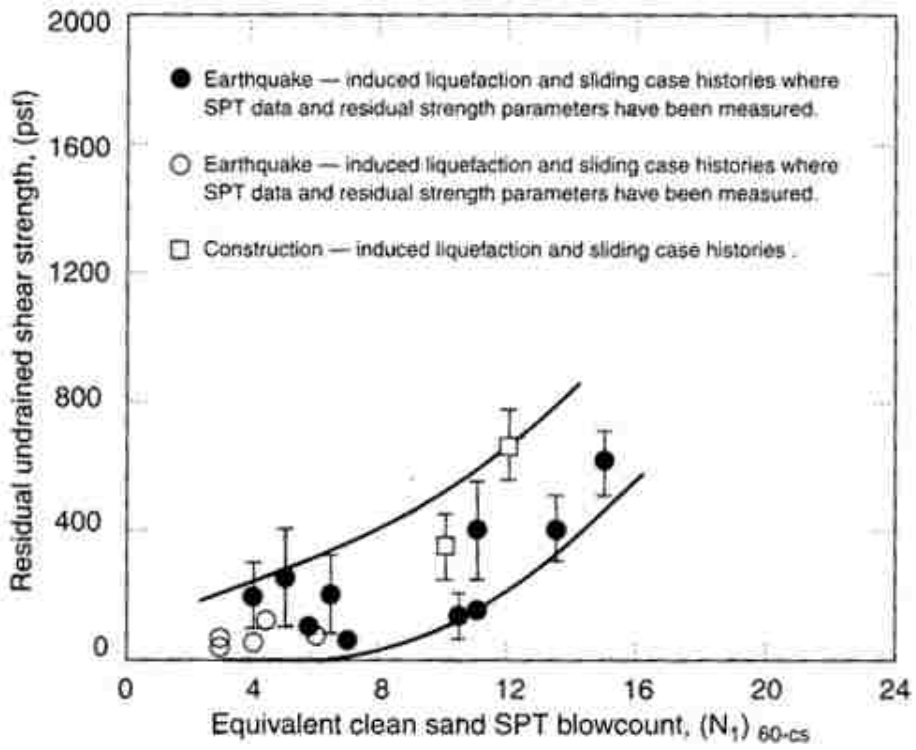

Figure 2.2. Relationship between corrected "clean sand" blowcount $(N_1)_{60\text{-}cs}$ and undrained shear strength (S_r) based on case studies (Seed and Harder, 1990)

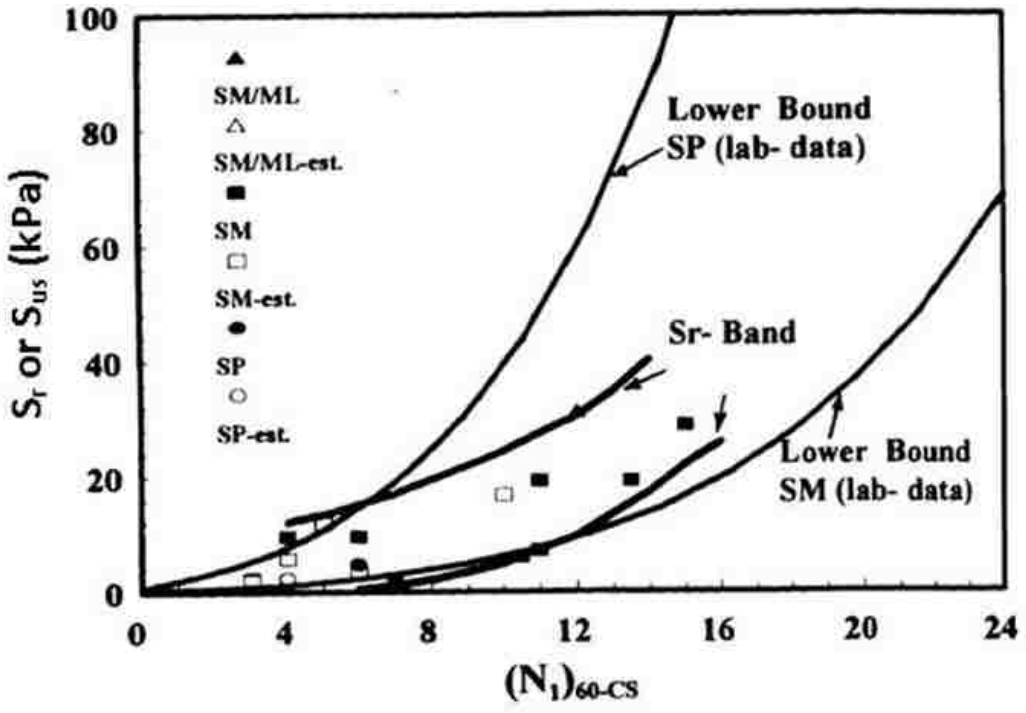

Figure 2.3. Comparison of steady-state strength (S_{us}) based on laboratory data with undrained shear strength (S_r) band determined from back-analysis of case histories for clean sands, silty sands, and silts (Based on Thevanayagam et al., 1996)

Based on liquefaction flow case histories, Olson and Stark (2002) presented equations to estimate liquefied shear strength ratio, $S_u(LIQ)/\sigma'_{v0}$, from the normalized tip resistance, q_{c1}, in cone penetration test (CPT):

$$S_u(LIQ)/\sigma'_{vo} = 0.03 + 0.0143 q_{c1} \pm 0.03 \qquad \text{for } q_{c1} \le 6.5 \text{ MPa} \qquad (2)$$

and from normalized SPT blowcount,$(N_1)_{60}$:

$$S_u(LIQ)/\sigma'_{vo} = 0.03 + 0.0075\left[(N_1)_{60}\right] \pm 0.03 \qquad \text{for } (N_1)_{60} \le 12 \qquad (3)$$

Olson and Stark (2003) verified the concept of liquefied shear strength ratio using laboratory testing. In earlier work (2002), they had found no trend in the liquefied strength ratio with respect to fines content. Although soils with higher fines content

should exhibit lower penetration resistance as a result of greater soil compressibility and smaller hydraulic conductivity, they are more likely to remain in undrained condition during flow.

Robertson (2010) proposed a relationship to estimate liquefied shear strength ratio:

$$\frac{S_u(LIQ)}{\sigma'_{vo}} = \frac{\left[0.02199 - 0.0003124 Q_{tn,cs}\right]}{1 - 0.02676 Q_{tn,cs} + 0.0001783 (Q_{tn,cs})^2} \quad (4)$$

where $0.03 \leq S_u(LIQ)/\sigma'_{v0} \leq \tan\phi'$, ϕ' is the effective friction angle of soil, and $Q_{tn,cs}$ is no more than 70. The equivalent clean sand value ($Q_{tn,cs}$) is related to the soil behavior type index, representing the type of soil, and its definition can be referred to Robertson (2010). Thus, Equation 4 can include the effect of fines content.

The studies described here suggest that the in situ test approach is quite promising to estimate the undrained shear strength of liquefied soil. However, laboratory testing is a strong tool to study the effect of some parameters on soil behavior because of the more controlled conditions in the laboratory. Further, the results of laboratory testing can be used as a guideline to make a judgment on in situ testing data.

2.2. SPECIMEN PREPARATION

Common methods to reconstitute soil specimens include moist tamping (MT), water pluviation (WP), air pluviation (AP), and slurry deposition (SD). Slurry deposition is also called slurry consolidation (SC) by some researchers, which was adopted herein. These approaches can yield different soil properties for the same materials under identical testing conditions due to variations in soil fabric (Ladd, 1977; Mulilis et al., 1977; Kuerbis and Vaid, 1988; Murthy et al., 2007). Soil specimens prepared by MT can have a

cyclic strength as much as 100% greater than those prepared by AP (Ladd, 1977). Specimens prepared by MT have considerably higher undrained shear strength and a slightly smaller flow potential than those prepared by the SD. However, at large strain, these differences in fabric vanish, leading to a unique fabric at the critical state (Murthy et al., 2007).

The MT method best models the soil fabric of rolled construction fills, for which the method was originally designed (Kuerbis and Vaid, 1988). Water tension forces exist in the specimen, and honeycomb structure forms easily (Guo and Wang, 2009). Vaid (1994) argued that the MT technique neither simulates the fabric of alluvial soil deposits nor guarantees specimen uniformity. Hoeg et al. (2000) investigated the effect of specimen preparation methods on the static behavior of silt with a PI of 5 in Borlange, Sweden. Using triaxial compression tests, they compared the strength of undisturbed specimens with that of reconstituted silt specimens under normal consolidation. Most of the specimens were prepared by MT, but one was created using the SD approach. The undisturbed specimens showed dilative and ductile behavior, whereas almost all the reconstituted specimens showed contractive and brittle behavior. Bradshaw and Baxter (2007) presented a new modified MT method and claimed that samples prepared with this method can exhibit cyclic strengths comparable to those of slurry consolidated sample and in situ block samples. They compared the method with the SC method for Wellington Avenue silt and with the block sample method for Olneyville silt. A direct comparison with the same silt material would be preferable.

The AP method models the natural deposition process of wind-blown Aeolian deposits (or loess), which generally consist of either poorly graded sand or poorly graded

silt (Kuerbis and Vaid, 1988). The AP method is not suitable for well-graded sand, which is easily segregated, since the process of sample saturation may disrupt the initial sand fabric, and fines are washed out of the sample (Kuerbis and Vaid, 1988; Carraro and Prezzi, 2007).

The WP method simulates the deposition of sand through water that occurs for many natural environments and mechanically placed hydraulic fills (Kuerbis and Vaid, 1988). It produces uniform samples of poorly graded sand, but particles size segregation is a problem. For well-graded soil, the WP results in larger maximum void ratio like that of a more poorly graded soil. Vaid et al. (1999) carried out an experimental program to study the influence of reconstituted methods on sand. They concluded that water-deposited specimens are very uniform compared to those prepared by MT. Vaid et al. (1999) compared the shear resistance of undisturbed frozen sand with that of sample prepared by other methods and argued that the WP can closely simulate the fabric of the natural alluvial and hydraulic fill sands. Hoeg et al. (2000) stated that the WP is promising, despite difficulties with segregation of sands with high fines content.

It is difficult to densify low-plasticity silt using vibration methods, and SD is a common technique to prepare silt specimens, and even sandy silt and silty sand specimens. Ishihara et al. (1978) developed the SD technique for silty sand and sandy silt, but their specimens were not very homogeneous when fines content was between 30% and 80%. Kuerbis and Vaid (1988) presented a new SD method to prepare sand specimens. Their specimens were exceptionally homogeneous with respect to void ratio and particle size gradation, regardless of gradation and fines content. This method effectively simulates well the soil fabric found in a natural fluvial or a hydraulic fill

deposit, yet creates homogenous samples that can be easily replicated as required. Carraro and Prezzi (2007) applied another new SD method for silty sands. They were able to reconstitute homogeneous specimens of sands containing fines, and they did not observe the characteristic strain-softening response associated with the usually collapsible fabric obtained by the AP and MT techniques. Yasuhara et al. (2003) used SD approach to prepare specimens to study the postcyclic degradation of strength and stiffness. Hyde et al. (2006) also prepared silt specimens using the SD approach and found non-uniformities due to the friction in the consolidation tubes and sample disturbance during preparation. They found that this method did not produce samples representative of silt placed as a coastal fill material, which would often be pluviated under water and then consolidated by an overburden. Instead, they applied a simple sedimentation technique to consolidate the slurry under a negative head of water. In addition to these SD approaches for silt, sandy silt, and silty sand, Khalili and Wijewickreme (2008) introduced a SD method to reconstitute gap-graded specimens (mixtures of waste rock and tailings) and overcame the difficulties of preparing such specimens.

Researchers have accepted the SD approach as the best method to reconstitute silt specimen. However, the problems shown by other researchers' work include the complexity and duration of specimen preparation. Section 4 describes a new SC approach to the preparation of low-plasticity silt specimens for triaxial tests, including a specimen movement technique to expedite the testing program.

2.3. MONOTONIC SHEAR BEHAVIOR OF LOW-PLASTICITY SILT

Several decades ago, Penman (1953) studied the static shear behavior of the non-plastic Braehead silt under normally consolidated conditions, both drained and undrained. The silt specimens showed dilative behavior. The same behavior has also found in the Alaska silts (Wang et al., 1982; Fleming and Duncan, 1990) and the Bonnie silt (Arulmoli et al., 1992), among others. Wang et al. (1982) found in Alaska silts no unique undrained shear strength with various effective consolidation pressures. They found that the ratio of undrained shear strength to effective consolidation pressure was higher than that for clay with an identical overconsolidation ratio.

Fleming and Duncan (1990) investigated the characteristics of undisturbed and reconstituted Alaskan silt specimens using a SD approach. In unconsolidated undrained (UU) tests, the reconstituted specimens exhibited undrained shear strength as much as 42% lower than that of undisturbed specimens. On the other hand, consolidated undrained (CU) tests indicated that the undrained strength of reconstituted specimens was higher than that of undisturbed specimens. Fleming and Duncan concluded that silt is more likely to be seriously affected by disturbance than clay. In general, the undrained strength of Alaskan silts can be normalized by effective consolidation pressure. As OCR increases, the normalized shear strength increases. Yasuhara et al. (2003) observed the same normalized behavior in the Keuper Marl silt with a PI of 19.7.

Brandon et al. (2006) studied the drained and undrained shear strength of two silts, undisturbed gray silt (called Yazoo silt, which is nonplastic) and disturbed tan silt (called LMVD silt with a PI of 4) from the Lower Mississippi Valley Division (LMVD). In undrained tests, both consolidated and unconsolidated, all specimens showed dilative

behavior. That study demonstrated that the UU tests provided no useful information on the undrained strengths of the Yazoo silts. The authors suggested that the constant Skempton pore pressure parameter A equal to zero was the failure criterion best used to determine the ratio of undrained shear strength to effective consolidation stress.

Izadi (2006) investigated the static behavior of Collinsville silt, sampled in the same region as the silt tested in the present research. Using a SD approach, he reconstituted his specimens in a large consolidometer. The soil showed fairly high dilative behavior, even normally consolidated. Without high enough B values after saturation, cavitation easily developed due to negative excess pore pressure, and the specimens became unsaturated at large strain.

Boulanger and Idriss (2006) reviewed the behavior of three blended silt mixtures under normally consolidated conditions, which was originally presented by Romero (1995). The specimen with a PI of 10.5 showed a plastic stress-strain response like that of normally consolidated clay. Its NCL and CSL were almost parallel, and it exhibited no quasi-steady-state behavior. Yasuhara et al. (2003) observed such plastic stress-strain behavior in the Keuper Marl silt with a PI of 19.7. Boulanger and Idriss (2006), on the other hand, noted that throughout the test, the silt specimen without plasticity exhibited strain hardening like that seen in loose sands, and its NCL and CSL were not parallel. However, the silt with a PI of 4 exhibited a behavior more like that of clay-like silt, but with a tendency toward some strain hardening and phase transformation behavior. Its NCL and CSL were approximately parallel, but it had a quasi-steady-state line. Boulanger and Idriss (2006), therefore, concluded that fine-grained soils with a PI greater than or equal to 7 can be expected to exhibit clay-like behavior, and fine-grained soils

with PI values ranging from 3 to 6 exhibit intermediate behavior. Nocilla et al. (2006) that the Italian silt with PIs of 11 and 13, no unique NCL and CSL were found because specimens prepared with slurries of different water content generated different fabrics.

Table 2.1 summarizes the monotonic shear behavior of low-plasticity silt, which can show strain-hardening behavior or plastic stress-strain behavior, depending primarily on PI, OCR, specimen preparation technique, and others.

Table 2.1. Summary of static shear behavior of low-plasticity silt

Silt Name	**Clay Content (<2μm)**	**LL**	**PI**	**Spec. Prep.**	**p'_c (kPa)**	**OCR**	**Strain Hardening or Softening**	**Reference**
Braehead Silt	0	24.6	NP	SD	34	1	Strain hardening	Penman (1953)
Alaskan OCS Silt	< 45%	Close to the A line		---	---	1-10.5	Strain hardening	Wang et al. (1982)
Tailing Slime	15-23%	25-40	5-19	---	144	1	Plastic stress-strain	Boulanger and Idriss (2006)
		just above A line			478			
Blended Silt	3%	26	0	SD	100	1	Strain hardening	
	11%	30	4		100	1	Little strain hardening	
	19%	36.5	10.5		100	1	Plastic stress-strain	
Tailing Slime	Sandy silt	---	0	US	270-720	1	Strain hardening	
	Clayey silt	---	9.6		270-720	1	Plastic stress-strain	

Note: p'_c - effective mean consolidation pressure, US – undisturbed sampling

Table 2.1. Summary of static shear behavior of low-plasticity silts (cont.)

Silt Name	Clay Content (<2μm)	LL	PI	Spec. Prep.	p'_c (kPa)	OCR	Strain Hardening or Softening	Reference
Alaskan Silt	23%	Closed to the A line		SD	---	1	Strain hardening	Fleming and Duncan (1990)
					---	2		
					---	8		
Bonnie silt	7%	29	15	SD	40	1	Strain hardening	Arulmoli et al. (1992)
					80	1		
					160	1		
Borlange Silt	5-10%	---	5	US	38.6	1	Strain hardening	Hoeg et al. (2000)
				MS	38.7	1		
				SD	38.5	1		
Keuper Marl silt	8%	---	19.7	SD	392	1	Plastic stress-strain	Yasuhara et al. (2003)
						2	Plastic stress-strain	
						4	Plastic stress-strain	
						10	Plastic stress-strain	
Silica flour	about 2%	29	<2	SD	100 and 200	1	Strain hardening	Silva and Bolton (2005)
Yazoo Silt	13-16%	Non-plastic		US	69 - 343	1	Strain hardening	Brandon et al. (2006)
Collinsvi-lle Silt	17%	30	6	SC	110 - 331	1	Strain hardening	Izadi (2006)

2.4. POSTCYCLIC BEHAVIOR OF SOIL WITH FULL LIQUEFACTION

Shear strength and stiffness of soil are recovered during reconsolidation after liquefaction. Here, *reconsolidation* refers to the process of volume change and dissipation of the excess pore pressure that builds up during cyclic loading up to liquefaction. Recovery of the shear strength and stiffness of low-plasticity silt takes time due to its low permeability and perhaps also as a result of poor drainage boundary conditions. Postliquefaction behaviors are different after various levels of reconsolidation. Some researchers have investigated the postliquefaction strength of soil, with a focus mainly on sand or sandy soil.

Vaid and Thomas (1995) performed triaxial tests on Fraser River sand using the WP approach to reconstitute specimens. They found that the liquefied sand deformed at virtually zero stiffness over a large range of axial strain (about 20%). With further straining, the sand always responded in a dilative manner under monotonic loading, even though the initial sand was contractive under static loading. The postliquefaction response represented continuous hardening and no approach to residual strength (Figure 2.4), regardless of density or effective consolidation pressure prior to cyclic loading, even after a postliquefaction strain of 32%. Amini and Trandafir (2008) also observed the dilation behavior in Bonneville silty sand, as did Liu et al. (2007) in silt. Vaid and Thomas (1995) explained that during the application of monotonic shearing, the grains in the liquefied specimen were rearranged. With increasing axial strain, the grains eventually regained contact. Subsequently, the pore water pressure started to decrease, and dilative behavior was measured. The findings of these studies overturned the assumption that if sand is contractive under static testing, its steady-state (or residual)

strength remains unaltered under monotonic loading following liquefaction induced by cyclic loading (Byrne et al., 1992).

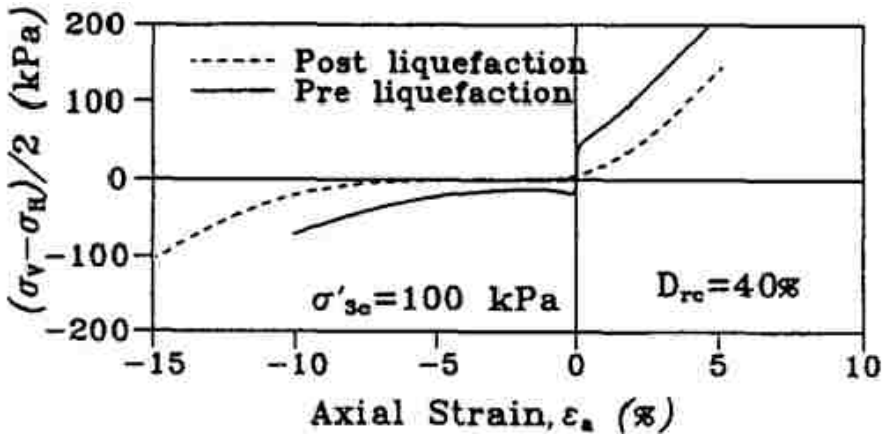

Figure 2.4. Comparison of static and postliquefaction response (σ_V and σ_H are vertical and horizontal stress, respectively) (Vaid and Thomas, 1995)

Other researchers have also examined the effect of specific factors on the postliquefaction behaviors, including density, axial strain induced by cyclic loading, and fine content. Vaid and Thomas (1995) found that the recovery rate of postliquefaction stiffness increased as relative density increased. Liu et al. (2007) found that the threshold strain after which stiffness increases quickly decreased as dry unit weight increased and maximum double axial strain decreased. Vaid and Thomas (1995) draw the same conclusion. Porcino and Caridi (2007) observed that the cyclic resistance of liquefied dense sand specimens remained practically unchanged under new cyclic loading. Conversely, in loose sand specimens, they observed decreased liquefaction resistance.

This effect was induced by the formation of looser and therefore weaker zones on top of the liquefied specimen. Therefore, a dense sample is more resistant to reduction in shear strength, and it recovers its stiffness more easily than a loose sample. Ashour et al. (2009) presented equations to assess the undrained response of liquefied sand based on drained test behavior formulation, indicating that the postcyclic excess pore pressure and associated residual effective confining pressure govern the postliquefaction undrained behavior of sand.

Most postliquefaction tests have been conducted on sand specimens under conditions of full reconsolidation or none at all. Work on postliquefaction behavior under various levels of reconsolidation has been extremely limited. The research presented here reconsolidated liquefied specimens at various levels, and ran monotonic shear tests to compare postliquefaction strength and stiffness with preliquefaction conditions.

2.5. POSTCYCLIC BEHAVIOR OF SOIL WITH LIMITED LIQUEFACTION

Limited liquefaction is common in connection with earthquakes of short duration or low magnitude, and in the case of soils highly resistant to liquefaction. However, studies of postcyclic behavior of low-plasticity silt under limited liquefaction conditions remain scarce.

Chern and Lin (1994) carried out cyclic loading and postcyclic consolidation tests on loose, clean sand and silty sand. They found that the reconsolidation volumetric strain is related to the maximum cyclic strain amplitude or residual pore pressure ratio developed during cyclic loading, regardless of the cyclic stress ratio or the number of stress cycles applied. For loose sand with accumulated, cyclic, single-amplitude axial

strain of less than 1% or a residual pore pressure ratio of less than 1.0, the magnitude of postcyclic reconsolidation volumetric strain is relatively small compared to that in liquefied specimens (Figure 2.5). Sanin and Wijewickreme (2006) presented similar findings after they conducted cyclic direct simple shear testing on Fraser River Delta silt. Chern and Lin (1994) proposed that full liquefaction (excess pore pressure equal to 1.0) is a prerequisite to significant volume change due to one-dimensional reconsolidation of loose deposits on level ground after an earthquake.

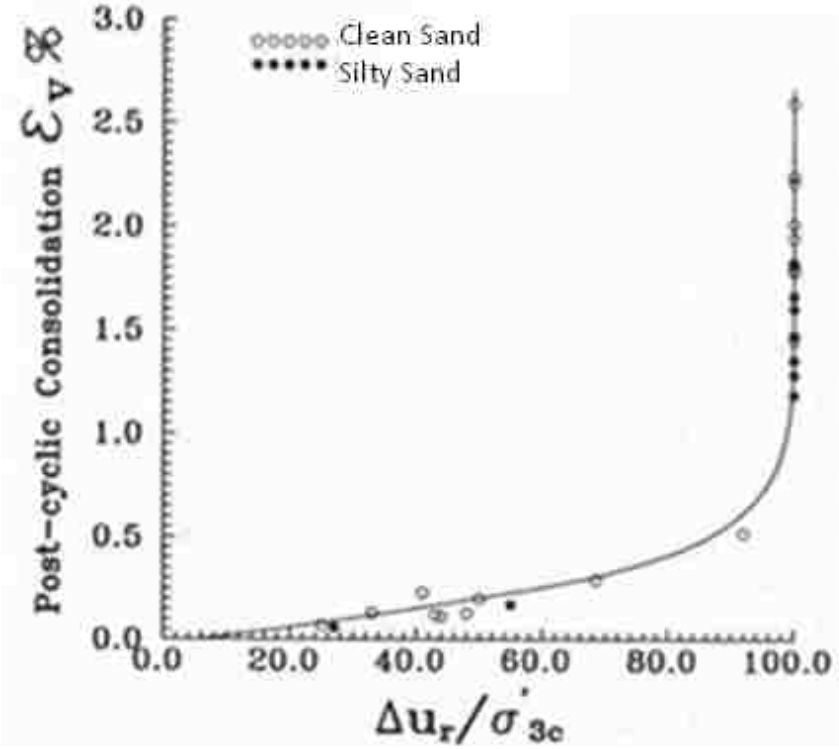

Figure 2.5. Relationship between postcyclic consolidation volumetric strain of sand and the residual pore pressure ratio (Chern and Lin, 1994)

Ashour et al. (2009) studied the undrained postcyclic response of sand following limited liquefaction. Under limited liquefaction, sand may exhibit initial (restrained) contractive behavior followed by dilative behavior. Here, the excess pore pressure and the associated residual effective confining pressure after cyclic loading (not initial density or confining pressure) governed the postcyclic undrained behavior (stress-strain relationship) of the sand. In limited liquefaction tests, Vaid and Thomas (1995) found that the postcyclic shear behavior approached to initial soil performance more closely with less excess pore pressure (Figure 2.6). With fewer loading cycles, there was lower excess pore pressure and so larger effective confining pressure. With larger effective confining pressure, postcyclic shearing behavior was more like the static shear behavior of soil without previous cyclic loading. Conversely, soil with low effective confining pressure due to large excess pore pressure has very low initial stiffness of soil at the beginning of postcyclic shearing.

Soroush and Soltani-Jigheh (2009) carried out strain-controlled cyclic triaxial testing on mixed clayey soils (clay-sand and clay-gravel mixtures). They concluded that the ratio of postcyclic undrained shear strength to initial undrained shear strength ($S_{u(PC)}/S_{u(M)}$) and the ratio of postcyclic secant deformation modulus to initial secant deformation modulus ($E_{50(PC)}/E_{50(M)}$) generally decreased as axial strain induced by cyclic loading increased. Further, they found that the reduction in the deformation modulus was more pronounced. Specimen behavior during postcyclic loading was similar to that of overconsolidated soils. Generally, the value of the apparent overconsolidation ratio (OCR_{app}) was proportional to the axial strain induced by cyclic loading. The *apparent overconsolidation ratio* is defined as the ratio of effective consolidation pressure before

cyclic loading to effective confining pressure at the beginning of postcyclic monotonic shearing. Soroush and Soltani-Jigheh (2009) presented charts to estimate postcyclic undrained shear strength, secant deformation modulus, and postcyclic excess pore pressures using the OCR_{app}.

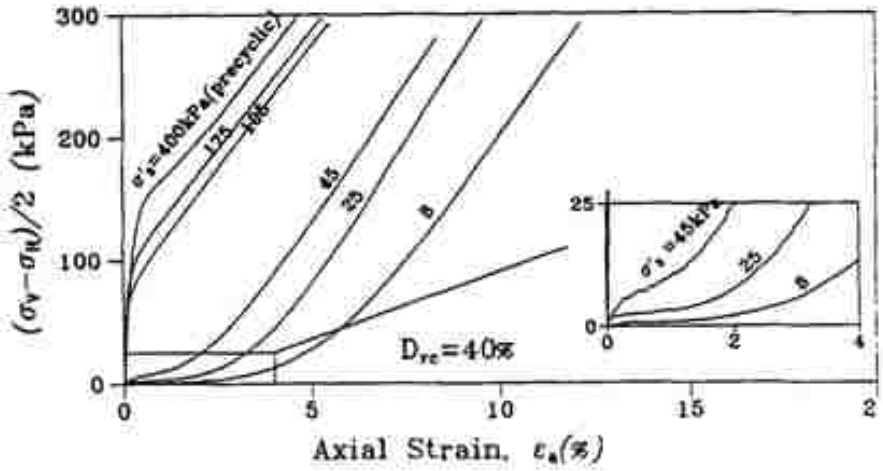

Figure 2.6. Postcyclic monotonic responses at various levels of liquefaction (The values close to the curves are effective confining pressures at the beginning of postcyclic shearing.) (Vaid and Thomas, 1995)

Little work has examined postcyclic behavior of silt, other than sand and mixed clayey soil. Yasuhara et al. (2003) carried out triaxial tests to study the postcyclic degradation of the strength and stiffness of low-plasticity silt (PI = 19.7). They applied cyclic loading under stress-controlled conditions until the sample experienced either 10% axial strain (single amplitude) or 100 cycles of undrained loading. With the same OCR, they found that postcyclic shear strength without reconsolidation decreased with an

increase in excess pore pressure ratio following cyclic testing. With increasing cyclic-induced excess pore pressure, stiffness at the beginning of postcyclic shearing decreased along with the peak deviator stress. Yasuhara's group observed that softening behavior occurred after the strength peaked, and this maximum value was reached at increasing strains with increasing OCR. After cyclic loading, the decrease in initial stiffness was more noticeable than the undrained shear strength, and this tendency was more marked for overconsolidated specimens. That work demonstrated that postcyclic stiffness of overconsolidated specimens correlates with excess pore pressure ratio generated during cyclic loading; however, compared to that for normally consolidated specimens, this correlation is not strong. By conducting direct simple shear tests on nonplastic silt, Song et al. (2004) found that the ratio of postcyclic maximum shear modulus to precyclic maximum shear modulus ($G_{max,cy}/G_{max,NCi}$) decreased rapidly with an increase in normalized pore pressure ($\Delta u/\sigma'_{vc}$). The rapid decrease in the stiffness ratio ($G_{max,cy}/G_{max,NCi}$) began at a lower excess pore pressure ratio with a higher initial shear stress (τ_s) (Figure 2.7).

Hyde et al. (2007) studied postcyclic behavior of a creamy powdered limestone (69.2% silt sized particles) with a PI of 6. The final change in specific volume was almost identical for all samples with identical axial strains induced by cyclic loading, irrespective of excess pore pressure. The change in specific volume, however, was expected to decrease with decreasing excess pore pressures developed during cyclic loading. The slope for postcyclic recompression was about 10 times steeper than that obtained from the isotropic swelling and recompression lines and rather similar to that of the isotropic consolidation line. This trend was quite different from the recompression

characteristics for more plastic soils reported by other researchers (Yasuhara et al., 1992, Hyde et al., 1997), who studied clay and plastic silts. Hyde et al. (2007) noted that for sands without full liquefaction and for clays; the excess pore pressure accumulated during cyclic loading is generally the main parameter to model postcyclic recompression, but for liquefied sand the volumetric strain model is often formulated using the shear strain developed as a result of liquefaction. Hyde's ground devoted more effort to studying the effect of anisotropic consolidation on postcyclic monotonic and cyclic behavior. They concluded that the ratio of undrained shear strength after and before cyclic loading decreases with an increase in the initial sustained deviator stress ratio (q_s/p'_c) in both compression and extension tests (Figure 2.8). On the other hand, the cyclic strength for second loading increased with an increasing initial sustained deviator stress ratio q_s/p'_c up to 0.75 (Figure 2.9).

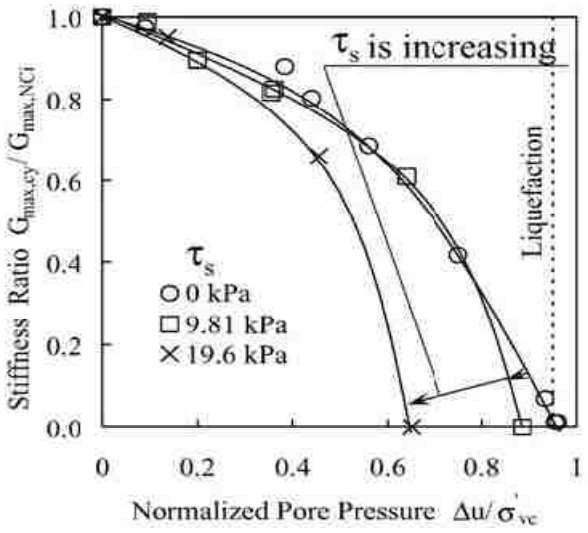

Figure 2.7. Stiffness-decreasing characteristics with normalized pore pressure (Song et al., 2004)

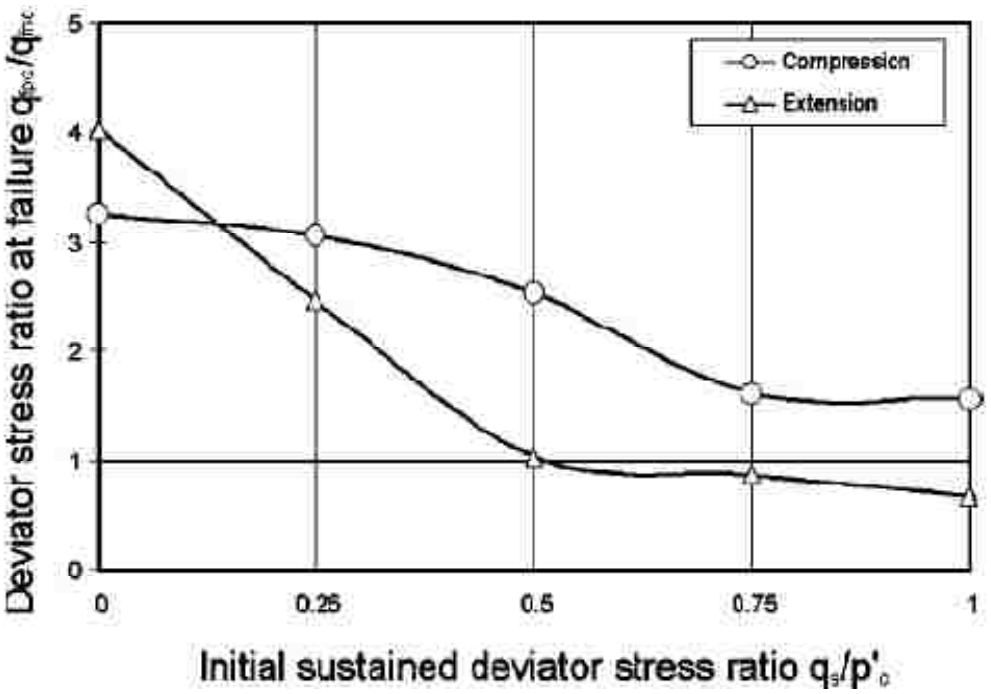

Figure 2.8. Comparison of deviator stress ratio at failure for samples with and without postcyclic recompression (Hyde et al., 2007)

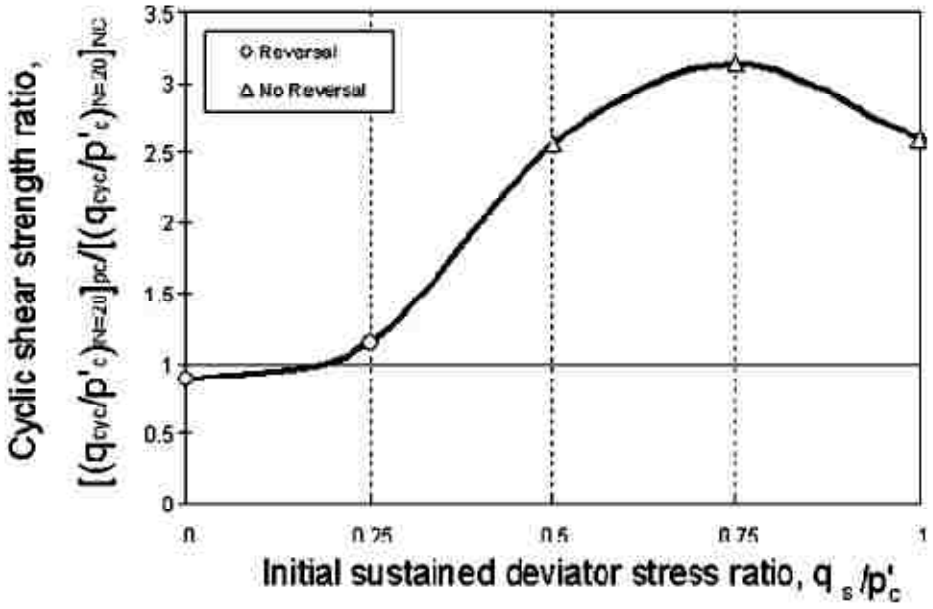

Figure 2.9. Comparison of cyclic shear strength for first loading and postdrainage second loading (Hyde et al., 2007)

In summary, the volume change in sand due to the reconsolidation after limited liquefaction is much lower than that after full liquefaction. Excess pore pressure after cyclic loading controls the postcyclic undrained shear behavior of sand and low-plasticity silt, irrespective of initial density or initial confining pressure. The greater the excess water pressure, the greater the reduction in undrained shear strength. The reduction in shear strength and stiffness of mixed clay soils is related to the axial strain induced by the cyclic loading. The reduction of stiffness is more marked than that of shear strength.

The research presented below attempts to close the gaps in published research on limited liquefaction of silts. It investigates the postcyclic behavior of low-plasticity silt at various levels of liquefaction, inducing various excess pore pressure ratios. It includes postcyclic monotonic shear tests under full and no reconsolidation.

2.6. EFFECT OF PLASTICITY ON POSTCYCLIC SHEAR BEHAVIOR

Plasticity has played an important role in liquefaction resistance. The PI may be used as a criterion to estimate the liquefaction potential of soil (Gratchev et al., 2006a, 2006b; Guo and Prakash, 1999). Guo and Prakash (1999) suggested that the liquefaction resistance of undisturbed samples first decreases with an increasing PI up to about 5, then increases as the PI rises beyond that level.

Logically, postcyclic behavior should be influenced by the PI; however, few reports address the effect of PI on the changes in shear strength and stiffness due to cyclic loading. Song et al. (2004) found that the tendency of the stiffness of nonplastic silt to decrease with the excess pore pressure ratio is less marked than that in plastic Arakawa clay with a PI of 17.3 (Figure 2.10). However, case histories indicate (Robertson, 2010)

that very young, very loose, nonplastic or low-plastic soils tend to be more susceptible to significant and rapid strength loss than older, denser, or more plastic soils. Alba and Ballestero (2008) stated that increasing fines content decreases the undrained shear strength of soil after liquefaction, but they did not investigate the effect of PI on the change of undrained shear strength due to cyclic loading.

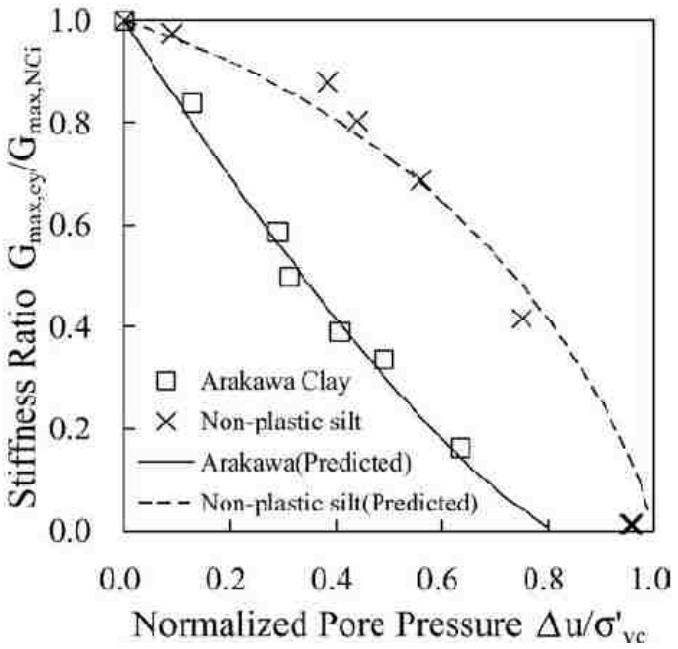

Figure 2.10. Relationship between shear modulus ratio and normalized pore pressure (Song et al., 2004)

Thus, according to existing reports, postcyclic shear strength decreases with an increase in PI. However, there was no consistent data reported on the effect of PI on reductions in shear strength and stiffness between Song et al. (2004) and Robertson

(2010). To study the role of plasticity on the postcyclic shear behavior of low-plasticity silt, this work investigated the effect of PI on changes of shear strength and stiffness due to cyclic loading with varying PI by adding bentonite to the silt.

2.7. SUMMARY

A review of the available literature shows that limited work has been done on the behavior of low-plasticity silt, especially after cyclic loading. Although its monotonic behavior has been studied for at least half a century, silt is usually treated as clay or sand regardless of its unique behavior, and more work is required. The research presented herein is based on an experimental program that provides important laboratory data to advance the understanding of the monotonic and postcyclic monotonic shear behavior of low-plasticity silt.

3. EXPERIMENTAL PROGRAM

3.1. SUBJECT SOIL

3.1.1 Material Description. Low-plasticity silt occupies the uppermost stratigraphic position over extensive areas of the central United States, and the thickest deposits occur adjacent to the Missouri and Mississippi Rivers to the leeward side of the prevailing westerly winds. The subject silt for this research was taken from Collinsville, Illinois, about 13 miles east of the Mississippi River. Figure 3.1 shows that Collinsville is located in NMSZ, a seismically unstable area of the central United States.

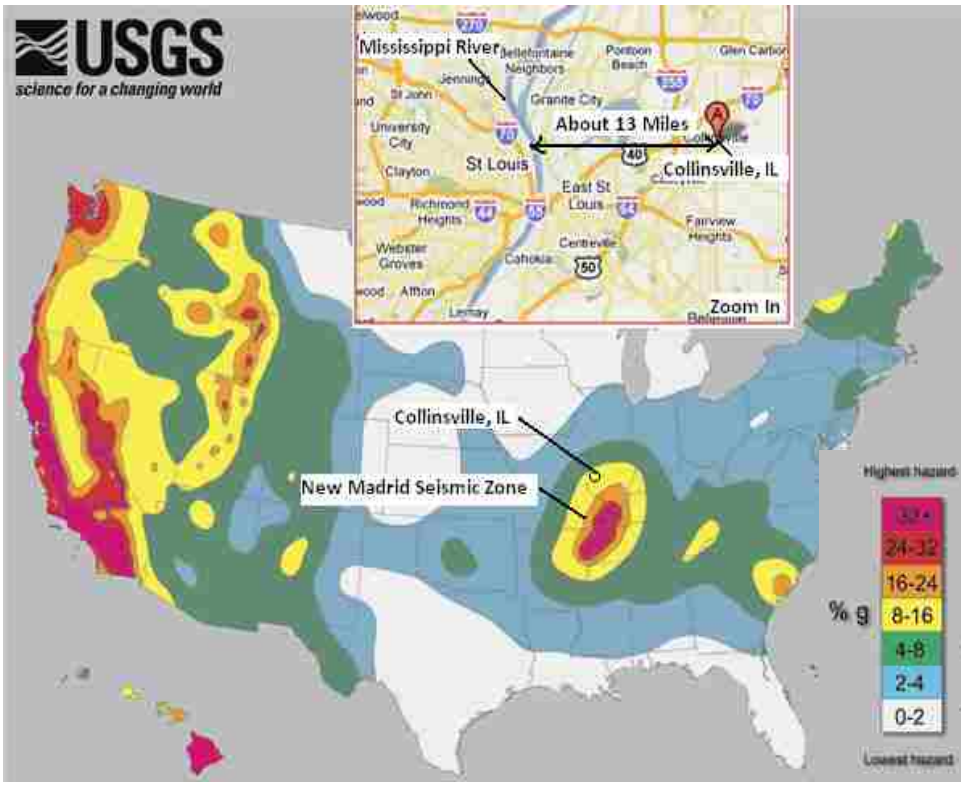

Figure 3.1. Silt source location (based on USGS, 2005)

The index properties of this silt were determined using multiple laboratory tests. Table 3.1 summarizes the index properties of MRV silt. The grain size distribution was obtained using sieve and hydrometer analysis (ASTM D 422), and the clay content was determined to be 14.5% (Figure 3.2). The specific gravity was 2.71, as measured according to ASTM standard D 854. The consolidation parameters were determined using isotropic consolidation pressure in a triaxial chamber. The Atterberg limits were determined based on ASTM standard D 4318; the PI was 5.8, and the liquid limit (LL) was 28.1.

Table 3.1. Index properties of the MRV silt

Index Property	**Value**
Clay content (< 2um)	14.5%
Liquid limit (LL)	28.1
Plastic limit (PL)	22.3
Plasticity index (PI)	5.8
Specific gravity (G_s)	2.71
Maximum void ratio (e_{max})	1.604
Minimum void ratio (e_{min})	0.436
Compression index (C_c)	0.0896
Recompression index (C_r)	0.0090

The LL of low-plasticity silt is difficult to determine. There are two common approaches to its measurements: Casagrande approach (ASTM D 4318-05) and Fall Cone

approach (BS 1377-2). Researchers have compared these two approaches comprehensively. The Casagrande approach yields slightly higher value than the Fall Cone approach for the upper range, but slightly lower values for the lower range (Koester, 1992; Sridharan and Prakash, 2000; Prakash and Sridharan, 2006). The Casagrande approach is popular in the United States; however, for low-plasticity silt, it is much more elaborate procedure than the Fall Cone approach, mainly because the silt cracks easily when the silt paste is cut using the grooving tool in the Casagrande cup. Thus, results based on the Casagrande approach are questionable and not easily reproduced for low-plasticity silt.

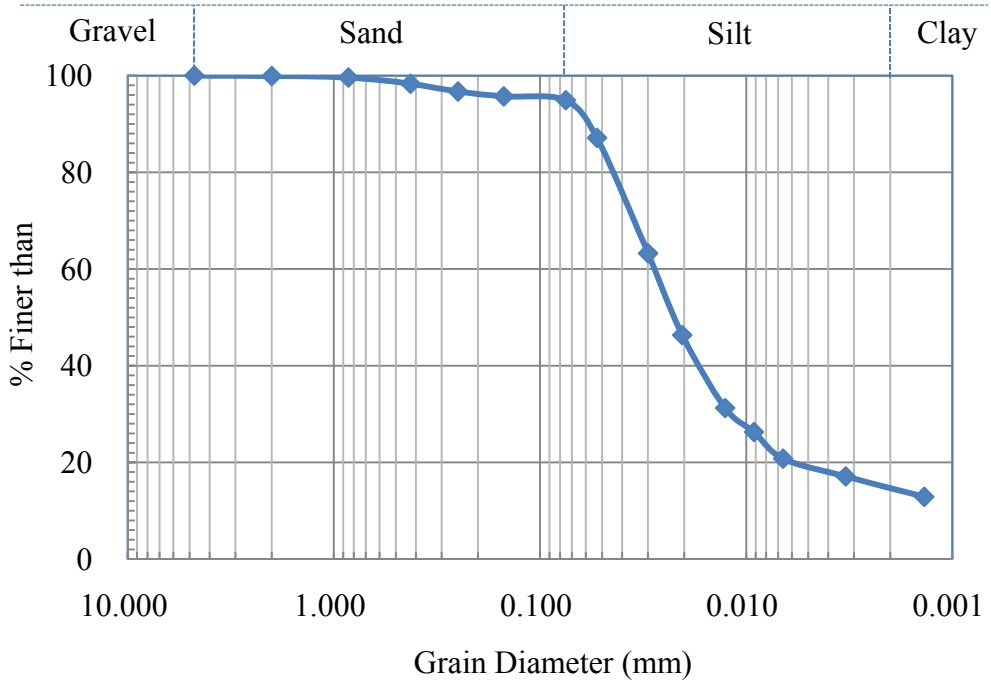

Figure 3.2. Grain size distribution of MRV silt

The Fall Cone approach was used to check the validity of the LL obtained from the Casagrande approach. The Casagrande approach yielded a LL of 28 and the Fall Cone method showed a value of 30. Figure 3.3 shows the data point for the subject silt material and the range plotted according to relationships summarized by Koester (1992). The point falls within the range identified by many researchers. The LL of 28 was used here to facilitate comparison with other silts, whose PIs have also been determined using the Casagrande approach.

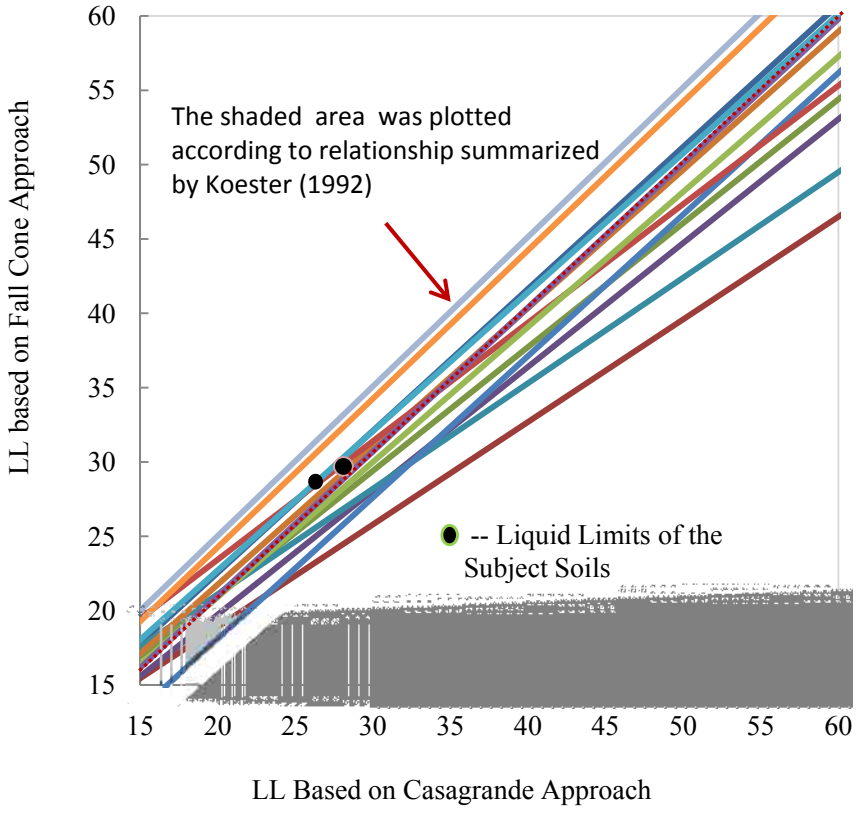

Figure 3.3. Relationship between liquid limits determined by Casagrande and Fall Cone approaches

The minimum and maximum void ratios were determined to compute relative density. The minimum void ratio (e_{min}) of sand is normally determined using the vibrating table method (ASTM D 4253-00). This method, however, is not as effective for increasing the density for silts. As recommended by Bradshaw and Baxter (2007), the minimum void ratio for silts can be measured using the modified compaction approach outlined in ASTM standard D 1557 based on Polito and Martin's demonstration (2001) that the modified compaction test gives results similar to those yielded by the vibrating table test for silty sand. Thus, the present work used the modified compaction method to determine the maximum dry unit weight ($\gamma_{dry,\ max}$) of the MRV silt and then computed its minimum void ratio. Figure 3.4 shows the modified Proctor compaction curve of the MRV silt. Its maximum dry unit weight is 18.5 kN/m^3 at an optimum water content (w_{optium}) of 10.6%. Its minimum void ratio was computed to be 0.44. The maximum void ratio (e_{max}) was obtained by allowing silt slurry to settle in a graduated cylinder, as suggested by Bradshaw and Baxter (2007), who stated that silts exhibit unreasonably high bulking when dry samples are used to determine the maximum void ratios based on ASTM standard D 4254. The maximum void ratio was determined to be 1.60.

3.1.2 Particle Morphology. This work investigated the shape and surface roughness of silt particles using a field emission gun scanning electron microscope (FEGSEM) with magnification ranging from 30X to 500,000X. The specimens were tilted up to 45˚. Two MRV silt samples were selected for particle morphology. From the silt sample #1, 0.25 g of the silt was mixed with 2 ml of distilled water. About 0.25 ml of the soil dilution was mixed with additional 2 ml of distilled water. This mixture was shaken, and approximately 0.25 ml of it was added to another 2 ml distilled water.

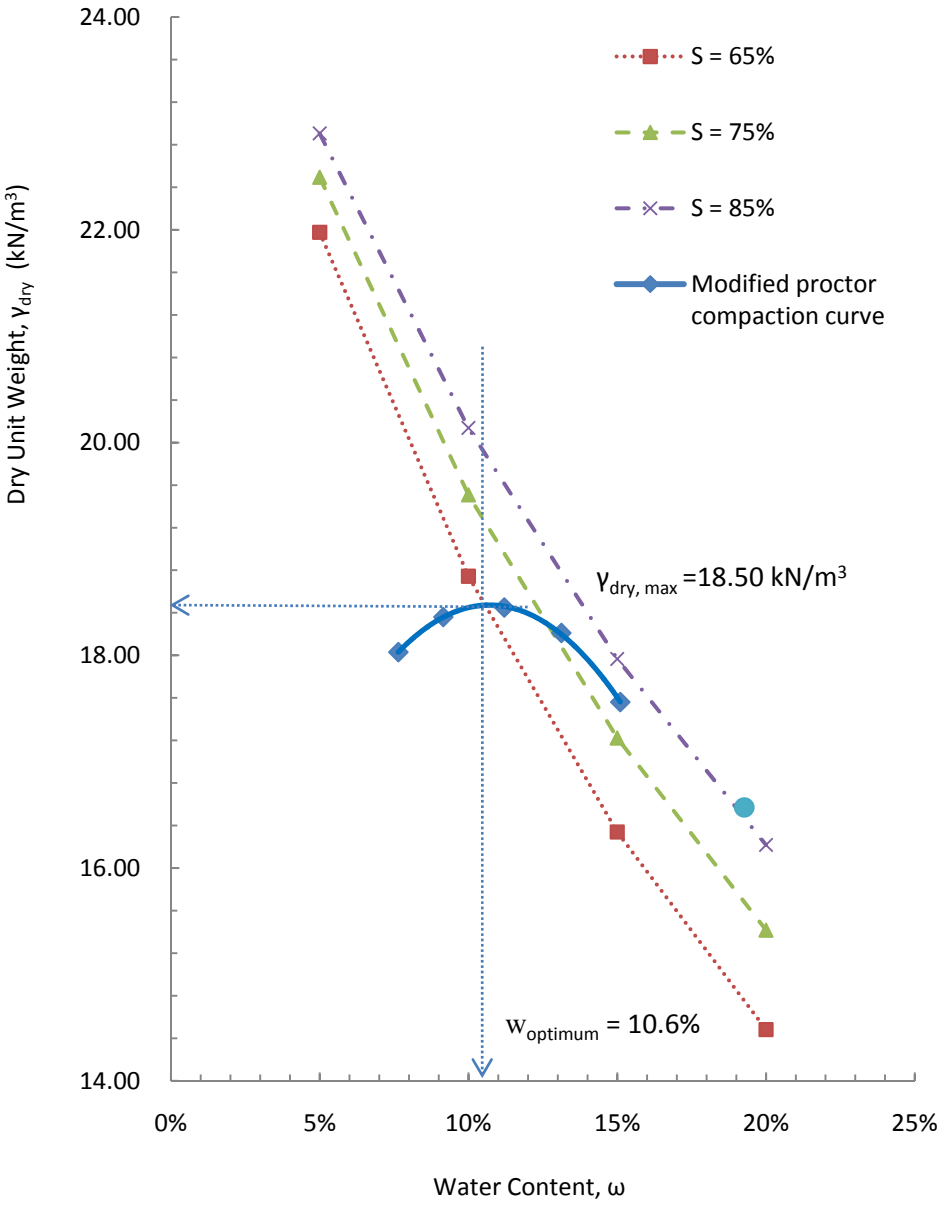

Figure 3.4. Modified Proctor compaction curve of MRV silt

A few drops of each suspension were placed on a smooth, clean aluminum stub, and the water was allowed to evaporate over a few hours. The stub was inserted in the FEGSEM specimen chamber and the silt particles dispersed under vacuum. Figure 3.5

shows brief steps to prepare the soil specimen. Sample #2 was chosen from a different location within the soil container with sample #1, but the same preparation procedures were applied.

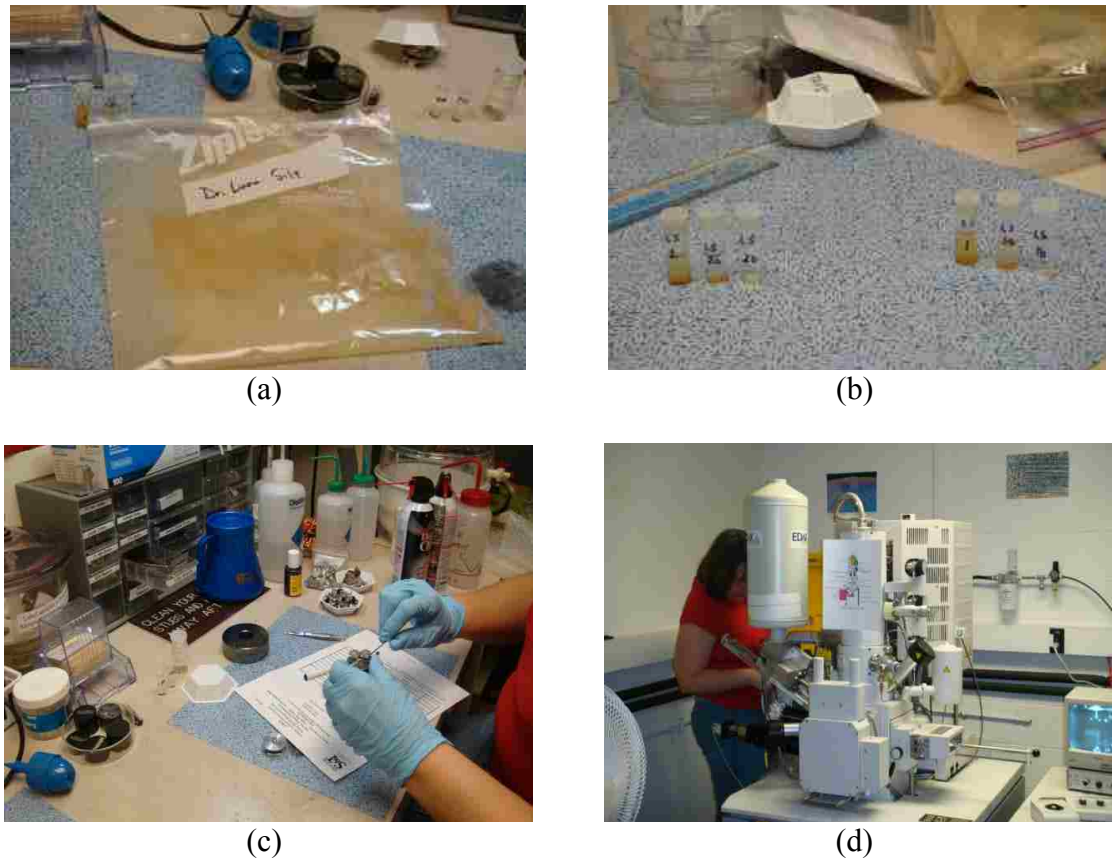

(a) (b)

(c) (d)

Figure 3.5. Preparation of MRV silt samples for particle morphology: (a) Silt sample, (b) Silt dissolved in distilled water, (c) Placement of silt suspension on a stub; (d) Insertion of stub to specimen chamber

Figure 3.6 shows a schematic illustration of the image acquisition. The soil particles in the specimen chamber were observed from the top and at a 45˚ angle from

four directions (east, south, west, and north). Table 3.2 lists the soil specimens for particle morphology. Six images captured the whole soil specimen, five of which were from sample #1 and one of which was from sample #2. To investigate particle shape and roughness, seven soil particles were observed, six from sample #1 and one from sample #2.

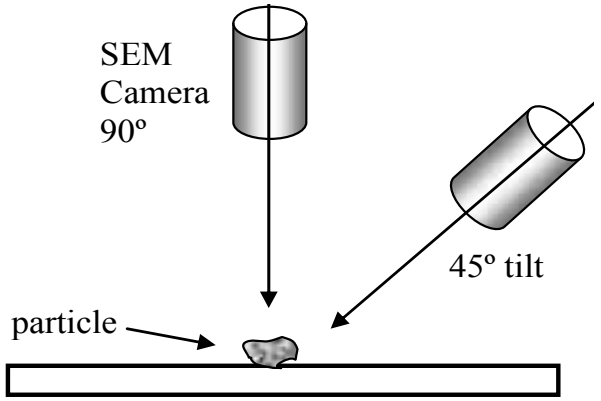

Figure 3.6. Image acquisition for MRV silt particle

Figure 3.7 shows two views of the soil specimen. The shape of the silt particles ranged from subangular to angular, and even very angular. Two particles were randomly selected and investigated from different directions. Figures 3.8 and 3.9 show the shape and surface roughness of those two particles observed from different directions. The surface of both particles was rough. These particle features contributed to the dilative behavior of the MRV silt during triaxial shearing tests, as explained in Section 5.

Table 3.2. List of MRV silt particles investigated using FEGSEM

Sample No.	View No.	Image Label	Magnification	View Direction
1	Overview 1	016-1bb	110x	Top
	Overview 2	016-1cc	350x	Top
	Overview 3	016-1e	130x	Top
	Overview 4	016-1f	250x	Top
	Overview 5	016-1g	1500x	Top
	Particle 1	016-1a	35000x	Top
	Particle 2	016-1c	35000x	Top
	Particle 3	016-1i	2500x	Top
	Particle 4	016-1m	2000x	Top
		016-1n	2000x	South, 45°tilt
		016-1o	2000x	East, 45°tilt
		016-1p	2000x	North, 45°tilt
		016-1q	2000x	West, 45°tilt
	Particle 5	016-1r	4500x	West, 45°tilt
		016-1s	4500x	North, 45°tilt
		016-1t	4500x	East, 45°tilt
		016-1u	4500x	South, 45°tilt
		016-1v	4500x	Top
	Particle 6	016-1w	2500x	Top
		016-1x	2500x	South, 45°tilt
		016-1y	2500x	East, 45°tilt
		016-1z	2500x	North, 45°tilt
		016-1aa	2500x	West, 45°tilt
2	Overview 6	016-2a	130x	Top
		016-2b	250x	Top
		016-2c	600x	Top
	Particle 7	016-2d	2500x	Side

(b) Overview 2

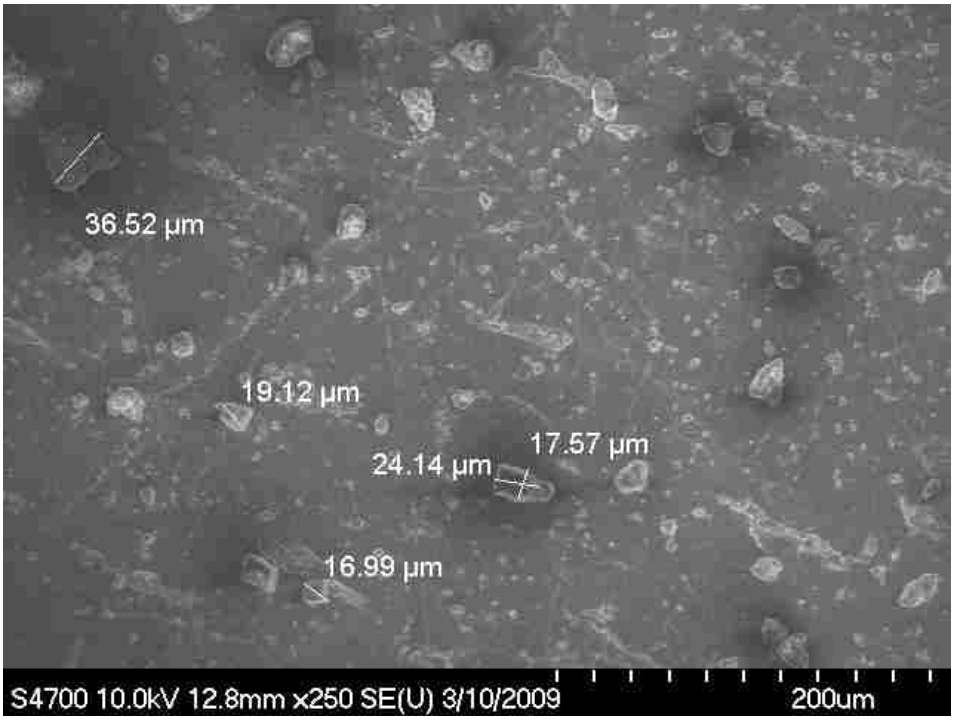

(a) Overview 4

Figure 3.7. Images of soil particles

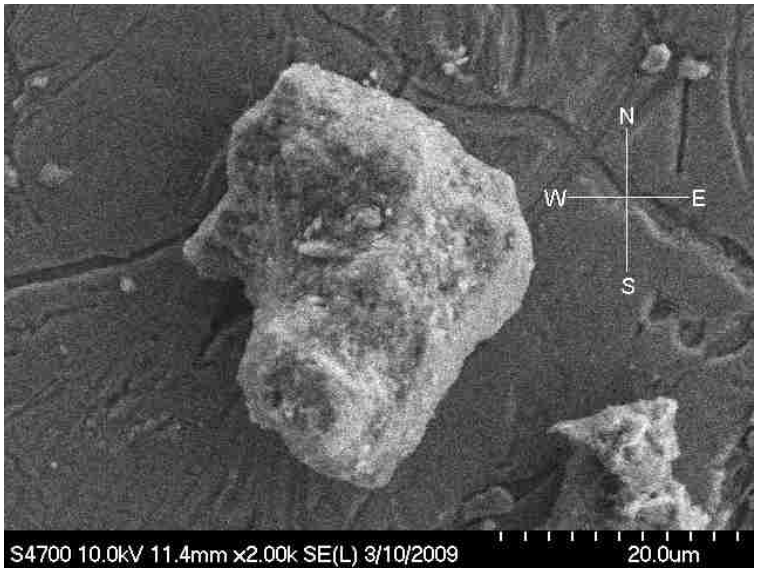

(a) Plan view

(b) North view at 45º angle

(c) East view at 45º angle

(c) South view at 45º angle

(d) West view at 45º angle

Figure 3.8. Images of particle #1 from different directions

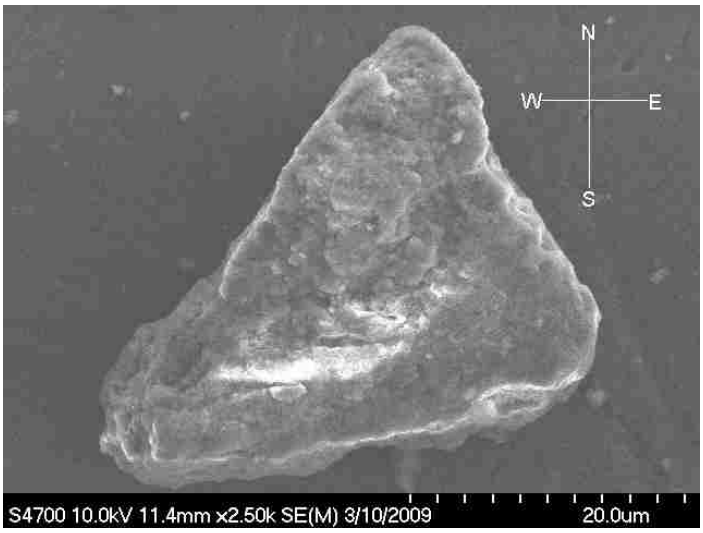

(a) Plan view

(b) North view at 45º angle

(c) East view at 45º angle

(d) South view at 45º angle

(e) West view at a tilt of 45º angle

Figure 3.9. Images of particle #3 from different directions

3.1.3 Liquefaction Potential. Several criteria have been used to evaluate the liquefaction potential of low-plasticity silt (Wang, 1979, 1981; Seed et al., 1983; Koester, 1992; Andrews and Martin, 2000; Seed et al., 2003; Bray et al., 2004; Bray and Sancio, 2006; Boulanger and Idriss, 2004, 2006). On the basis of Wang (1979 and 1981), Seed and Idriss (1983) proposed the following Chinese criteria: Clayey soils with less than 15% of particles finer than 5 μm, a LL less than 35, and a water content greater than 0.9 LL may be vulnerable to liquefaction as a result of shaking during an earthquake. These criteria were widely applied for two decades to estimate the susceptibility of low-plastic soil to liquefaction. Recently, however, researchers have found that at some sites, these Chinese criteria did not predict the liquefaction that occurred (Boulanger, 1998; Bray et al., 2004; Bray and Sancio, 2006). Table 3.3 shows a matrix developed by Andrews and Martin (2000) for liquefaction evaluation. If a soil has a LL less than 32 and fewer than 10% of its particles are less than 2 μm, it could liquefy during an earthquake. The MRV silt tested here had a LL of 29, and 14.5% of its particles were smaller than 2 μm, and it does liquefy. Therefore, further investigation was required to evaluate its susceptibility to liquefaction based on Andrews and Martin's criteria.

Bray et al. (2004) showed that soils with PI ≤ 12 and water content > 85% of the LL are susceptible to liquefaction, whereas soils with a PI between 12 and 20 and water content > 80% of the LL are "systematically more resistant to liquefaction but still susceptible to cyclic mobility." Based on this criterion, the MRV silt tested here was liquefiable. Seed et al. (2003) presented another guideline for evaluation of liquefaction potential; their method, which is based on observations of ground failure in fine-grained soils in the 1999 Kocaeli and Chi-Chi earthquakes, relies on the plasticity chart shown in

Figure 3.10. According to these criteria, the MRV silt should be susceptible to liquefaction during earthquakes.

Table 3.3. Liquefaction susceptibility criteria proposed by Andrews and Martin (2000)

	LL<32	**LL>=32**
Minus 2 µm fraction < 10%	Susceptible to liquefaction	Further studies required (consider plastic nonclay sized grains)
Minus 2 µm fraction > 10%	Further studies required (consider nonplastic clay sized grains)	Not susceptible to liquefaction

(LL determined by Casagrande-type percussion apparatus.)

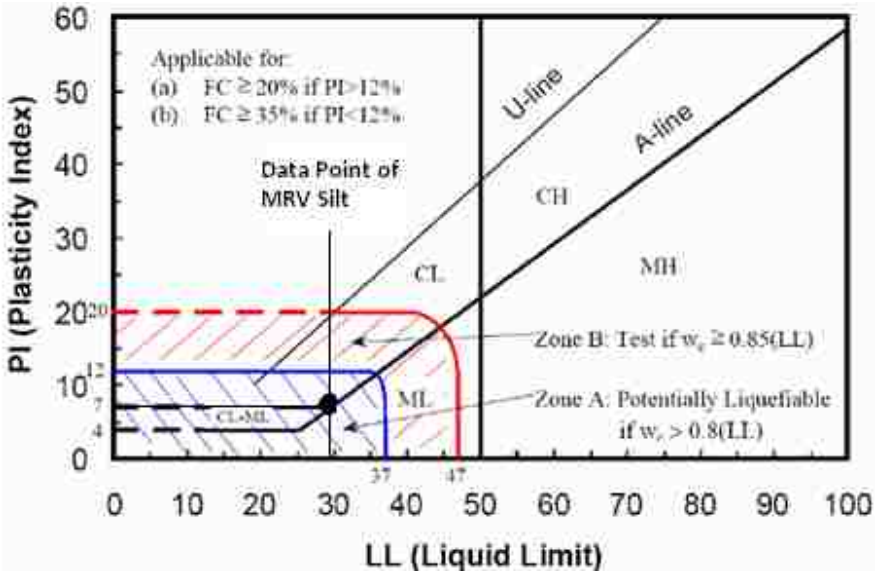

Figure 3.10. Recommendations of Seed et al. for assessment of liquefiable soil types (based on Seed et al. 2003)

In summary, the MRV silt tested here may be susceptible to liquefaction according to the criteria of Bray and Seed's groups, but further tests must be conducted to evaluate their liquefaction potential based on the criteria proposed by Andrews and Martin. Thus, there is still no consensus on the criteria for evaluation of the liquefaction potential of such soil.

3.2. TRIAXIAL TESTING EQUIPMENT

The triaxial testing program conducted for this research included static, cyclic, and postcyclic monotonic testing. It used the Humboldt triaxial system to conduct static and postcyclic monotonic testing and the GCTS (i.e., Geotechnical and Consulting Testing System) triaxial system to conduct cyclic triaxial testing. The axial load was applied as a displacement controlled platform on the Humboldt load frame (Figure 3.11) and pneumatically from the Belloframe actuator on the GCTS load frame (Figure 3.12).

The Humboldt triaxial testing system was operated manually via the pressure panel during saturation and consolidation. The GCTS STX-50 system was supposed to be more advanced, allowing each stage to be controlled by the computer program (CATS). However, the equipment used here was about eight years old and not easily operated by servo control. Therefore, the saturation and consolidation were controlled manually before cyclic loading. In particular, monotonic loading applied by the axial pneumatic actuator was not effective on the GCTS STX-50 system. The load was not maintained because it was increased during the axial compression triaxial test. The deviator stress applied fluctuated by plus or minus 10 kPa, which was considered unacceptable.

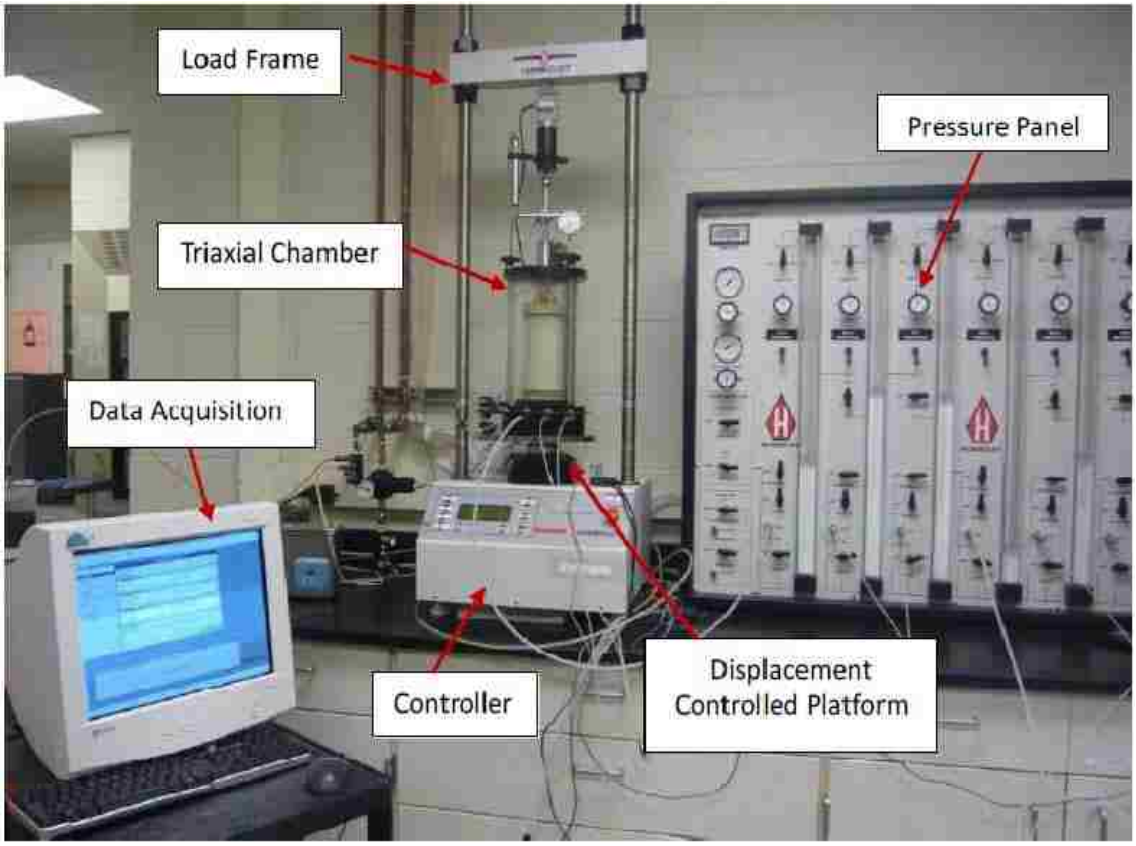

Figure 3.11. Humboldt triaxial testing system

After many trials to adjust the PIDs and repair the actual servo-valve, all static tests and postcyclic monotonic tests were conducted on the Humboldt load frame, which applies the load using a displacement-controlled platform. After cyclic loading was complete and full or limited liquefaction reached, the triaxial chamber with the liquefied specimen was slid onto the platen of the Humboldt loading frame. Further details of this procedure are presented Section 3.3.5 below. Table 3.4 shows the Humboldt and GCTS equipment specifications (Izadi, 2008). The air pressures, which can be regulated by triaxial pressure panels, are 0-1,400 kPa in the Humboldt system and 0-1,000 kPa in the

GCTS system. Nevertheless, the highest pressure achievable using an air compressor in the laboratory is about 1,200 kPa. The maximum pressure used in this research was about 1100 kPa in the Humboldt system and about 950 kPa in the GCTS system.

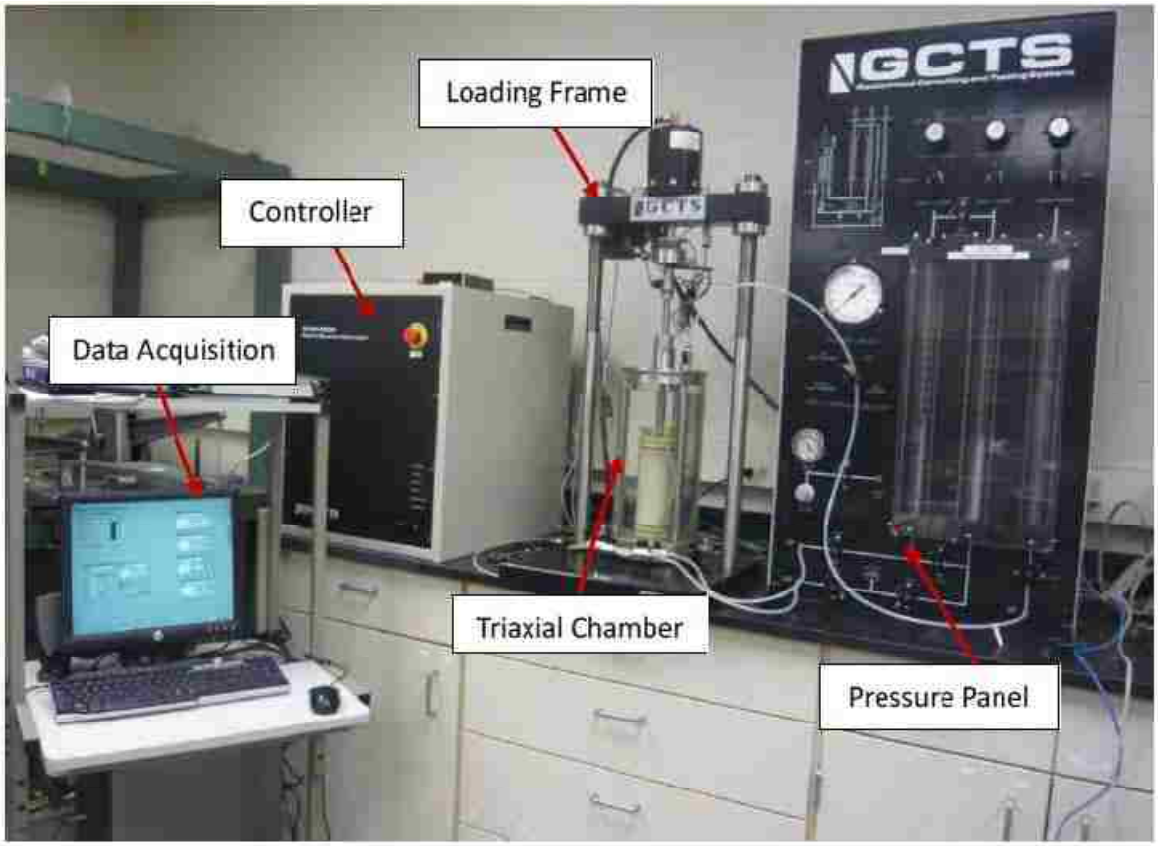

Figure 3.12. GCTS triaxial testing system

The tubing connection system in the GCTS chamber was modified as shown in Figure 3.13 so that the specimen could be more easily saturated. In order that the reading in the pore pressure transducer would more accurately represent the value throughout the

specimen, one of the ports on the top cap (location “D”) was connected to location “C” with tubing. After the specimen was partially saturated under vacuum, the vacuum was removed and the deaired water was drained from the bottom back pressure burette to the top back pressure burette under a back pressure difference with valves opened in locations “A”, “B”, and “C”, while maintaining an effective confining pressure less than the effective consolidation pressure planned for the test. With this process, the air bubbles in the tubing and top porous stone were easily removed to the top burette. The valve was then closed at location “A” to start saturation under back pressure. Although the back pressure was supplied only from the bottom burette, it reached the bottom and top ends of specimens simultaneously through the tubing connecting locations “C” and “D”. Additionally, the distance of back pressure transmission during saturation and of water drainage during consolidation was shortened, expediting both processes. Furthermore, the pore pressure in the transducer represents the average of the top and bottom pore pressures during shearing.

Table 3.4. Humboldt and GCTS triaxial equipment specifications

Item	**Sensor**	**Capacity**		**Resolution**	
		Humboldt	**GCTS**	**Humboldt**	**GCTS**
Axial Load	Load Cell	500 lbs	±500 lbs	1 lbs	±1 lbs
Axial Deformation	LVDT	2 inches	2 inches	0.005 inches	± 0.005 inches
Cell Pressure	Pressure Transducer	200 psi	±145 psi	0.1 psi	±0.1 psi
Pore Water Pressure	Pressure Transducer	200 psi	±145 psi	0.1 psi	±0.1 psi

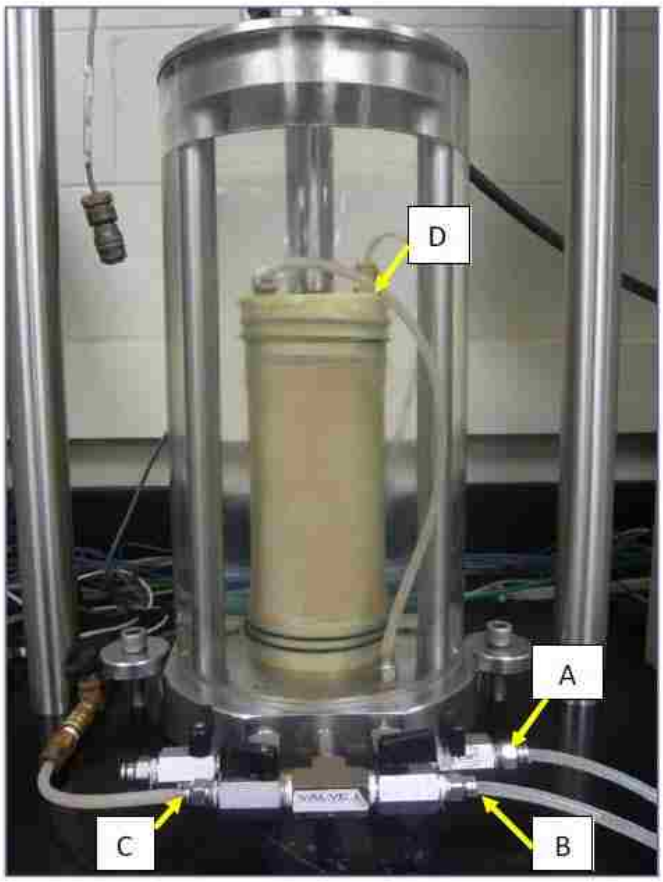

Figure 3.13. Modified tubing connection system in the GCTS equipment

3.3. TRIAXIAL TESTING PROCEDURES

Three types of triaxial testing were performed: static, cyclic, and postcyclic monotonic testing. The deviator stress was applied by means of axial compression in the triaxial chamber. All types of tests involved saturation and consolidation in early stages.

3.3.1 Saturation. It is crucial to achieve specimen saturation for liquefaction tests. Without a high degree of saturation, liquefaction is difficult to achieve (Nagao et al.

2010). Here, the necessary degree of saturation was achieved with vacuum, followed by back pressure.

After the reconstituted specimens (target dimensions: 71 by 142 mm) were seated on the triaxial base, a strong vacuum (less than effective consolidation pressure) was applied for eight hours to remove the entrapped air bubbles and saturate the specimen. When bentonite was added to the silt, more than eight hours were required. During this time, the specimen was held with a split mold to prevent disturbance. After the vacuum period, the specimen was measured. Its height was measured with a caliper, as shown in Figure 3.14. After the split mold was removed, the diameter was measured with a π-tape. The triaxial chamber was then secured on the base with enough grease around the O-rings to prevent water and pressure leakage.

Cell pressure and back pressure were added incrementally to continue saturating the specimen (ASTM standard D 5311-92). The increments of pressure and the duration of each pressure were significant. The difference between cell pressure and back pressure must always be smaller than the effective consolidation pressure; and enough time must be allowed for the air bubbles to dissolve into the water. To determine the pressure increments and their duration, the transmission 25 kPa back pressure from the bottom end to the top end of one specimen was timed by supplying back pressure at the bottom end of the specimen and monitoring it at the top end of the specimen. Because the back pressure is applied to the specimen simultaneously from the bottom and top ends during saturation, a quarter of the previously determined transmission time is required to transmit back pressure from ends to the specimen center, following the recommendation by Izadi (2008). It was found that about 105 min were required for the transmission of

pressure from the bottom to the top of the natural MRV silt specimen. Thus, the duration of about 26 min (= 105/4 min) was required when supplying back pressure simultaneously at the bottom and top ends of the specimen. In addition to transmission time, additional time was allowed for the dissolution of air into the water under back pressure. At least 45 min were required for each cell and back pressure increment of 25 kPa. When bentonite was added to the silt, more time was required for each pressure increment.

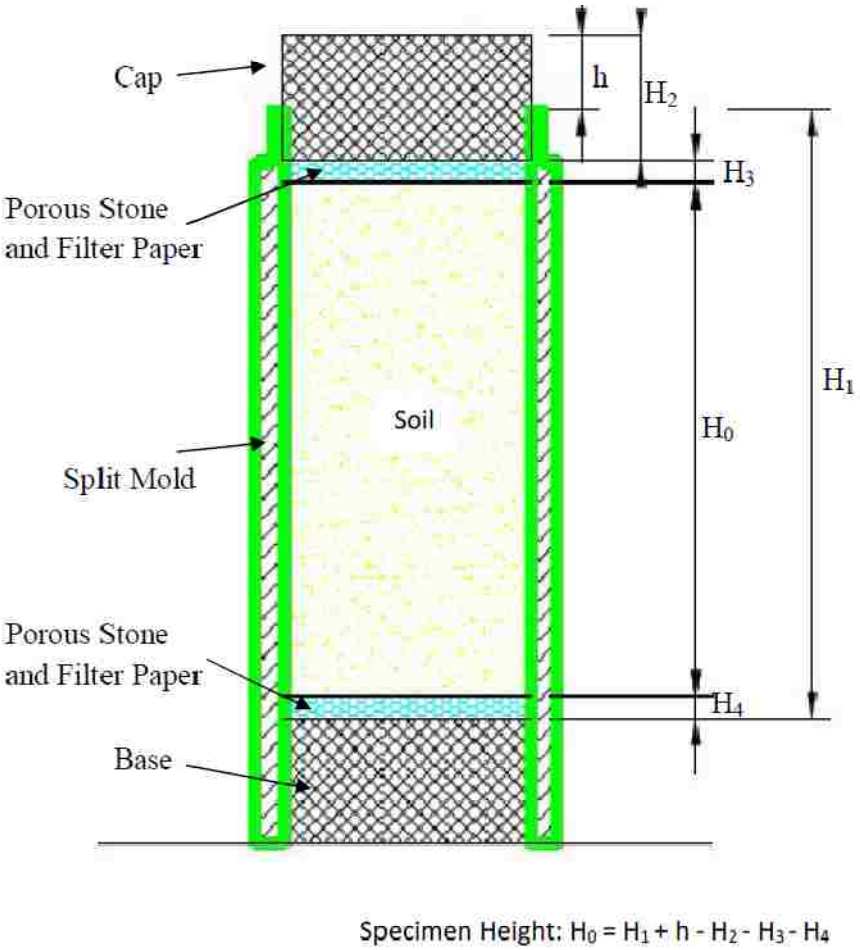

Figure 3.14. Measurement of soil specimen height

The cell and back pressures were increased incrementally until the Skempton B-value remained constant. For tests conducted on the Humboldt system, the B-value obtained for most tests was greater than 0.98. For tests conducted on the GCTS system, the B-value of about 0.94 was achieved. This smaller B-value was probably due to differences in system configuration (tubing, valves, etc). Because negative excess pore pressure appeared especially for highly overconsolidated silt specimens, additional pressure (at least 100 kPa) was supplied to ensure that the specimen remained saturated and thus prevent cavitation during shearing.

After saturation, the change in the height of the specimen was measured, and the change in its volume was calculated based on ASTM standard D 5311-92:

$$\Delta V_{sat} = 3V_0 \left[\Delta H_s / H_0 \right] \tag{5}$$

Where:

V_0 – initial volume of the specimen,

ΔH_s – change in height of the specimen during saturation, and

H_0 – initial height of the soil specimen.

3.3.2 Consolidation. Isotropic consolidation was achieved by applying isotropic cell pressure around the specimen. The change in specimen volume was monitored to determine the time of primary consolidation according to the change in water level in the bottom burette on the pressure panel. Figure 3.15 shows the volume change curve for one of natural MRV silt specimens; it indicates that only 14 minutes were required to reach 100% primary consolidation. For silt with added bentonite, the consolidation time was longer and will be discussed in Section 8. If the specimens were overconsolidated, the

cell pressure was increased by the value of OCR multiplied by effective consolidation pressure. The cell pressure was then reduced again, and time was allowed for swelling (ASTM D 4767-04). The change in the height and volume of the specimens was measured during consolidation; the final volume and height were then updated for use in triaxial shear testing stages.

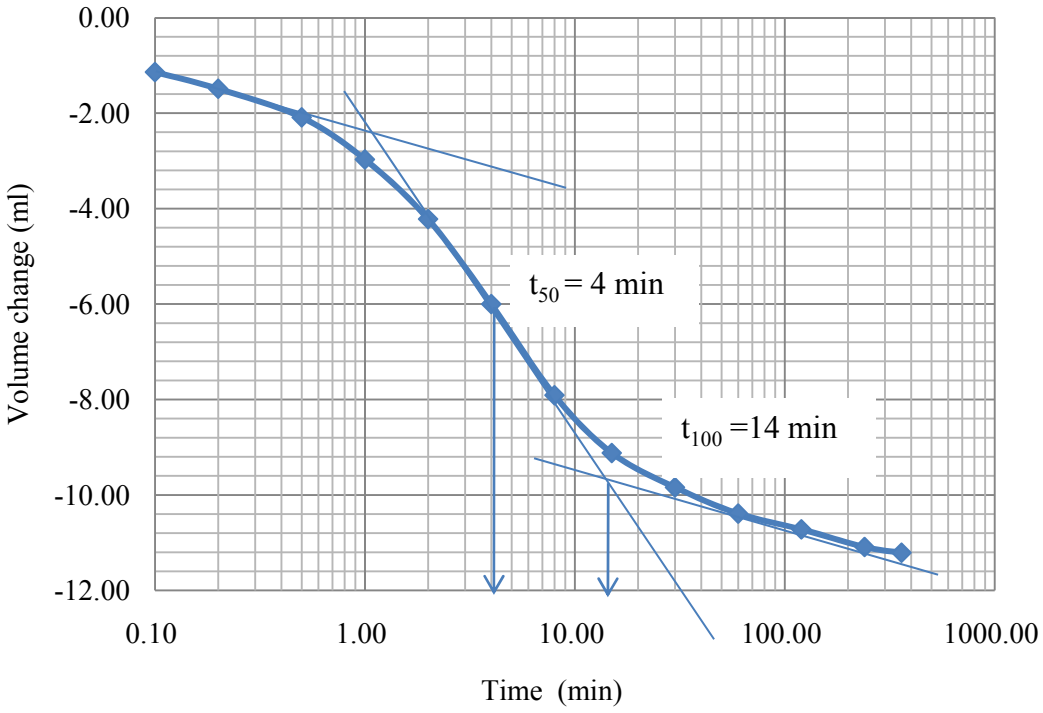

Figure 3.15. Consolidation time of MRV silt specimen (t_{50} – time of 50% primary consolidation; t_{100} – time of 100% primary consolidation)

3.3.3 Static Triaxial Testing. Undrained triaxial shear testing was conducted to study the monotonic shear behavior of the MRV silt. The tests were conducted on the Humboldt system with drainage valves closed, and pore pressure measurements were taken. The deformation rate was calculated based on ASTM D4767 – 04:

$$d' = H \times \varepsilon' = H \times 4\% / (10 t_{50}) \tag{6}$$

where:

d′ – deformation rate,

ε′– strain rate (summarized for all tests in section 3.4),

H – updated height of the specimen after consolidation, and

t_{50} – time of 50% primary consolidation.

Based on the time required to reach 50% primary consolidation, the strain rates for all static triaxial tests were 0.08 - 0.13%/min. Most tests were normally stopped at a large axial strain (> 30%). The deviator stress (Δσ) was calculated by dividing the axial load (N) by the corrected cross area, which was computed as

$$A_{corrected} = A_0 / (1 - \varepsilon_1) \tag{7}$$

where $A_{corrected}$ is the corrected cross area, A_0 is initial cross area, and ε_1 is axial strain.

3.3.4 Cyclic Triaxial Testing. Undrained cyclic triaxial testing was performed to study the liquefaction resistance of the MRV silt. It also induced excess pore pressure (u_e) and axial strain (ε_1), facilitating investigation of the postcyclic behavior. The tests were conducted on the GCTS system with the deviator stress controlled. The cyclic stress was set by following the sine function. Here, the cyclic stress ratios (CSR) of 0.10, 0.18, 0.25,

and 0.35 were selected. The maximum and minimum deviator stresses during the cyclic loading were computed according to ASTM standard D 5311 – 92:

$$\Delta\sigma_{cyc} = \pm 2 \times \sigma_c' \times CSR \tag{8}$$

where $\Delta\sigma_{cyc}$ is the peak cyclic deviator stress.

Cyclic loading was continued until the excess pore pressure ratio (R_u) reached 1.0 for full liquefaction, and 0.85, 0.70, and 0.35 for limited liquefaction of the natural MRV silt. For the silt with added bentonite, the cyclic test indicated that the specimen had no initial liquefaction (R_u lower than 1.0). Therefore, the cyclic loading was not stopped until a specific axial strain (discussed in Section 8). The frequency of cyclic loading is crucial for measurement of excess pore pressure. The predominant frequency of earthquake loading tends to be around 1~5 Hz (Kramer, 1996, Izadi, 2008). If this frequency was applied to supply cyclic loading for the low-plasticity MRV silt, not enough time would remain for transmission of excess pore pressure from the inside of the specimens to the pore pressure transducer. Typically, a lower frequency is used, and this work used a frequency of 0.1 Hz. Comparison of the results to those achieved with loading frequency of 1 Hz indicates that cyclic stress ratios should be adjusted accordingly (Lefebvre and LeBoeuf, 1987; Boulanger et al., 1998). Cyclic strength increases about 9% per log cycle of the loading rate (Boulanger and Idriss, 2007).

3.3.5 Postcyclic Monotonic Triaxial Testing. Postcyclic monotonic triaxial tests were conducted with full and limited liquefaction. Once cyclic loading was completed, the deviator stress was slowly set back to zero to return to an isotropic confining pressure for reconsolidation. The following remainder of the procedure depended on the type of postcyclic monotonic testing to be conducted.

Study of postliquefaction behavior at various levels of reconsolidation began with determination of the reconsolidation curve, so that the time required for various levels of reconsolidation can be obtained. Section 6 reports the reconsolidation curve of specimens with full liquefaction. Table 3.5 shows the time required to achieve various reconsolidation levels. By controlling the reconsolidation time, various levels of reconsolidation could be obtained after liquefaction. For example, it took 5.0 min to achieve 60% reconsolidation for postcyclic monotonic shearing. After the various levels of reconsolidation were reached, postcyclic monotonic triaxial compression was applied.

Table 3.5. Time required for various levels of reconsolidation

Reconsolidation Level	**Volume Change (ml)**	**Reconsolidation Time (min)**
0%	0	0
30%	9.7	2.4
50%	12.8	3.9
60%	14.3	5.0
100%	20.5	13.0

During the study of postcyclic behavior under various levels of limited liquefaction, the specimens were sheared after each of two cases: full and no

reconsolidation. First, with full reconsolidation, the drainage valve was opened, the excess pore pressure was allowed to dissipate completely, the drainage valves was closed again. Second, with no reconsolidation, the drainage valve remained to be closed, and 30 minutes were allowed for pore water pressure in the specimen to reach equilibrium. The MRV silt-bentonite mixtures required more time.

If reconsolidation was required, the specimen dimensions were updated for postcyclic monotonic triaxial compression. As noted above, postcyclic monotonic testing was conducted on the Humboldt loading frame. After the loading rod was locked, the triaxial chamber was moved by sliding carefully to the Humboldt loading frame, which was placed by the GCTS loading frame, to reduce disturbance as much as possible, (Figure 3.16). This move was accomplished by placing the two load frames on the same level and then carefully sliding the triaxial chamber and leaving all the tubing connected to the same triaxial pressure panel (see Figure 3.16). The pore water pressure just changed slightly (about 1 kPa) with the drain valves closed during the sliding process. Thus, the specimen was not disturbed significantly during sliding.

Ten minutes were allowed for pore water pressure to reach equilibrium after sliding the triaxial chamber to the Humboldt platen. Postcyclic triaxial compression testing was then conducted by controlled deformation. The deformation rate was computed according to Equation 3.2 using the 50% reconsolidation time, which was almost constant among all tests with the same testing conditions. For more details, see Section 6. The strain ratio was determined to be 0.10% for all postcyclic monotonic tests of the natural MRV silt.

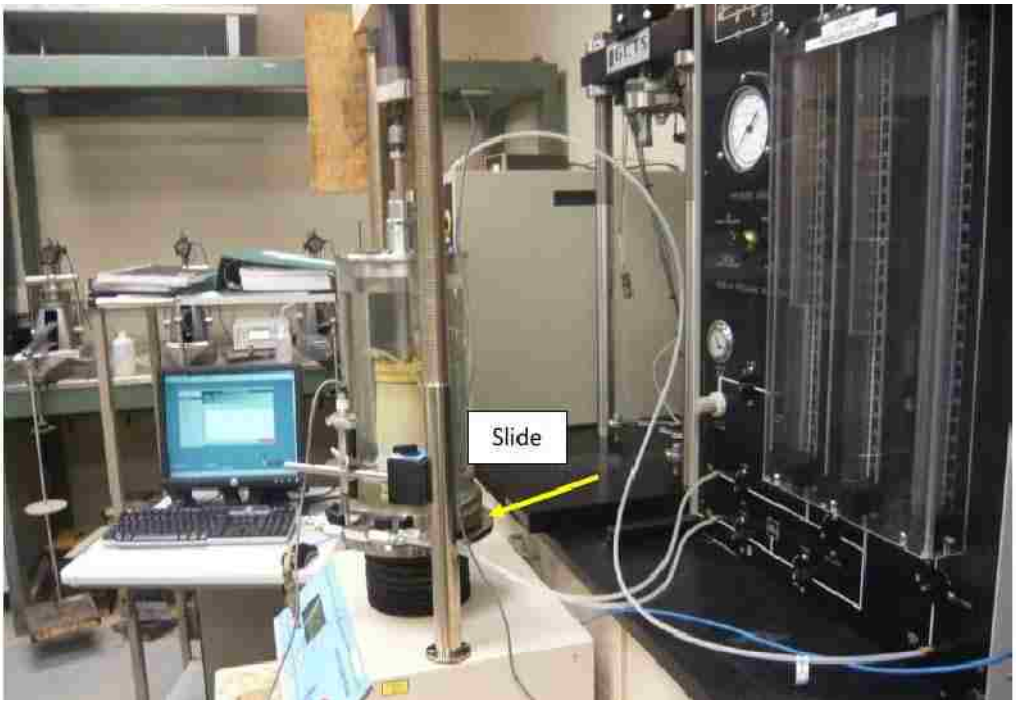

Figure 3.16. Sliding of triaxial chamber from the GCTS to the Humboldt load frame

3.4. SUMMARY

This experimental program included saturation, consolidation, static triaxial testing, cyclic triaixal testing, and postcyclic monotonic triaxial testing, in addition to multiple tests to determine the soil index properties. Saturation was achieved by supplying vacuum and then high back pressure. Consolidation was achieved using isotropic three-dimensional consolidation pressure. Static and postcyclic monotonic triaxial testing was conducted on the Humboldt system, and cyclic triaxial testing on the GCTS system. The Skempton B-values were greater than 0.98 and 0.94 for almost tests on the Humboldt and GCTS system, respectively.

Table 3.6 lists all triaxial tests for this experimental program. There were 47 triaxial tests in total. The static triaxial tests for the MRV silt and its mixture with bentonite were conducted to obtain monotonic behavior as a reference for the postcyclic monotonic behavior. They were conducted under both normal consolidation and overconsolidation and with different effective consolidation pressure, but all cyclic and postcyclic tests under normal consolidation and with only effective consolidation pressure of about 90 kPa. As shown in Table 3.6, the tests marked with ID including a letter "R" were conducted to repeat the corresponding test to verify the repeatability of triaxial tests with identical conditions. For example, the test MS1R was conducted with the same testing conditions with the test MS1. For postcyclic monotonic tests with full liquefaction, various reconsolidation levels (100%, 60%, 30%, and 0%) were allowed after cyclic loading to study the effect of reconsolidation level on postcyclic shear behavior. With limited liquefaction, two kinds of postcyclic monotonic tests with various levels of limited liquefaction were operated to investigate the variation in postcyclic monotonic behavior with liquefaction level, respectively, at full and no reconsolidation. With bentonite added, postcyclic monotonic tests were conducted to investigate the effect of plasticity on postcyclic monotonic behavior with a comparison to monotonic behavior.

Table 3.6. Summary of all triaxial tests

Task	Test ID	Added Bentonite Content (%)	Saturation	Consolidation				Cyclic Loading				Reconsolidation			Shearing
			B-Value	σ'_c	OCR	t_{50}	e	CSR	N_{cyc}	R_u	ε_{cyc}	U_r	t_{50}	e'	ε'
				kPa		min					%	%	min		%/min
Static Triaxial Tests on MRV Silt	MS1	--	0.99	50.0	1	8.5	0.700	--	--	--	--	--	--	--	0.05
	MS1R	--	0.98	50.0		NA	0.730	--	--	--	--	--	--	--	0.05
	MS2	--	0.98	90.0		5.5	0.679	--	--	--	--	--	--	--	0.05
	MS3	--	0.98	129.0		NA	0.652	--	--	--	--	--	--	--	0.05
	MS4	--	0.99	51.2	2	4	0.665	--	--	--	--	--	--	--	0.11
	MS5	--	0.99	90.0		3.2	0.653	--	--	--	--	--	--	--	0.10
	MS6	--	1.00	50.0	4	3.2	0.647	--	--	--	--	--	--	--	0.13
	MS7	--	0.99	91.2		NA	0.612	--	--	--	--	--	--	--	0.10
	MS8	--	0.98	50.0	8	6.5	0.648	--	--	--	--	--	--	--	0.06
	MS9	--	1.00	90.0		NA	0.591	--	--	--	--	--	--	--	0.10
Cyclic Triaxial Tests on MRV Silt	MD1	--	0.95	91.1	1	9.6	0.669	0.10	66.2	1.00	0.4	--	--	--	--
	MD2	--	0.94	91.2		30	0.661	0.18	35.2	1.00	10.5	--	--	--	--
	MD2R	--	0.95	90.8		10	0.686	0.18	33.2	1.00	11.2	100	3.8	0.624	--
	MD3	--	0.94	90.0		22	0.680	0.25	3.2	1.00	11.8	--	--	--	--
	MD4	--	0.94	90.0		6	0.676	0.35	1.2	1.00	11.1	100	3.8	0.618	0.11
	MD4R	--	0.94	89.7		8.5	0.682	0.35	1.2	1.00	11.4	100	3.5	0.624	--
Postcyclic Tests on MRV Silt with	MF1	--	0.95	90.6	1	--	0.665	<0.18	66.2	1.00	11.7	100	4.0	0.598	0.11
	MF1R1	--	0.94	90.4		10	0.660	0.18	27.1	1.00	9.8	100	4.0	0.593	0.11
	MF1R2	--	0.94	89.9		6.5	0.669	0.18	31.1	1.00	8.9	100	4.1	0.602	0.11
	MF2	--	0.95	90.7		7	0.657	0.18	27.2	1.00	11.3	60	NA	0.615	0.11

Table 3.6. Summary of all triaxial tests (cont.)

Task	Spec. ID	Added Bentonite Content (%)	Saturation	Consolidation				Cyclic Loading				Reconsolidation			Shearing
			B Value	σ'_c kPa	OCR	t_{50} min	e	CSR	N_{cyc}	R_u	ε_{cyc} %	U_r %	t_{50} min	e'	ε' %/min
Full Liquefaction	MF3	--	0.95	90.5	1	8	0.663	0.18	24.1	1.00	14.5	30	NA	0.637	0.11
	MF4	--	0.95	90.3		8.5	0.659	0.18	18.1	1.00	11.5	0	NA	0.659	0.11
	MF5*	--	0.94	90.2	1	NA	0.655	0.18	45.2	1.00	8.9	100	8.9	0.566	0.11
Postcyclic Tests on MRV Silt with Limited Liquefaction	ML1	--	0.95	90.5	1	NA	0.653	0.18	26.2	0.85	1.23	100	--	0.621	0.11
	ML2	--	0.93	91.1		9.5	0.674	0.18	22.2	0.70	0.21	100	--	0.666	0.11
	ML3	--	0.94	90.7		NA	0.662	0.18	6.2	0.30	0.18	100	--	0.660	0.11
	ML4	--	0.94	90.5		NA	0.643	0.18	25.2	0.85	0.95	0	--	--	0.11
	ML5	--	0.94	91.1		NA	0.645	0.18	18.1	0.70	0.23	0	--	--	0.11
	ML6	--	0.94	90.7		NA	0.667	0.18	4.0	0.35	0.09	0	--	--	0.11
Static Triaxial Tests on MRV Silt with Bentonite Added	MSB1	1.25	0.99	90.0	1	18	0.653	--	--	--	--	--	--	--	0.02
	MSB2	2.50	1.00	50.0	1	85	0.721	--	--	--	--	--	--	--	0.01
	MSB3	2.50	0.98	90.0	1	NA	0.649	--	--	--	--	--	--	--	0.01
	MSB4	2.50	0.98	243.0	1	50	0.609	--	--	--	--	--	--	--	0.01
	MSB5*	2.50	1.00	90.0	8	44	0.559	--	--	--	--	--	--	--	0.01
	MSB6	5.00	1.00	50.0	1	160	0.745	--	--	--	--	--	--	--	0.01
	MSB7	5.00	0.99	90.0	1	360	0.628	--	--	--	--	--	--	--	0.01
	MSB8*	5.00	0.97	90.0	8	380	0.506	--	--	--	--	--	--	--	0.01
	MSB9	7.50	0.95	49.4	1	700	0.783	--	--	--	--	--	--	--	0.01

Table 3.6. Summary of all triaxial tests (cont.)

Task	Spec. ID	Added Bent. Cont. (%)	Satur-ation	Consolidation				Cyclic Loading				Reconsolidation			Shear-ing
			B-Value	σ'_c kPa	OCR	t_{50} min	e	CSR	N_{cyc}	R_u	ε_{cyc} %	U_r %	t_{50} min	e'	ε' (%/min)
Postcyclic Tests on MRV Silt with Bentonite Added	MFB1	1.25	0.95	90.5	1	40	0.675	0.25	5.5	0.89	20.5	NA	NA	NA	NA
	MFB2	2.50	0.95	91.3	1	93	0.660	0.25	7.2	0.86	16.1	100	65	0.571	0.009
	MFB3	2.50	0.94	91.9	1	NA	0.667	0.18	126	0.89	16.9	0	NA	NA	0.009
	MFB4	2.50	0.93	91.2	1	100	0.648	0.18	160	0.92	9.0	100	40	0.591	0.009
	MFB5	2.50	0.95	90.4	1	NA	0.675	0.18	89.2	0.86	9.0	0	NA	NA	0.009
	MFB6*	2.50	0.93	90.6	1	40	0.660	0.35	1.1	0.78	9.0	100	28	0.569	NA
	MFB7	5.00	0.95	91.2	1	190	0.690	0.18	407	0.82	9.0	100	110	0.646	0.004
	MFB8	5.00	0.95	91.3	1	NA	0.688	0.25	12.1	0.64	9.4	0	NA	NA	0.004
	MFB9*	5.00	0.94	91.3	1	180	0.685	0.35	1.2	0.55	9.0	100	140	0.574	NA

Note: 1. The specimens marked with an "*" were also used to determine consolidation parameters.

2. N_{cyc} is the number of loading cycle during cyclic loading;
e is the void ratio of the specimen after consolidation;
e′ is the void ratio of the specimen after reconsolidation;
NA - not available
Other symbols have the same meanings elsewhere in the dissertation.

4. SPECIMEN PREPARATION

Ideally, laboratory testing of natural soil deposits should use undisturbed soil samples; however, low-plasticity soils are difficult to recover and they are easily disturbed in the process. Undisturbed specimens can be recovered using freezing, but this method is expensive and of limited availability. Another method is to inject a gel or similar material to solidify so that it can then be cored. The gel is then removed in the laboratory under controlled conditions. This process, however, is also difficult to do with low permeability soils, and it can also disturb the soil. Consequently, the most common technique is to reconstitute low-plasticity soil specimens in the laboratory. The key objective of specimen reconstitution is to obtain properties identical or at least very close to those of in situ soils. As noted by Kuerbis and Vaid (1988), a technique to prepare reconstituted sand sample for laboratory testing must meet five criteria: the ability of preparing the desired density, the uniformity in void ratio, full saturation, no particle size segregation, and simulation of natural soil deposition. These criteria also apply to the preparation of silt specimens. Here, full saturation was achieved using vacuum and back pressure, as described in Section 3.3.1

The most common methods to reconstitute soil specimens include moist tamping, water pluviation, air pluviation, and slurry consolidation. Based on the literature review presented in Section 2, this research relied on the slurry consolidation method to reconstitute specimens for triaxial tests.

4.1. SPECIMEN RECONSTITUTION

4.1.1 Reconstitution Procedures. The silt specimens were reconstituted using slurry consolidation in a 71.1 mm diameter split vacuum mold. The target dimensions of the specimen were 71.1 by 142.2 mm to accommodate static and dynamic triaxial testing. The silt slurry was consolidated under incremental dead weights and vacuum. The procedure to prepare specimens is presented as follows (Figure 4.1):

1. Preparation of silt slurry

Originally silt was dry and in clumps breaking and grinding, then sieved. The portion of the silt that passed through a No. 40 sieve (0.425 mm) was selected for the slurry. One kilogram of dry silt was mixed with deaired water, resulting in a water content of 44%. The slurry was then covered with plastic wrap to prevent water from evaporating and left to soak overnight (for about 10 hours) to complete absorption of the water. Finally, the slurry was mixed thoroughly for 15 min using an industrial Hobart electric mixer with a flat paddle (and taking care to avoid air entrapment during mixing).

2. Pouring of slurry into split vacuum mold

After the silt slurry was mixed, it was poured into a split vacuum mold. Because the volume of slurry was larger than the split vacuum mold, an extension tube with internal graduated marks was place on the top of split mold (Figure 4.1a). The slurry was poured through a funnel to the desired height. The excess slurry was collected in a bowl so that the mass of the soil specimen could be determined.

3. Consolidation of the silt slurry in the split mold

The slurry was left to settle under its own weight for three hours to prevent slurry from squeezing out under the dead weights. A plastic cap was placed on the slurry for

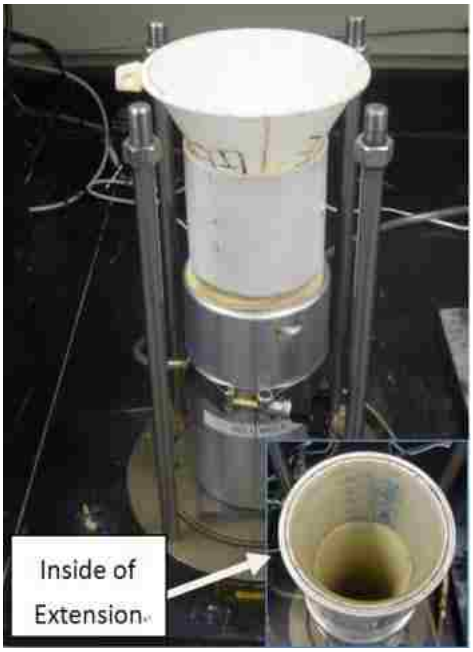

(a)

(b)

(c)

Figure 4.1. Experimental setup used to reconstitute silt specimens: (a) slurry holder, (b) slurry consolidated under dead weight, (c) Specimen consolidated under the vacuum

two hours, and a loading rod was placed overnight. The loading times were determined based on several trials in order to avoid squeezing slurry out of mold during incremental weight placement. As shown in Figure 4.1b, dead weights were then added, and primary consolidation was achieved under each load increment before the next weight was added. Consolidation progress was monitored using a digital gauge on the loading rod to monitor specimen deformation. The vertical stress (less than 32.3 kPa) imposed by all the weights was less than the desired minimum effective consolidation pressure of 50 kPa.

4. Use of vacuum to improve consolidation pressure

Due to the friction that develops between the membrane and the consolidating soil in the mold, the effective vertical consolidation pressure tends to decrease from the top (loading) to the bottom of the specimen (base), resulting in a non-uniform void ratio. To improve the uniformity of the specimen, identical vacuum pressures (45 kPa) were applied simultaneously at the top and bottom of the specimen. The vacuum was applied using a unique differential vacuum control apparatus (R. W. Stephenson, personal communication). Thus, the specimen consolidated under the same top and bottom pressures. Before placing the vacuum, the weights were removed and the top porous stone and filter paper were replaced with clean ones. The consolidation process under the vacuum was also monitored using the digital gauge (Figure 4.1c). The specimen was then ready for saturation and consolidation with the triaxial pressure panel.

The soil adhering to the porous stone and filter paper was cleaned. After the soil particles settled out of suspension, the surface water was removed, and the excess soil was dried and weighed to obtain the total weight of the silt solids in the specimen. Each

incremental pressure took about eight hours to consolidate. Preparation of one specimen under all loads took a total of about two days.

4.1.2 Specimen Uniformity. The uniformity of the silt specimens was verified by measuring the variation in water content and particle size distribution throughout the specimen. Assuming that the degree of saturation was identical throughout the specimen, water content is a measure of void ratio. The grain size distribution indicated whether particles had been segregated by size.

The silt specimens were cut into seven slices, and the water content of each slice was measured. Figure 4.2 shows the variation in water content versus height of the specimen. As expected, the water content was lower towards the top and bottom ends of the specimen where the vacuum was applied and the pressure gradients were the highest. The maximum difference in water content ($\Delta\omega$) throughout the specimen was just 1.20%.

To verify that the specimen preparation was not dependent on the fines content, two other silt specimens were prepared with addition of 2.5% and 5% bentonite. With the added bentonite, the variation in water content was even smaller, as seen in Figure 4.2. These results make it reasonable to conclude that the void ratio was essentially uniform throughout the specimen.

Once the water content was determined, 50 g were cut from each silt slice and placed in a 250-mL beaker mixed with 125 ml of sodium hexametaphosphate solution (40 g/L) for hydrometer analysis (ASTM D 422-63). The dry silt slices were easily disaggregated into the solution. Figure 4.3 shows the particle size distributions, which were very consistent. The deposition of silt slurry is different from that of sand. For sand, the larger particles settle easily and quickly so that segregation is common. However, for

a silt slurry, the water content is only about 1.6 times the liquid limit. Voids among the silt particles are insufficient to allow the larger particles to pass and settle down to induce segregation.

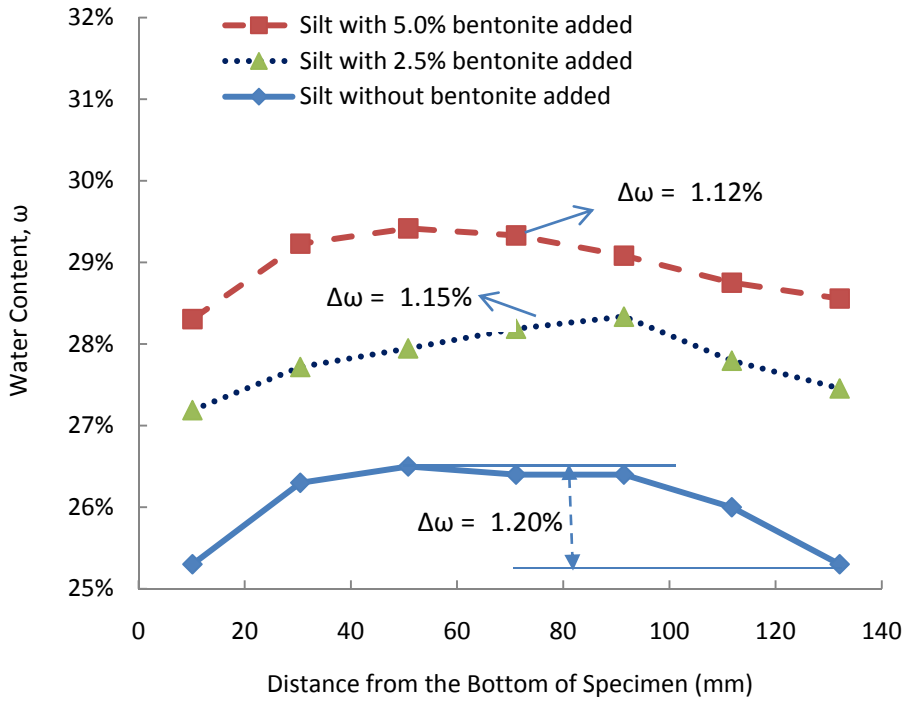

Figure 4.2. Variation in water content from top to bottom of specimen

The distribution of water content and particle size in the reconstituted specimens of natural silt and silt with bentonite indicated that the specimens were quite uniform and could be used to prepare nearly identical reconstituted silt specimen.

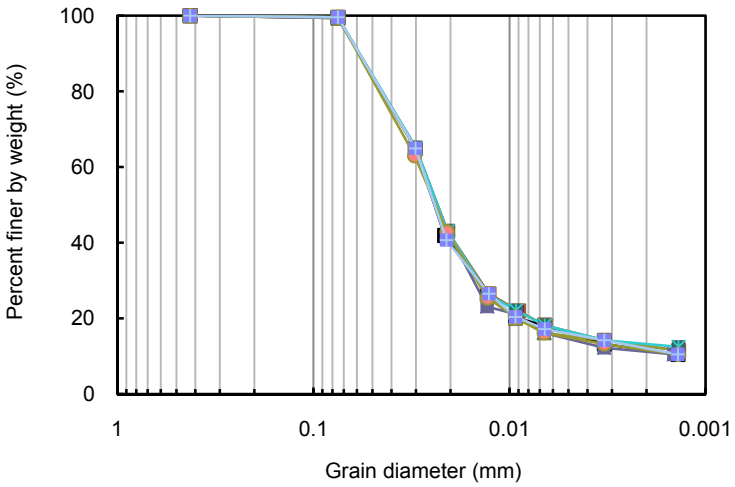

Average	
Diameter (mm)	% finer
0.4250	100.00
0.0750	99.51
0.0302	64.72
0.0208	42.48
0.0129	25.76
0.0093	20.88
0.0066	17.15
0.0033	13.61
0.0014	11.04

(a)

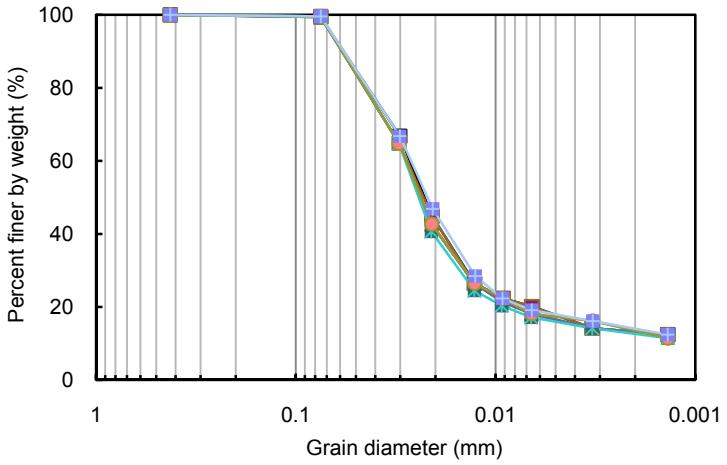

Average	
Diameter (mm)	% finer
0.4250	100.00
0.0750	99.51
0.0303	65.37
0.0208	43.62
0.0127	26.49
0.0092	21.77
0.0066	18.70
0.0033	14.74
0.0014	12.15

(b)

Figure 4.3. Variation in grain size distribution for seven (7) slices of silt specimen reconstituted by slurry deposition: (a) natural silt, (b) silt with adding 2.5% bentonite

4.2. SPECIMEN PREPARATION FOR TESTING

4.2.1 Movement Procedures. Specimens can be prepared directly on the triaxial base platen. Saturation, consolidation, and shearing can then be completed with the

specimen on the same position. This process, however, makes a complete test sequence time consuming. To expedite the testing process, this project developed a special procedure. The specimen was prepared on another base platen, which was then moved to the triaxial base platen. A key requirement of this process was that the specimen be moved with as little disturbance as possible. A following procedure was developed to accomplish this (Figure 4.4):

1. The split vacuum mold was removed while the vacuum was kept on the specimen. A split miter sample mold with diameter of 71.1 mm was used to hold the specimen. A clamp was used to hold the split mold together (Figure 4.4a).

2. The vacuum was then reduced to zero. After a 30-minute waiting period to dissipate the vacuum and avoid entrainment of air in the specimen, the O-rings and the membrane were stretched around the bottom of the split miter sample mold (Figure 4.4b).

3. The top porous stone and top cap were left attached to the specimen, and the specimen with the bottom porous stone was slid onto a metal plate. The plate was then placed next to the base so that the specimen could be moved onto it with the bottom porous stone level (Figure 4.4c).

4. The specimen, with the porous stones and top cap, was moved onto the triaxial base platen and fixed with another clamp (Figure 4.4d).

5. The membrane and O-rings were stretched down to the triaxial base platens (Figure 4.4e).

6. The plastic cap was removed, and the triaxial top cap was carefully placed (Figure 4.4f).

(a)

(b)

(c)

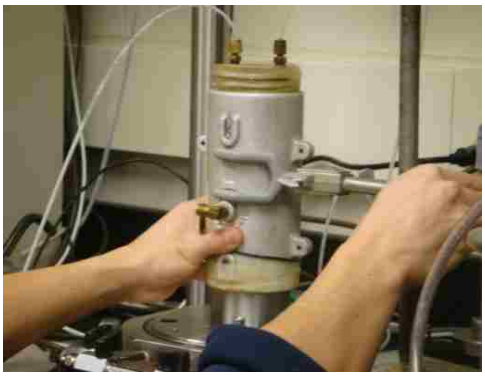

(d)

(e)

(f)

Figure 4.4. Specimen movement from preparation location to triaxial base platen on load frame pedestal: (a) Remove the split vacuum mold and use a split miter box to hold the silt specimen, (b) Move o-rings up and stretch the membrane upwards, (c) Slide silt specimen onto a metal plate, (d) Move silt specimen to a triaxial base platen and fix it with a clamp, (e) Stretch membrane down and move o-rings down to the triaxial base, (f) Set triaxial cap with screw (g) Place vacuum at top and bottom of specimen for 2 hours to remove air, (h) Remove split miter mold, and silt specimen ready for testing

(g)

(h)

Figure 4.4. Specimen movement from preparation location to triaxial base platen on load frame pedestal: (a) Remove the split vacuum mold and use a split miter box to hold the silt specimen, (b) Move o-rings up and stretch the membrane upwards, (c) Slide silt specimen onto a metal plate, (d) Move silt specimen to a triaxial base platen and fix it with a clamp, (e) Stretch membrane down and move o-rings down to the triaxial base, (f) Set triaxial cap with screw (g) Place vacuum at top and bottom of specimen for 2 hours to remove air, (h) Remove split miter mold, and silt specimen ready for testing (cont.)

7. A 45-kPa vacuum was applied for 2 hours to remove any air in the specimen, stones, and lines. The vacuum system allowed the vacuum to be increased as necessary to remove more air bubbles from the specimen to expedite saturation using back pressure. However, the vacuum was always smaller than the effective consolidation pressure (Figure 4.4g).

8. The split miter mold was removed. At this time, the specimen was ready for triaxial testing (Figure 4.4h).

While testing was conducted in the triaxial chamber, another specimen was prepared on the special experimental setup. Since the time to prepare a specimen was almost equal to that required for saturation, consolidation, and shearing, this process reduced the time for the whole testing program by about 50%.

4.2.2 Disturbance during Handling and Moving of Specimens. Observations indicated that there was very little disturbance of specimens during movement as long as the specimen remained vertical. This technique required no direct handling to trim of the specimen. Trimming is normally required if silt sedimentation occurs in a large-scale consolidometer into which sampling tubes are pushed to subsample the specimen.

To verify that there was very little disturbance of the specimens during movement to the triaxial base platen, the specimen size under 45 kPa vacuum was measured with a π-tape before and after the movement (Table 4.1). This value was recorded as an initial diameter before the vacuum was removed. Removal of the vacuum unloads the specimen and can cause swelling. The vacuum was left on the specimen for 8 hours to remove the air after movement. This process behaved as a recompression and the size of specimen may recover. The diameter was then recorded at the same location and compared to the original measurement (Table 4.1). If handling and movement had disturbed the specimen, the two diameters would have varied. The difference, however, was very small, confirming that the handling and movement process created only minimal disturbance.

Table 4.1. Change in diameter (mm) of specimen due to movement and handling

Location	Before Movement	After Movement	Difference
Top	70.45	70.40	-0.05
Middle	69.06	68.95	-0.11
Bottom	69.40	69.50	0.10

4.3. TESTING REPLICAS

The ability to produce identical specimens was verified by conducting additional tests under identical conditions. The objective was to quantify the reproducibility of the testing protocols and assess their quality. For this purpose, two static triaxial compression tests and several cyclic triaxial tests were conducted.

4.3.1 Static Triaxial Tests. Two normally consolidated undrained (CU) triaxial tests with an effective consolidation stress of 50.0 kPa were conducted to verify the repeatability of static testing under the same conditions. A Humboldt triaxial system was used for the static triaxial compression tests. After the specimens of the natural MRV silt were moved to the triaxial base platen, vacuum and then back pressure were applied to saturate the specimens, resulting in a Skempton B-value higher than 0.98. Figure 4.5 shows the testing results.

The stress-strain curves are nearly identical in shape at the initial phase of shearing; they become dissimilar at large strains. The differences in deviator stress and excess pore pressure between the tests were insignificant under large strain. The percent differences are 5.9% and 10.4% of the average values of deviator stresses and excess pore pressures, respectively. The stress and strain computations at large strain values (> 10%) are inherently unreliable because of the area corrections at these levels. These small differences, however, are acceptable and attributable to unavoidable variations in testing and to human factors. These results confirm the repeatability of static triaxial compression testing on specimens prepared as described here.

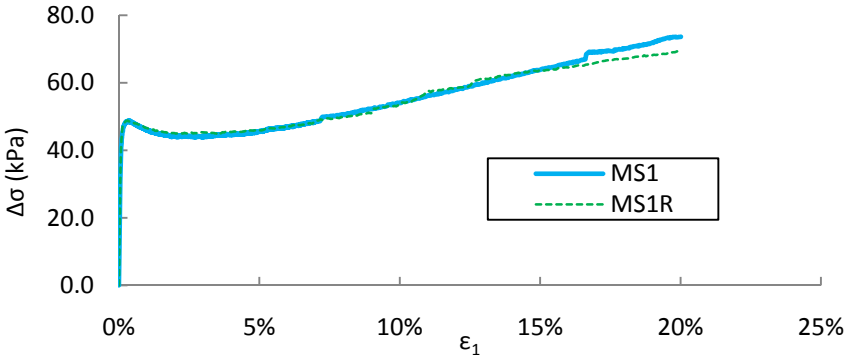

(a)

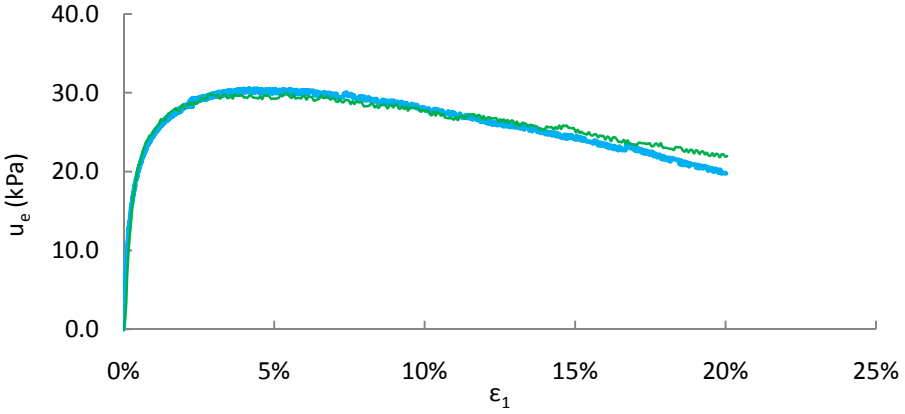

(b)

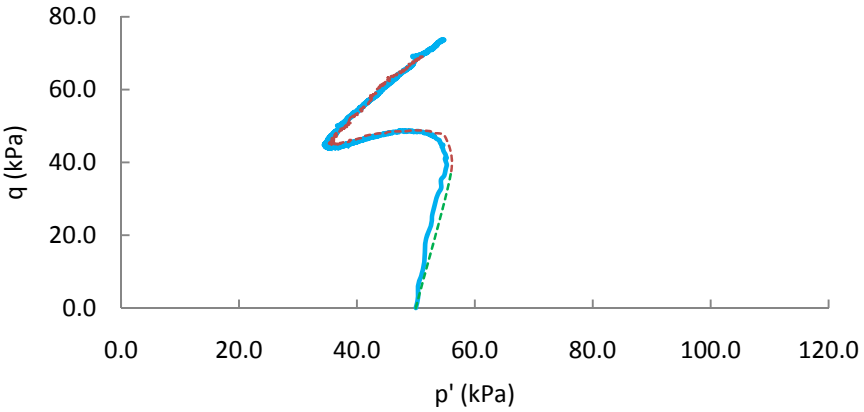

(c)

Figure 4.5. Repeatability of Static Testing ($p' = (\sigma'_1 + \sigma'_2 + \sigma'_3)/3$, $q = \sigma_1 - \sigma_3$): (a) $\Delta\sigma$ vs. ε_1, (b) u_e vs. ε_1, (c) q vs. p'

4.3.2 Cyclic Triaxial Tests. Cyclic triaxial tests were conducted at two cyclic stress ratios (CSR) of 0.18 and 0.35, normally consolidated to an effective confining stress (σ'_c) of 90 kPa (Figure 4.6). For a CSR of 0.18, specimens MD2 and MD2R required 35.2 and 32.2 cycles of loading, respectively, to liquefy. The average number of cycles was 33.7. The difference between the average number and 35.2 or 32.2 is 1.5, or just 4.5% of the average 33.7. Thus, the difference in the number of cycles between two tests was small. For the higher CSR of 0.35, specimens MD4 and MD4R shown in Figure 4.7 presented even smaller differences. Both liquefied at only 1.2 cycles of load. The excess pore pressure and stress paths were nearly identical. Thus, the replicated specimens produced near identical dynamic failure conditions of liquefaction.

This specimen preparation technique was also used to study the postcyclic behavior of silt soils. Seven cyclic triaxial tests were conducted, each with a CSR of 0.18 and a σ'_c of 90 kPa. Table 4.2 shows the void ratio (e) after normal consolidation and the number of loading cycles (N_{cyc}) to liquefy the specimens. The MD and MF tests were used to study liquefaction resistance and postliquefaction behavior, respectively. The coefficient of variation of the e was 0.0125, and that of the N_{cyc} was 0.1023. These small coefficients of variation are considered as acceptable for a research quality testing program.

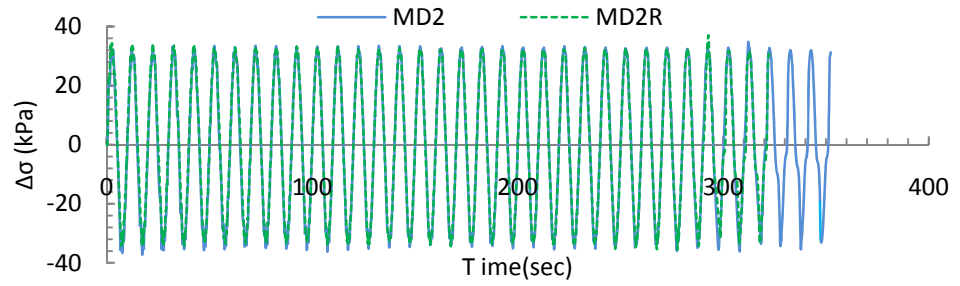

(a)

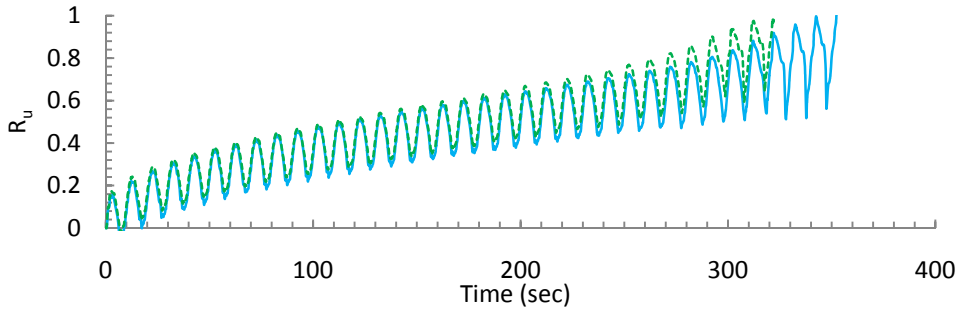

(b)

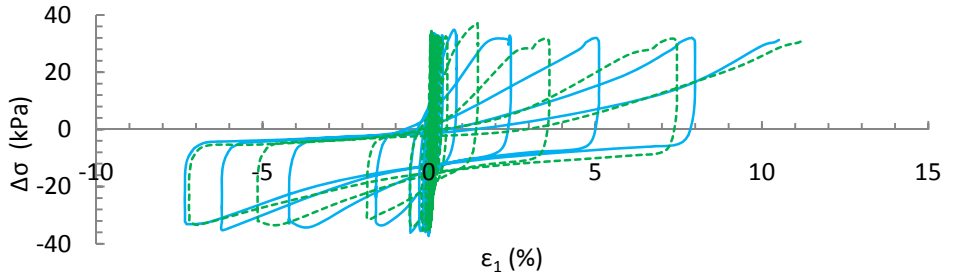

(c)

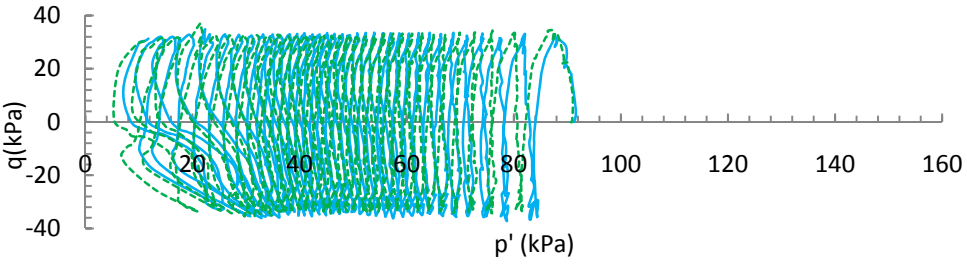

(d)

Figure 4.6. Repeatability of cyclic testing with a CSR of 0.18: (a) Δσ vs. Time, (b) R_u vs. Time, (c) Δσ vs. ε_1, (d) q vs. p'

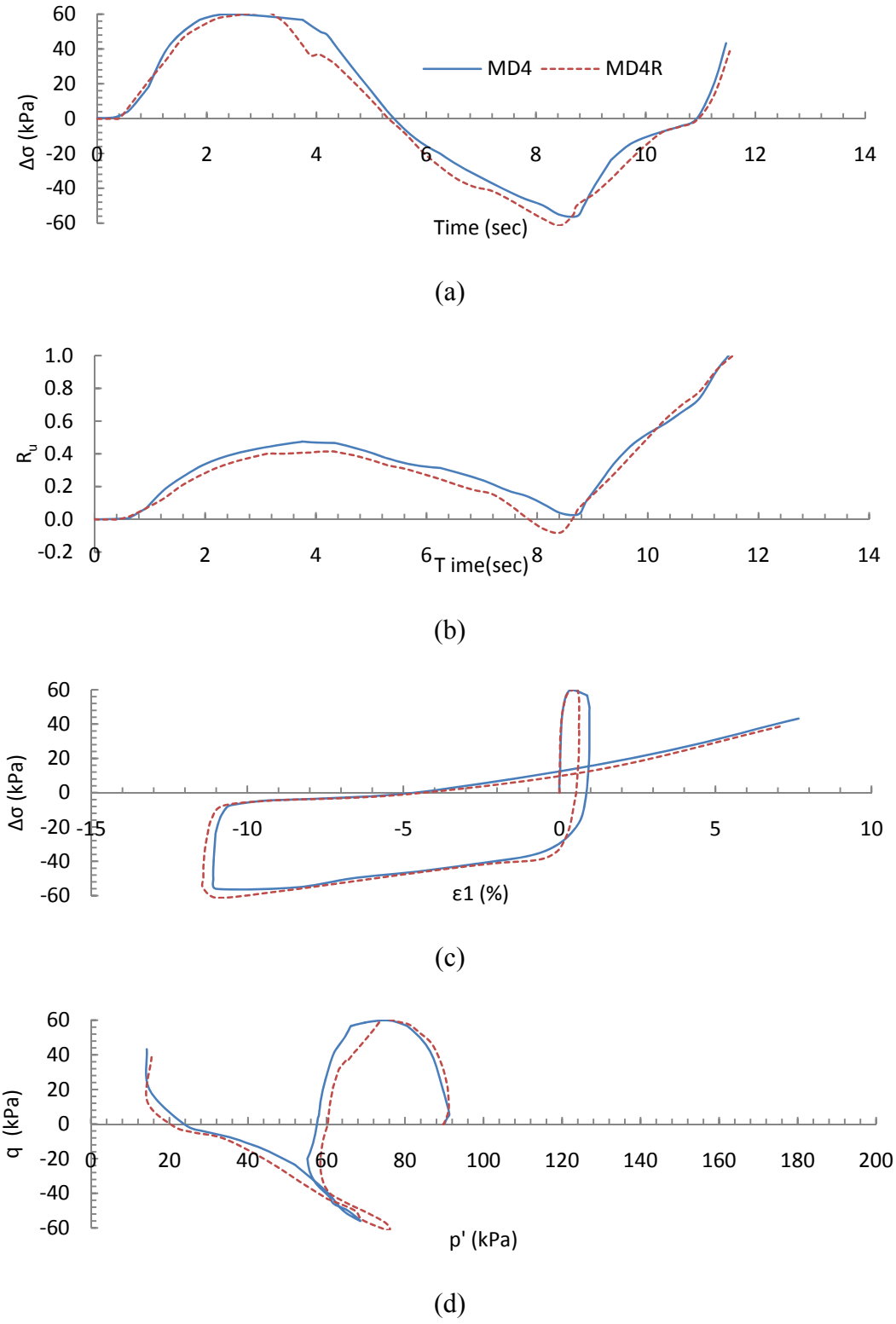

Figure 4.7. Repeatability of cyclic testing with a CSR of 0.35: (a) Δσ vs. Time, (b) R_u vs. Time, (c) Δσ vs. ε_1, (d) q vs. p'

Table 4.2. Statistics on number of loading cycles required to liquefy specimens with a CSR of 0.18

Test ID	MD2	MD2R	MF1R1	MF1R2	MF2	MF3	MF4	Mean	Standard deviation	Coefficient of variation
e	0.661	0.681	0.660	0.669	0.657	0.663	0.659	0.664	0.008	0.0125
N_{cyc}	35.2	33.2	27.1	31.1	27.2	30.1	28.1	30.3	3.1	0.1023

4.4. SUMMARY

This section presented a new slurry consolidation method, describing a procedure using MRV silt. Specimen uniformity was verified by measuring the water content and particle size distribution for seven slices of the silt specimens. These measurements showed very little variation over the length of the specimens. The testing program was expedited with a special handling and moving technique to permit simultaneous specimen preparation and triaxial testing. The reliability of this technique was verified by confirming minimal disturbance of the specimen during movement. To further verify the validity of this approach, tests were repeated for both static and cyclic triaxial conditions, and the results compared. The differences between original and replicated specimens were minimal. Thus, this new approach can be effectively used to reconstitute specimens of low-plasticity silt.

5. MONOTONIC AND CYCLIC SHEAR BEHAVIOR OF LOW-PLASTICITY SILT

This section describes triaxial tests on the MRV silt conducted to study monotonic and cyclic shear behavior of low-plasticity silt. These determined the best failure criterion to compute effective friction angle and the effect of OCR on monotonic undrained shear behavior. They also permitted identification of the critical state line and normalized behavior for the MRV silt, and finally report the cyclic behavior and liquefaction resistance of the silt.

5.1. MONOTONIC SHEAR BEHAVIOR

This work carried out static consolidated undrained triaxial compression tests on low-plasticity silt specimens with various OCRs and effective consolidation pressures (σ'_c). The specimens were saturated with back pressures (σ_{BP}) until a B-value of at least 0.98 was reached. To avoid the development of cavitation due to negative excess pore pressure generated during generated shearing of overconsolidated specimens, the back pressures applied were greater than what was required to produce a B-value of 0.98 (Table 5.1). After saturation, the specimens were consolidated at OCRs of 1, 2, 4, and 8 and effective consolidation pressures of 50, 90, and 129 kPa. The OCRs were achieved by consolidating the specimens to preconsolidation pressure ($\sigma'_p = \sigma'_c \times OCR$) and rebounding them to effective consolidation pressure.

5.1.1 Undrained Shear Behavior. Figure 5.1 shows the deviator stress and excess pore pressure response of the MRV silt specimens. Although the shearing of specimens with an OCR of 1 was stopped at 20% axial strain due to the small

measurement range (0 ~ 1 inch) of the initial LVTD, the specimens could be expected to reach critical state at an axial strain of about 25%. In slightly overconsolidated specimens MS4 and MS5 each with an OCR of 2, there were no great increases in the deviator stress after the axial strain was larger than 20%. The deviator stresses ($\Delta\sigma$) and excess pore pressures (u_e) at the critical state of normally consolidated specimens and other overconsolidated specimens which did not reached critical state were estimated by extrapolation for later analysis (Table 5.1).

Table 5.1. Static triaxial compression tests on MRV silt

Test ID	σ_{BP} at B = 0.95	σ_{BP} at end of saturation	B-value	σ'_p	σ'_c	OCR	e	u at critical state	$\Delta\sigma$ at Critical state	A_f
	(kPa)	(kPa)		(kPa)	(kPa)			(kPa)	kPa	
MS1	241.3	289.6	0.99	--	50.0	1	0.700	300.6	85.0	0.13
MS2	217.2	241.3	0.98	--	90.0	1	0.679	269.2	144.0	0.19
MS3	217.2	241.3	0.98	--	129.0	1	0.652	299.4	154.8	0.38
MS4	241.3	337.8	0.99	102.4	51.2	2	0.665	337.3	113.7	0.00
MS5	193.1	265.4	0.99	180.0	90.0	2	0.653	263.6	198.9	-0.01
MS6	241.3	337.8	1.00	200.0	50.0	4	0.647	306.3	191.0	-0.16
MS7	265.6	362.0	0.99	364.8	91.2	4	0.612	287.2	370.3	-0.20
MS8	265.4	360.6	0.98	400.0	50.0	8	0.648	284.6	296.5	-0.26
MS9	248.2	386.1	1.00	720.0	90.0	8	0.591	255.6	513	-0.25

Note: e – void ratio of specimen after it was rebounded to effective consolidation pressure (σ'_c);
A_f – ratio of excess pore pressure to deviator stress at the critical state

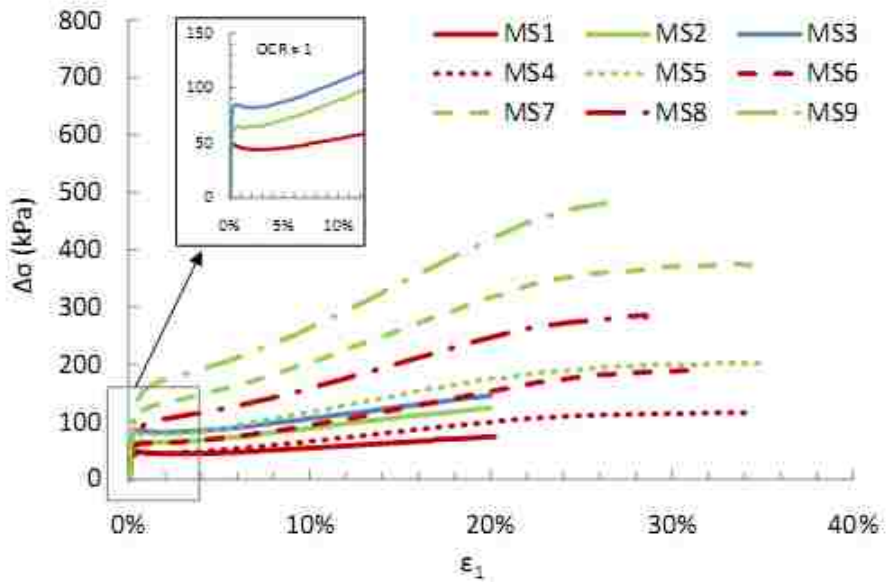

(a)

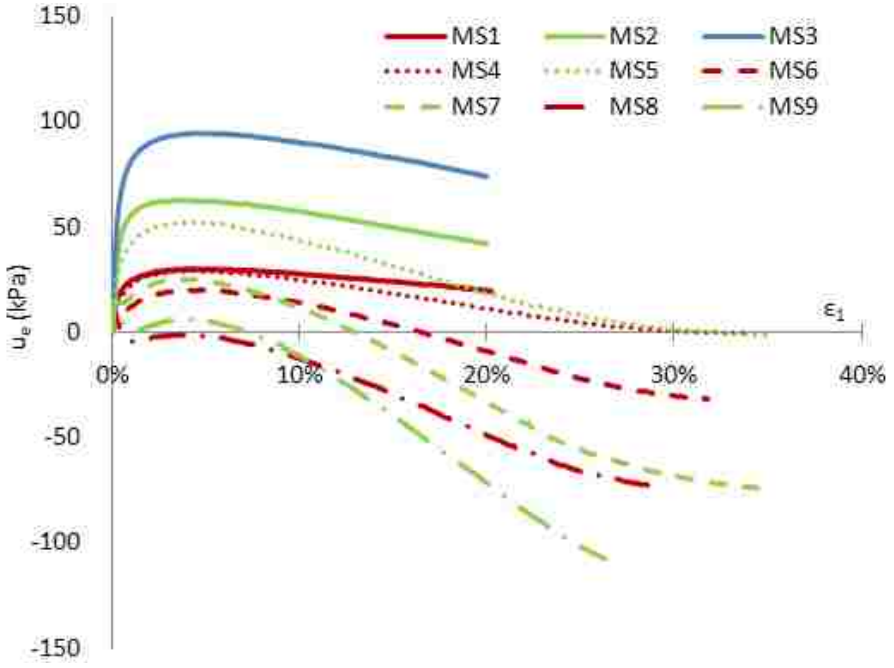

(b)

Figure 5.1. Static testing results of MRV silt: (a) $\Delta\sigma$ vs. ε_1, (b) u_e vs. ε_1

Figure 5.1a indicates that all overconsolidated specimens with an OCR equal to or larger than 2 showed continuous dilative behavior (strain-hardening), but the normally consolidated specimens had a slight strain-softening stage after the initial peak deviator stress. After this strain-softening stage, the higher deviator stress built up, and the normally consolidated specimens showed strain-hardening behavior. Under higher OCRs, the dilative behavior became more obvious for specimens with identical effective consolidation pressures. The A_f value in Table 5.1 also indicated this behavior. As the OCR increased, the A_f value decreased.

The dilative behavior at the large deformation, especially for overconsolidated specimens, can be explained by the MRV silt particle features. As stated in Section 3, the shapes of the silt particles ranged from subangular to angular, and even very angular. The surface of the silt particles was rough. These features tended to contribute to the dilative behavior of this material.

5.1.2 Effective Friction Angle. The effective effective friction angle (ϕ') can be obtained based on various failure criteria. Possible failure criteria include maximum deviator stress ($(\sigma_1 - \sigma_3)_{max}$), maximum principal stress ratio ($(\sigma'_1 / \sigma'_3)_{max}$), maximum excess pore pressure ($u_{e,\,max}$), stress path reaching K_f line, limiting strain, and excess pore pressure of zero ($u_e = 0$) (Brandon et al., 2006). The effective friction angle for the low-plasticity MRV silt tested here was calculated using all these failure criteria (Figure 5.2). Since the silt showed only slightly dilative behavior at an OCR of 1, the excess pore pressure did not reach zero. Thus, the Mohr circles in Figure 5.2e are based on overconsolidated specimens only. The failure criteria of $(\sigma_1 - \sigma_3)_{max}$, $(\sigma'_1 / \sigma'_3)_{max}$, and 15% limiting strain yielded relatively consistent effective friction angles for the MRV silt.

Conversely, the effective friction angles based on $u_{e,\,max}$, $u_e = 0$, and stress path reaching K_f line are widely scattered. Two criteria in particular, $(\sigma'_1 / \sigma'_3)_{max}$ and 15% limiting strain, produced effective friction angles of approximately 35°. However, the effective friction angle was about 32° based on the criterion of $(\sigma_1 - \sigma_3)_{max}$, which was obtained at the point of large strain, under which an earth structure would fail. Thus, the $(\sigma_1 - \sigma_3)_{max}$ is not an appropriate criterion for calculation of the effective friction angle of the MRV silt. Brandon et al. (2006) conducted a similar research for the normally consolidated Yazoo silt (nonplastic) and LMZD silt with PI of 4 and found that, for both silts, all of the previously mentioned failure criteria except the $u_{e,\,max}$ can result in a effective friction angle within a narrow range.

To analyze the influence of each failure criterion on the calculated effective friction angle of low-plasticity silt, the results of this work were combined with those reported by Brandon et al. (2006) and Izadi (2006). Figure 5.3 shows that the failure criteria of $(\sigma'_1 / \sigma'_3)_{max}$, 15% limiting strain, and stress path reaching K_f lines yielded a higher effective friction angle than other criteria. The effective friction angle is lowest based on the criterion of $u_{e,\,max}$ because full strength in terms of effective stress had not been mobilized. Although Brandon et al. (2006) concluded that any of the failure criteria except the u_{max} could be used to evaluate the effective friction angle of low-plasticity, dilative silts, the criteria of $u_e = 0$ and stress path reaching K_f line could not be used for the MRV silt tested here, because this silt did not dilate enough to induce negative excess pore pressure and large ranges of stress paths touched the K_f line in the stress space, respectively. The criteria of 15% limiting strain and $(\sigma'_1 / \sigma'_3)_{max}$ estimated the effective friction angle consistently. For the MRV silt tested here, the maximum σ'_1 / σ'_3 appeared at

around 10% axial strain. However, for other low-plasticity silts, the axial strain at the maximum σ'_1 / σ'_3 is probably larger than 15%. Thus, it is recommended that a 15% limiting strain is the best criterion to calculate the effective effective friction angle of low-plasticity silt.

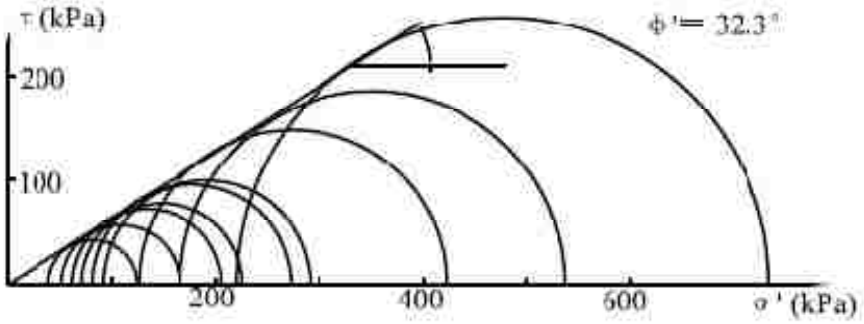

(a)

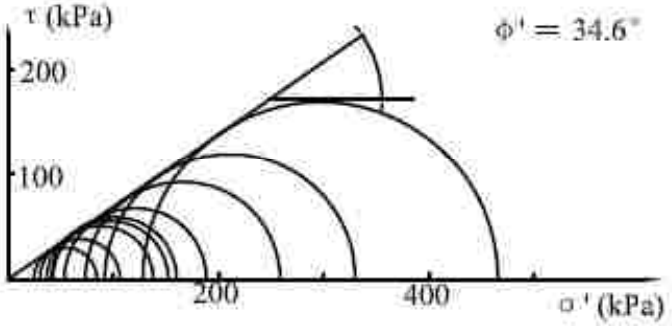

(b)

Figure 5.2. Effective friction angle based on various failure criteria: (a) $(\sigma_1 - \sigma_3)_{max}$, (b) $(\sigma'_1 / \sigma'_3)_{max}$, (c) limiting strain 15% , (d) $u_{e,\,max}$, (e) $u_e = 0$, (f) stress path reaching K_f line

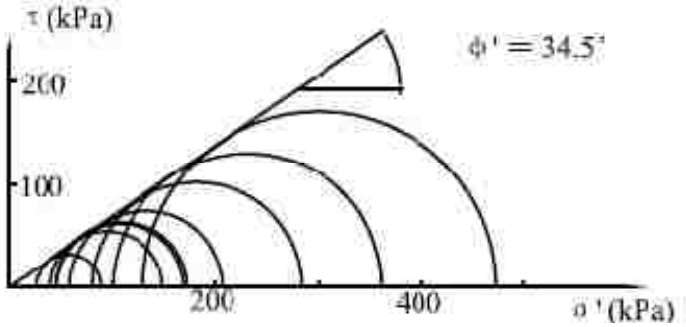

(c)

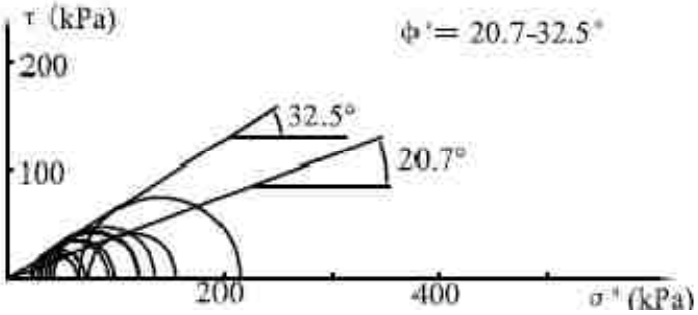

(d)

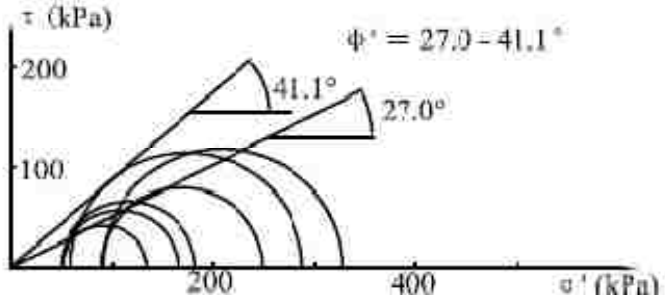

(e)

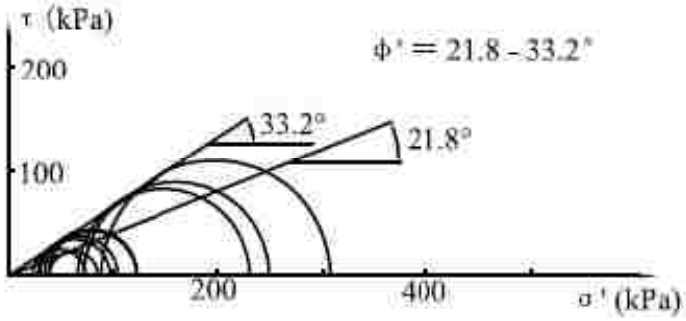

(f)

Figure 5.2. Effective friction angle based on various failure criteria: (a) $(\sigma_1 - \sigma_3)_{max}$, (b) $(\sigma'_1/\sigma'_3)_{max}$, (c) limiting strain 15% , (d) $u_{e,\,max}$, (e) $u_e = 0$, (f) stress path reaching K_f line (cont.)

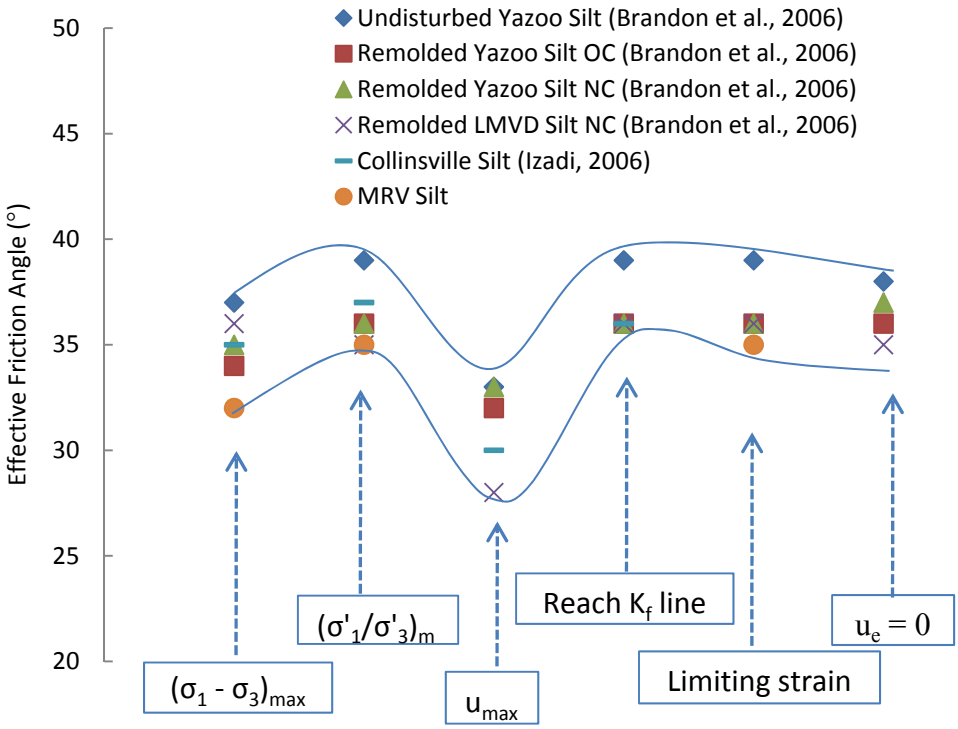

Figure 5.3. Variation in effective friction angle based on various failure criteria

5.1.3 Critical State Line. The stress paths of all static tests were plotted in the Cambridge stress space (see Figure 5.4, $p' = (\sigma'_1 + 2\sigma'_3)/3$; $q = \sigma_1 - \sigma_3$). All stress paths rose along one line (K_f line) after the phase transformation points were reached. The phase transformation point is defined as the state at which the reversal from contractive to dilative behavior occurs (Ishihara et al., 1975). A failure line (K_f line) was plotted with the slope (M) of about 1.4 in the stress space; therefore, the effective friction angle was computed to be 34.6° using $\sin\phi = 3M/(6+M)$; this angle is comparable to those using the failure criteria discussed above.

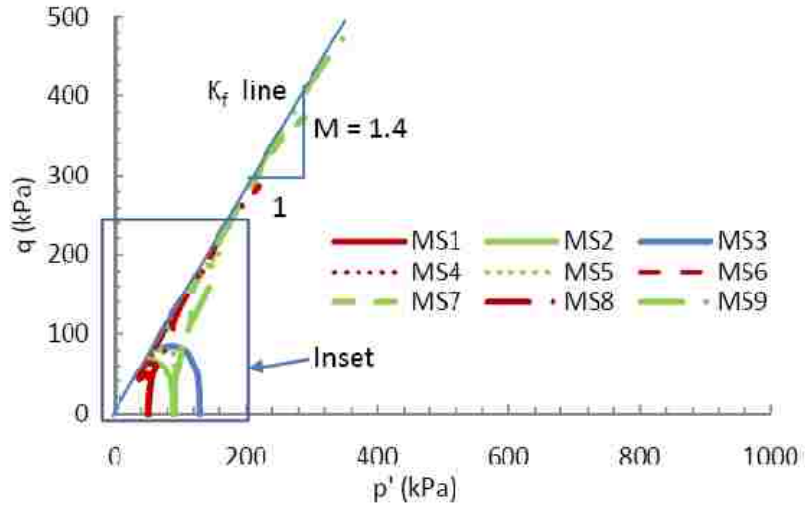

(a)

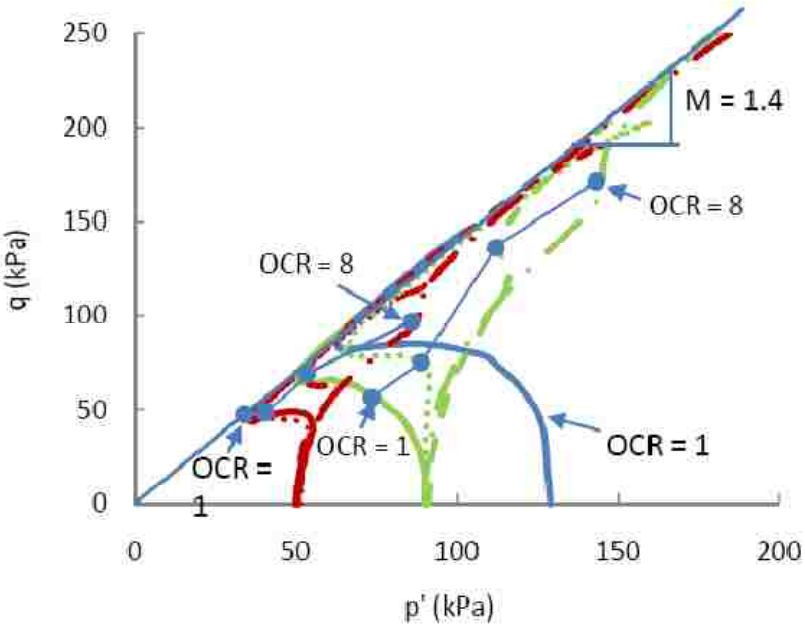

(b)

Figure 5.4. Stress paths in Cambridge space: (a) showing all data, (b) enlarged inset

To study the stress paths more closely, Figure 5.4b was enlarged to focus on the early stages of stress paths. The OCRs are marked for each stress path from 1 to 8. In general, the stress path indicates that the silt specimens became more dilative as the OCR

increased. Further investigation identified the following phenomenon: Specimens with an OCR of 1 or 2 showed initial contraction followed by continuous dilation behavior. With an OCR of 4 and an effective consolidation pressure of 50 kPa, the specimen showed behavior similar to that of specimens with an OCR of 1 or 2. At an effective consolidation pressure of 90 kPa, however, the specimen with an OCR of 4 showed continuous dilation, as did the specimens with an OCR of 8. Thus, specimen with higher effective consolidation pressure dilated more when the OCR was equal to 4. This behavior is the opposite to that is expected from typical soils (sands and clays). Normally, with increasing effective consolidation pressure, soil specimens tend to contract. Yamamuro and Lade (1998) also observed this unexpected behavior in silty sand. They noted that a specimen with an effective consolidation pressure of 25 kPa showed static liquefaction. As the pressure increased, the silty sand developed more resistance (i.e., it became more dilated). Thus, the low-plasticity silt tested here showed a behavior different from that observed in typical sands and clays.

This work also studied the lab data to investigate the critical state in the e-lnp' space. Figure 5.5 shows one critical state line obtained for the tested silt. Since the void ratio remains constant during undrained shearing, the stress path in the e-lnp' space can only move horizontally towards the CSL depending on the pore pressure response. Figure 5.5 indicates that, due to the negative pore pressure induced by the tendency to dilate, all data points moved starting with the initial state point (ISP), continuing through the phase transformation point (PTP), and ending at the critical state point (CSP). All specimens near the end of shearing showed dilative behavior compared to the state at the beginning of shearing. Even the normally consolidated and slightly overconsolidated specimens

showed a decrease in pore pressure (dilative response) at the end of shearing after the expected contraction in the initial shearing (see Figure 5.1b). This behavior agreed with the findings in the stress space, since all stress paths rose along the critical state line in the stress space after the phase transformation stage. The critical state line was not parallel to normal consolidation line. As noted by Boulanger and Idriss (2006), if the normal consolidation and critical state lines are not parallel, the silt behaves like a sand. Thus, the silt tested here had sand-like behavior. However, the work of Boulanger and Idriss does not address the effect of OCR on silt behavior. As noted in Section 5.1.4 below, the OCR played a significant role in the normalized behavior of the tested silt, as it did in that of clay, so that the silt did not behave exactly like a sand.

From the initial state to the critical state, the critical state diagram revealed general dilation behavior. However, as mentioned above, specimens with an OCR of 1 or 2 initially contracted, and then dilated. To identify the initial dilation or contraction in the e-lnp space, a phase transformation line was also plotted in the Figure 5.5. Only the data points for specimens MS7, MS8, and MS9 are located to the left of the phase transformation line. Due to the magnitude of negative excess pore pressure compared to other specimens, these overconsolidated specimens tended to dilate from their initial state to the phase transformation state.

5.1.4 Normalized Behavior. The deviator stress of some clays can be normalized by effective consolidation pressure, as suggested by Ladd and Foott (1974) and Ladd et al. (1997). Fleming and Duncan (1990) demonstrated that the undrained strength of low-plasticity Alaskan silts can also be normalized, producing relatively small variations.

These small variations in the normalized values for identical OCRs are believed to result from sample preparation and reconsolidation effects.

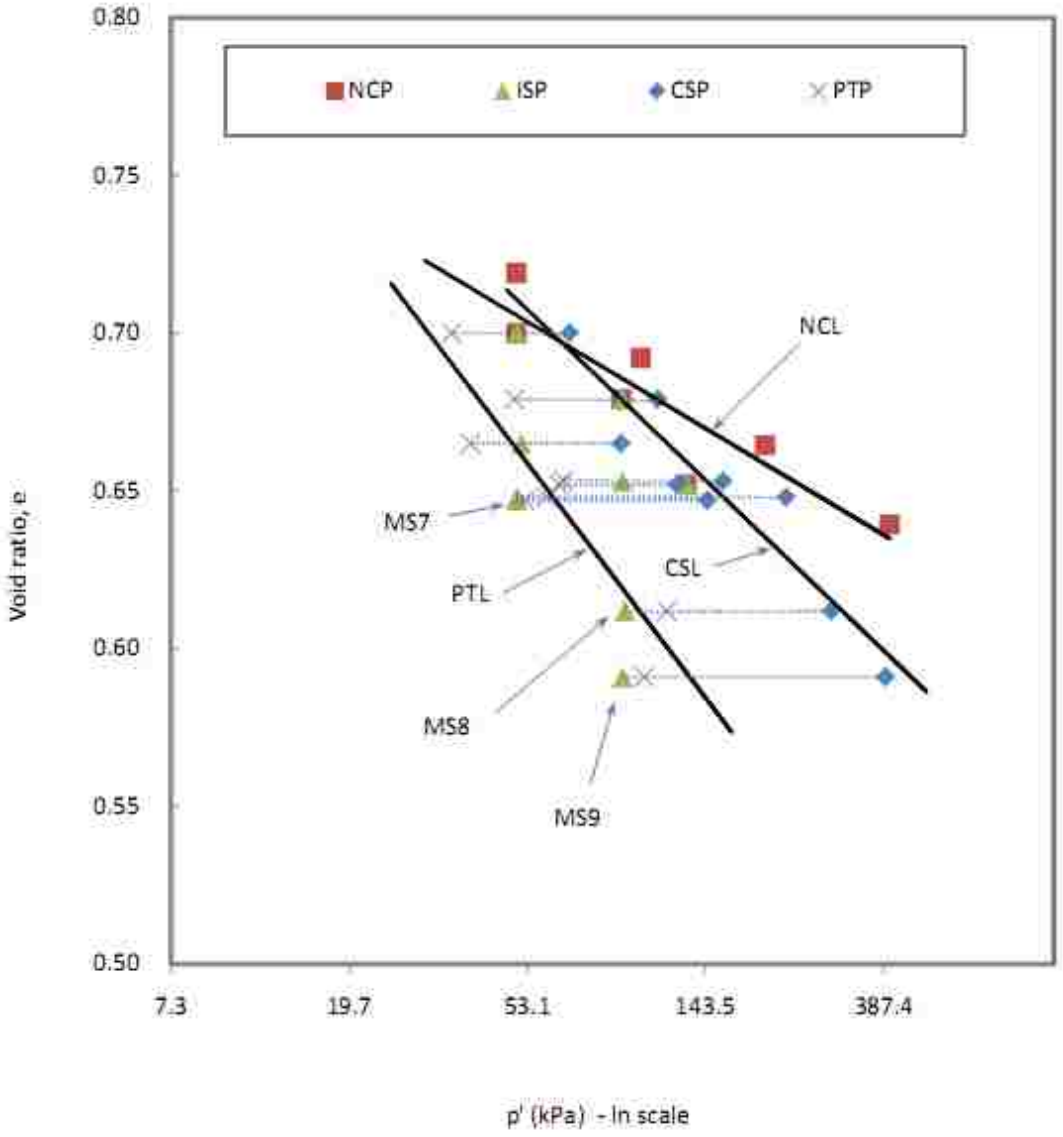

Figure 5.5. Critical state diagram obtained from consolidated undrained tests (NCP – normally consolidation point)

Figure 5.6 shows the normalized behavior plots with respect to effective consolidation stress for the MRV silt tested here. With higher OCR, the normalized deviator stress was higher, and more negative normalized excess pore pressure was generated (Figure 5.6a and 5.6b). In the normalized stress space (Figure 5.6c), a higher OCR generally resulted in a more dilative response, except for the specimen with an effective consolidation pressure 50 kPa and an OCR of 1. Therefore, the OCR played a significant role in normalized stress-strain behavior. Furthermore, under the same OCR, normalized behaviors were different for different effective consolidation pressures. When the OCR was equal to 1 or 8, the normalized deviator stress decreased with increasing effective consolidation pressure. On the other hand, when the OCR was 4, the normalized deviator stress increased with increasing effective consolidation pressure. Specimens with an OCR of 2 had intermediate behavior, as indicated by closely matching curves of normalized deviator stress and excess pore pressure against axial strain.

The stress-strain behavior appears not to have been normalized by effective consolidation pressure. However, the variations of normalized stress-strain behavior induced by the effective consolidation pressure were much lower than those induced by the OCR. These small variations were caused in part by inevitable variations in procedures from one test to another. Thus, the MRV silt tested here can be said to have normalized behavior. Similarly, the excess pore pressure could also be normalized by effective consolidation pressure.

Based on many tests of six clays, Ladd et al. (1997) developed the following equation to consider the effect of OCR on the normalized shear strength of clay:

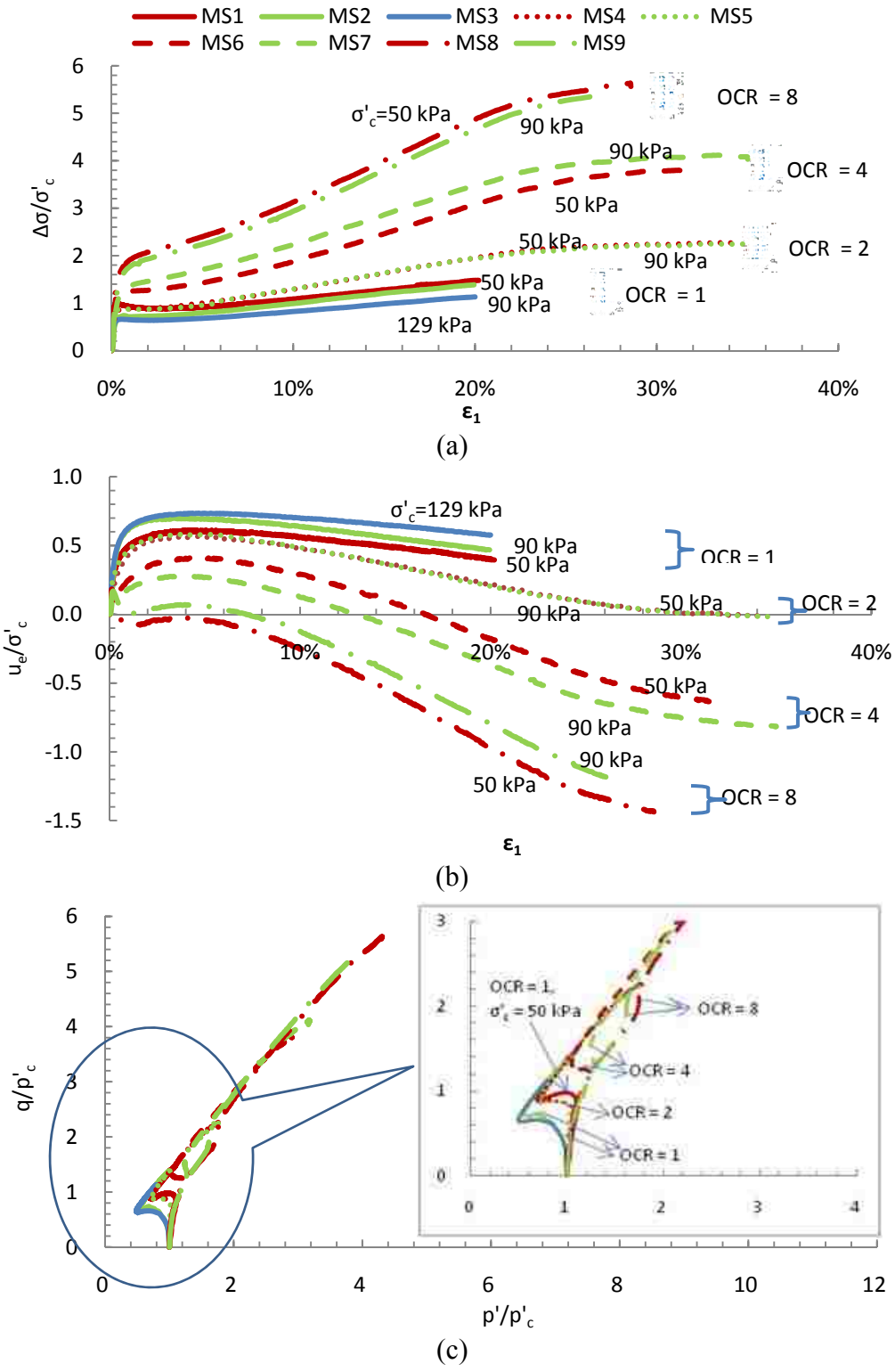

Figure 5.6. Normalized behaviors of the silt: (a) normalized deviator stress, (b) normalized excess pore pressure, (c) normalized stress path

$$\frac{(S_u / \sigma'_C)_{(OC)}}{(S_u / \sigma'_C)_{(NC)}} = OCR^m \quad (9)$$

where S_u is undrained shear strength, and σ'_c is effective consolidation pressure. Here, the *m* value is normally equal to 0.80, but it varies from 0.75 to 0.85 based on the OCR. A higher OCR is probably associated with a higher value of m.

Furthermore, Ladd (1991) presented the following equation to calculate the S_u/σ'_c:

$$\frac{S_u}{\sigma'_c} = S \times OCR^m \quad (10)$$

where *S* is 0.22 and 0.25 for clay and silt, respectively; *m* is 0.80 for both clay and silt.

By combining the results reported by Fleming and Duncan (1990), Yasuhara et al. (2003), and Izadi (2006), this work studied the effect of OCR on the normalized shear strength of low-plasticity silt under isotropic consolidation. Table 5.2 shows these comparisons. The undrained shear strength was determined here as one-half of the deviator stress at an axial strain of 15%, as done by Fleming and Duncan (1990) for the Alaskan Silt. They proposed a range of S_u/σ'_c, and the present work took the middle value for comparison herein. The Keuper Marl silt studied by Yasuhara et al. (2003) had a plasticity index of 19.7 and a liquid limit of 38.6, and is thus classified as a lean clay (CL) using the Unified Soil Classification System. However, the silt fraction was nearly 70% based on the grain size distribution curve, and it was considered a low-plasticity silt (Yasuhara et al., 2003). Izadi (2006) reported normalized deviator stress curves of Collinsville silt, and these curves were used to determine the undrained shear strength. The same data shown in Table 5.2 is plotted in Figure 5.7, which clearly shows that, for all four silts, the S_u/σ'_c increases as the OCR increases (Figure 5.7a).

Table 5.2. Variation in normalized shear strength with OCR

Silt	**PI**	**OCR**				
		1	2	4	8	10
Alaskan	Close to A-line in Plasticity Chart	0.925	1.775	---	2.925	---
Keuper Marl	19.7	0.34	0.565	0.85	---	1.7
Collinsville	6	1.325	2.625	3.2	---	---
MRV	5.8	0.566	0.820	1.332	1.951	---

For the silt materials compared above, it was impossible to relate S_u/σ'_c to OCR using as single expression such as Equation 10. Ladd et al. (1997) also used the ratio of normalized shear strength of overconsolidated specimens to that of normally consolidated specimens as shown in Equation 9. Figure 5.7b indicates that there was no significant difference among the various silts. Thus, the PI has no significant effect on the normalized shear strength ratio for the low-plasticity silt.

The data points in Figure 5.7b can be fitted using Equation 9 with an *m* value of 0.58; the data point with an OCR of 10 is the only exception. Ladd et al. (1997) tested clays and found the *m* value to be 0.8 and also required a larger *m* value for higher OCRs. As is possible with clayey soil, the equation permits convenient prediction of the undrained shear strength of overconsolidated silty soil using the known shear strength of normally consolidated specimen.

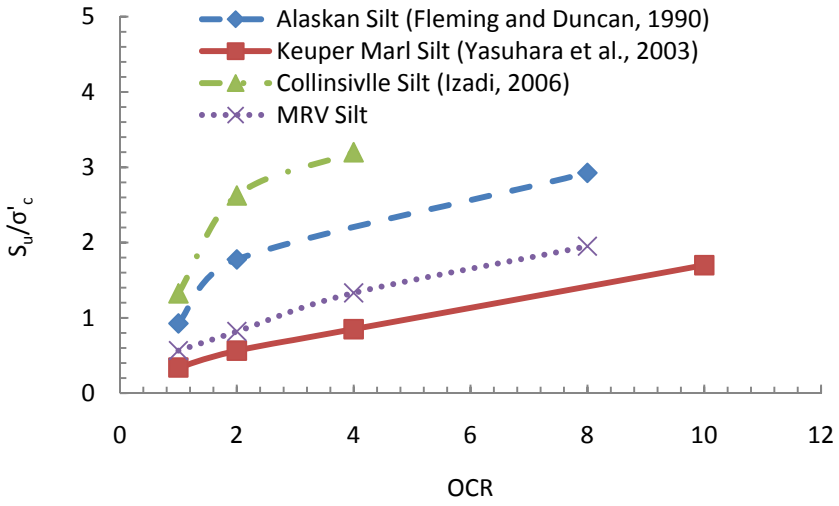

(a)

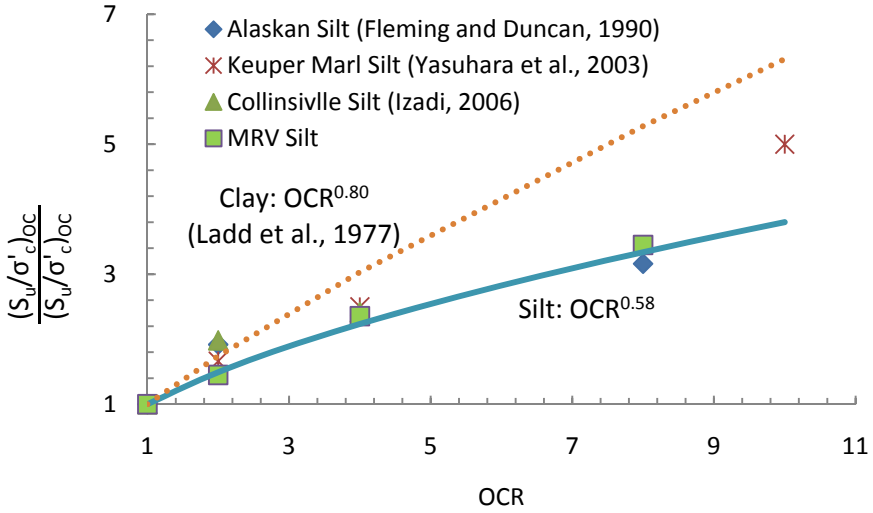

(b)

Figure 5.7. Effect of OCR on normalized shear strength: (a) S_u/σ'_C vs. OCR, (b) $\frac{(S_u/\sigma'_C)_{(OC)}}{(S_u/\sigma'_C)_{(NC)}}$ vs. OCR

Figure 5.7b also plots the curve used to demonstrate the effect of OCR on the normalized shear strength ratio of a clay. The curve for the clay is above that for the silt, indicating that the OCR affects the normalized shear strength ratio of the silt less than it

does that of the clay. The *m* value is probably related to the plasticity of the silt. This hypothesis is supported by the fact that low-plasticity silts behave like an intermediate soil. The *m* value for the silts was determined based on the limited data available for four kinds of low-plasticity silt. Additional research data could verify the validity of an *m* value of 0.58 for low-plasticity silt.

Figure 5.8 plots the curve of principal stress ratio (σ'_1/σ'_3) against axial strain. The maximum values of this ratio are located in a narrow zone of 3.45 to 3.77, which explains why the failure criterion of $(\sigma'_1/\sigma'_3)_{max}$ can yield a relatively constant effective friction angle. Thus, stress-strain behavior can be normalized using effective confining stress during the shearing.

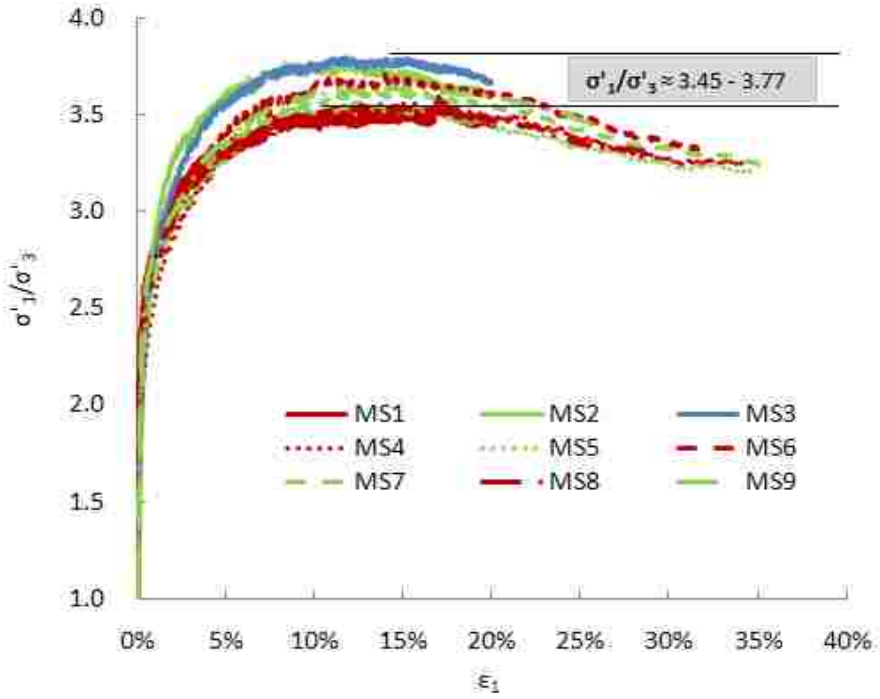

Figure 5.8. Principal stress ratio versus axial strain of MRV silt

5.2. CYCLIC SHEAR BEHAVIOR

Cyclic shear behavior of the tested MRV silt was investigated using cyclic triaxial tests. Table 5.3 lists the tests, including those (MD2, MD2R, MD4, and MD4R) used to verify the repeatability of the cyclic tests described in Section 4. Specimen MD1 with a CSR of 0.10 did not liquefy and developed a cyclic strain (ε_{cyc}) of only 0.39%. With higher CSRs, the MRV silt reached initial liquefaction (i.e. excess pore pressure ratio equal to 1.0). The curves of cyclic tests can be found in the Appendix.

Table 5.3. Summary of cyclic triaxial tests on MRV silt normally consolidated to an effective consolidation pressure of about 90 kPa

Test ID	B-Value	e	CSR	N_{cyc}	ε_{cyc} (%)
MD1	0.948	0.669	0.10	66.17	0.39
MD2	0.944	0.661	0.18	35.2	10.51
MD2R	0.952	0.686	0.18	33.2	11.21
MD3	0.944	0.680	0.25	3.15	11.80
MD4	0.940	0.676	0.35	1.15	11.10
MD4R	0.944	0.682	0.35	1.15	11.42

The liquefaction resistance of the MRV silt was evaluated according to the criterion of the R_u equal to 1.0. Figure 5.9 shows the curve of CSR versus number of loading cycle (N_{cyc}). This curve is comparable to the liquefaction resistance of other silty soils (Boulanger et al. 1998, Guo and Prakash 1999). The CSR required to liquefy specimen decreased with an increase in N_{cyc}.

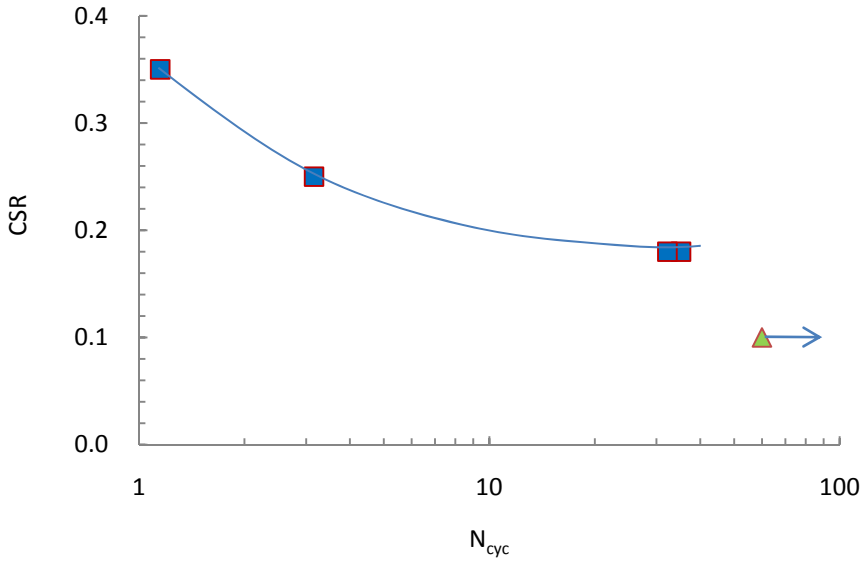

Figure 5.9. Liquefaction resistance of MRV silt normally consolidated to effective confining pressure of about 90 kPa

5.3. SUMMARY

The MRV silt specimens with an OCR of 1 or 2 initially contracted, and then dilated. With an OCR of 8, the silt dilated continuously. All these specimens (OCR = 1, 2, and 8) exhibited normal behavior; that is, they showed less dilation with higher effective consolidation pressure. For an OCR of 4, however, the specimens showed reverse behavior; that is, higher dilation with higher effective consolidation pressure.

The critical state line was not parallel to the normal consolidation curve in the *e-lnp'* space. According to Boulanger and Idriss (2006), the silt shows a sand-like behavior. However, in this work, the OCR did play a significant role in the stress-strain behavior of the silt, as it does in that of clay. These findings indicated that the behavior of the silt was unique, and thus more complex than previously thought.

With the failure criteria of u_{max}, u = 0, and a stress path reaching the K_f line, the effective friction angle of the silt tested here was difficult to determine. This work suggests that limiting strain is the criterion best suited to calculate the effective friction angle because it generates a more consistent effective friction angle for low-plasticity silt.

The stress-strain behavior of the MRV silt can be normalized by effective consolidation pressure and effective confining pressure. As the OCR increased, the shear strength normalized by effective consolidation pressure increased. An *m* value of 0.58 was used to estimate the overconsolidated shear strength of low-plasticity silt using Equation 1 when the normally consolidated shear strength was known. Although this value should be verified with more testing data, it provides a means to relate the shear strength of low-plasticity silt to its OCR. However, Equation 10 cannot be used to relate normalized shear strength to OCR because there are large differences in the curve of S_u/σ'_c versus OCR among different silts, a characteristic that makes each unique.

The MRV silt can reach initial liquefaction under cyclic loading with a CSR no less than 0.18. With a CSR of 0.10, the specimen cannot liquefy. This work has presented the curve of CSR versus N_{cyc}.

6. POSTCYCLIC BEHAVIOR OF LOW-PLASTICITY SILT WITH FULL LIQUEFACTION

6.1. EXPERIMENTAL PROGRAM: FULL LIQUEFACTION

To investigate the postcyclic behavior of low-plasticity silt, various reconsolidation levels (U_r = 100%, 60%, 30%, and 0%) were achieved by controlling the dissipation time of excess pore pressure after the specimens were completely liquefied (R_u = 1),

Figure 6.1 shows the reconsolidation curves from the available specimens. Although the postcyclic monotonic shear tests on specimens MD2R and MD4R, which were used to replicate the tests MD2 and MD4 (see Section 4), did not succeed, their postcyclic reconsolidation curves were available and thus included in Figure 6.1. The CSRs of MD4 and MD4R were 0.35, and that of MF1 was less than 0.18, the other tests were conducted under cyclic loading with a CSR of 0.18. Figure 6.1 indicates that the time required to fully reconsolidate the specimens did not vary significantly ($t_{100} \approx 13$ min). This consistency confirms that the specimens prepared using the slurry consolidation method were identical, and the preparation method is reliable. Figure 6.1 shows the time required for various reconsolidation levels ($t_{30,}$ $t_{60,\text{ and}}$ t_{100}) for postcyclic monotonic triaxial compression tests.

Figure 6.2 shows the testing procedures via stress paths for cyclic and postcyclic monotonic tests with full liquefaction. The specimens were normally consolidated to 90 kPa. Cyclic loading continued until liquefaction (i.e., R_u = 1.0). After pore water pressure equalized, the specimens were allowed to reconsolidate to various degrees. Finally, the deviator stress was increased to failure, prompting the postcyclic behavior.

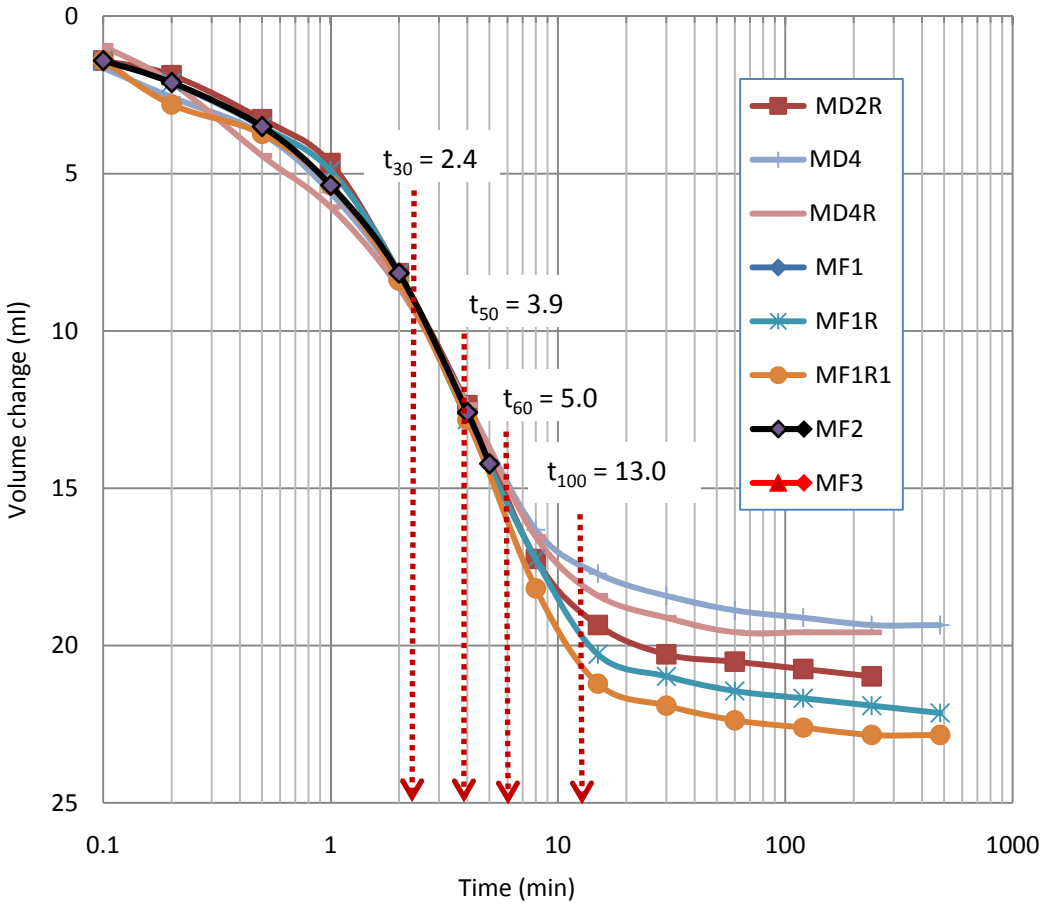

Figure 6.1 Time required to reach various reconsolidation levels after liquefaction (e.g., t_{30} indicates time for 30% reconsolidation)

6.2. VOLUME CHANGE DUE TO FULL RECONSOLIDATION

Soil fabric can change due to cyclic loading; therefore, permeability and compressibility varied for the MRV silt with and without previous cyclic loading. This section compares permeability and compressibility with and without previous cyclic loading.

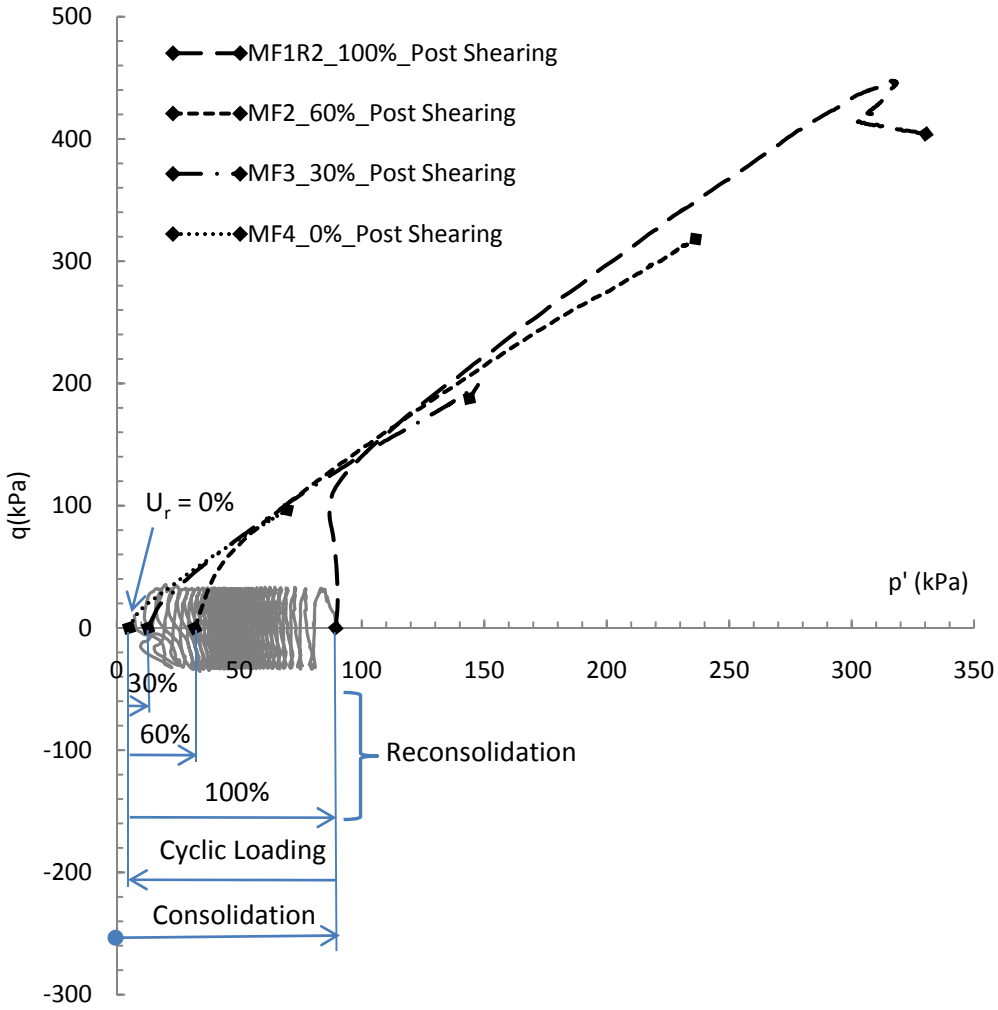

Figure 6.2. Testing procedures via stress paths to study postliquefaction behavior of MRV silt with various reconsolidation levels

6.2.1 Permeability. Permeability was compared before and after cyclic loading to study the effect of liquefaction on permeability. Permeability was computed as (Holtz and Kovacs, 2010):

$$k = \frac{a_v \rho_w g c_v}{1 + e_0} \tag{11}$$

where:

a_v – coefficient of compressibility, both prior to and after liquefaction, calculated in the σ'_c of 90 kPa

ρ_w – density of water,

g – gravity acceleration,

c_v – coefficient of consolidation, $c_v = TH_{dr}^2/t_{50}$,

H_{dr} – drainage distance (i.e. half of specimen height), and

T – time factor, equal to 0.197 for the 50% primary consolidation.

The above equation was applied from Terzaghi's one-dimensional consolidation theory, which assumes one dimensional drainage and compression. However, the specimen was consolidated under isotropic pressure, so one should be careful in the use of this value. It is only being used to compare the permeability of the specimen before and after liquefaction. The permeability prior to liquefaction (k) and after liquefaction (k') from five available tests was compared in Figure 6.3. Average permeability was 5.744×10^{-7} cm/s and 5.544×10^{-7} cm/s for the soil prior to and after liquefaction, respectively. The permeability remained essentially constant; therefore, cyclic loading had no significant effect on the permeability characteristics of the MRV silt. All permeability was within the same order of magnitude. However, Figure 6.3 indicates that the variation of k' was smaller than that of k, because the difference between the maximum permeability and the minimum permeability was greater for preliquefaction ($\Delta k = 2.85\times10^{-7}$ cm/sec) than for postliquefaction ($\Delta k' = 0.72\times10^{-7}$ cm/sec). The smaller variation of k' indicated a smaller difference in the soil fabric among specimens after liquefaction. The greater variation in permeability prior to liquefaction was induced by

the inevitable variations in procedures from one test to another. With cyclic loading, the soil grains were rearranged to similar microstructural state. It could be said that the process of liquefaction (R_u=1) reproduced a similar permeability for the different specimens. As noted by Thevanayagam et al. (2001), the soil is completely remolded during cyclic loading, and it behaves as a freshly deposited soil. Thevanayagam's group investigated the effect of liquefaction on the permeability of soil materials from sand (Foundry sand #55) to silt (Sil-co-sil#40). They reported the coefficient of consolidation instead of the permeability and found that the coefficient of consolidation prior to and after liquefaction were nearly the same at identical effective consolidation pressure.

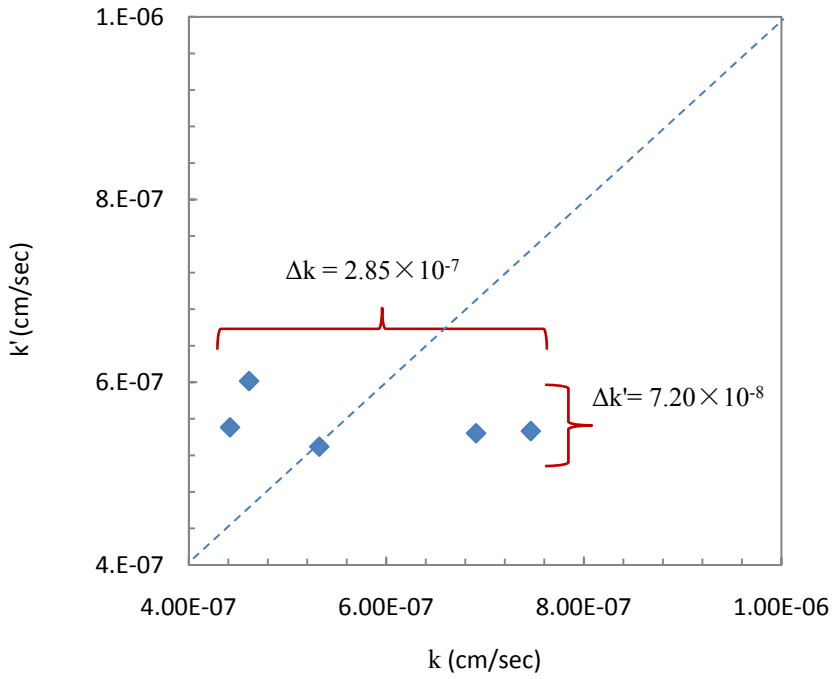

Figure 6.3. Comparison of the permeability of MRV silt before and after liquefaction

6.2.2 Compression and Recompression Indices. During reconsolidation, excess pore pressure was reduced from sustained excess pore pressure to 0 kPa. Excess pore pressure decreased by 5-10 kPa due to its equilibrium throughout specimens after liquefaction; thus, the excess pore pressure at the beginning of reconsolidation was 80-85 kPa. Correspondingly, the mean principal stress (p') increased from a range of 5–10 kPa to about 90 kPa during reconsolidation. In the meantime, the specimens became denser due to dissipation of excess pore pressure. Figure 6.4 shows the reconsolidation curves and includes all available reconsolidation data. The compression index (C_c) and recompression index (C_r) of the soil prior to liquefaction are 0.0896 and 0.0090, respectively, as indicated in Section 3. The slopes of the reconsolidation lines of the soil after liquefaction range from 0.0502 to 0.0604. Thus, they are much closer to the compression index than the recompression index. In Figure 6.4, therefore, the reconsolidation lines are more parallel to the compression line than to the recompression line.

Thevanayagam et al. (2001) presented similar findings for artificial soil mixtures of a sand and nonplastic silt. Likewise, Hyde et al. (2007) reported similar results for a creamy powdered limestone with 69.2% silt sized particles and a PI of 6. Thevanayagam et al. (2001) found that the postliquefaction reconsolidation line was nearly parallel to the compression line than to the recompression line. For a creamy powdered limestone, Hyde et al. (2007) found that the slope of postcyclic reconsolidation line was about 10 times steeper than that obtained from the precyclic recompression line and rather similar to that the compression line.

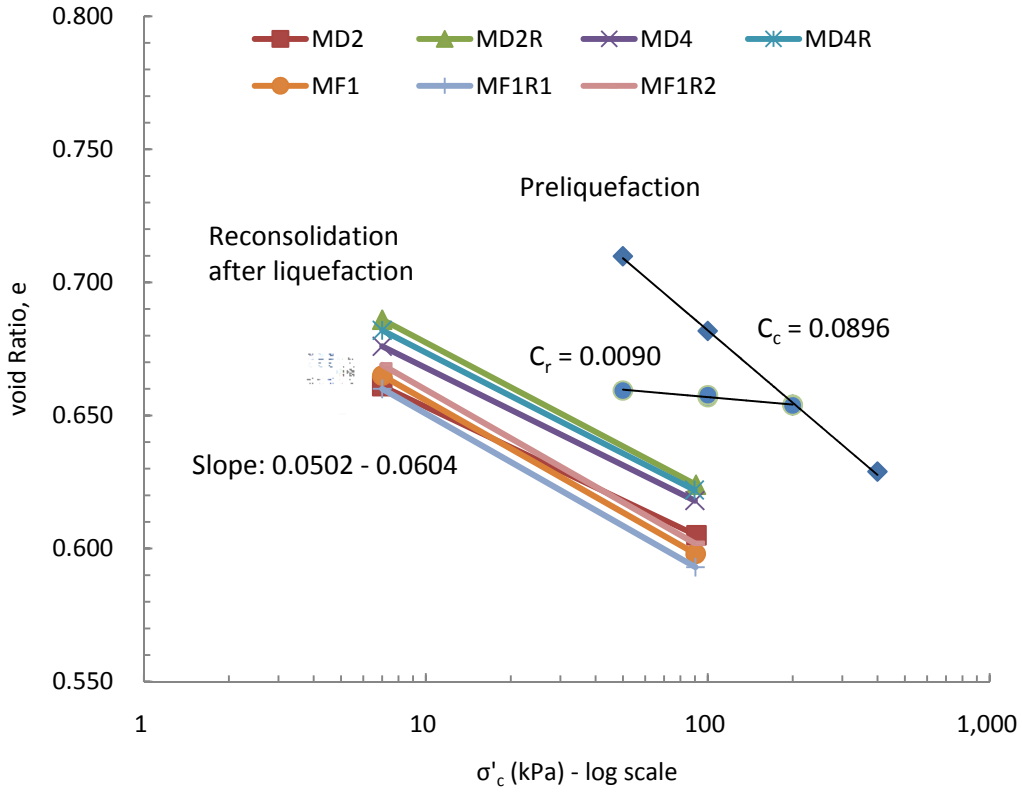

Figure 6.4. Reconsolidation curves of MRV silt after full liquefaction

On the other hand, some have reported opposite results for clays and plastic silts (Yasuhara and Andersen, 1991, Yasuhara et al., 1992; Hyodo et al., 1994; and Hyde et al., 1997). For example, Yasuhara and Andersen (1991) and Yasuhara et al. (1992) found that slopes of the reconsolidation lines after cyclic loading were as small as 1.5 times recompression index for Drammen clay with a PI of 27 and Ariake clays with PIs of 69 and 72. Hyde et al. (1997) observed that the slope of reconsolidation line of the Keuper Marl silt with a PI of 19 after cyclic loading was almost identical to that of recompression line without previously cyclic loading.

Thus, the effect of liquefaction on the compression index varies from one soil to another. However, previous research appears to indicate that the reconsolidation line after cyclic loading is more parallel to the compression line for sands and low-plasticity silts. The present research has verified this result for the MRV silt. For clays and high-plasticity silts, the reconsolidation line is more parallel to the recompression line. The consensus appears to be that the soil fabric of plastic soils is more difficult to change by cyclic loading than that of low-plasticity soils. The latter are more easily remolded during cyclic loading, and after liquefaction they tend to behave as freshly deposited soils. Section 8 discusses further the effect of plasticity in the change of consolidation parameters of MRV silt due to cyclic loading.

Figure 6.5 compares the compression and recompression indices of postliquefaction MRV silt with those of the preliquefaction MRV silt. The compression and recompression indices of the silt with previously cyclic loading were measured on the specimen that finished reconsolidation to recover effective confining pressure from 10 kPa to 90 kPa. After the effective confining pressure was recovered to 90 kPa, more effective confining pressure was provided incrementally to determine the compression and recompression indices. In Figure 6.5, the data points in the reconsolidation stage with effective confining pressure from 10 kPa to 90 kPa are aligned with the data points from 90 kPa to 360 kPa, suggesting that reconsolidation is actually a process of compression rather than recompression. The compression index (C'_c) and recompression index (C'_r) after liquefaction were respectively 0.0589 and 0.0071, and both were are smaller than those before liquefaction. Therefore, the compressibility of MRV silt decreases due to the change in fabric induced by cyclic loading, but still significant in compression range.

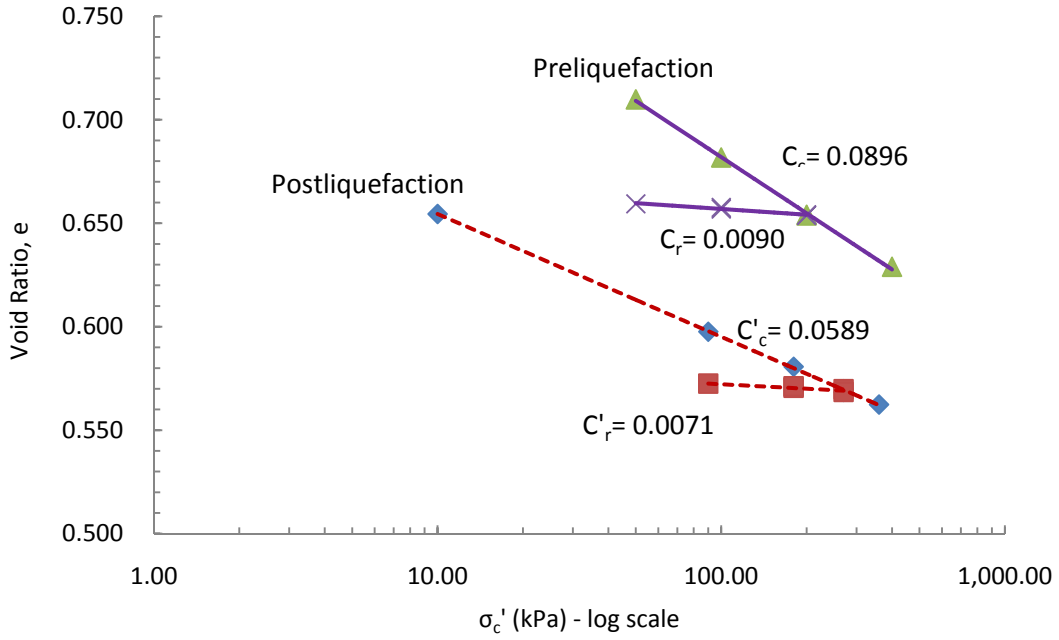

Figure 6.5. Comparison of compression and recompression indices before and after liquefaction of MRV silt

6.3. EFFECT OF CSR ON POSTLIQUEFACTION MONOTONIC BEHAVIOR

This section addresses the effect of CSR on the postcyclic monotonic shear behavior of the MRV silt. As indicated in Table 6.1, specimen MF1 with a CSR of less than 0.18 took 66.17 cycles of loads to liquefy; specimens MF1R1 and MF1R2, both with CSRs of 0.18, required an average of 29 cycles to liquefy; and specimen MD4 with a CSR of 0.35 required only one cycle to liquefy. All specimens induced identical excess pore pressures of about 90 kPa. However, the development of cyclic axial strain (ε_1) at the end of cyclic loading varied slightly, and there was no obvious relationship between axial strain and CSR.

Table 6.1. Summary of postliquefaction triaxial compression tests to investigate the effect of CSR on postliquefaction shear behavior

Test ID	B-value	σ'_c (kPa)	e	CSR	N_{cyc}	ε_{cyc} (%)	e'	Δe	ε_v (%)
MD4	0.940	90.0	0.676	0.35	1.15	11.09	0.618	0.058	3.57
MF1	0.948	90.6	0.665	<0.18	66.17	11.68	0.598	0.067	4.02
MF1R1	0.944	90.4	0.660	0.18	27.14	9.79	0.593	0.062	4.04
MF1R2	0.944	89.9	0.669	0.18	31.14	8.85	0.602	0.067	4.01

Note:

N_{cyc} – number of loading cycles;

ε – axial strain induced by cyclic loading

e' - void ratio after reconsolidation;

Δe – change of void ratio due to reconsolidation;

ε_v – volumetric strain due to reconsolidation, $\varepsilon_v = \Delta e/(1+e)$

Figure 6.6 shows the postcyclic behavior of all four specimens. For specimens with CSRs less than or equal to 0.18, the results of postcyclic shear tests produced curves demonstrating that deviator stress, excess pore pressure, and stress path were similar among all specimens. There was a slight drop in deviator stress at large deformation for specimens MF1, MF1R1, and MF1R2. Specimen MD4 with a CSR of 0.35 showed no obvious drop in deviator stress, which was slightly higher than that of other specimens at the end of tests. However, there was no significant difference in maximum deviator stress among the specimens. Thus, CSR has no significant effect on the postcyclic shearing behavior of MRV silt.

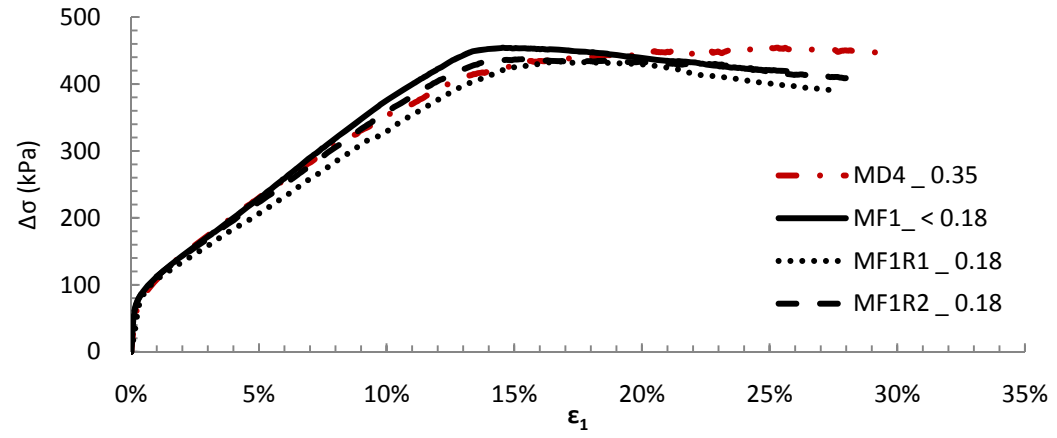

(a)

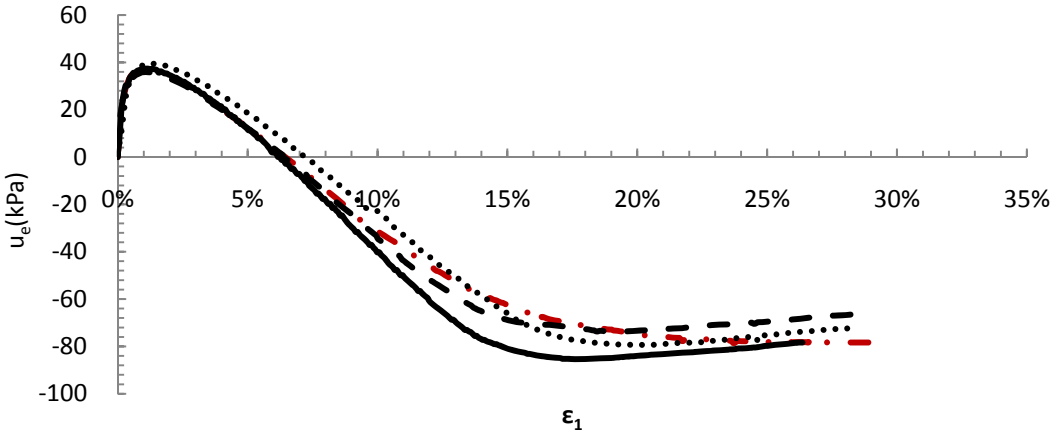

(b)

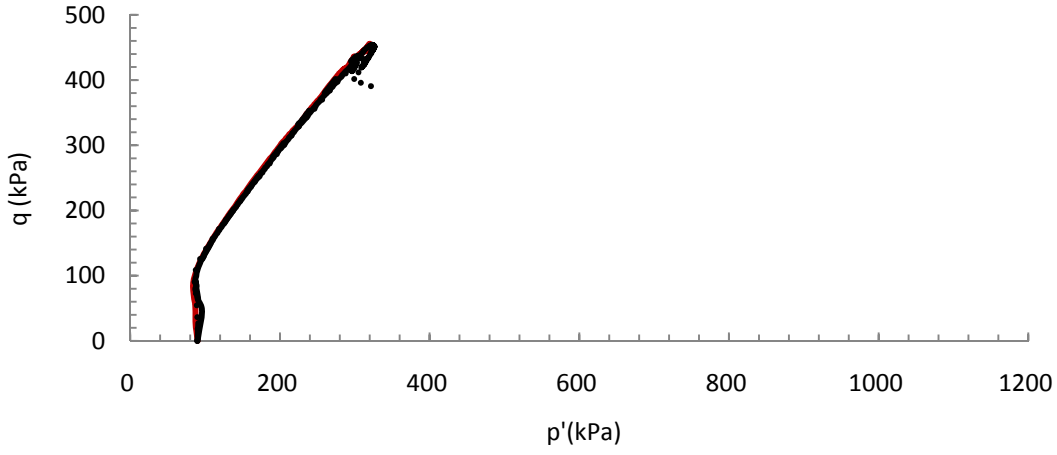

(c)

Figure 6.6. Postliquefaction monotonic shear behavior of MRV silt with full reconsolidation with various CSRs: (a) $\Delta\sigma$ vs. ε_1, (b) u_e vs. ε_1, (c) q vs. p'

Table 6.1 also shows the volumetric strain due to the reconsolidation after full liquefaction. Specimen MD4 had a slightly smaller volumetric strain than others, but the difference was not significant. This observation was similar to the behavior of sand tested by Chern and Lin (1994) and that of clay tested Yasuhara et al. (1992). Chern and Lin (1994) carried out postcyclic consolidation tests on loose, clean sand and silty sand and found that the reconsolidation volumetric strain was related to the residual pore pressure ratio developed during cyclic loading, regardless of the cyclic stress ratio or the number of loading cycles. Similarly, Yasuhara et al. (1992) concluded that the volumetric strains of Ariake clays with PIs of 69 and 72 were governed by the excess pore pressure ratio.

The results of the present study suggest that excess pore pressure after cyclic loading govern the postcyclic behavior of MRV silt (not initial density or confining pressure before cyclic loading). This finding can be explained by two factors affected by liquefaction and reconsolidation: One is the fabric of the soil, and the other is the density of the soil. On one hand, the liquefaction identically induced excess pore pressure of about 90 kPa for this work. The interlocking arrangement of soil particle was loosened to the same degree. On the other hand, the change of void ratio induced by reconsolidation was close, and so the density of specimens was close. These characteristics contributed to the similarity of postliquefaction behavior among specimens with various CSRs.

6.4. EFFECT OF RECONSOLIDATION LEVEL ON POSTLIQUEFACTION MONOTONIC SHEAR BEHAVIOR

This section describes the effect of reconsolidation level on postliquefaction undrained monotonic shear behavior. Once the desired reconsolidation level was

achieved for each test, the undrained triaxial compression was applied on the liquefied specimens, and the effects of reconsolidation level on the shear strength and stiffness were observed. Additionally, this work examined the apparent overconsolidation due to excess pore pressure induced by cyclic loading. Table 6.2 summarizes postliquefaction triaxial compression tests at various reconsolidation levels.

Table 6.2. Postliquefaction triaxial compression tests at various reconsolidation levels

Test ID	B-value	σ'_c (kPa)	e	CSR	N_{cyc}	U_r (%)	e'	Δe	ε_v (%)
MF1R2	0.944	89.9	0.669	0.18	31.14	100	0.602	0.067	4.0
MF2	0.945	90.7	0.657	0.18	27.16	60	0.615	0.042	2.5
MF3	0.947	90.5	0.663	0.18	30.14	30	0.637	0.026	1.6
MF4	0.948	90.3	0.659	0.18	28.14	0	0.659	0	0

6.4.1 Undrained Shear Behavior. Figure 6.7 shows the postliquefaction monotonic behavior of MRV silt after various reconsolidation levels. With full reconsolidation, specimen MF1R2 contracted initially then dilated continuously (Figure 6.7c). As indicated by the deviator stress-strain curve of the Figure 6.7a, the deviator stress reached a peak value of about 437 kPa at an axial strain of 14%. The deviator stress drops slightly after continued axial strain. On the other hand, the other three specimens dilated continuously until they reached the critical state at the axial strain larger than 25%.

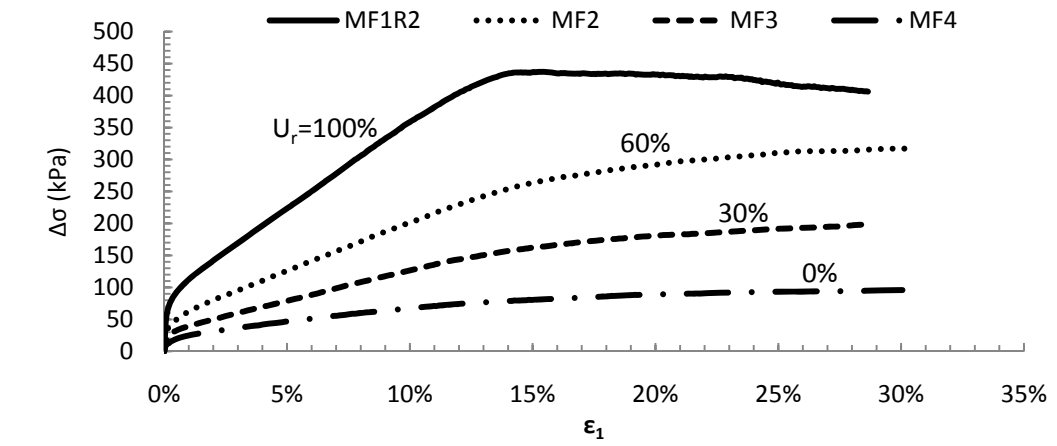

(a)

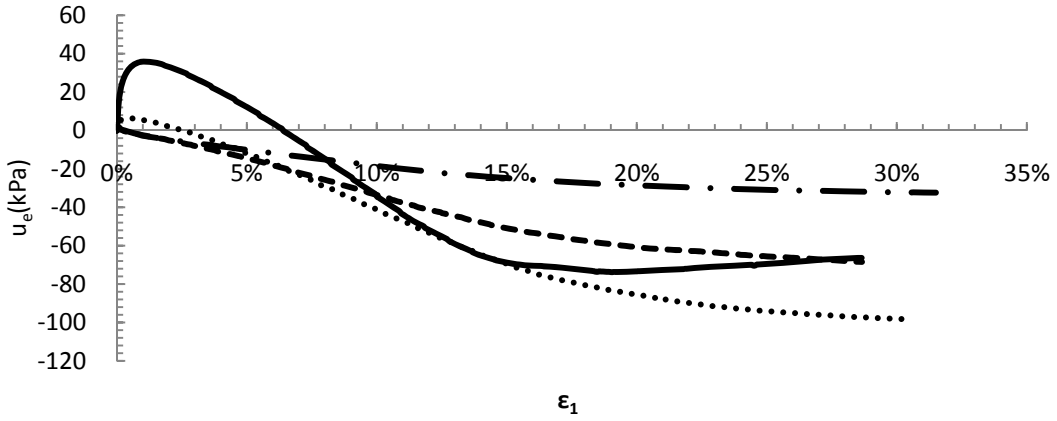

(b)

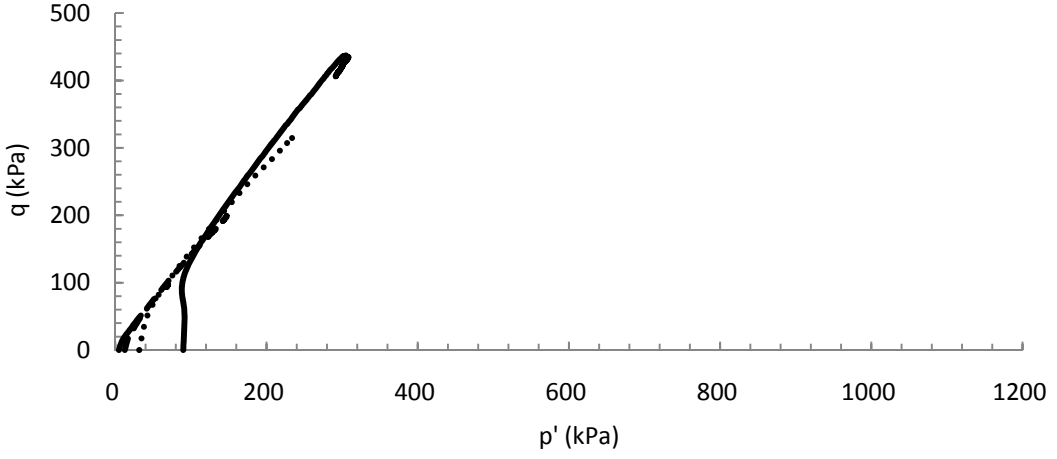

(c)

Figure 6.7. Postliquefaction undrained shear behavior of MRV silt under various reconsolidation levels after full liquefaction: (a) $\Delta\sigma$ vs. ε_1, (b) u_e vs. ε_1, (c) q vs. p'

Figure 6.7b shows the excess pore pressure response. A higher reconsolidation level resulted in a higher initial effective confining pressure at the beginning of postcyclic monotonic shearing. As a result, higher excess pore pressure occurred at the initial stage of the postliquefaction monotonic shearing. On the other hand, when the reconsolidation level was low, the initial effective confining pressure was low. Thus, the specimens with a low reconsolidation level dilated early. At the large deformation, however, all specimens dilated along the same failure line (Figure 6.7c), indicating that the reconsolidation level does not change the slope of the failure line (or the effective friction angle at this critical state).

6.4.2 Shear Strength and Stiffness at Small Deformation. As shown in Figure 6.7a, the slope of the curve of stress-strain clearly decreased at small strain (about 1%). At axial strain larger than 1%, the deviator stress increased almost linearly with an increase in axial strain until critical state. In this work, both shear strength and stiffness were addressed at small and large deformation separately. The shear strength and stiffness at small deformation were called as yield shear strength and initial stiffness, respectively; and the shear strength and stiffness at large deformation were called as undrained shear strength and secant modulus, respectively.

Figure 6.8 shows the method by which initial stiffness (E_i) and yield shear strength (S_y) were determined. The initial stiffness is the initial tangential modulus, which is in turn the slope of the curve of deviator stress versus axial strain at the axial strain of 0%. To get the yield shear strength, two tangential lines were plotted, as indicated in Figure 6.8. The yield shear strength was half of the deviator stress at an axial strain, in which those two tangential lines intersect (Wood, 1990).

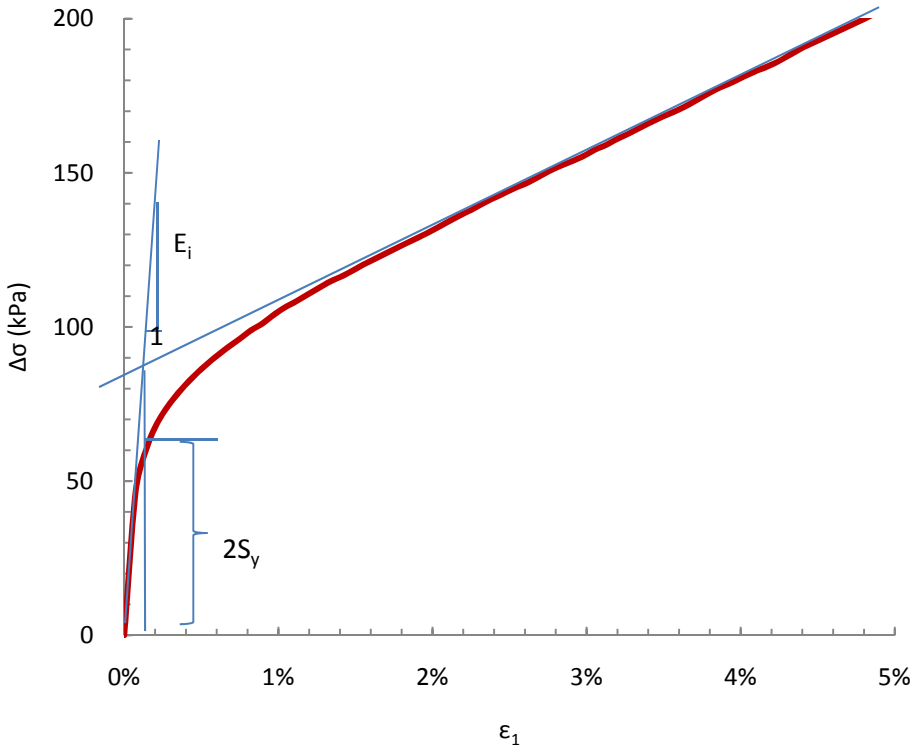

Figure 6.8. Determination of yield shear strength and initial stiffness

Figures 6.9 show the increase in initial stiffness and yield shear strength with an increase in reconsolidation level. To express the effect of reconsolidation level, Figure 6.10 shows the ratios of initial stiffness and yield shear strength, each at any reconsolidation, to those with no reconsolidation (i.e., $S_y/S_{y,\,Ur\,=\,0\%}$, and $E_i/E_{i,Ur\,=\,0\%}$). With full reconsolidation, yield shear strength and initial stiffness of the liquefied silt were as large as 6.25 times the yield shear strength and 5.91 times the initial stiffness of the liquefied silt with no reconsolidation, respectively. Thus, yield shear strength increased slightly more than initial stiffness due to reconsolidation.

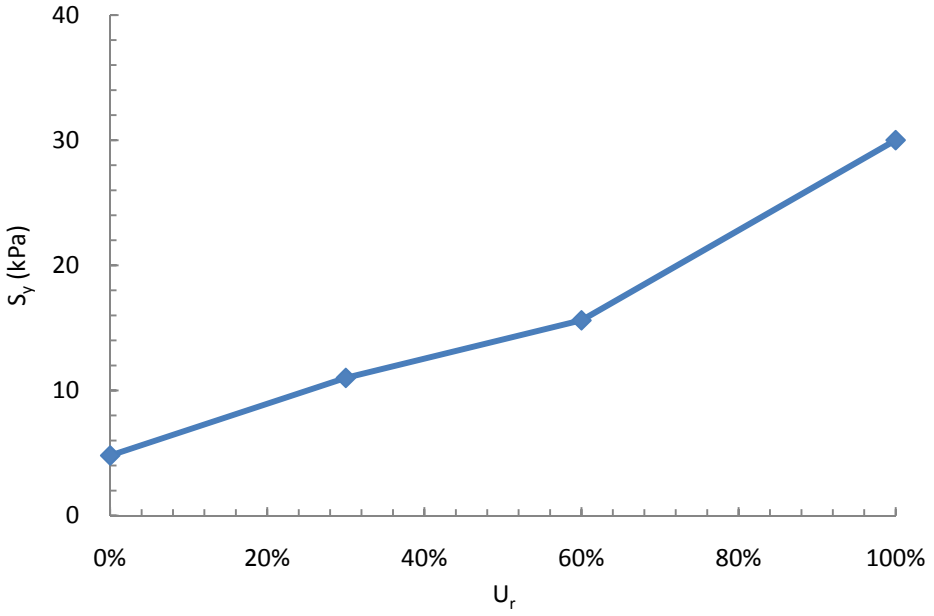

(a)

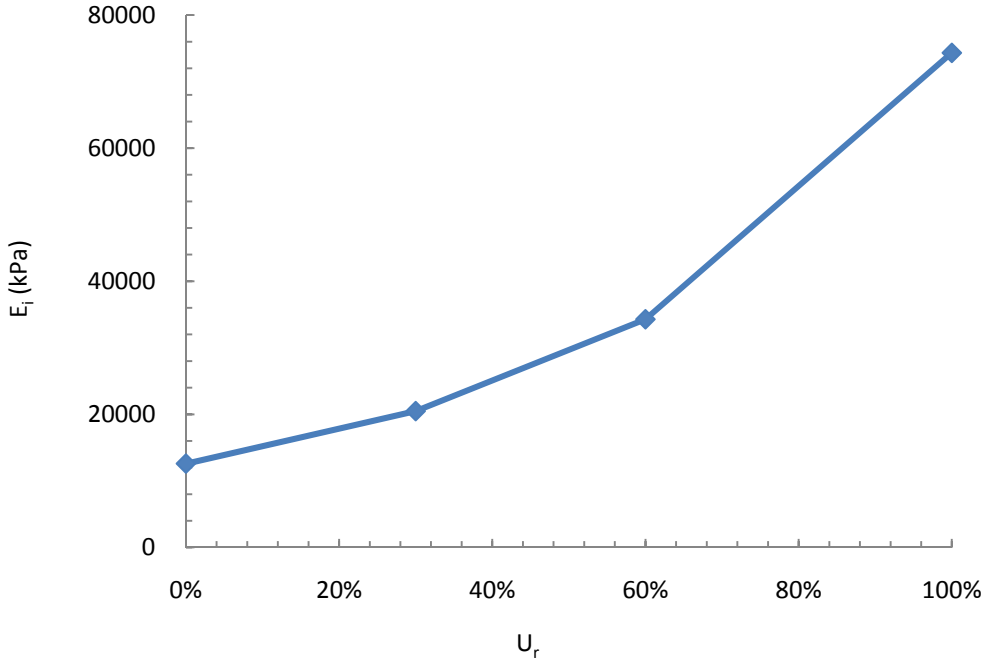

(b)

Figure 6.9. Variation in yield shear strength and initial stiffness with reconsolidation level: (a) S_y vs. U_r; (b) E_i vs. U_r

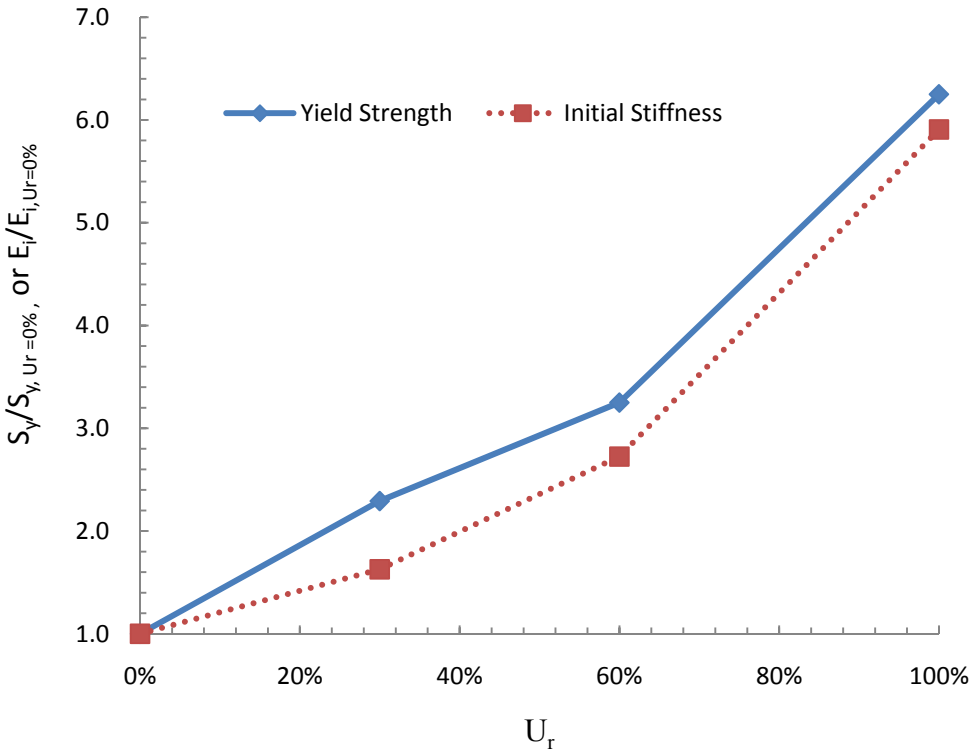

Figure 6.10. Recovery of yield shear strength and initial stiffness with reconsolidation

6.4.3 Shear Strength and Stiffness at Large Deformation. As shown in Figure 6.11, the undrained shear strength was determined to be half of the deviator stress at the critical state, at which there is no change in deviator stress with continued axial strain. The secant modulus is the ratio of deviator stress to axial strain, at which the deviator stress is equal to one half of deviator stress at critical state (Yasuhara et al., 2003). Raising the reconsolidation level increased the undrained shear strength and secant modulus of the liquefied silt (Figure 6.12). Similarly, like shear strength and stiffness at the small deformation, each of undrained shear strength and secant modulus at any

reconsolidation level was divided by the same parameter with no reconsolidation to express the effect of the reconsolidation level. As shown in Figure 6.13, the $E_i/E_{i,Ur = 0\%}$ increased as reconsolidation level increased. The same was true of the $S_y/S_{y,\ Ur\ =\ 0\%}$; however, the increase was not as great at an U_r of 100%. The undrained shear strength of the fully reconsolidated liquefied silt was 4.21 times larger than that of the unreconsolidated liquefied silt. The secant modulus of the fully liquefied silt was 5.34 times larger than that of the unreconsolidated liquefied silt.

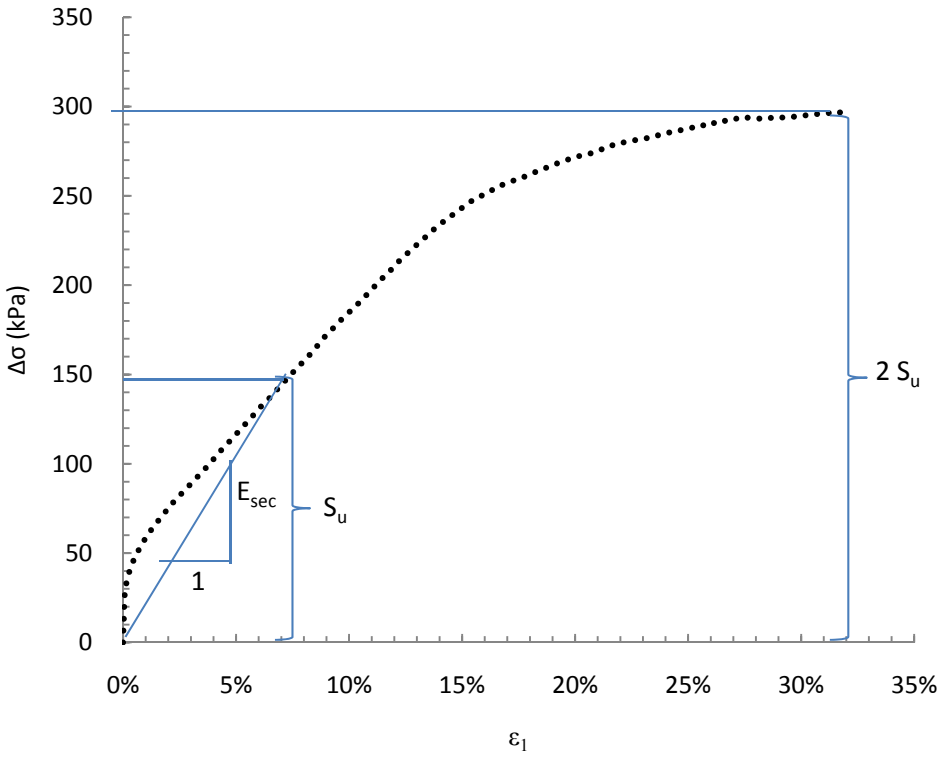

Figure 6.11. Illustration of determination of undrained shear strength and secant modulus

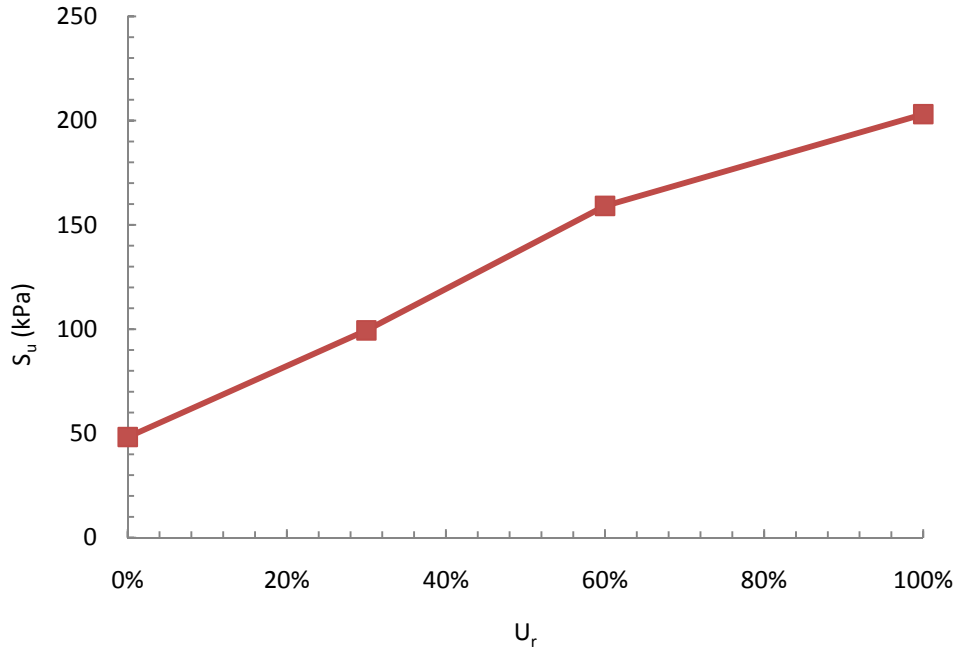

(a)

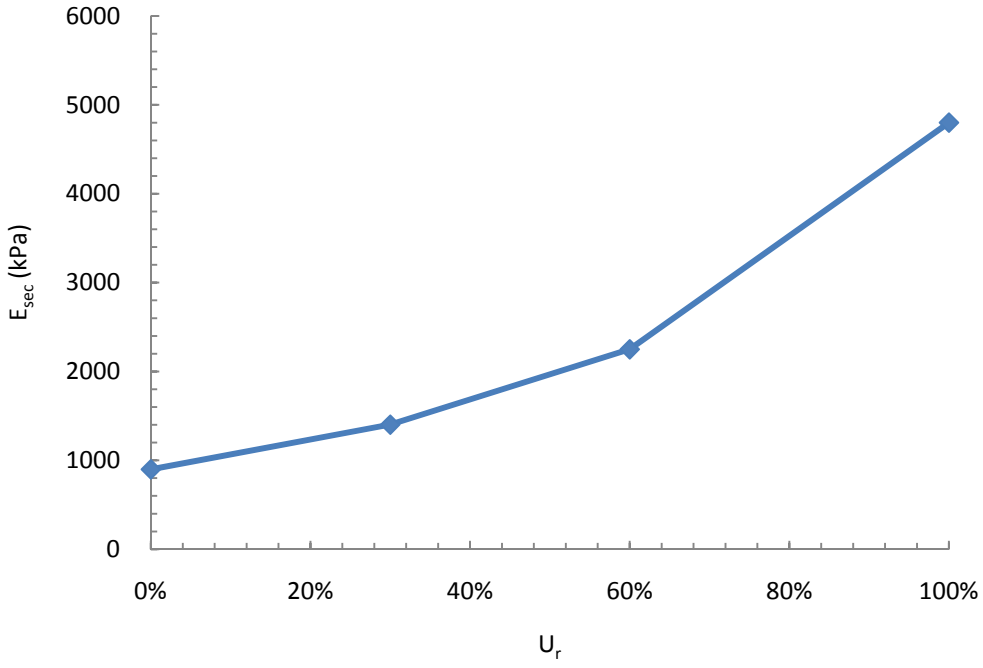

(b)

Figure 6.12. Variation in undrained shear strength and secant modulus with reconsolidation level: (a) S_u vs. U_r, (b) E_{sec} vs. U_r

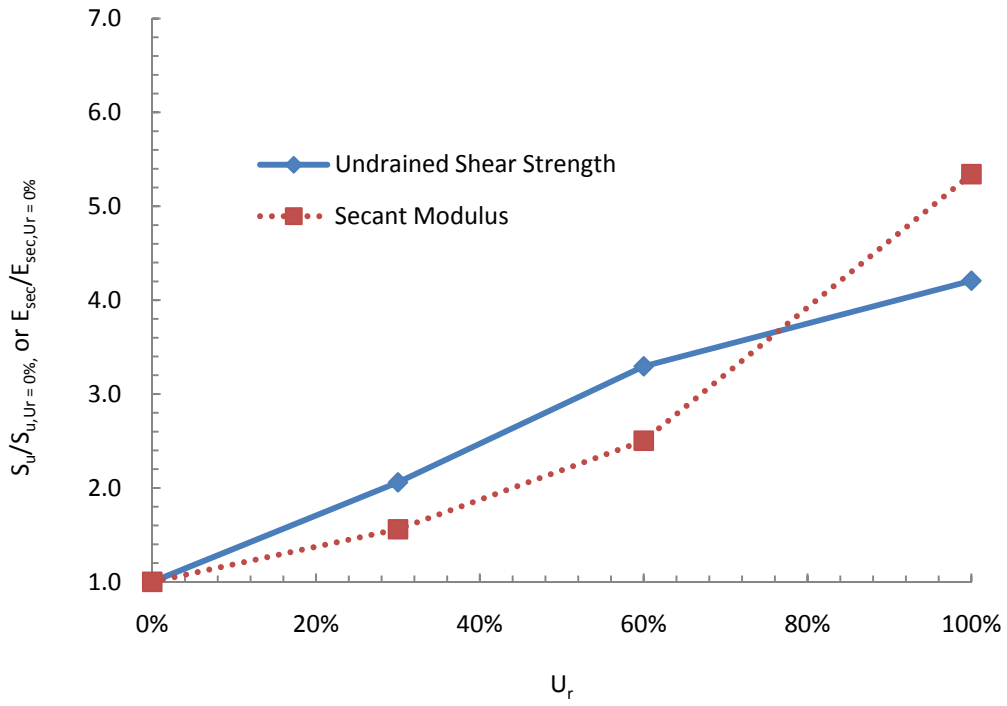

Figure 6.13. Recovery of undrained shear strength and secant modulus with reconsolidation

6.4.4 Apparent OCR. Several researchers have used the term apparent overconsolidation ratio (OCR_{app}) to study postcyclic undrained shear strength (Yasuhara et al., 2003; Soroush and Soltani-Jigheh, 2009; Ashour et al., 2009). This OCR_{app} is defined as the ratio of initial effective consolidation pressure (σ'_c) before cyclic loading to effective confining pressure (σ'_3) at the beginning of postliquefaction shearing. It is induced by excess pore pressure during cyclic loading. This work computed the OCR_{app} for the MRV silt with various levels of reconsolidation (Figure 6.14). As reconsolidation level increased, the OCR_{app} decreased because the effective confining pressure increased as excess pore pressure decreased.

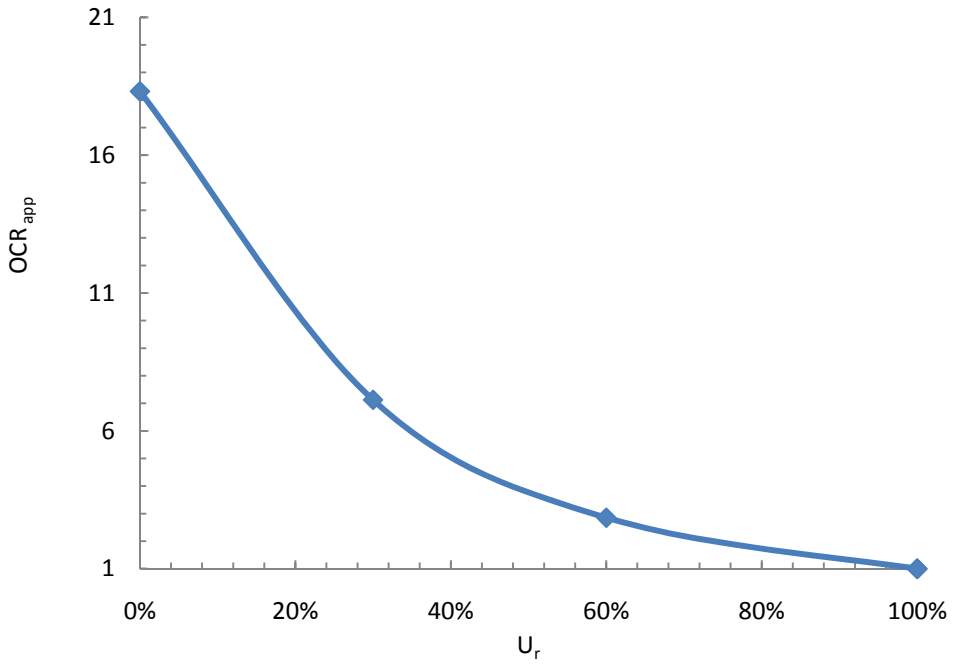

Figure 6.14. Variation in apparent overconsolidation ratio with reconsolidation level

The undrained shear strength (S_u) was normalized by the effective confining pressure at the beginning of postcyclic shearing. Figure 6.15 shows the effect of OCR_{app} on the normalized shear strength (S_u/σ'_3) of the tested silt. The normalized shear strength ratio $((S_u/\sigma'_3)_{OC}/(S_u/\sigma'_3)_{NC})$ is defined as the ratio of the normalized shear strength of the overconsolidated specimen to that of the normally consolidated specimen. For a comparison, Figure 6.15 also shows the normalized shear strength ratio $((S_u/\sigma'_c)_{OC}/(S_u/\sigma'_c)_{NC})$ of the silt for static triaxial tests described in Section 5. It should be noted that undrained shear strength was defined as half of deviator stress at an axial strain of 15% in Section 5. Here, for comparison, half of the deviator stress at the critical state is defined instead as the undrained shear strength.

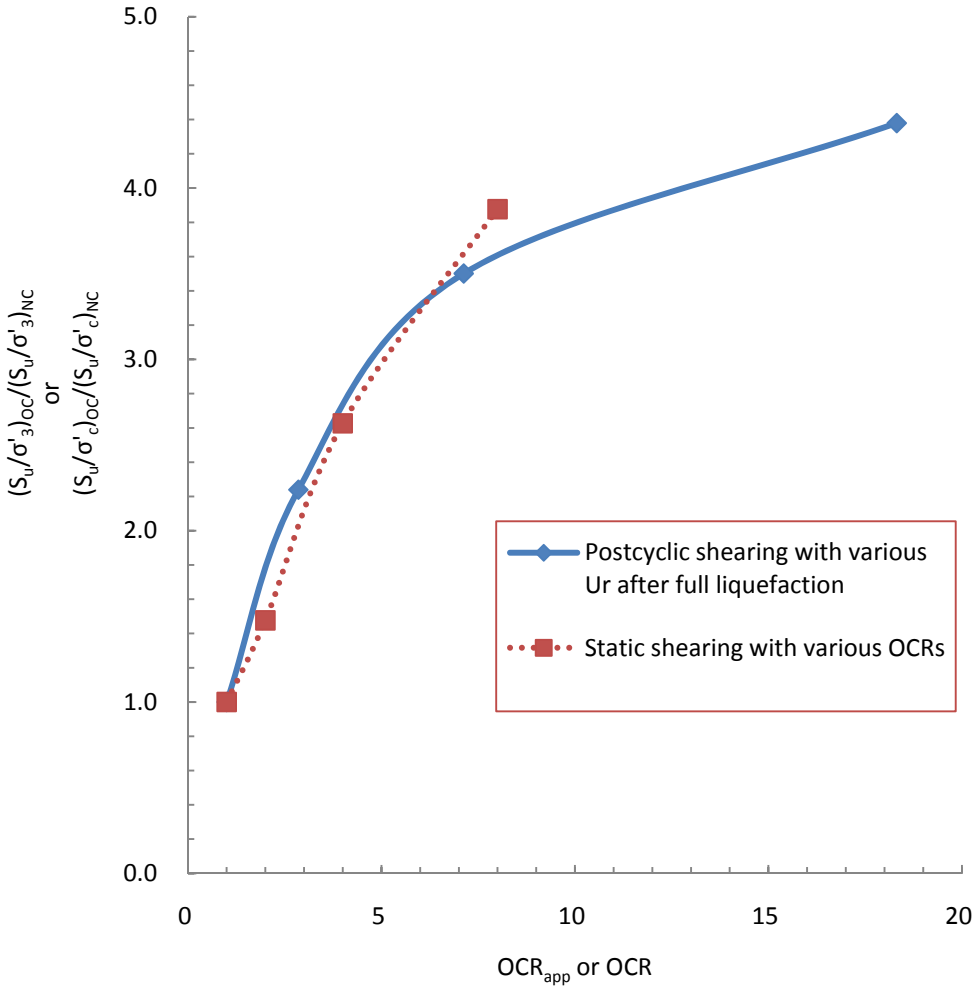

Figure 6.15. Effect of OCR or OCR_{app} on the normalized undrained shear strength

Figure 6.15 indicates no significant difference between the static and postcyclic monotonic test in the variation in the normalized shear strength ratio with the OCR or OCR_{app}. Thus, the OCR and OCR_{app} have the same effect on the increase in normalized shear strength ratio. With identical effective consolidation pressure, overconsolidation produces the same increase in undrained shear strength regardless of how the

overconsolidation condition was developed. Actually, the OCR and OCR_{app} represent two different overconsolidation processes. The OCR is formed by reducing cell pressure while keeping pore pressure constant so that the effective consolidation pressure is reduced from OCR × σ'_c to σ'_c. Conversely, the OCR_{app} is formed by increasing pore pressure while keeping cell pressure constant to change effective consolidation pressure. In other words, the OCR and OCR_{app} just represent two different ways to produce overconsolidation, and they have the same effect on normalized shear strength ratio. For the OCR_{app}, however, soil was loaded dynamically and liquefied.

6.5. COMPARISON WITH MONOTONIC SHEAR BEHAVIOR

6.5.1 Undrained Stress-strain Behavior. Figure 6.16 compares postcyclic monotonic behavior of the liquefied silt to that of the silt without previous cyclic loading. The static test on static specimen (MS2) had a slightly drop of deviator stress after initial peak point, indicating a quasi-steady state, but specimens with previous cyclic loading (MF1R2 and MF4) showed continuous strain-hardening behavior. The undrained shear strength of the liquefied specimen MF4 was lower than that of specimen MS2 without previous cyclic loading. Specimen MF4 was compressed monotonically with no reconsolidation after its liquefaction; therefore, the specimen did not become dense and had a void ratio relatively close to that of specimen MS2. However, specimen MF4 had a lower initial effective confining pressure than the static specimen MS2 due to the remaining excess pore pressure induced by cyclic loading. Thus, the specimen MF4 was less stiff at the early stage. Although specimen MF4 dilated continuously with deformation, its undrained shear strength was not identical to that of specimen MS2.

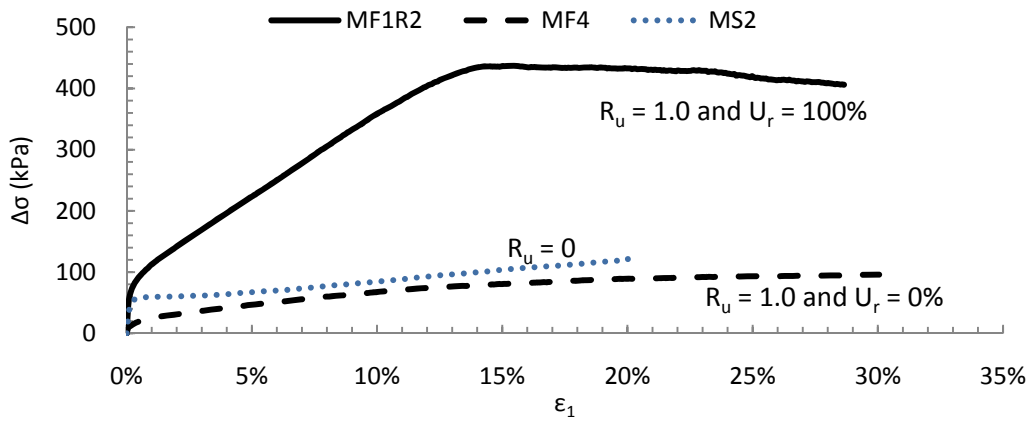

(a) $\Delta\sigma$ vs. ε_1

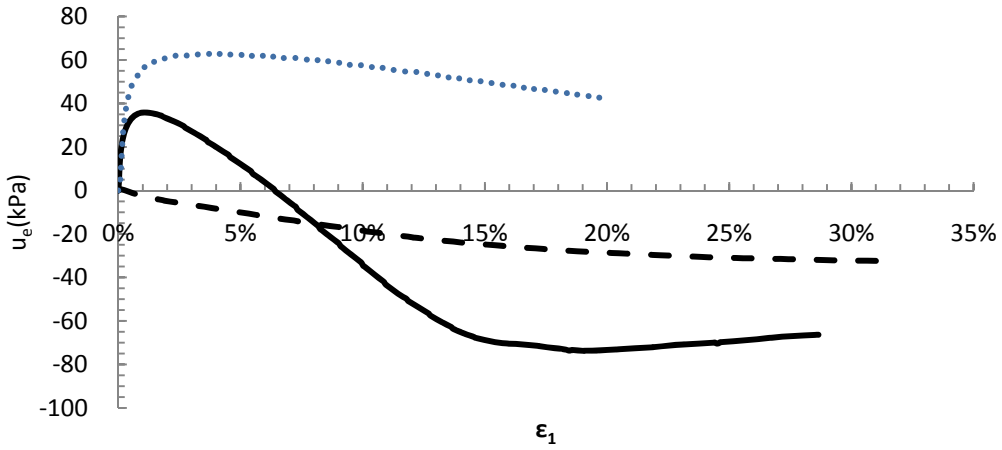

(b) u_e vs. ε_1

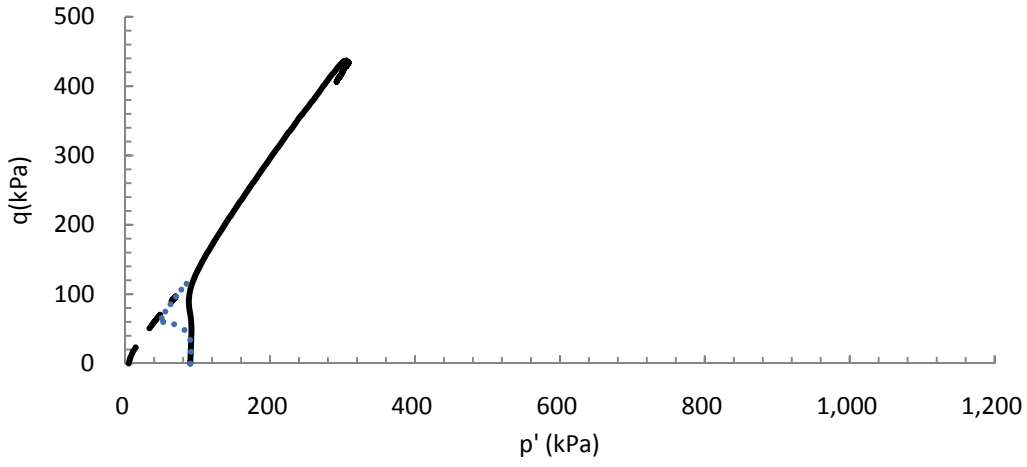

(c) q vs. p'

Figure 6.16. Comparison of undrained stress-strain behavior of MRV silt with and without liquefaction: (a) $\Delta\sigma$ vs. ε_1, (b) u_e vs. ε_1, (c) q vs. p'

It is believed that the damage of the soil fabric due to cyclic loading is attributable to the reduced undrained shear strength. Such limited recovery of deviator stress with deformation is also indicated in the work of Yasuhara et al. (2003), who studied the postcyclic degradation of strength and stiffness for low-plasticity silt with a PI of 19.7. The undrained shear strength cannot be recovered completely.

With full reconsolidation, specimen MF1R2 gained undrained shear strength about 4 times that of the static specimen MS2. Although the interlocking of soil particles in specimen MF1R2 was weakened by cyclic loading, its void ratio was largely decreased due to reconsolidation (Table 6.2). The decrease in the void ratio is attributable to the large increase in the undrained shear strength.

6.5.2 Critical State Line. Figure 6.17 is a plot of the CSL of the liquefied specimens against that of static specimens with no previous cyclic loading. To provide more data points, the plot includes specimens MF1 and MF1R1. The CSL of the liquefied specimens is not parallel to that of the soil specimens without previous cyclic loading, suggesting that the CSL of the MRV silt may change as the soil fabric changes due to cyclic loading, and that no unique CSL exists for the MRV silt.

The CSL of the postliquefaction soil in Figure 6.17 is not parallel to its NCL, confirming that the MRV silt behaves like sand, displaying one aspect of the unique static behavior described in Section 5. Figure 6.17 also shows that, in the tested range of mean effective principal pressure, the CSL of the silt after liquefaction is below that before liquefaction because the void ratio of the specimens was reduced due to reconsolidation. The soil weakening is also indicated by the variation of undrained shear strength with void ratio shown in Figure 6.18. For soil specimens both with and without cyclic loading,

undrained shear strength decreased as the void ratio increased. However, the undrained shear strength of the liquefied specimens decreased more quickly than that of the specimens without liquefaction. With an identical void ratio > 0.570, the liquefied specimens had lower undrained shear strength than the specimens without liquefaction. When the void ratio became higher and the silt was looser, the difference in the undrained shear strength grew. When the void ratio was < 0.570, however, there tends to be little difference in undrained shear strength of the soil before and after liquefaction. Thus, cyclic loading has no effect on undrained shear strength when the MRV silt is dense.

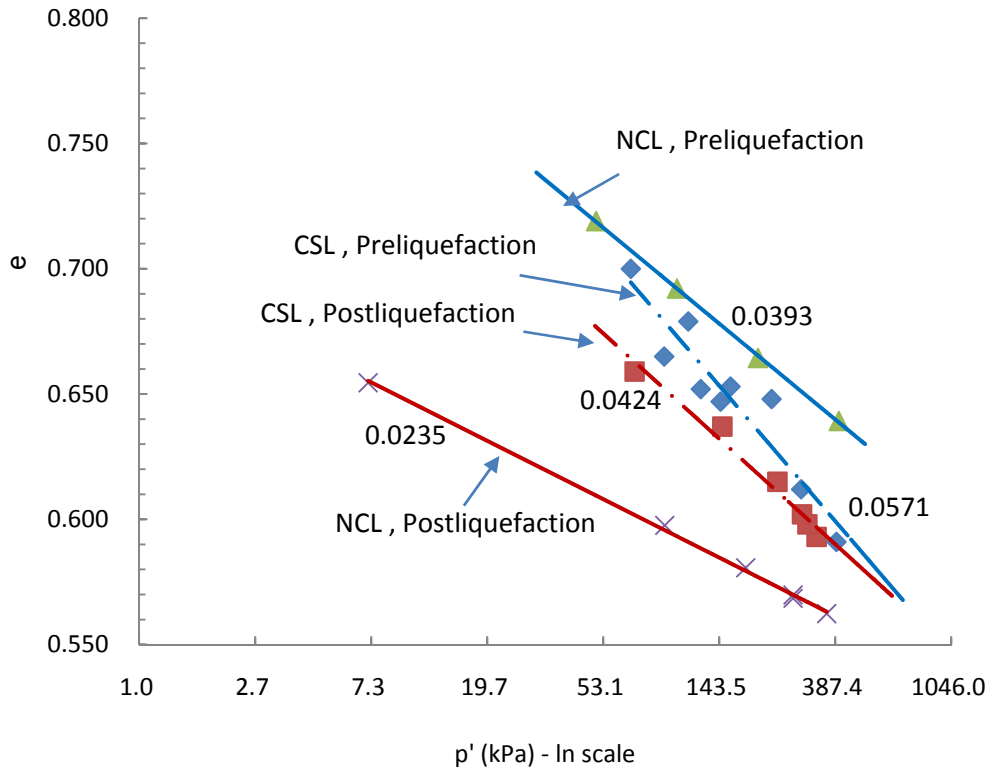

Figure 6.17. Critical state lines of MRV silt prior to and after liquefaction (the value next to each line is the slope)

6.6. DISCUSSION

6.6.1 Void Ratio Change and its Role. Reconsolidation makes excess pore pressure dissipate in the liquefied soil, which then becomes denser. The reduction in void ratio may contribute to an increase in undrained shear strength, as indicated in Figure 6.18. For example, silt with a void ratio of 0.60 had an undrained shear strength of about 195 kPa, as about 4.2 times the 46 kPa of the undrained shear strength at the void ratio of 0.66. On the other hand, a large change in void ratio can induce large volumetric deformation after reconsolidation. The field consequences are large settlements under buildings and earth structures.

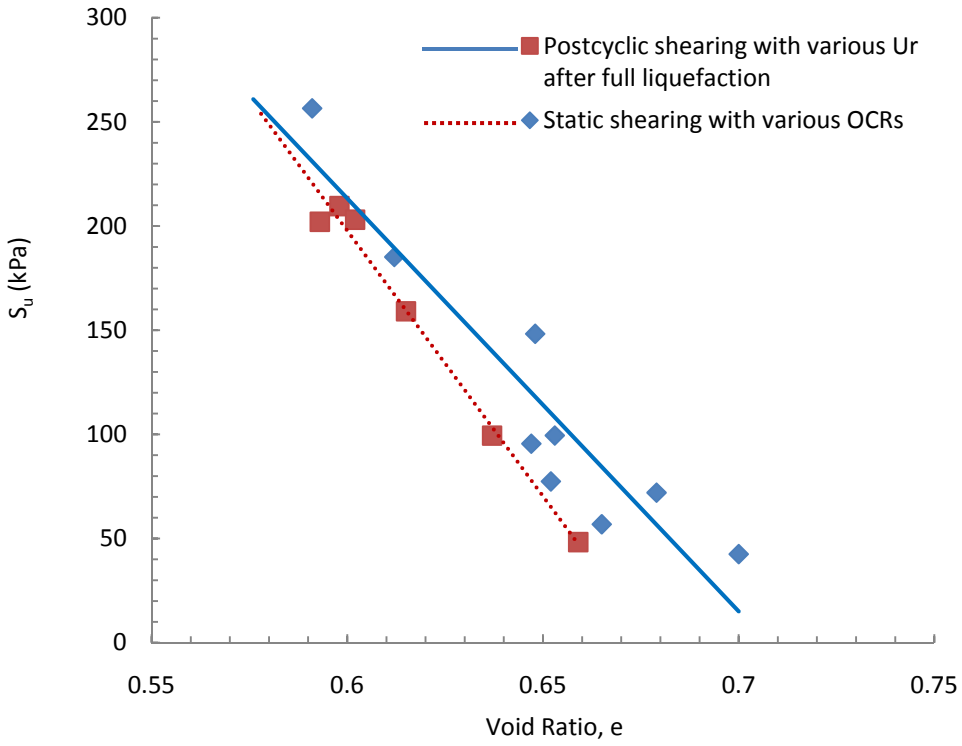

Figure 6.18. Variation in undrained shear strength of MRV silt with void ratio prior to and after liquefaction

Compared to silt without previous cyclic loading, liquefied silt has no decrease in undrained shear strength if the silt is dense enough (Figure 6.18). Porcino and Caridi (2007) studied the postliquefaction response of Ticino sand and reported that the cyclic resistance of dense sand specimens after liquefaction remains practically unchanged after a new cyclic loading. Although this project did not examine the reliquefaction characteristics of the MRV silt, it is reasonable to suppose that the liquefaction resistance of dense MRV silt decreases less than that of loose MRV silt due to previous cyclic loading.

6.6.2 Critical State Line. Although the fabric of the silt was damaged by cyclic loading and the liquefied silt had lower undrained shear strength than the original silt at the identical void ratio, the reduction in void ratio due to reconsolidation played a significant role in increasing the undrained shear strength of the tested silt. Without reconsolidation, undrained shear strength decreased due to fabric modification. This response contradicts to the concept of critical state, indicating that various soils have the same undrained shear strength at the large deformation and a unique critical state regardless of the difference in initial fabric of the soil. This is not true for MRV silt. The fabric change due to liquefaction is probably attributable to the different critical state of the tested silt. As indicated by Seed (1987), Vaid and Chern (1985), Stark and Mesri (1992) and others, the CSL may be influenced by the shear mode, effective confining pressure, and sample preparation method, all of which may vary the arrangement of soil grains (or fabric).

Further study of Figure 6.17 suggests that the data points for postliquefaction monotonic tests can be fitted with a straight line in semi- logarithmic space more easily

than those for static tests. A reasonable explanation for this phenomenon is that the fabric of liquefied soil specimens is more similar than that of static specimens without previous cyclic loading. During liquefaction, the soil skeleton is completely remolded, and soil behaves as if it has been freshly deposited (Thevanayagam et al. 2001).

6.6.3 Drainage for Reconsolidation. The required conditions for reconsolidation are the drainage of water and the dissipation of excess pore pressure. These are controlled by the permeability of soil, the length of the drainage path, and the drainage boundary. As indicated by Figure 6.3, the permeability of MRV silt is slightly different prior to and after liquefaction.

The MRV silt specimens tested here were about 5.0-inch high after liquefaction and required only about 13 minutes to fully reconsolidate. Thus, undrained shear strength can be recovered quickly after liquefaction. Certainly, the reconsolidation time also depends on the boundary and length of drainage path. If there are few or no permeable soil layers above and below an MRV silt layer in the field, dissipation of excess pore pressure and reconsolidation the liquefied silt layer take more time. Besides the reduced undrained shear strength in the liquefied silt layer, the high excess pore pressure may produce a crack or gap in the deposit. If this happens in an earth dam, the dam may fail. The 1965 seismic failures of Chilean tailings dams indicated that the cores of several dams liquefied first, and excess pore pressure and erosion of the flowing material widened the gap in the dam deposit (Dobry and Alvarez, 1967). The dam cores were made of tailings with diameters of 87.5-100% smaller than 0.075 mm, making them a kind of silt, according to the USCS soil classification. Thus, the good drainage flow may reduce the risk of earth dam failure.

Additionally, the big increase in the undrained shear strength due to full reconsolidation after liquefaction may provide a method to improve the soil for ground mitigation. As noted by Thevanayagam et al. (2001), an installation of supplementary wick drains can help relieve excess pore pressure developed during dynamic compaction and stone column installation in silty soils. With the installation of supplementary wick drains in low-plasticity silts, cyclic loading is applied to induce liquefaction and thus to allow full reconsolidation. The MRV silt can gain considerable undrained shear strength by using the mitigation techniques, such as blasting (Towhata, 2008).

6.7. SUMMARY

Based on an analysis of the results of triaxial tests on MRV silt with various reconsolidation levels after full liquefaction, this study supports the following findings:

There was no significant difference in permeability between before and after liquefaction. However, cyclic loading remolded the specimens and produced similar permeability among specimens due to the more consistent soil fabric after liquefaction. In the $e\text{-}log\sigma'_c$ space, the data points for reconsolidation are on the same straight line as those for the compression of the liquefied silt, suggesting that reconsolidation behaved like a process of compression rather than recompression. Cyclic loading made the MRV silt less compressible because the compression and recompression indices were reduced to a point below those for silt without previous cyclic loading.

The CSR for cyclic loading had no effect on volumetric strain due to reconsolidation and postcyclic shear behavior. They were governed by excess pore pressure rather than CSR.

The shear strength and stiffness of MRV silt with both small and large deformation increased with an increase in the reconsolidation level. For small deformation, yield strength always increased more than initial stiffness with an increase in reconsolidation level. For large deformation, however, undrained shear strength and secant modulus increased significantly for low and high reconsolidation levels, respectively. The failure line (or effective friction angle) in the stress space was not changed by cyclic loading.

The MRV silt specimens had lower OCR_{app} with higher reconsolidation levels after liquefaction. The normalized shear strength ratio increased with increasing OCR_{app}. The relationship of the normalized shear strength ratio to OCR_{app} after liquefaction was almost identical to that for specimens with no cyclic loading.

Compared to specimens subjected to static triaxial test without previous cyclic loading, the specimen with no reconsolidation after liquefaction had lower undrained shear strength. With a reduction in void ratio, a specimen with full reconsolidation gained undrained shear strength as high as about 4 times that of a specimen without previous cyclic loading.

Specimens with and without previous cyclic loading had different CSLs. With identical void ratio, the undrained shear strength of soil with previous cyclic loading was lower than that of soil without previous cyclic loading. When the void ratio increased, the difference in undrained shear strength without and with cyclic loading grew larger. However, with a void ratio less than 0.57, there tends to be no reduction in undrained shear strength.

7. POSTCYCLIC BEHAVIOR OF LOW-PLASTICITY SILT WITH LIMITED LIQUEFACTION

7.1. EXPERIMENTAL PROGRAM: LIMITED LIQUEFACTION

This section investigated the effect of limited liquefaction on monotonic shear behavior of low-plasticity silt. When the desired liquefaction level (i.e., excess pore pressure ratio, R_u) of 0.85, 0.70, or 0.35 was reached, cyclic loading was stopped and the deviator stress was slowly reset to zero. Two sets of tests were conducted. Figure 7.1 shows the testing procedures via stress paths for these two sets of tests, during which the CSR remained at 0.18.

The first set of specimens (ML1, ML2, and ML3) was dynamically loaded at various liquefaction levels, then fully reconsolidated, and finally sheared monotonically in undrained conditions (see Figure 7.1a). Section 7.2 describes this first series of tests.

The second set of specimens (ML4, ML5, and ML6) was also dynamically loaded at various liquefaction levels, but they were not reconsolidated. Instead, undrained shearing took place once excess pore pressure reached equilibrium (see Figure 7.1b). Section 7.3 describes this series of tests.

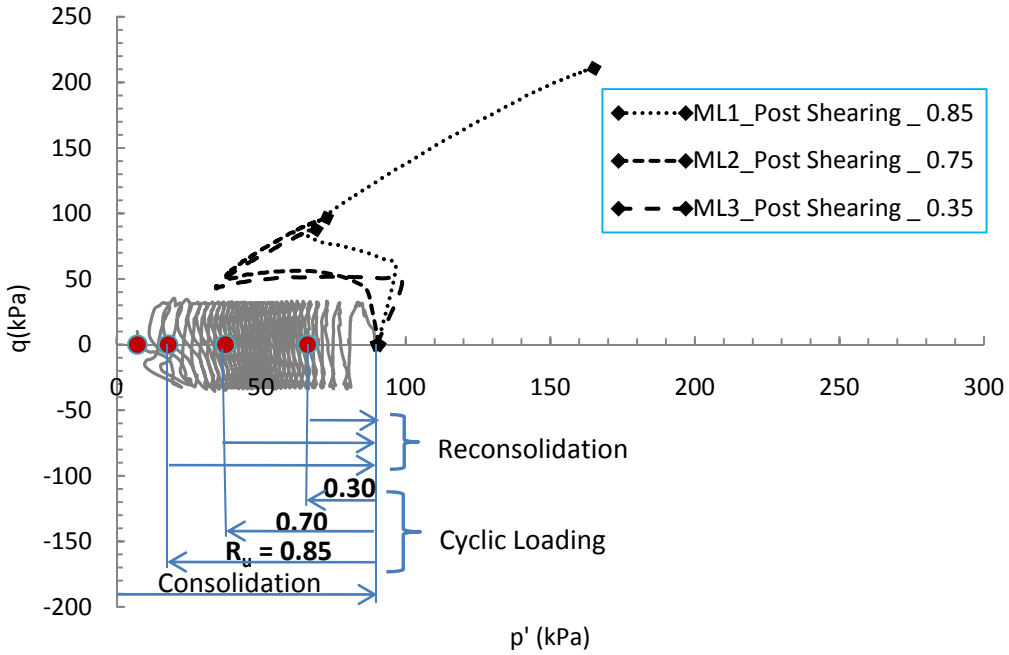

(a)

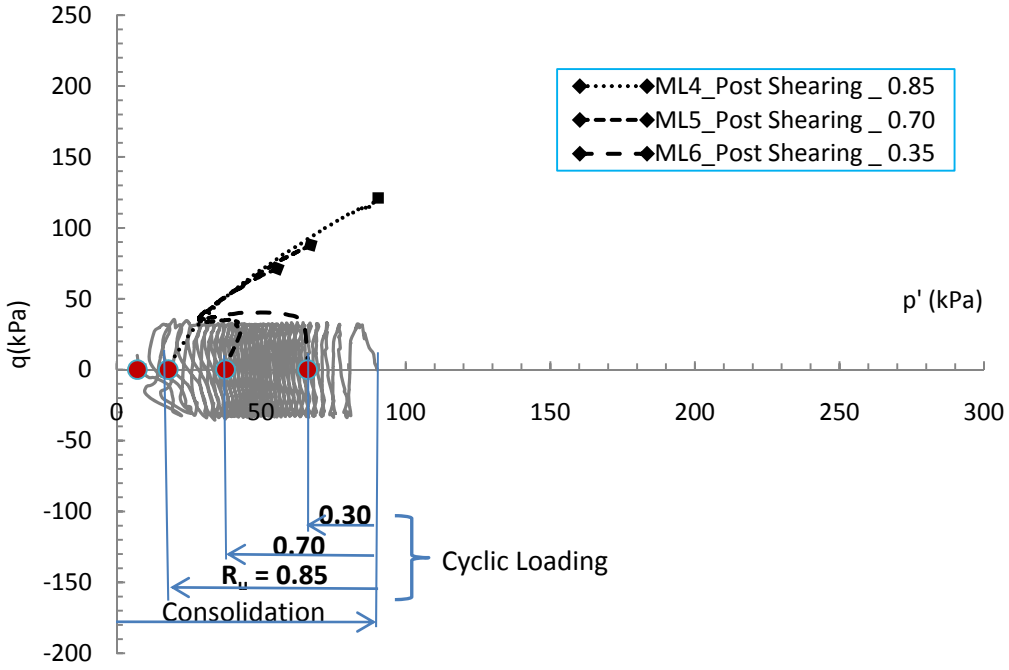

(b)

Figure 7.1. Testing procedures via stress paths to study postcyclic behavior of MRV silt with limited liquefaction: (a) with full reconsolidation, (b) with no reconsolidation

7.2. POSTCYCLIC SHEAR BEHAVIOR WITH FULL RECONSOLIDATION

If the drainage conditions are good, excess pore pressure can dissipate quickly so that soil structure in the field tends to shear after full reconsolidation. Table 7.1 lists the tests conducted to study the effect of liquefaction level on the postcyclic monotonic behavior of the MRV silt with full reconsolidation after cyclic loading. For comparison, this table provides information on both the fully liquefied specimen MF1R2 (with a R_u = 1.0) and the static specimen MS2 (with no liquefaction). Thus, the specimens with liquefaction levels ranging from 0 to 1.0 can be compared.

Table 7.1. Summary of triaxial tests of MRV silt with full reconsolidation after various liquefaction levels

Test ID	B-value	σ'_c (kPa)	e	N_{cyc}	R_u	$u_{e,\,cyc}$	e'	ε_v (%)
MF1R2	0.94	89.9	0.669	31.14	1.00	89.9	0.602	*4.0*
ML1	0.93	90.5	0.653	26.18	0.85	76.9	0.621	*1.9*
ML2	0.93	91.1	0.674	22.15	0.70	63.4	0.666	*0.5*
ML3	0.94	90.7	0.662	6.22	0.35	27.2	0.660	*0.1*
MS2	0.98	90.0	0.679	0	0	0	0.679	*0*

Note: $u_{e,cyc}$ – excess pore pressure induced by cyclic loading

7.2.1 Undrained Shear Behavior. Figure 7.2 shows deviator stress, excess pore pressure, and stress paths for the monotonic loading after limited liquefaction. At about 25% axial strain, all specimens except MF1R2 reached the critical state at a constant deviator stress. Clearly, except for static specimen MS2, the specimen with greater

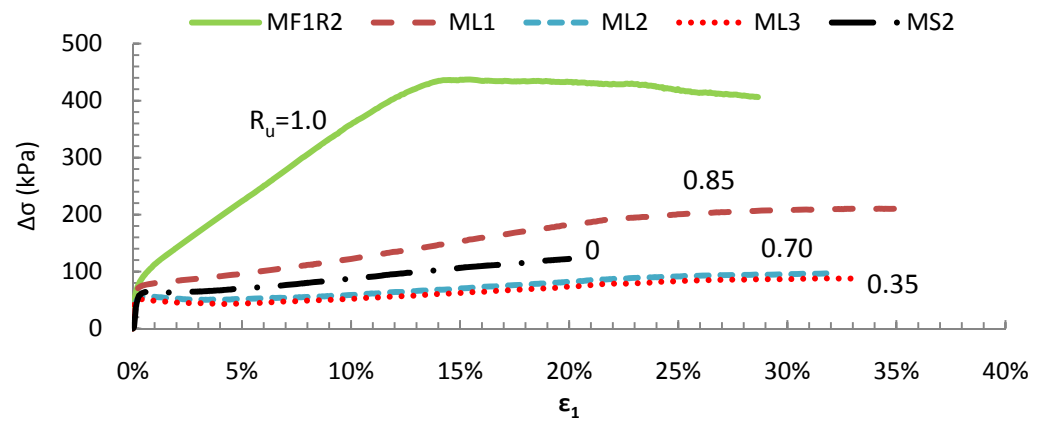

(a)

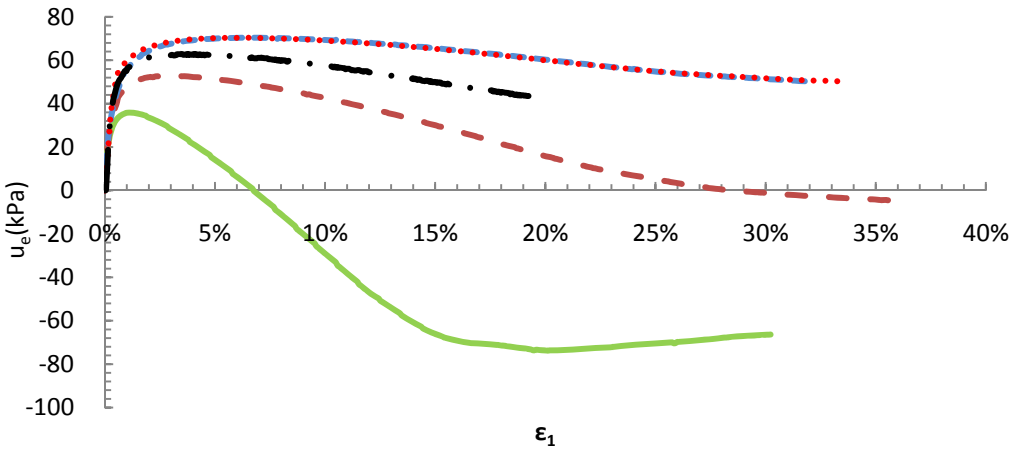

(b)

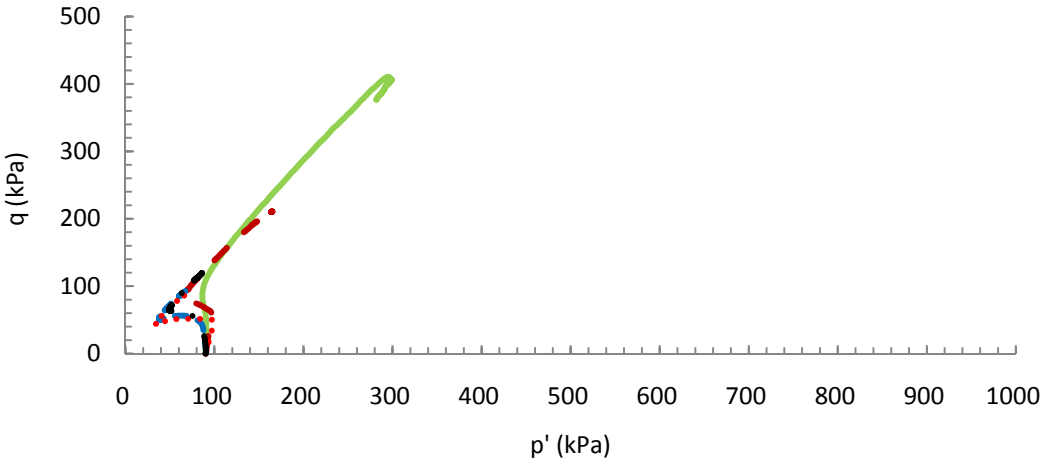

(c)

Figure 7.2. Postcyclic shear behavior of MRV silt with full reconsolidation after various liquefaction levels: (a) $\Delta\sigma$ vs. ε_1, (b) $\Delta\sigma$ vs. ε_1, (c) q vs. p'

liquefaction had a larger deviator stress and developed more positive excess pore pressure (Figure 7.2a and 7.2b). The stress paths in Figure 7.2c indicate that all specimens initially contracted; however, the specimen with 100% liquefaction (MF1R2) contracted less than the other specimens. Compared to the specimens MS2 without previous cyclic loading, specimens ML2 and ML3 had less continuous dilation (Figure 7.2c). Specimens ML2 (R_u = 0.70) and ML3 (R_u = 0.35) had nearly identical curves of deviator stress and excess pore pressure versus axial strain. When liquefaction level was increased to R_u = 0.85, the deviator stress resistance increased and the excess pore pressure decreased further after the initial peak value (Figures 7.2a and 7.2b).

7.2.2 Shear Strength and Stiffness at Small Deformation. This work studied the effect of limited liquefaction on strength and stiffness at small deformation. Figure 7.3 shows the variations in yield shear strength (S_y) and initial modulus (E_i) versus the liquefaction level. The yield shear strength increased with an increase in liquefaction level up to R_u=0.85, as indicated in Figure 7.3a. Beyond that, there was a small reduction in the yield shear strength. The initial modulus increased with an increase in liquefaction level, as indicated in Figure 7.3b. When the liquefaction level was larger than 0.70, it increased less.

In Figure 7.4, each of yield shear strength and initial stiffness at any liquefaction level was normalized by those with 0% liquefaction (i.e. without previous cyclic loading). With an increase in liquefaction level, the increase in initial stiffness of the MRV silt was larger than that in yield shear strength, suggesting that limited liquefaction with full reconsolidation has a greater impact on initial stiffness than on yield shear strength.

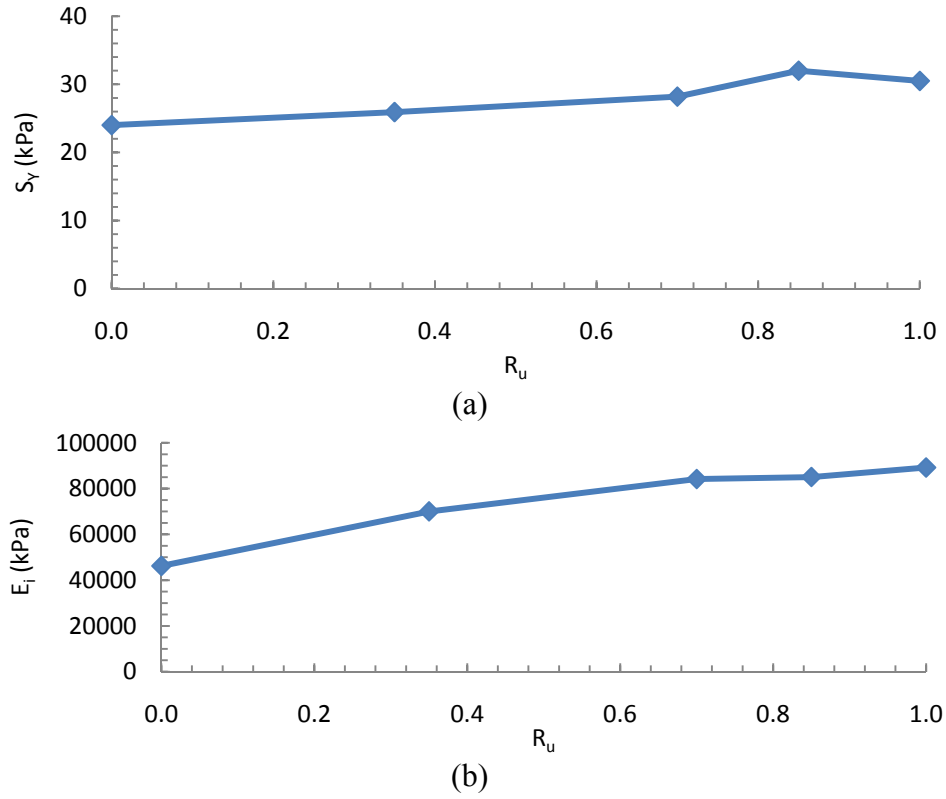

Figure 7.3. Variation in yield shear strength and initial modulus with liquefaction level of MRV silt after full reconsolidation: (a) S_y vs. R_u, (b) E_i vs. R_u

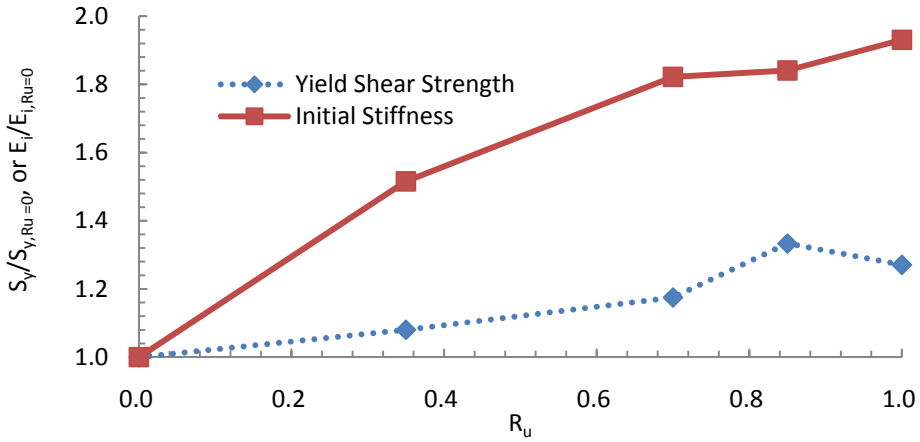

Figure 7.4. Variation in yield shear strength and initial stiffness of MRV silt with increased liquefaction level

7.2.3 Shear Strength and Stiffness at Large Deformation. In Figure 7.5, undrained shear strength (S_u) is plotted against liquefaction level. It was only slightly lower than that of static specimen MS2, which had no previous cyclic loading, when the excess pore pressure ratios were 0.35 and 0.70. When the excess pore pressure ratio was 0.85, the undrained shear strength increased. The reason why the S_u of the specimens with R_u of 0.35 and 0.70 decreased compared to the static specimen MS2 probably included: the fabric of the soil was damaged during the cyclic loading; the decrease in void ratio due to reconsolidation was not enough to increase the undrained shear strength. In Figure 7.6, the volumetric strain (ε_v) due to reconsolidation is plotted against liquefaction level. When the liquefaction level was up to 0.70, the volumetric strain was small. Beyond that point, there was a larger volumetric strain due to reconsolidation. Together, Figures 7.5 and 7.6 demonstrate that an excess pore pressure ratio of 0.70-0.80 is a prerequisite for significant volume reduction and thus for an increase in undrained shear strength due to reconsolidation after cyclic loading.

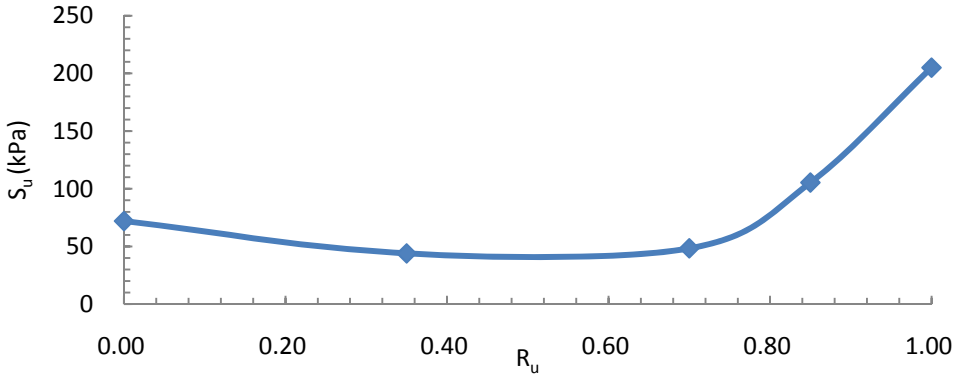

Figure 7.5. Effect of liquefaction level on undrained shear strength of MRV silt with full reconsolidation

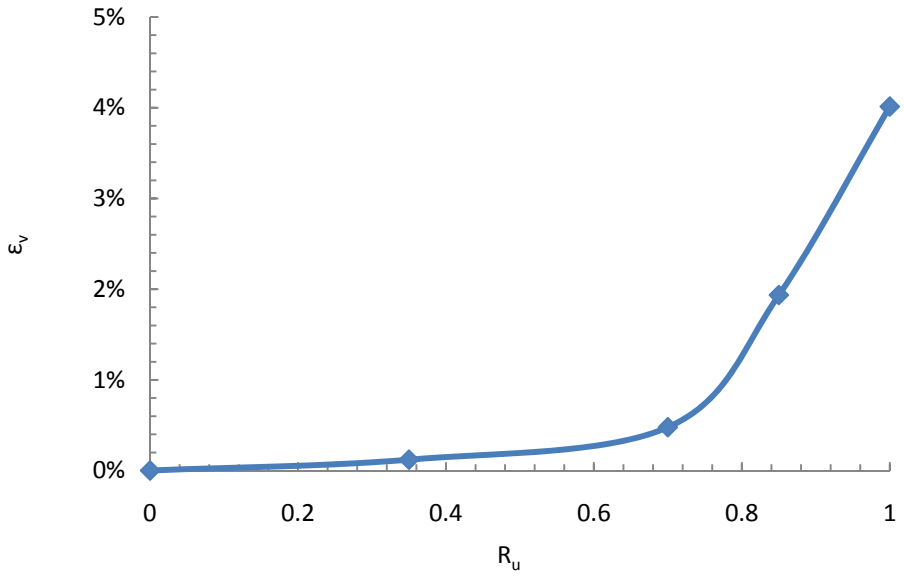

Figure 7.6. Volumetric strain of MRV silt due to reconsolidation after various liquefaction levels

In Figure 7.7, the secant modulus is plotted against liquefaction level. In contrast to the undrained shear strength, there was no apparent relationship between secant modulus and liquefaction level. The secant modulus was larger at liquefaction levels of 0.35 and 0.70 than other levels because the soil did not dilate significantly after deviator stress exceeded yield stress. As an example, Figure 7.8 help demonstrates this phenomenon with a comparison between ML1 and ML3. The $\Delta\sigma_{max}/2$ of the specimen ML3 occurred before yield stress; therefore, the secant modulus was almost equal to the initial stiffness. Thus, the small strain governs the deviator stress-strain behavior of the postcyclic specimens with excess pore pressure ratios of 0.35 or 0.70, but large strain governs that of the static specimen and postcyclic specimens with excess pore pressure ratios greater than 0.70.

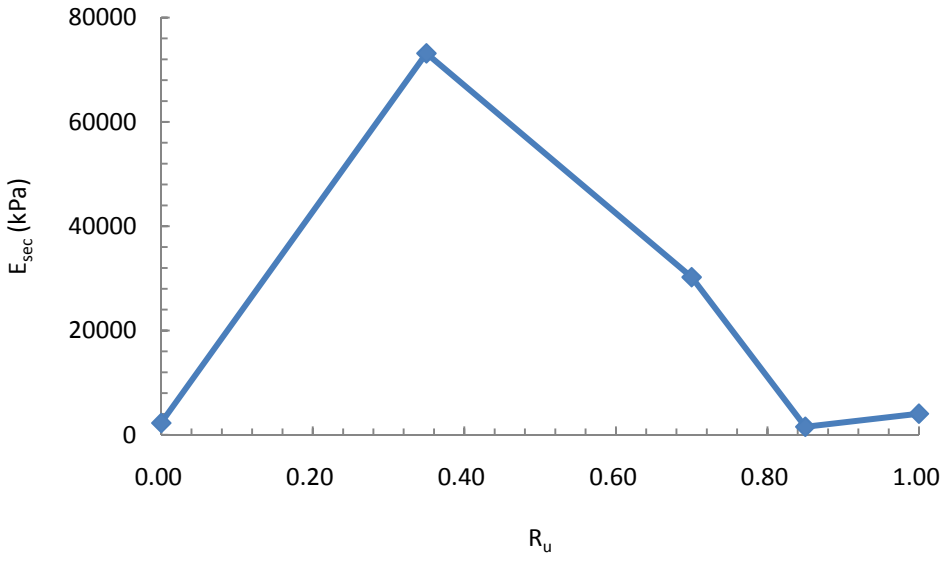

Figure 7.7. Effect of liquefaction level on secant modulus of fully reconsolidated MRV silt

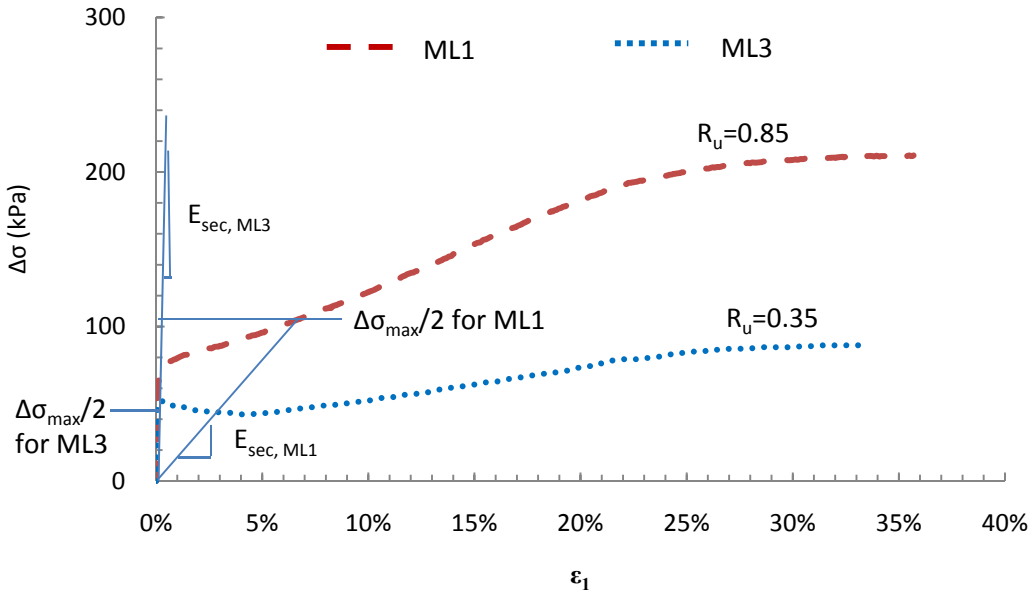

Figure 7.8. Determination of secant modulus for specimens with two liquefaction levels

7.3. POSTCYCLIC SHEAR BEHAVIOR WITHOUT RECONSOLIDATION

Because excess pore pressure can remain for a long time if the drainage conditions in the field are poor, this section addresses postcyclic behavior without reconsolidation. Table 7.2 lists the tests conducted to study the effect of limited liquefaction on the postcyclic monotonic behavior of the MRV silt with no reconsolidation after cyclic loading. Postcyclic monotonic triaxial compression tests were conducted once the excess pore pressure reached equilibrium. Similarly, as in the previous section, the information on the fully liquefied specimen MF4 with a liquefaction level of 1.0 and the static specimen MS2 with no liquefaction are included for comparison in Table 7.2.

Table 7.2. Summary of triaxial tests of MRV silt with no reconsolidation after various liquefaction levels

Test ID	B-value	σ'_c (kPa)	e	N_{cyc}	R_u	$u_{e,\,cyc}$	u_e after equilibrium	σ'_3 after equilibrium
MF4	0.94	90.3	0.660	28.14	1.00	90.3	85.1	5.2
ML4	0.93	90.5	0.643	25.17	0.85	76.9	72.9	17.6
ML5	0.93	91.1	0.645	18.12	0.70	63.4	58.1	33.0
ML6	0.94	90.7	0.667	4.01	0.35	27.21	23.7	67.0
MS2	0.98	90.0	0.679	-	-	-	0	90.0

7.3.1 Undrained Shear Behavior. Figure 7.9 shows the deviator stress and excess pore pressure versus axial strain, and stress paths for various excess pore pressure

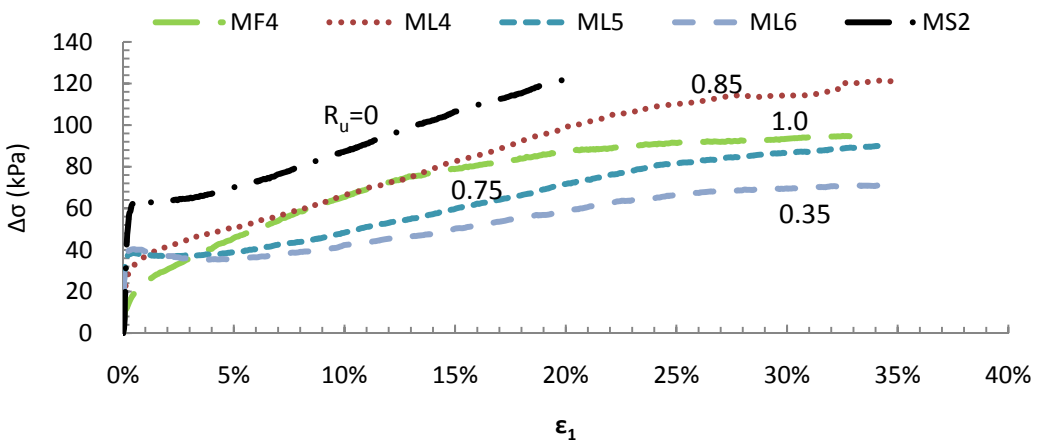

(a)

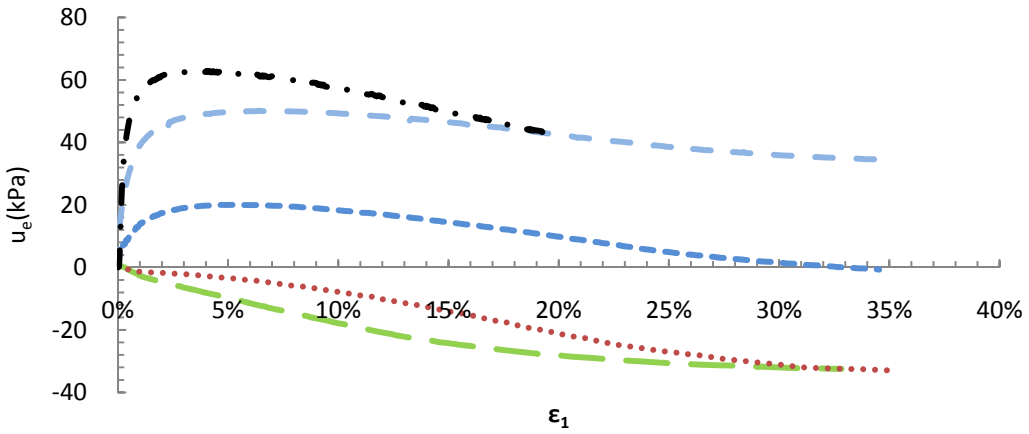

(b)

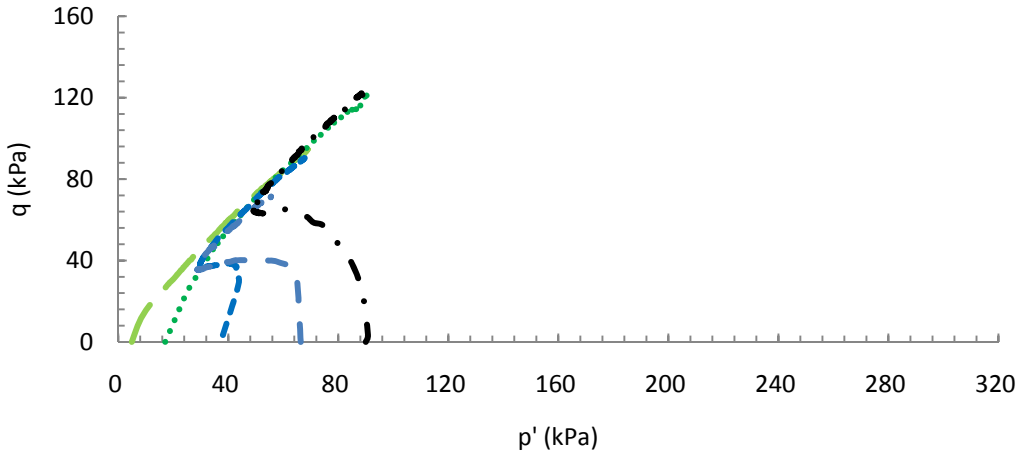

(c)

Figure 7.9. Postcyclic behavior of MRV silt without reconsolidation after various liquefaction levels: (a) Δσ vs. ε_1, (b) Δσ vs. ε_1, (c) q vs. p'

ratios. As shown in Table 7.2, the effective confining pressure at the beginning of postcyclic monotonic compression was lower at higher excess pore pressure ratio. Specimens with lower effective confining pressure developed more negative excess pore pressure during postcyclic shearing and dilated earlier. As indicated in Figure 7.8c, specimens MF4 and ML4 dilated initially, but the other specimens contracted initially, then dilated after the phase transformation point. There was no apparent relationship between the stress-strain curve at the large strains and the excess pore pressure ratio, although a lower deviator stress at identical axial strain was expected at higher R_u.

To further analyze the stress-strain behavior, Figure 7.10 plots the principal stress ratio (σ'_1/σ'_3) against axial strain. Specimen MF4 had the highest peak point of principal stress ratio, indicating the greatest dilation behavior. All specimens, however, converged to a similar principal stress ratio at the large strain (> 20%).

7.3.2 Shear Strength and Stiffness at Small Deformation. Figure 7.9a is enlarged in Figure 7.11 to show the details of relationships between the deviator stress and axial strain at small deformation. Specimens ML5 (R_u=0.70) and ML6 (R_u=0.35) had a small drop in deviator stress beyond the yield stress, so they had quasi-steady states, as did static specimen MS2. Conversely, specimens ML4 (with a liquefaction level of 0.85) and MF4 (with a liquefaction level of 1.0) continued dilating after they reached critical state (Figure 7.9). As indicated in Figure 7.12, yield shear strength and initial stiffness decreased significantly when the liquefaction level was larger than 0.7. Figure 7.13 compares these decreases by normalizing them with respect to yield shear strength and initial stiffness of MRV silt without previous cyclic loading (MS2). Yield shear strength decreased more with liquefaction level than did initial stiffness.

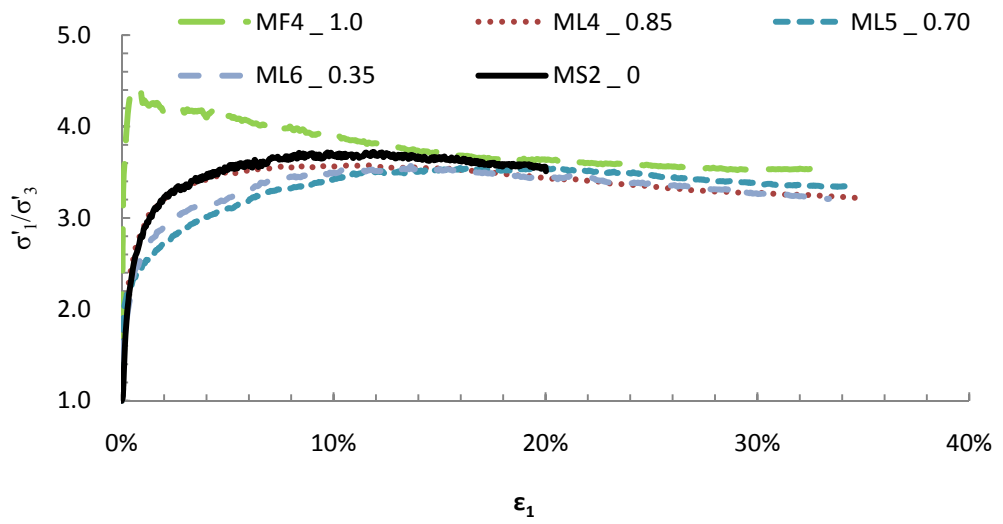

Figure 7.10. Principal stress ratio versus axial strain of MRV silt without reconsolidation after limited liquefaction

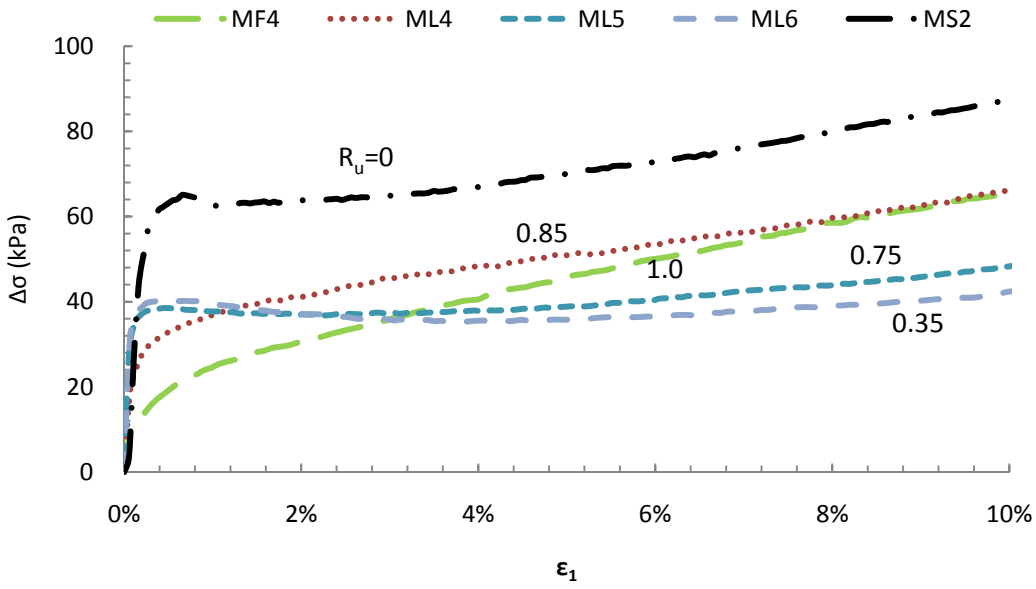

Figure 7.11. Postcyclic behavior of MRV silt without reconsolidation after limited liquefaction at small deformation

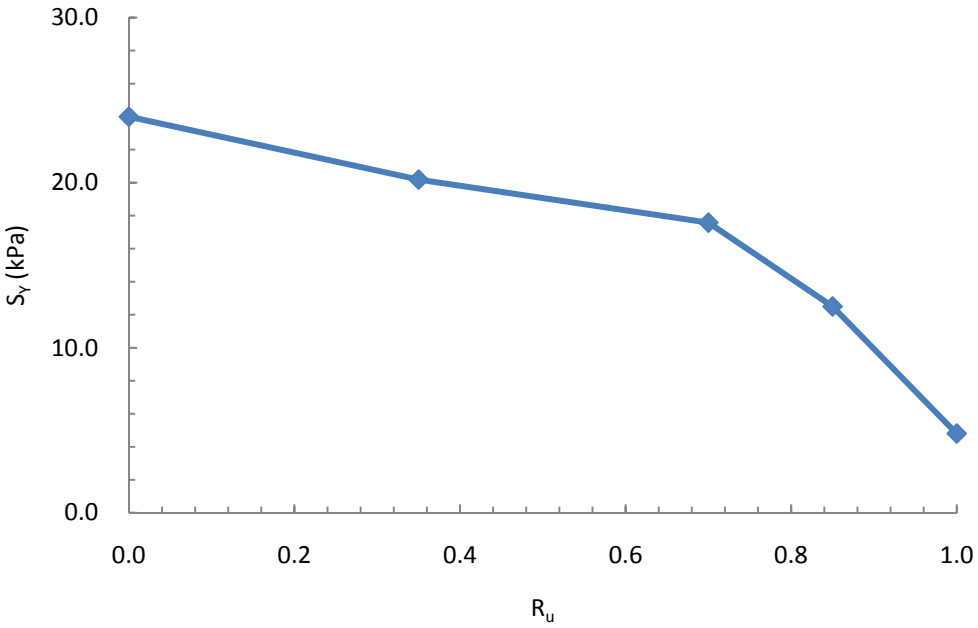

(a)

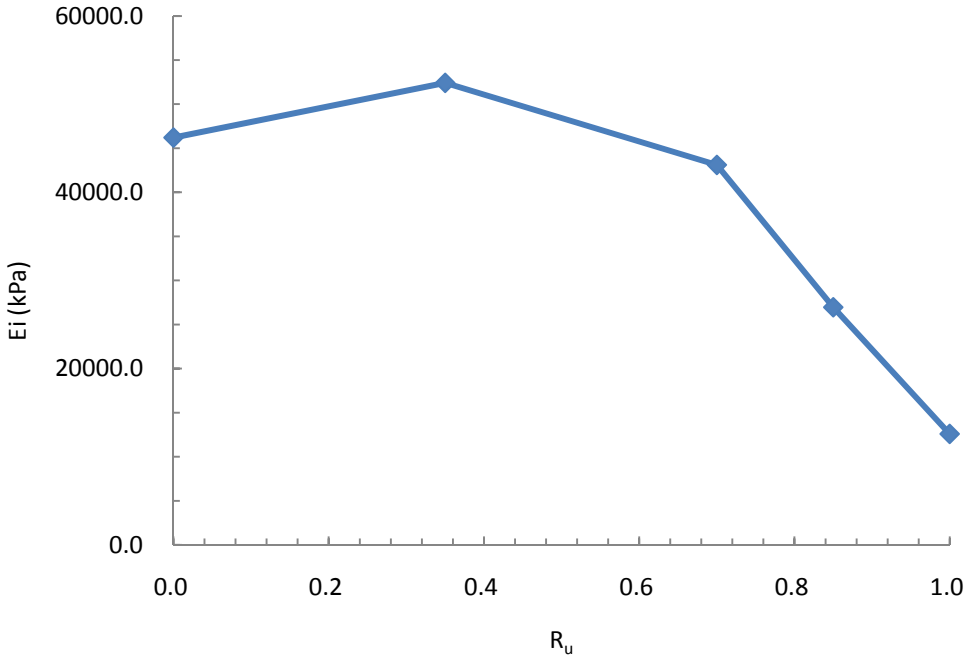

(b)

Figure 7.12. Reductions in yield shear strength and initial stiffness of MRV silt with no reconsolidation after limited liquefaction

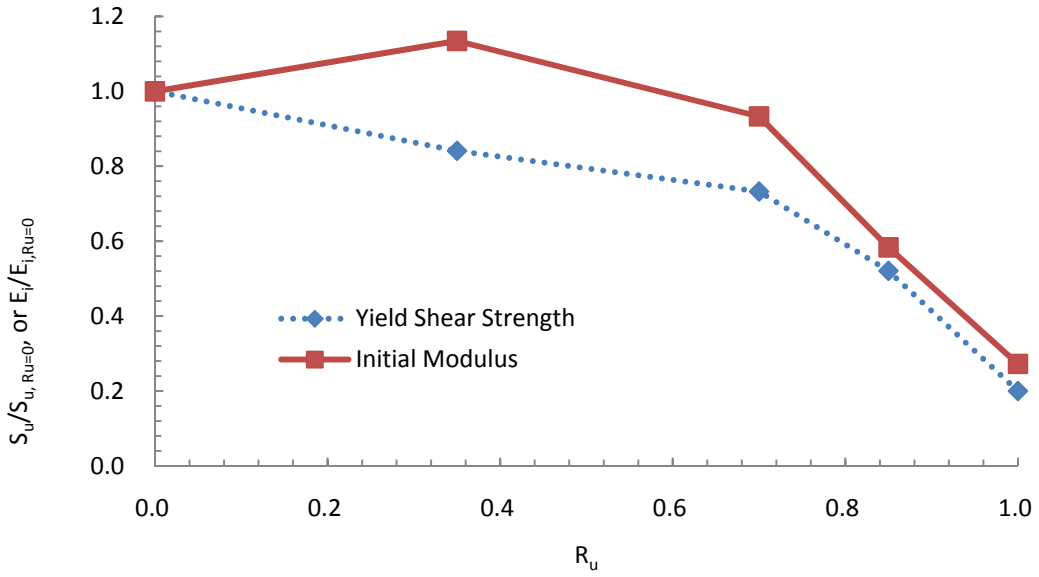

Figure 7.13. Effect of liquefaction level on normalized yield shear strength and initial stiffness of MRV silt without reconsolidation

7.3.3 Shear Strength and Stiffness at Large Deformation. Undrained shear strength had been expected to increase as liquefaction level decreased because the fabric of the specimen with a lower liquefaction level was less affected by cyclic loading, and it had higher effective confining pressure. As indicated in Figure 7.14, however, there was no apparent relationship between undrained shear strength and liquefaction level.

Figure 7.15 plots the secant modulus against excess pore pressure ratio. As for fully reconsolidated specimens, there was no apparent relationship between secant modulus and excess pore pressure ratio. Secant modulus was greatest at a excess pore pressure ratio of 0.30. As for fully reconsolidated soil, soil with no reconsolidation dilated little after yield stress, and small strain governed the postcyclic deviator stress-strain behavior.

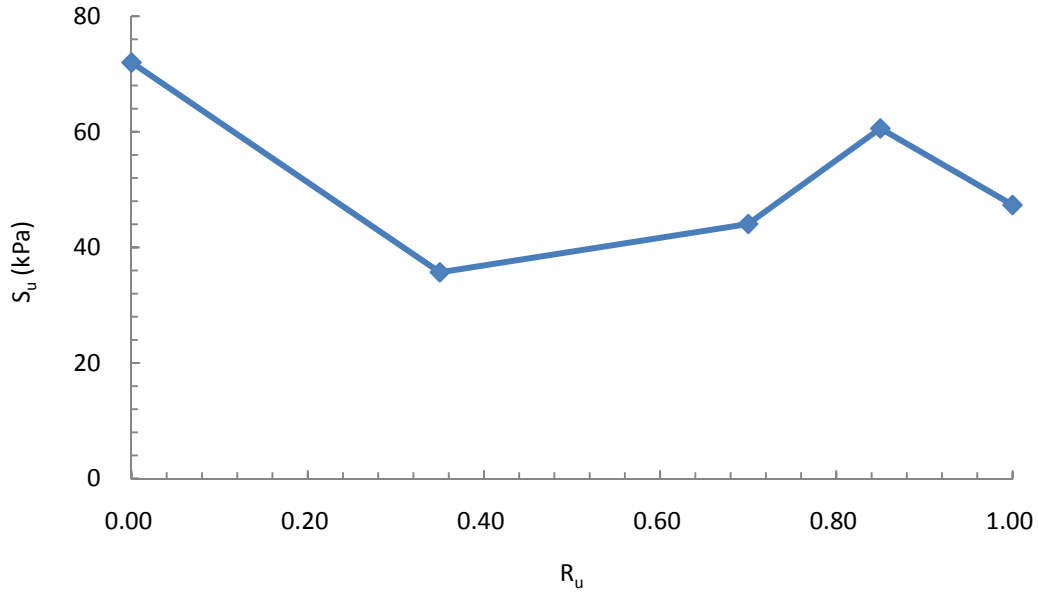

Figure 7.14. Effect of liquefaction level on undrained shear strength of unreconsolidated MRV silt

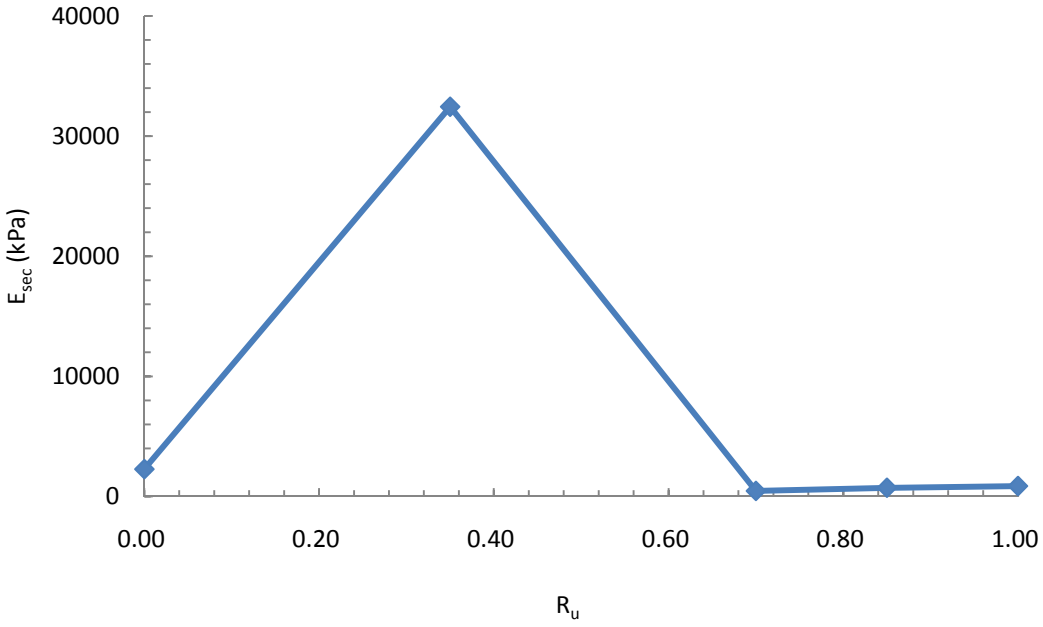

Figure 7.15. Effect of liquefaction level on secant modulus of unreconsolidated MRV silt

7.4. DISCUSSION

7.4.1 No Reconsolidation and Full Reconsolidation. Figure 7.16 shows the effect of reconsolidation on the yield shear strength and initial stiffness after limited liquefaction. The yield shear strength and initial stiffness of fully reconsolidated specimens were higher than those of specimens with no reconsolidation. The differences in yield shear strength and initial stiffness of the soil with full reconsolidation and no reconsolidation became significant at a liquefaction level greater than 0.70.

Figure 7.17 shows the variation in undrained shear strength and secant modulus in relation to liquefaction level. The fully reconsolidated specimen had higher undrained shear strength and secant modulus than did the static specimen (with a liquefaction level of 0). Figure 7.17a indicates that the change in undrained shear strength due to full reconsolidation was minimal at a liquefaction level below 0.70. Conversely, it was significant if the liquefaction level was higher than 0.70. Thus, reconsolidation may significantly increase the undrained shear strength only when the magnitude or duration of cyclic loading produces a liquefaction level higher than 0.70. The increase in secant modulus due to full reconsolidation was minimal when the liquefaction level was higher than 0.70 (Figure 17b); and it was significant when the liquefaction level was lower than 0.80. Again, it should be stressed that the high secant modulus at a liquefaction level lower than 0.80 was induced by limited dilation when the deviator stress was larger than the yield stress.

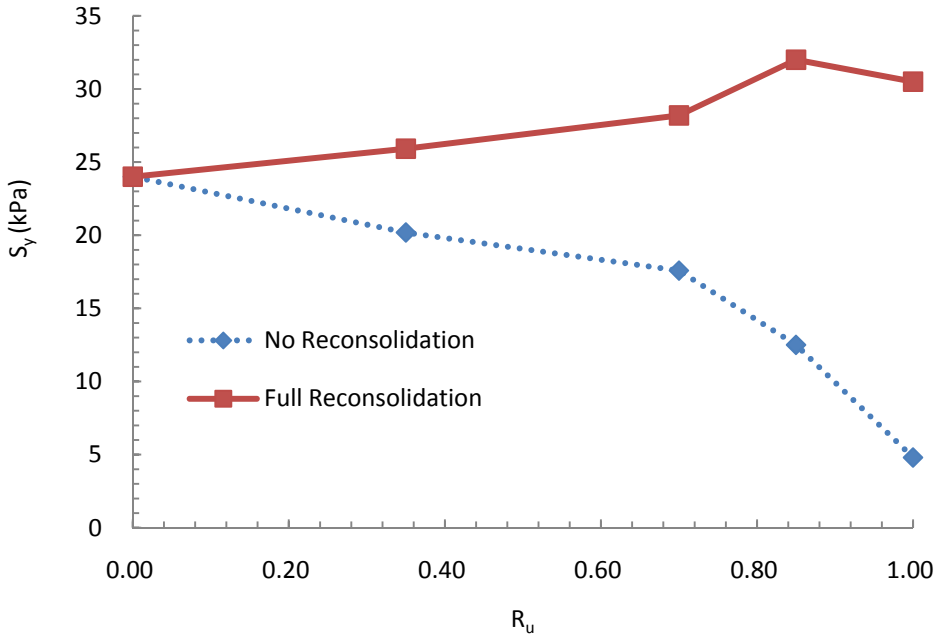

(a)

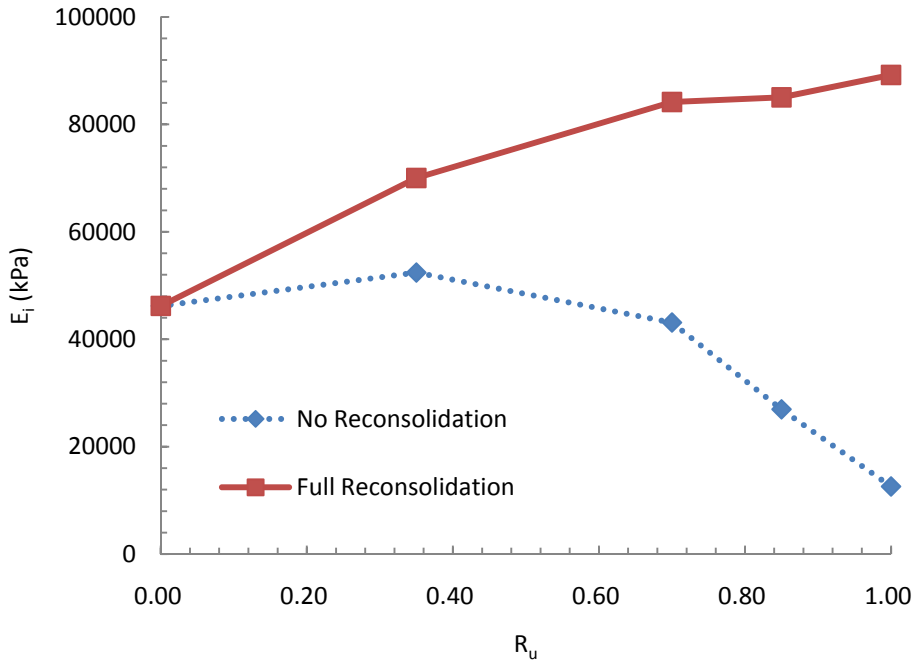

(b)

Figure 7.16. Effect of reconsolidation on yield shear strength and initial stiffness of MRV silt after limited liquefaction: (a) S_y vs. R_u, (b) E_i vs. R_u

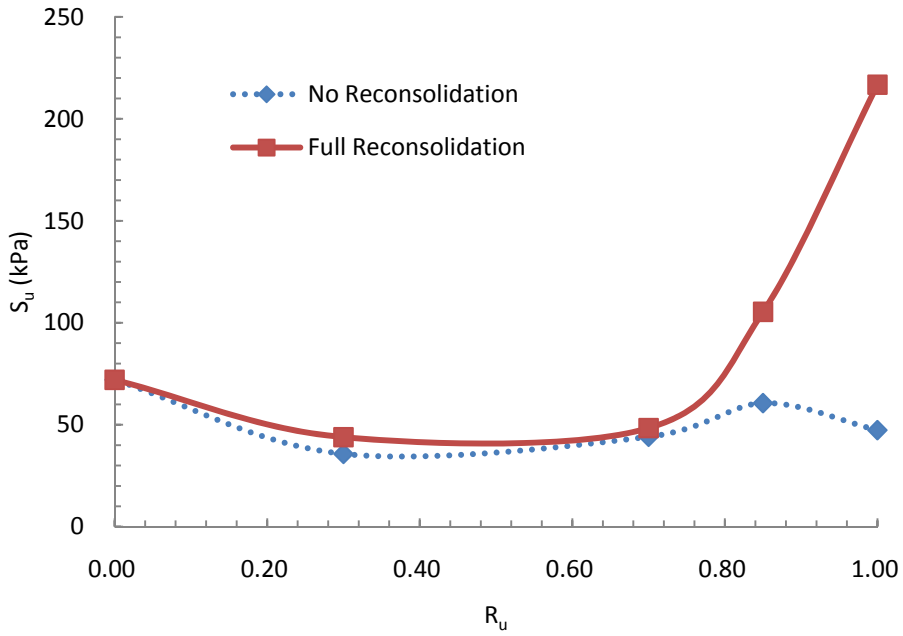

(a)

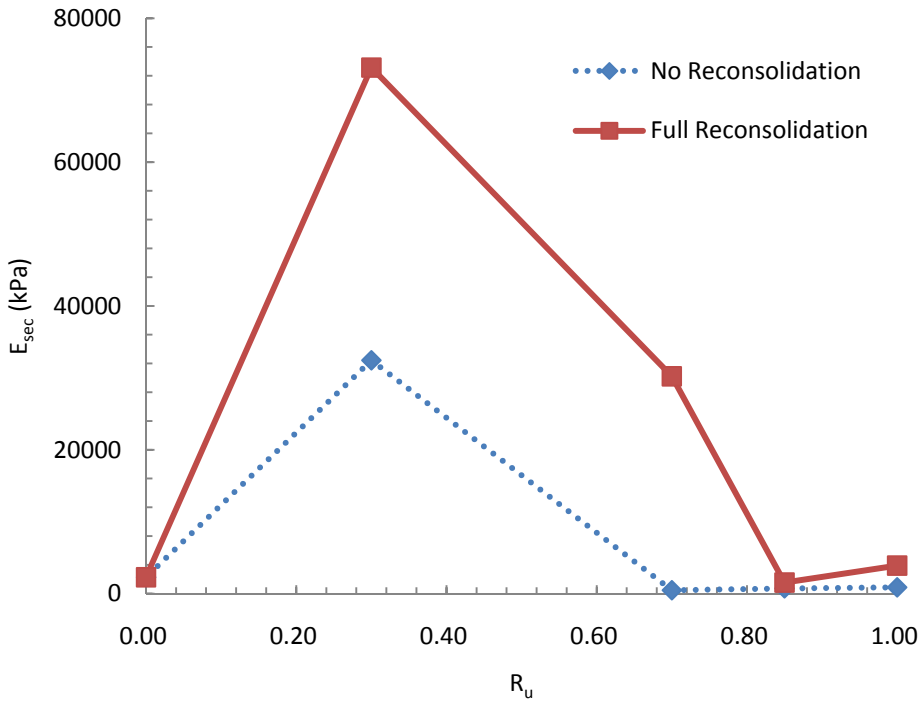

(b)

Figure 7.17. Effect of reconsolidation on undrained shear strength and secant modulus after limited liquefaction

A liquefaction level greater than 0.70 is a prerequisite for an increase in the yield shear strength (S_y), initial stiffness (E_i) and undrained shear strength (S_u) due to full reconsolidation. The reasonable explanation for why these values increase significantly only when the R_u is higher 0.70 is that the increase in soil density is insufficient to compensate for their reduction due to the weakened fabric during cyclic loading, when the R_u is lower than 0.70. As shown in Figure 7.6, volumetric strain increased significantly when the liquefaction level was higher than 0.70. This finding for MRV silt was similar to the result for slightly overconsolidated Fraser River Delta silt with a PI of 4.0 (Sanin and Wijewickreme, 2006) but contradicts that for clean and silty sands (Chern and Lin, 1994). Sanin and Wijewickreme (2006) stated that the specimens with R_u close to 1.0 suffered to significant postcyclic volume strain for Fraser River Delta silt (Figure 7.18). Chern and Lin (1994) presented that initial liquefaction ($R_u = 1.0$) is a prerequisite to significant volume change due to reconsolidation in clean and silty sands. Thus, cyclic loading damages the fabric of MRV silt earlier than it does that of clean and silty sand.

This study of strength and stiffness change due to cyclic loading and reconsolidation is beneficial not only for stability and deformation evaluation in earthquake engineering, but also as a means to develop guidelines for ground mitigation such as dynamic compaction and stone column installation in low-plasticity silts. The installation of remedial wick drains can help reconsolidate the ground and increase shear strength (Thevanayagam et al., 2001).

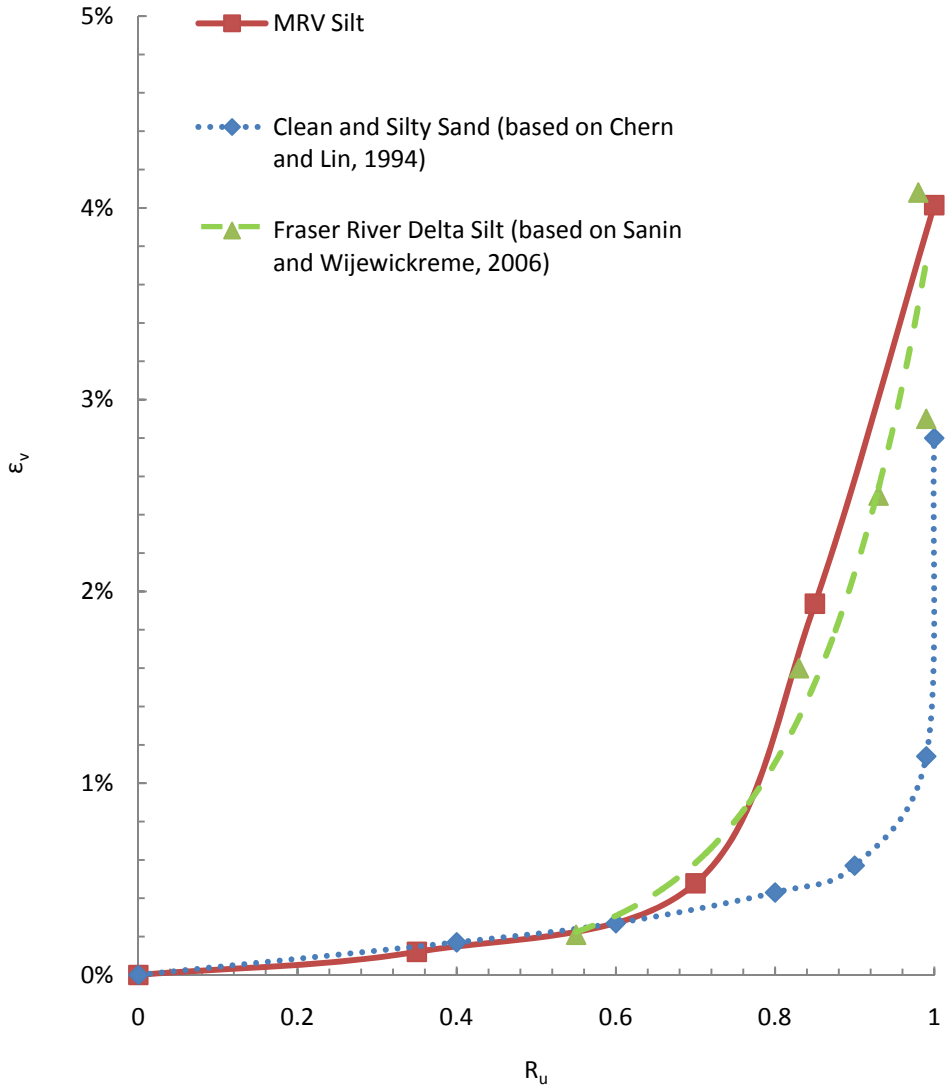

Figure 7.18. Variation in volumetric strain with liquefaction level in MRV silt and clean and silty sand

7.4.2 Comparisons with Other Available Laboratory Data. Several researchers have studied postcyclic undrained shear strength; these included Poulos et al. (1985),

Seed (1987), Ishihara et al. (1990), Seed and Harder (1990), Thevanayagam et al. (1996), Olson and Stark (2002, 2003), Robertson (2010), and others. Generally, there are three approaches to predict the undrained shear strength of soil with previous cyclic loading: laboratory testing, in situ testing, and normalized strength (Kramer, 1996). Each approach has its own advantages and limitations, and each yields somewhat different undrained shear strengths, indicated in Section 2. Thevanayagam et al. (1996) analyzed the postcyclic undrained shear strength of 24 sandy soils (including one sandy silt) and presented equations for the lower bounds of undrained shear strength for clean sands and silty sands.

$$\mathrm{Log}\,(S_u) = -0.32 + 0.04D_r, \text{ for clean sands (SP)} \quad (12)$$

and

$$\mathrm{Log}\,(S_u) = -1.12 + 0.04D_r, \text{ for silty sands (SM)} \quad (13)$$

where D_r is relative density. The data for the sandy silt was located below the SM lower bound.

Figure 7.19 shows the lower bound for clean sands and silty sands. The data of the MRV silt tested here were added to Figure 7.19. All are below the SM lower bound. The undrained shear strength increased sharply with a small increase in relative density. This phenomenon presents a challenge for the estimation of undrained shear strength, especially for in situ testing. It also requires that relative density be measured accurately; otherwise, the results will be inaccurate. However, the relative density of low-plasticity silts cannot be easily measured for in situ testing.

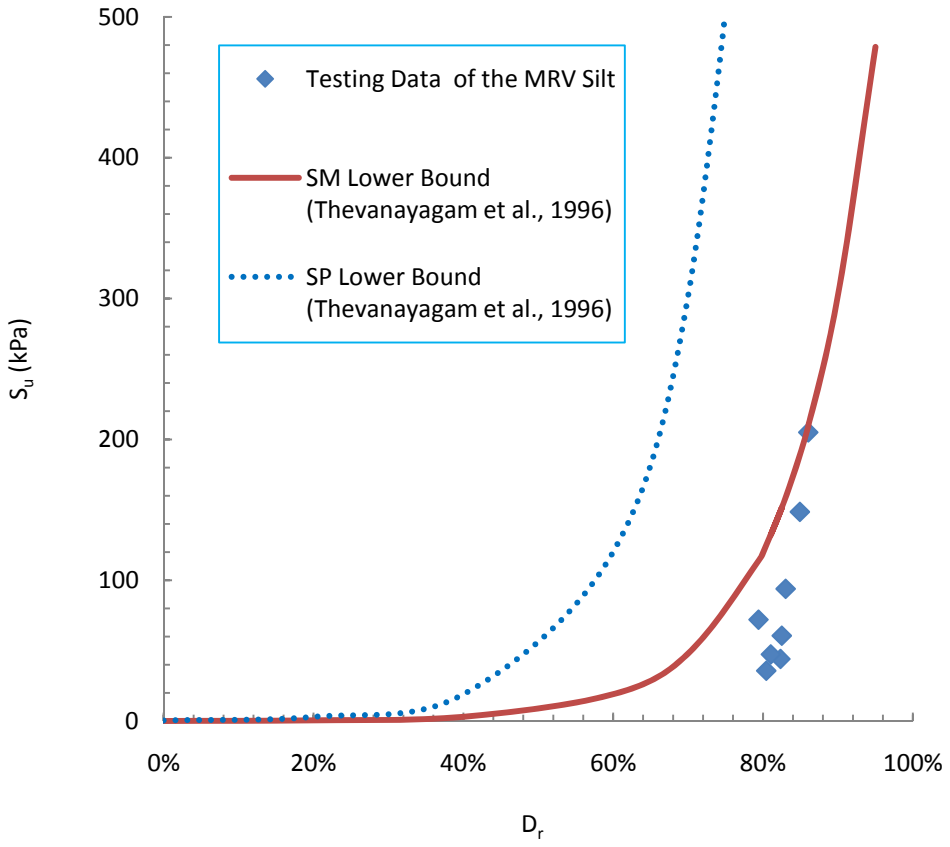

Figure 7.19. Relationship between undrained shear strength and relative density

7.5. SUMMARY

This work used laboratory tests to study the effect of limited liquefaction on monotonic shearing behavior of the MRV silt with full and no reconsolidation. With full reconsolidation, yield shear strength and initial stiffness generally increased with liquefaction level, the latter more than the former. Undrained shear strength decreased slightly with a liquefaction level lower than 0.70, because the increase in soil density was insufficient to compensate for the reduction in undrained shear strength due to weakened

soil fabric. Conversely, with a liquefaction level higher than 0.70, undrained shear strength increases significantly. Thus, the liquefaction level higher than 0.70 is a prerequisite for a significant increase in undrained shear strength. There was no apparent relationship between secant modulus and liquefaction level for the fully reconsolidated silt and at low levels liquefaction (0.35 and 0.70) the secant modulus is large because the soil does not dilate after yield stress and small strain governs postcyclic deviator stress-strain behavior.

Without reconsolidation, liquefaction level had no apparent effect on the reductions in undrained shear strength and secant modulus. Compared to the silt with no previous cyclic loading, there was a reduction only in undrained shear strength but no apparent change in secant modulus due to limited liquefaction. Yield shear strength and initial stiffness decrease with an increase in liquefaction level. These decreases were large when the liquefaction level was higher than 0.70. Cyclic loading tends to damage the fabric of the tested MRV silt at similar liquefaction level as it does that of the Fraser River Delta silt but at lower liquefaction level than it does that of clean and silty sand.

The undrained shear strength of MRV silt falls within the range reported by Thevanayagam et al. (1996). Due to the reconsolidation after cyclic loading, undrained shear strength increases significantly with an increase in relative density, indicating that determination of accurate relative density is crucial to estimate undrained shear strength of MRV silt after cyclic loading.

8. EFFECT OF PLASTICITY ON PRECYCLIC AND POSTCYCLIC BEHAVIOR OF LOW-PLASTICITY SILT

8.1. INDEX PROPERTIES OF SOIL MIXTURES

This section investigates the effect of PI on the precyclic and postcyclic behavior of low-plasticity silt. Bentonite was added to the MRV silt to form the silt-clay mixtures with added bentonite content of 1.25%, 2.5%, 5.0%, 7.5%, and 10.0% by weight. The clay content of each mixture was computed; and the results are listed in Table 8.1. Based on ASTM standard D 854, the specific gravity of the bentonite was measured to be 2.24, lower than results published by others (Delage et al., 2006; Ito and Komine, 2008). With the natural MRV silt's specific gravity of equal to 2.71, that of each silt-clay mixture with bentonite was computed (Table 8.1). The liquid limits (LL) were determined using the Casagrande and Fall Cone approaches, which were used for the natural MRV silt. The PI was computed using LL determined using the Casagrande approach minus PL. Figure 8.1 shows the variation in Atterberg limits with added bentonite. As the percentage of bentonite increased, the PI also increased. However, the increase in PI was minimal when the added bentonite content was no more than 2.5% of the total weight of the soil specimen. Beyond 2.5%, the PI increased significantly.

Table 8.1. Index properties of the silt-bentonite mixtures

Index Property	**Added Bentonite Content**				
	0%	2.5%	5.0%	7.5%	10.0%
Clay Content	14.5%	16.6%	18.8%	20.9%	23.1%
Specific Gravity	2.71	2.70	2.68	2.67	2.65
LL by Casagrande	28.1	28.9	32.7	36.9	42.2
LL by Fall Cone	29.9	30.1	35.0	38.8	44.5
PL	22.3	22.7	23.3	23.4	24.8
PI	5.8	6.2	9.4	13.5	17.4

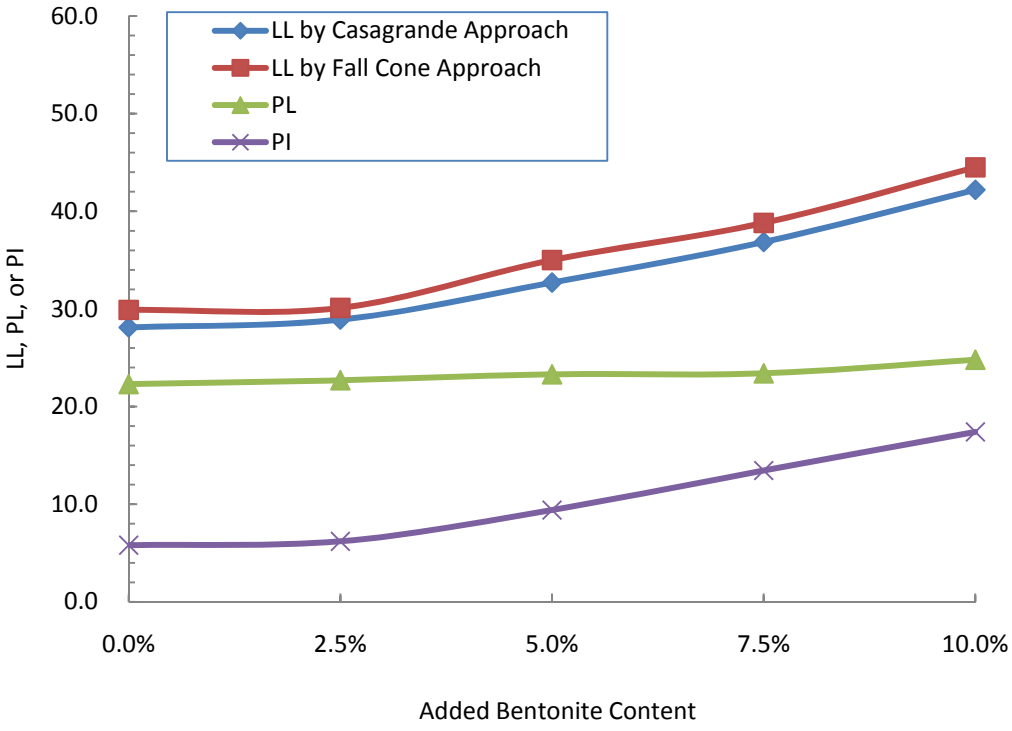

Figure 8.1. Variation in Atterberg limits with added bentonite content

For the silt-clay mixtures with added bentonite contents of 2.5% and 5.0%, as for the natural MRV silt, the consolidation parameters were determined using isotropic consolidation pressure (Table 8.2). The coefficients of compressibility (a_v) were computed at an effective consolidation pressure of 90 kPa. Figure 8.2 indicates that the silt-clay mixtures became less permeable with an increase in added bentonite content. The consolidation parameters t_{50} and c_v reflected the effect of reduced permeability (k). In particular, the permeability decreased significantly when added bentonite content increased from 0% to 2.5%. With a further increase in added bentonite content to 5.0%, the reduction in permeability was diminished. On the other hand, Figure 8.3 shows the variation in compressibility of the silt-clay mixtures; the added bentonite made the material more compressible as it became more plastic. The coefficient of compressibility (a_v), the compression index (C_c), and the recompression index (C_r) increased steadily with the increase in the bentonite content from 0% to 5.0%.

Table 8.2. Consolidation parameters of MRV silt-bentonite mixtures

Consolidation Parameter	**Added Bentonite Content**		
	0%	2.50%	5.0%
k (cm/s)	5.74×10^{-7}	1.09×10^{-7}	4.90×10^{-8}
t_{50} (min)	8.3	70	185
c_v (cm^2/sec)	0.0226	0.0032	0.0011
a_v (/kPa)	0.00043	0.00057	0.00076
C_c	0.0896	0.128	0.1991
C_r	0.009	0.0096	0.0156

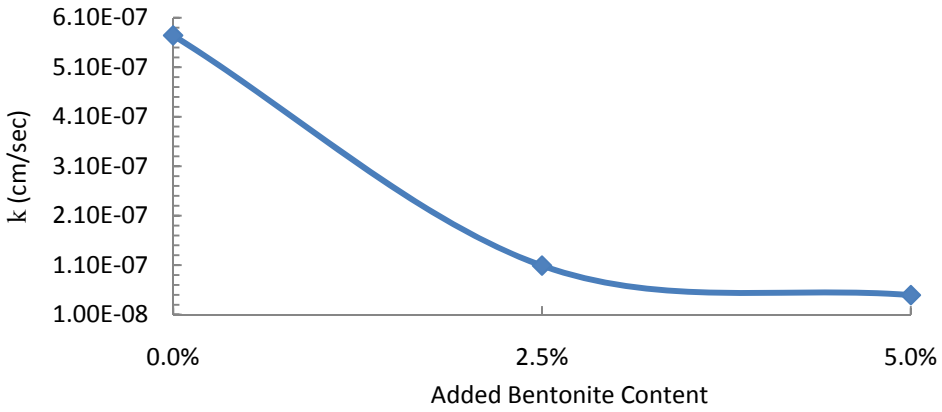

(a)

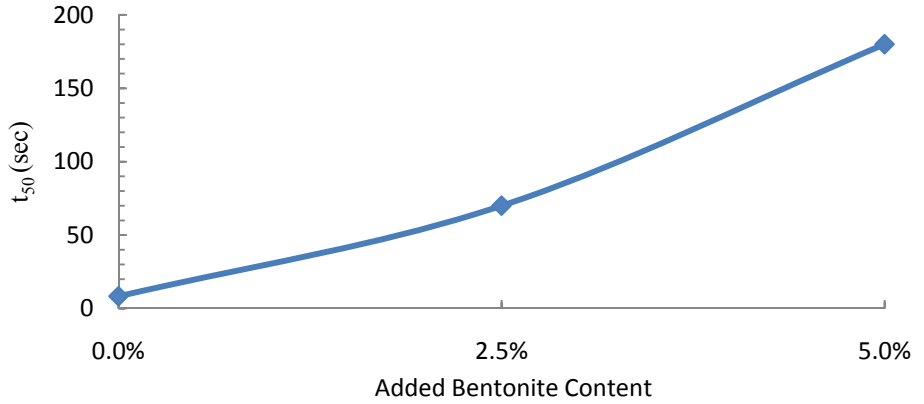

(b)

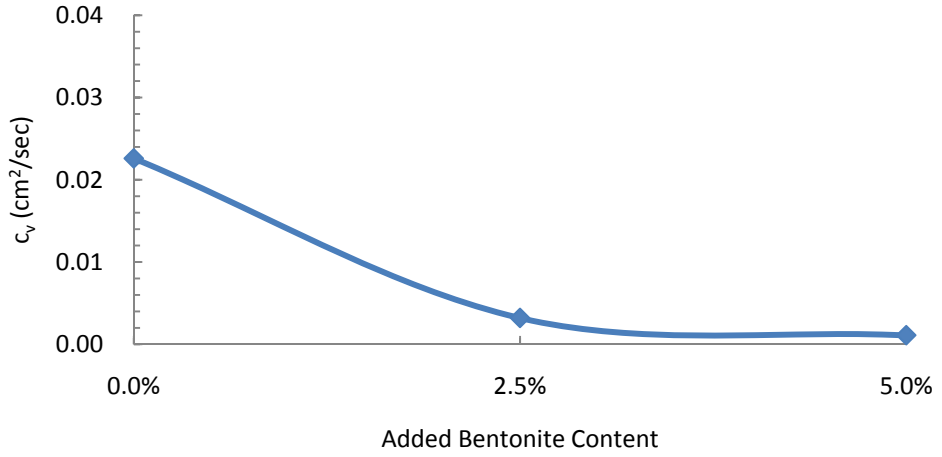

(c)

Figure 8.2. Variation in permeability and related parameters of MRV silt-bentonite mixtures with added bentonite content: (a) k vs. added bentonite content, (b) t_{50} vs. added bentonite content, (c) c_v vs. added bentonite content

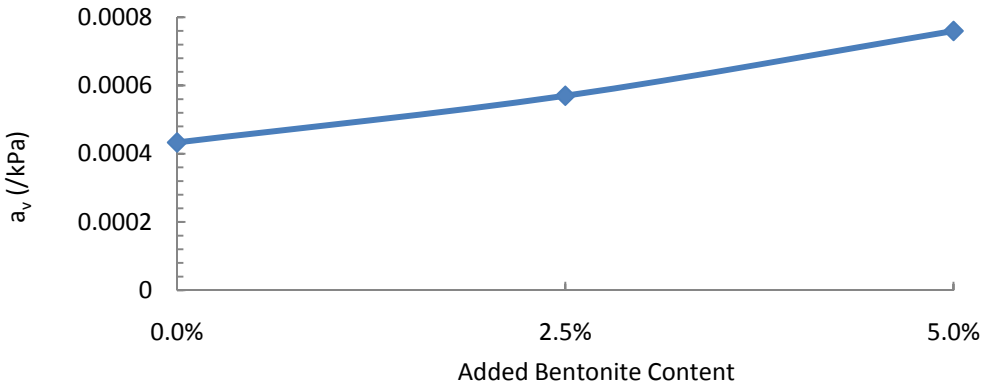

(a)

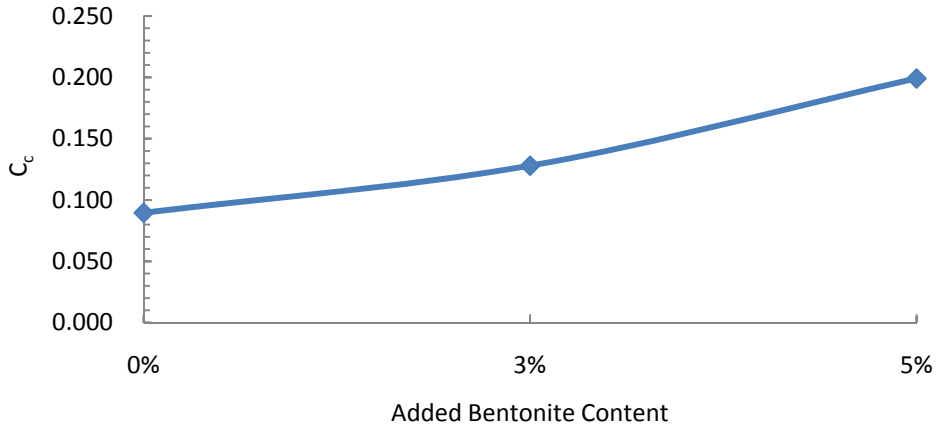

(b)

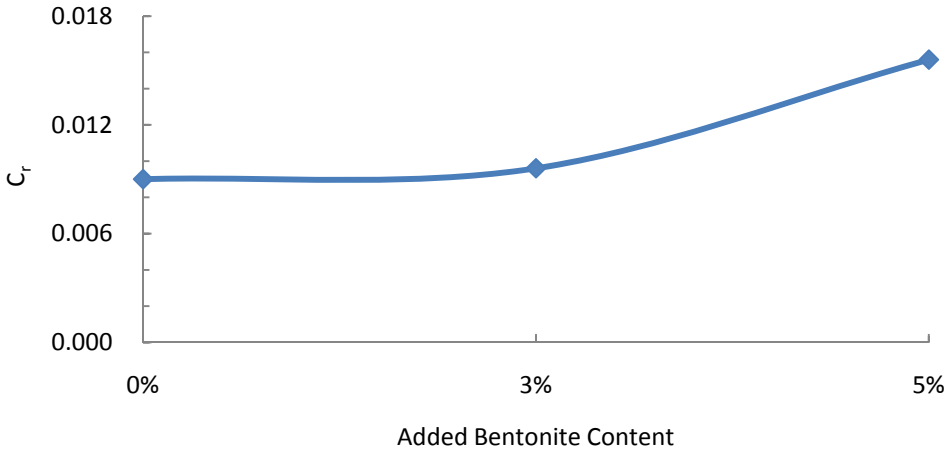

(c)

Figure 8.3. Variation in consolidation parameters related to compressibility of MRV silt-bentonite mixtures with added bentonite content: (a) a_v vs. added bentonite content, (b) C_c vs. added bentonite content, (c) C_r vs. added bentonite content

8.2. EFFECT OF PLASTICITY ON MONOTONIC SHEAR BEHAVIOR

Static triaxial consolidated undrained tests were conducted to study the effect of soil plasticity on the monotonic shear behavior of MRV silt and to provide a reference for postcyclic shear behavior. Table 8.3 lists all static triaxial compression tests on the MRV silt-bentonite mixtures. Here, the specimen MSB1 had an added bentonite content of 1.25%, and its PI was not determined using tests, but rather predicted to be 6.0 based on PIs of soil mixtures with added bentonite content of 0% and 2.5%.

Table 8.3. Static triaxial compression tests on the MRV silt-bentonite mixtures

Test ID	PI	B-value	σ'_c (kPa)	OCR	e	t_{50} (sec)	Strain rate (/min)
MSB1	6.0	0.99	90.0	1	0.653	18	0.022%
MSB2	6.2	1.00	50.0	1	0.721	85	0.005%
MSB3	6.2	0.98	90.0	1	0.649	NA	0.009%
MSB4	6.2	0.98	243.0	1	0.609	25	0.008%
MSB5	6.2	1.00	90.0	8	0.559	44	0.009%
MSB6	9.4	1.00	50.0	1	0.745	160	0.003%
MSB7	9.4	0.99	90.0	1	0.628	360	0.005%
MSB8	9.4	0.97	90.0	8	0.506	380	0.005%
MSB9	9.4	0.98	49.4	1	0.783	700	0.005%

Mainly, the normally consolidated tests were run on the specimens with bentonite added, except for the specimens MSB5 and MSB8, which were applied to determine the consolidation parameters. To make use of these tests, the effective consolidation pressures were rebound from 720 kPa to 90 kPa to obtain OCRs of 8. The undrained compression tests were conducted on these overconsolidated specimens to study the effect of PI on the shear behavior of overconsolidated specimens.

To equalize pore pressure throughout the soil specimens, suitable strain rates were required for static shear tests. Except for silt-clay specimens with added bentonite contents of 5.0% and 7.5%, the strain rates for shearing were computed based on the t_{50} (ASTM standard D 4767-04). If the strain rates for the soils with the bentonite contents of 5.0% and 7.5% were determined based on the t_{50}, it would take over 20 days for shearing. Figure 8.2c indicates that there was no significant difference in permeability among specimens with added bentonite contents of 2.5% and 5.0%; therefore, the strain rate for specimens MSB7, MSB8, and MSB9 was determined to be 0.005%/min.

8.2.1 Undrained Shear Behavior: Normally Consolidated. Figure 8.4 shows the undrained shear behavior of the specimens consolidated normally to an effective consolidation pressure of 50 kPa. The natural MRV silt specimen (MS1) had greater yield strength than the specimens with added bentonite (MSB2, MSB6, and MSB9). After yield stress, the deviator stress in the natural MRV silt specimen temporarily decreased more than in the soil mixtures, suggesting a more obvious quasi-steady state. The same occurred in specimens consolidated normally to an effective consolidation pressure of 90 kPa, as shown in Figure 8.5.

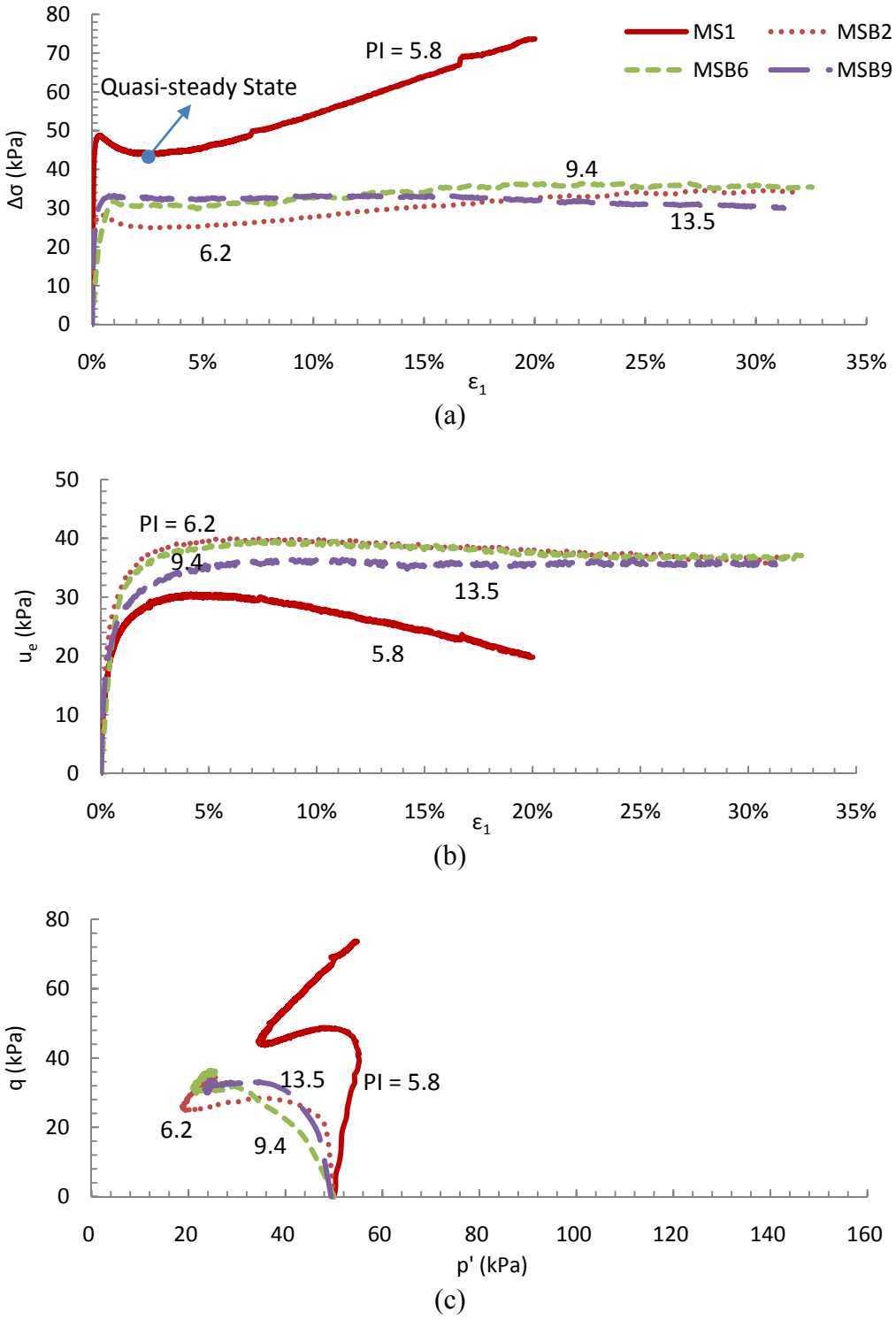

Figure 8.4. Monotonic shear behavior of MRV silt-bentonite mixtures consolidated normally to an effective consolidation pressure of 50 kPa: (a) $\Delta\sigma$ vs. ε_1, (b) u_e vs. ε_1, (c) q vs. p'

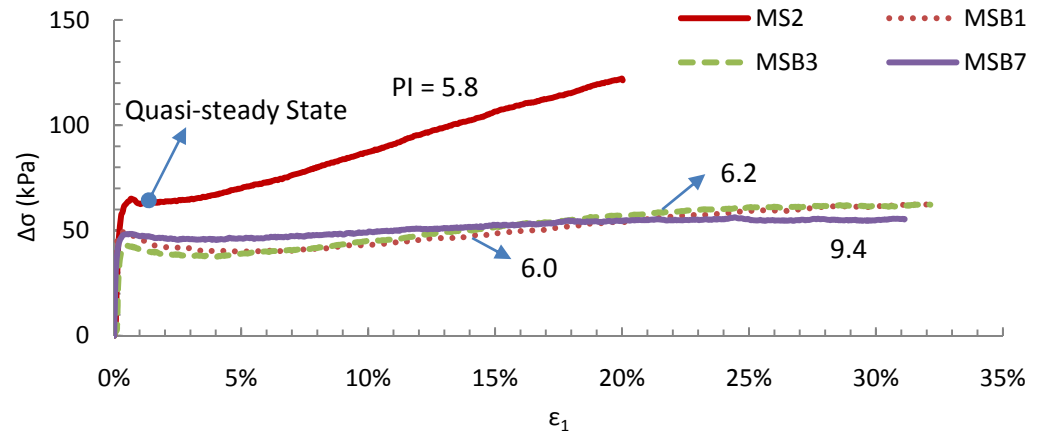

(a)

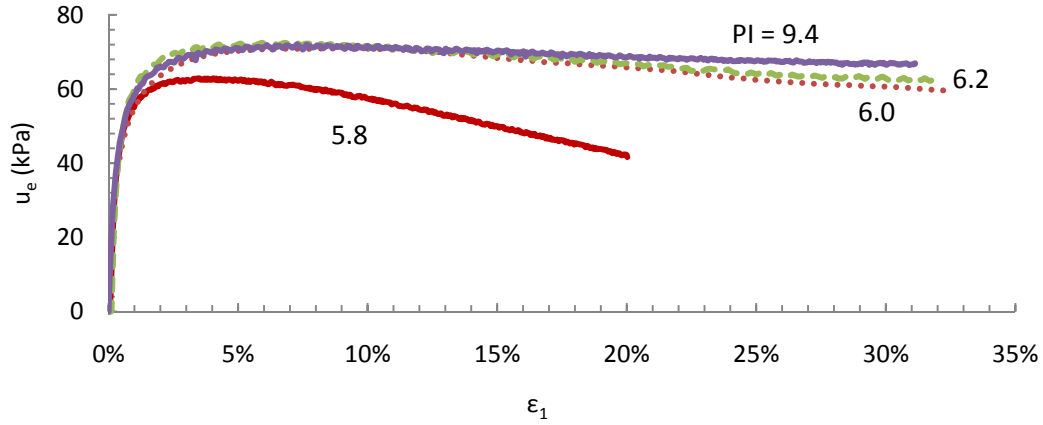

(b)

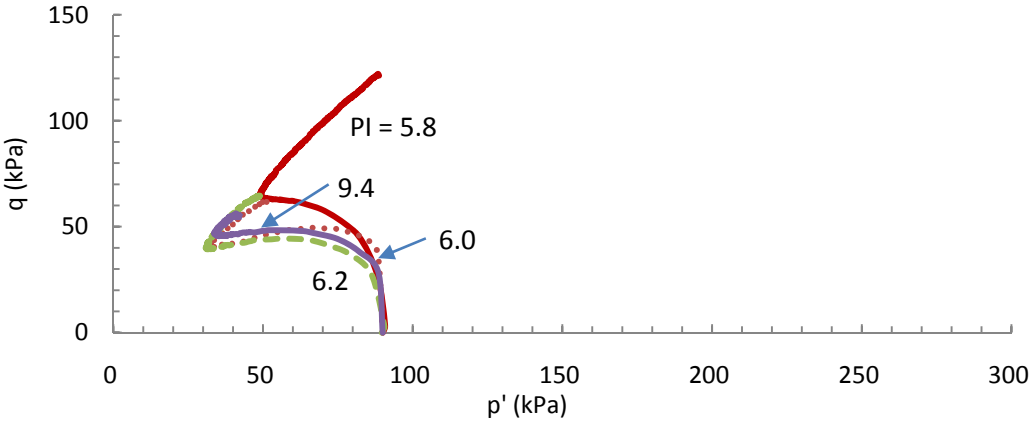

(c)

Figure 8.5. Monotonic shear behavior of MRV silt-bentonite mixtures consolidated normally to an effective consolidation pressure of 90 kPa: (a) $\Delta\sigma$ vs. ε_1, (b) u_e vs. ε_1, (c) q vs. p'

After the quasi-steady state, most soil specimens (except that with a PI of 13.5) displayed strain-hardening behavior until the critical state, which was reached at large strain (> 25%). For specimens with lower percentage of bentonite, the strain-hardening was more obvious, as shown in Figures 8.4a and 8.5a. The deviator stress-strain curve is almost flat for the soil mixture with a PI of 13.5 at an effective consolidation pressure of 50 kPa (Figure 8.4a), indicating perfectly plastic behavior. However, generally, there was no significant difference in undrained shear strength or in shape of the curves of deviator stress versus axial strain, excess pore pressure versus axial strain, and stress path among the specimens with PIs in the range of 6.0-13.5.

8.2.2 Undrained Shear Behavior: Overconsolidated. Figure 8.6 shows the undrained shear behavior of specimens at an effective consolidation pressure of 90 kPa and an OCR of 8. For comparison, Figure 8.6 also plots the curves for the normally consolidated soils at effective consolidation pressure of 90 kPa. With OCR of 8, none of specimens exhibited quasi-steady state because the deviator stress kept increasing regardless of a significant reduction in the slope of the deviator stress-strain curve (Figure 8.6a). Further, negative excess pore pressure developed in these specimens (Figure 8.6b), and they dilated more than the normally consolidated soils (Figure 8.6c).

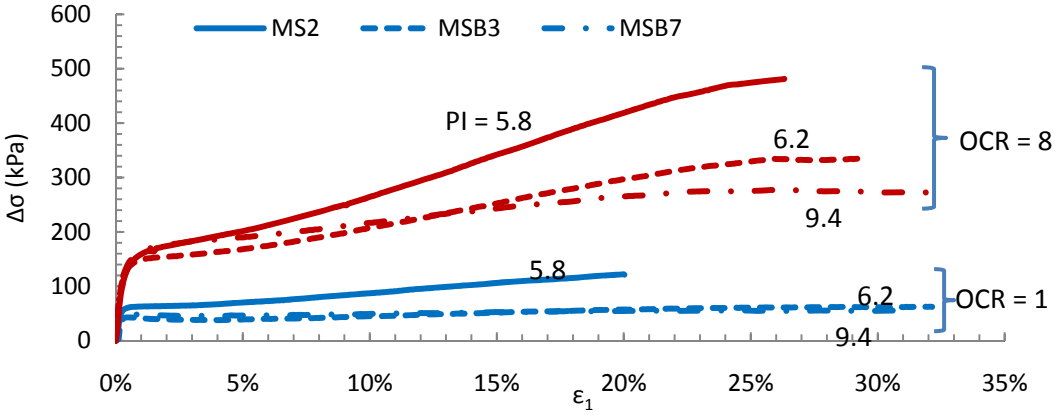

(a)

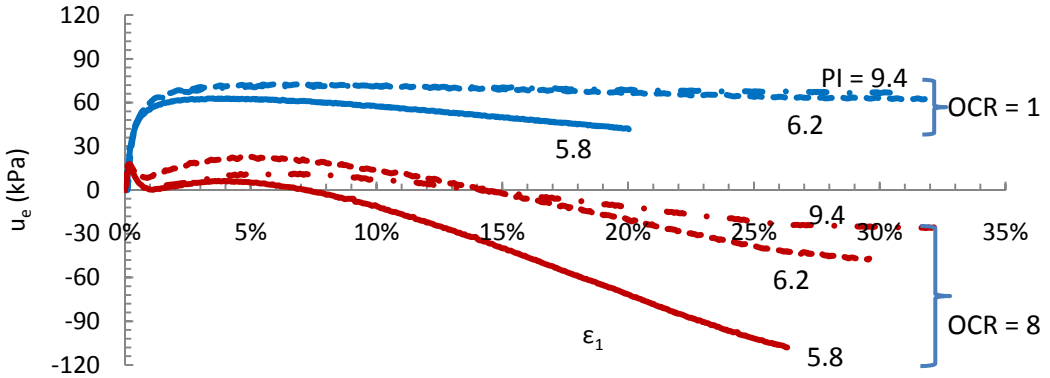

(b)

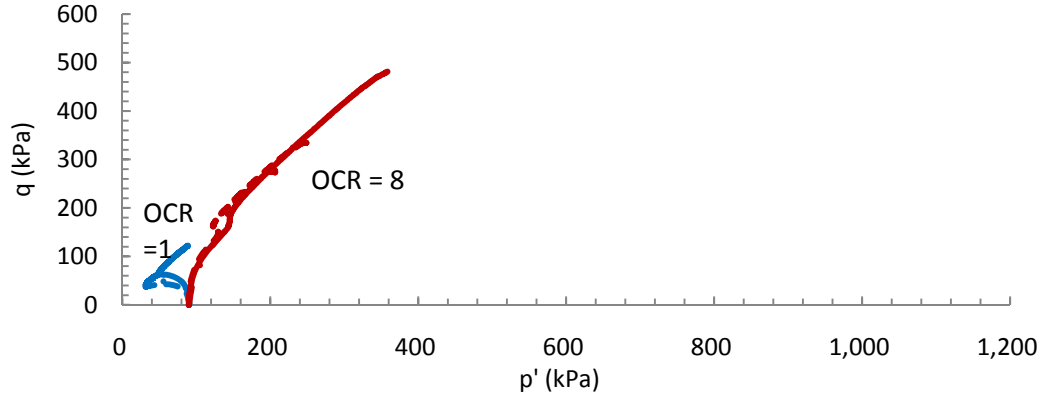

(c)

Figure 8.6. Monotonic shear behavior of MRV silt-bentonite mixtures at effective consolidation pressure of 90 kPa and OCRs of 1 and 8: (a) $\Delta\sigma$ vs. ε_1, (b) u_e vs. ε_1, (c) q vs. p'

Figure 8.7 reexamines the excess pore pressure response of the overconsolidated soils at small strain. Surprisingly, the curves of excess pore pressure versus axial strain of all specimens with OCRs of 8 have two peaks: one at an axial strain of about 0.2% and the other at an axial strain within the range of 3-7%. This response has never been observed in other soils, based on the knowledge of the author. Normally, highly overconsolidated soil has one peak excess pore pressure; positive excess pore pressure develops initially, then drops to negative excess pore pressure. The two peaks observed in the curves required further investigation.

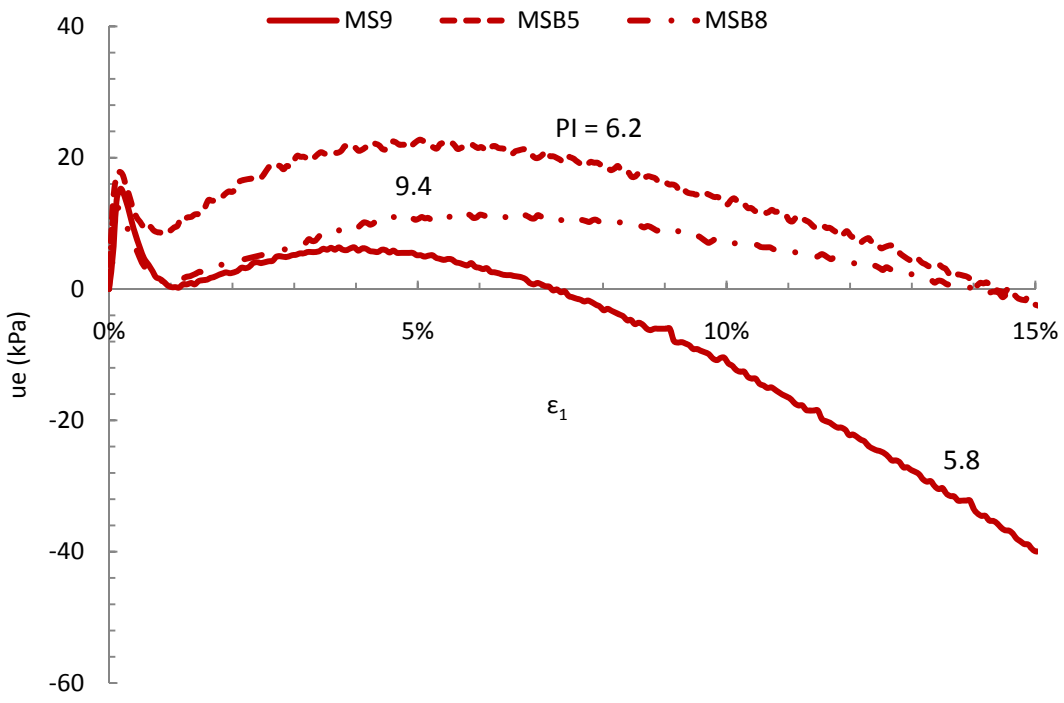

Figure 8.7. Excess pore pressure responses of MRV-bentonite mixtures at effective consolidation pressure of 90 kPa and OCR of 8

Section 5 demonstrated that the curves of $\Delta\sigma$ vs. ε_1, u_e vs. ε_1, and q vs. p' can be normalized by effective consolidation pressure. As shown in Figure 8.8, the deviator stress was normalized by effective consolidation pressure for MRV silt-bentonite mixtures at OCRs of 1 and 8. The normalized deviator stress ($\Delta\sigma/\sigma'_c$) at a large strain (> about 11%) of the overconsolidated soils decreased with an increase in PI from 5.8 to 9.4. For normally consolidated soils, the normalized deviator stress decreased sharply with an increase in PI from 5.8 to 6.0. A further increase in PI produced no significant difference in the normalized deviator stress at large strain.

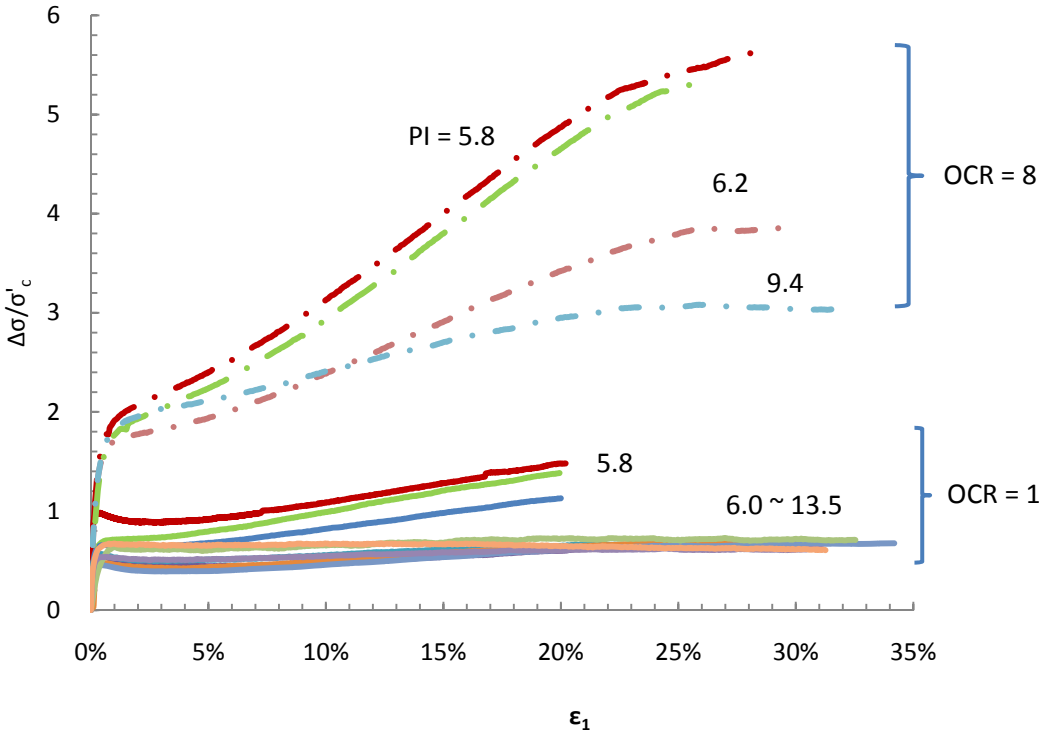

Figure 8.8. Normalized deviator stress of the MRV silt and its mixtures with bentonite at an effective consolidation pressure of 90 kPa and OCRs of 1 and 8

8.2.3 Effective Friction Angle. Using a failure criterion of 15% axial strain, which is preferred for calculation of the effective friction angle, as noted in Section 5, Figure 8.9 shows the determination in effective friction angles of the MRV silt-bentonite mixtures. For comparison, the figure also includes the result for the natural MRV silt. Overconsolidation did not change the effective friction angle for the natural MRV silt because a straight line was plotted to best-fit all Mohr circles of normally consolidated and overconsolidated specimens. For the soil mixtures with PIs of 6.2 and 9.4, however, it was difficult to use a straight line to best-fit all Mohr circles in the τ-σ' space. Thus, the effective friction angle of the MRV silt-bentonite mixtures with a high OCR may be different from that of normally consolidated soils. The difference is likely a result of the fact that the soil mixtures with PIs greater than 6.2 have "memory" of stress history like clays.

The effective friction angles of the soil mixtures with added bentonite were determined based only on the normally consolidated specimens. As shown in Figure 8.9, the soil mixtures with PIs of 6.2 and 9.4 had effective friction angles of 32.3° and 31.8°, respectively. Additionally, the soil mixture with a PI of 9.4 had cohesion (c) of 2.9 kPa. Thus, the effective friction angle decreased with an increase in PI.

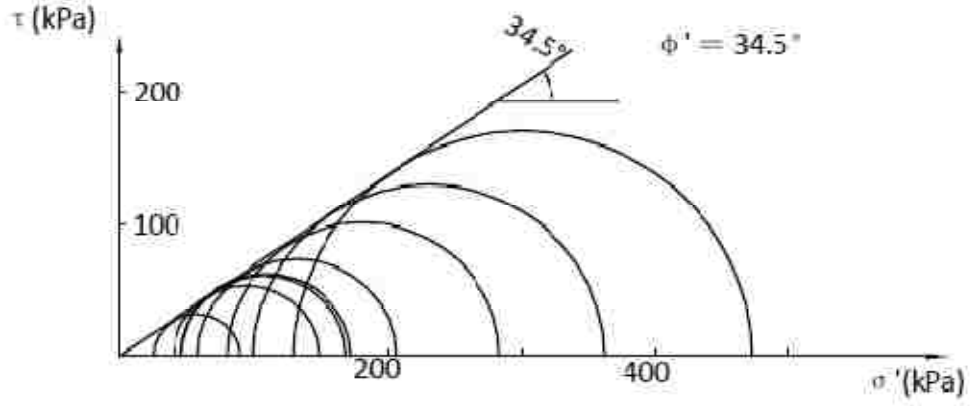

(a)

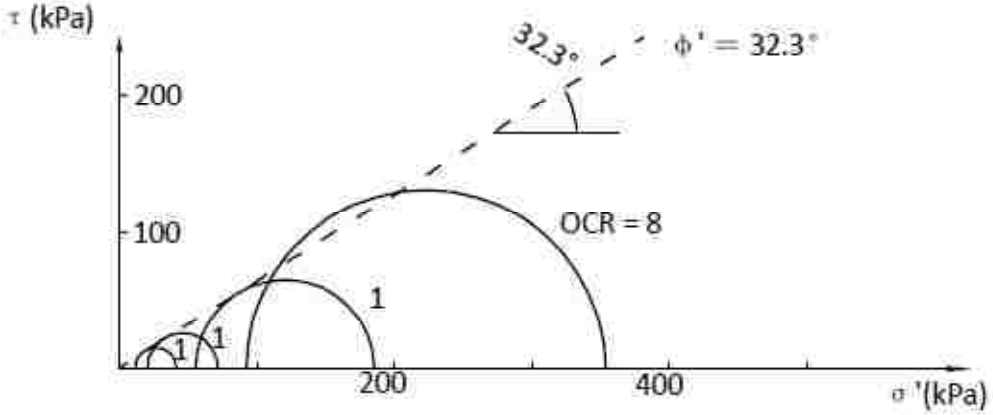

(b)

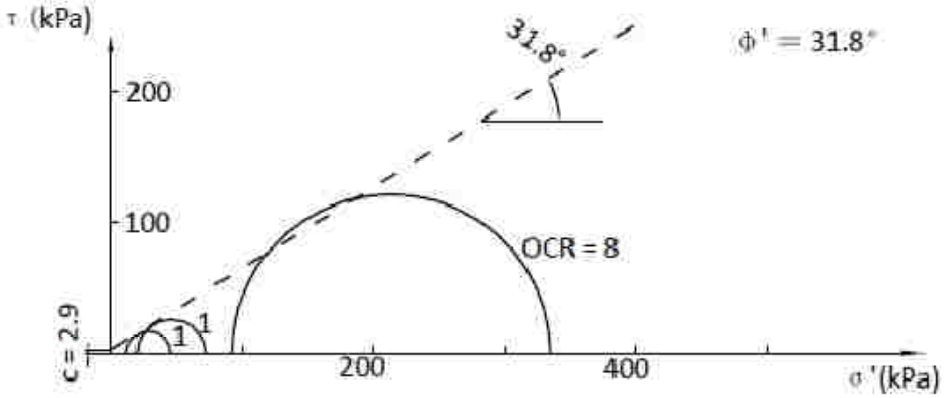

(c) PI = 9.4

Figure 8.9. Effective friction angles of MRV silt and its mixtures with bentonite using failure criterion of 15% axial strain: (a) PI = 5.8, (b) PI = 6.2, (c) PI = 9.4

8.2.4 Critical State Line. Figure 8.10 shows the CSLs of the MRV soil mixtures with PIs of 6.2 and 9.4. For comparison, it also plots the CSL of the natural MRV silt. As noted in Section 5, the CSL of the natural silt is not parallel to its NCL (Figure 8.9a). It has a phase transformation line (PTL). Figures 8.9b and 8.9c indicate that, when the bentonite was added to the MRV silt, the resulting mixtures had CSLs but not PTLs. Furthermore, the CSLs of the soil mixtures with PIs of 6.2 and 9.4 are almost parallel to their NCLs, as in most clays. Thus, the natural MRV silt behaves like an intermediate soil, which has both sand-like (CSL nonparallel to NCL) and clay-like (normalized behavior) behavior, as noted in Section 5. The soil mixtures with PIs greater than 6.2 behave more like clay in that their CSLs are almost parallel to their NCLs, and they do not have PTLs.

This observation is in agreement with testing results of three blended silt mixtures obtained from an aggregate mine's tailings pond reported by Romero (1995). The NCL and CSL for nonplastic silt #1 of Romero are not parallel; Silt #3 with a PI of 10.5 had essentially parallel NCL and CSL lines and did not exhibit quasi-steady state line (QSSL) behavior; Silt #2 with a PI of 4 had approximately parallel ICL and CSL lines like silt #3, but with a QSSL (Boulanger, 2006). It should be noted that the QSSL called by Boulanger (2006) was changed to be PTL in this work.

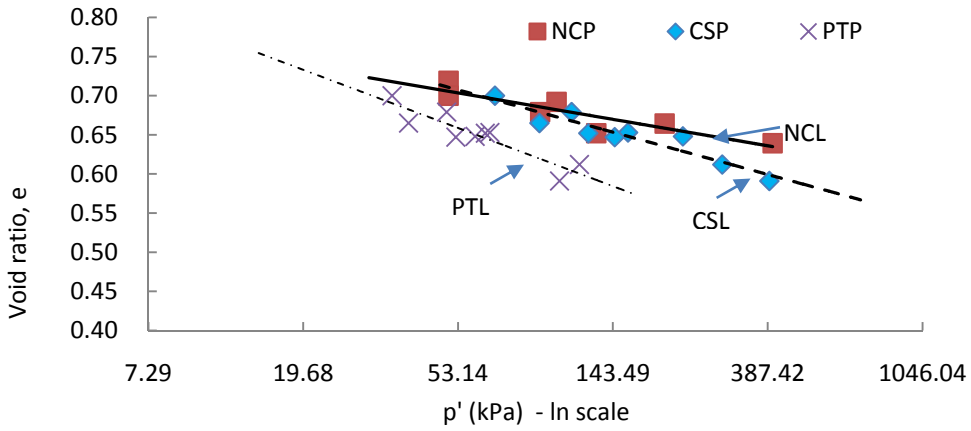

(a)

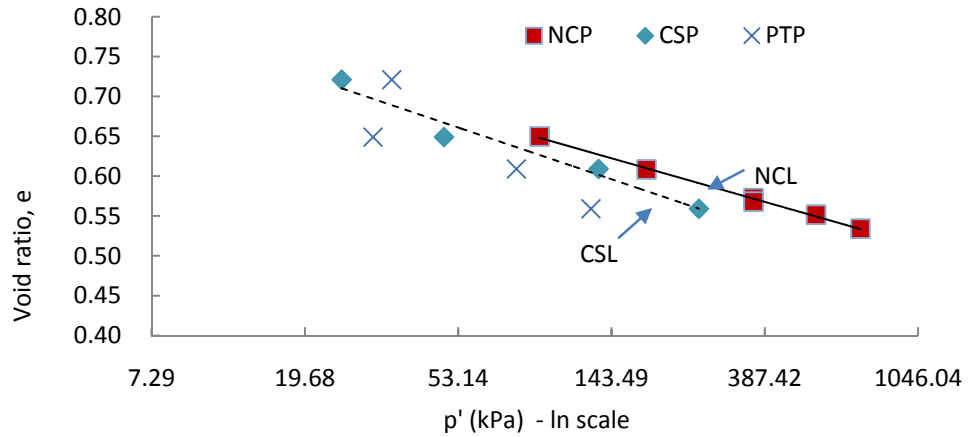

(b)

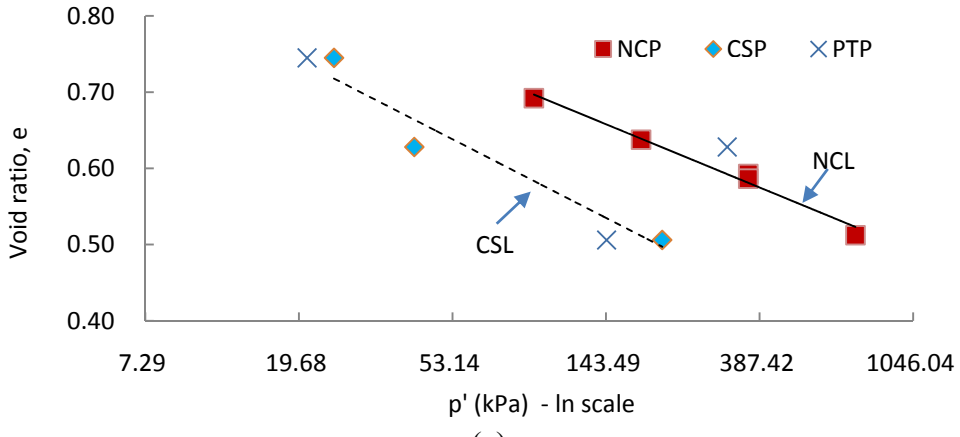

(c)

Figure 8.10. Critical state lines of MRV silt-bentonite mixtures: (a) PI = 5.8, (b) PI = 6.2; (c) PI = 9.4

8.3 EFFECT OF PLASTICITY ON CYCLIC SHEAR BEHAVIOR

Cyclic triaxial tests were conducted to investigate the cyclic shear behavior of the MRV silt mixtures with bentonite. Two levels of plasticity were tested: PIs of 6.2 and 9.4. Table 8.4 summarizes all cyclic triaixal tests. Initially, the cyclic tests on the natural MRV silt were conducted using a controlled excess pore pressure ratio (R_u) controlled. The cyclic tests were designed to stop when the excess pore pressure ratio reached 1.0. However, early test results indicated that the excess pore pressure of the MRV silt mixtures with bentonite could not reach 1.0; thus, the cyclic tests were stopped at the desired cyclic strains.

Table 8.4. Cyclic triaxial tests on the MRV silt-bentonite mixtures

Test ID	PI	B-value	σ'_c (kPa)	e	CSR	N_{cyc}	R_u	$u_{e,\,cyc}$ (kPa)	ε_{cyc} (%)
MFB1	6.0	0.95	90.5	0.675	0.25	5.46	0.89	80.9	20.53
MFB2	6.2	0.95	91.3	0.660	0.25	7.23	0.86	78.7	16.1
MFB3	6.2	0.94	91.9	0.667	0.18	126.17	0.89	81.7	16.9
MFB4	6.2	0.93	91.2	0.648	0.18	160.37	0.92	83.9	9.02
MFB5	6.2	0.95	90.4	0.675	0.18	89.18	0.86	77.5	8.99
MFB6	6.2	0.93	90.6	0.660	0.35	1.13	0.78	70.9	9.04
MFB7	9.4	0.95	91.2	0.690	0.18	407.29	0.82	74.6	8.99
MFB8	9.4	0.95	91.3	0.688	0.25	12.13	0.64	58.9	9.44
MFB9	9.4	0.94	91.3	0.685	0.35	1.15	0.55	50.0	8.98

8.3.1 Excess Pore Pressure Response. Figures 8.11-8.13 show the cyclic shear behavior of the MRV silt and its mixtures with bentonite. For all soils, the excess pore

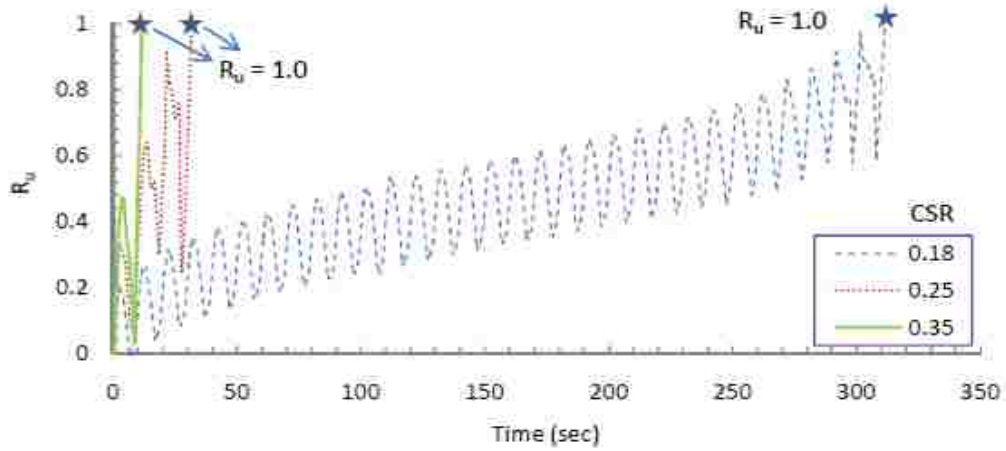

(a)

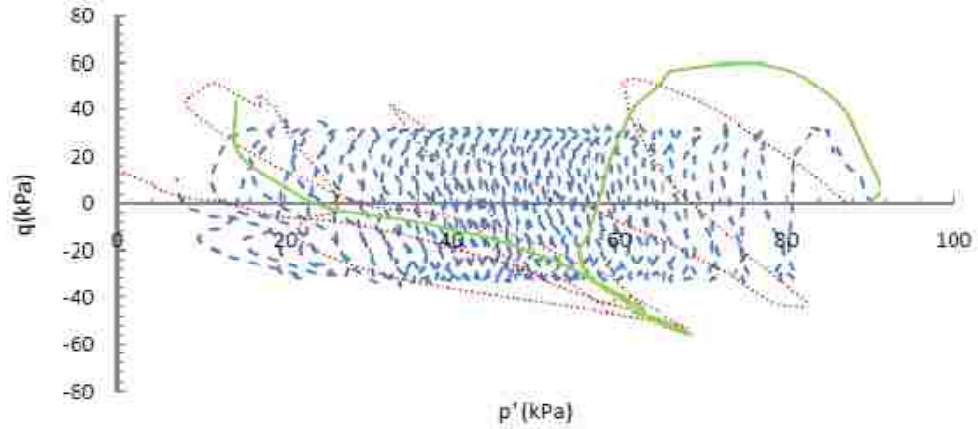

(b)

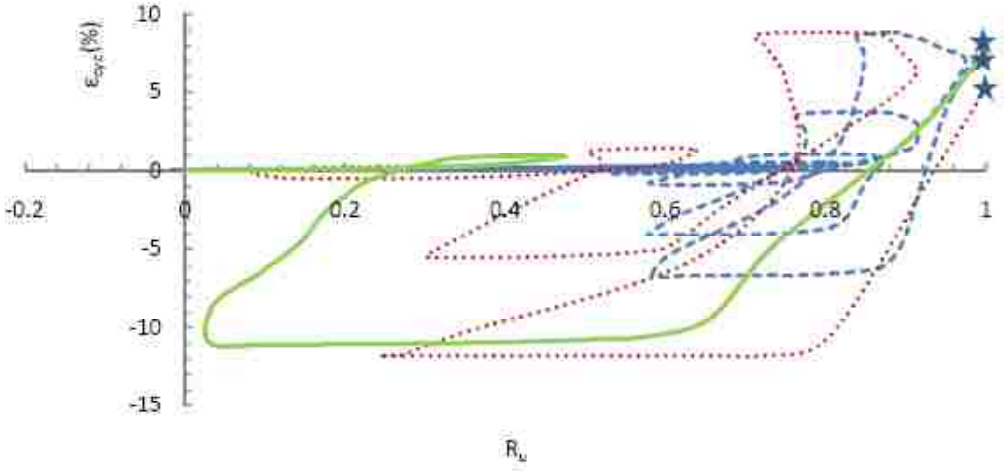

(c)

Figure 8.11. Cyclic shear behavior of MRV silt with a PI of 5.8: (a) R_u vs. Time, (b) q vs. p', (c) ε_{cyc} vs. R_u

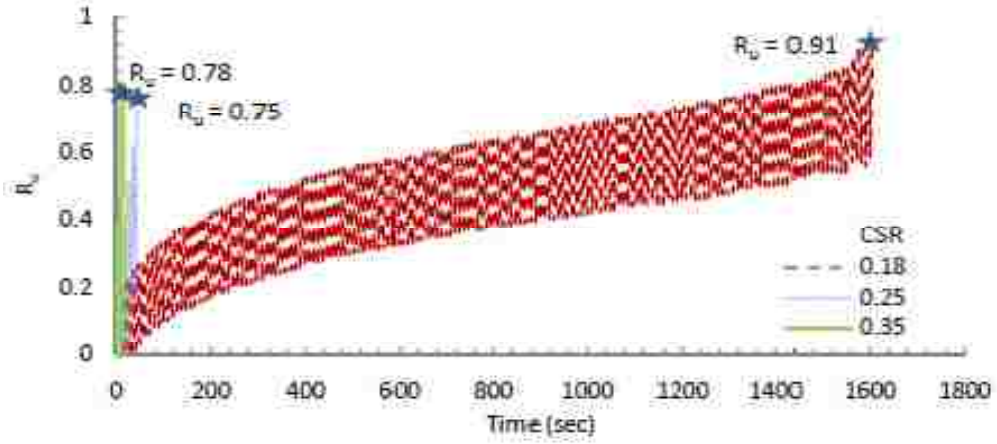

(a)

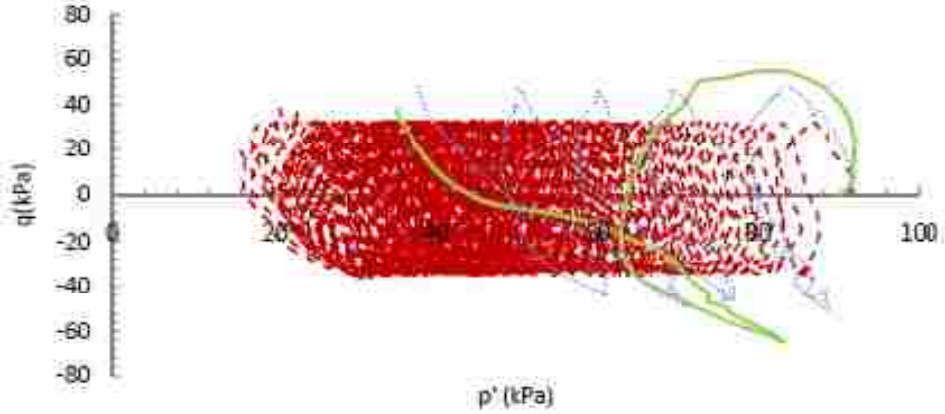

(b)

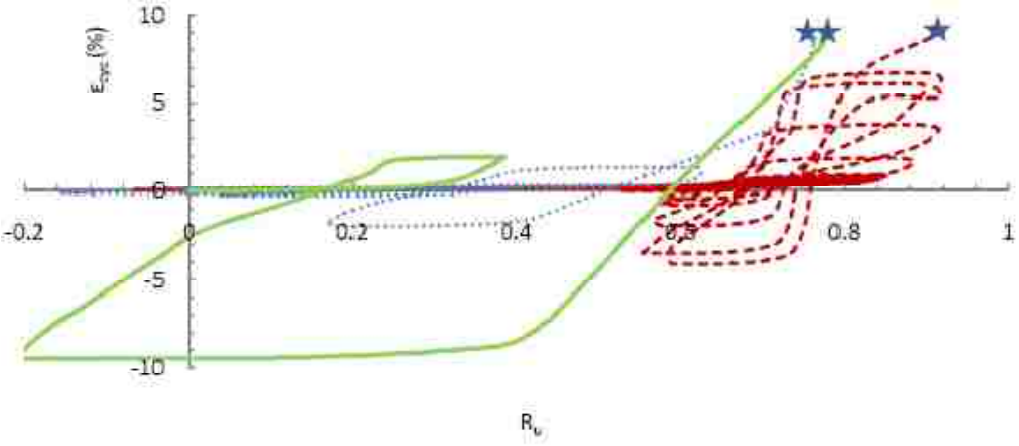

(c)

Figure 8.12. Cyclic shear behavior of MRV silt-bentonite mixture with a PI of 6.2: (a) R_u vs. Time, (b) q vs. p', (c) ε_{cyc} vs. R_u

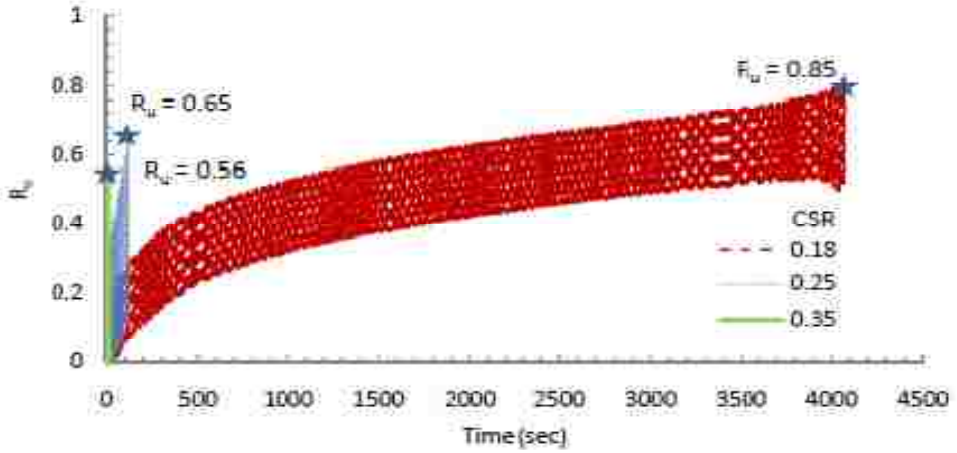

(a)

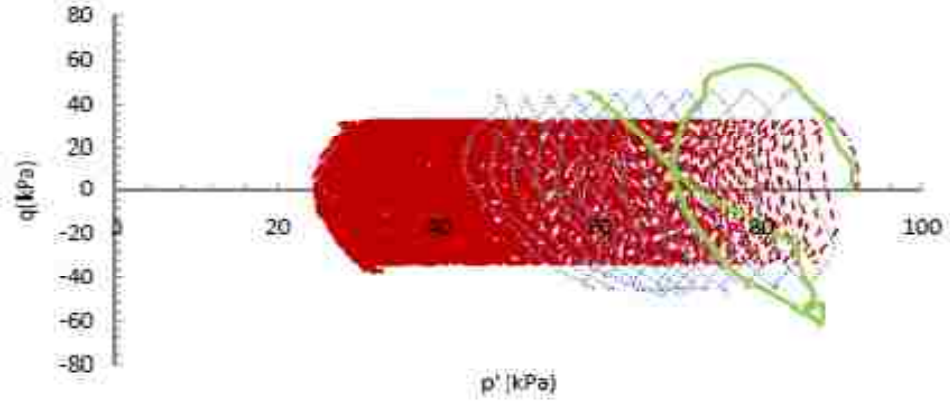

(b)

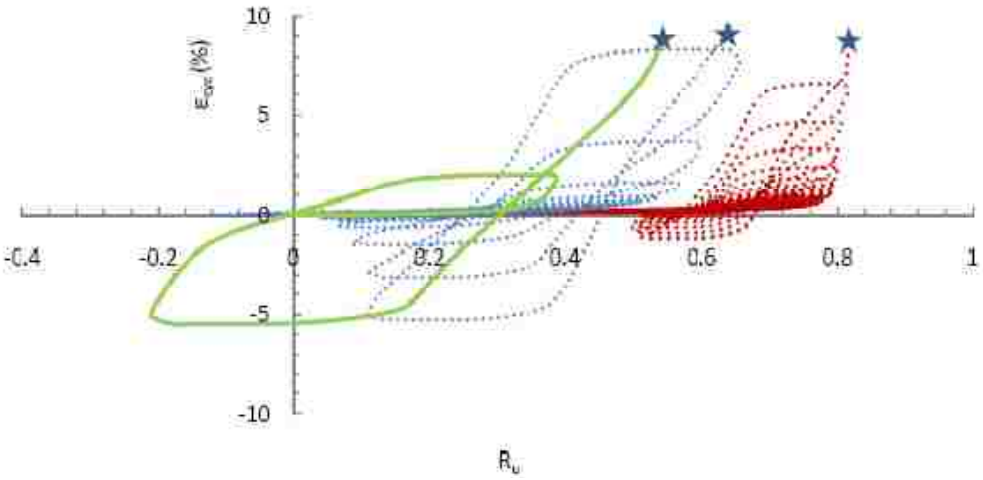

(c)

Figure 8.13. Cyclic shear behavior of MRV silt-bentonite mixture with a PI of 9.4: (a) R_u vs. Time, (b) q vs. p', (c) ε_{cyc} vs. R_u

pressure ratio build-up was more quickly with an increase in CSR. The soil with different added bentonite content had different excess pore pressure ratio at the cyclic strain (ε_{cyc}) of up to 9.0%. The natural MRV silt with a PI of 5.8 reached an R_u of 1.0 at the end of cyclic loading with a CSR of 0.18. However, the soil mixtures with PIs of 6.0, 6.2, and 9.4 only developed excess pore pressure ratios of less than 1.0 at end of tests (Table 8.4). To show the effect of PI on the development of excess pore pressure, Figure 8.14 shows the curves of excess pore pressure ratio versus time for all specimens with CSRs of 0.18. The three curves with PIs of 5.8, 6.2, and 9.4 were obtained from specimens MF1R2, MFB4, and MFB7, respectively, all of which had positive cyclic strain of about 9.0% at the end of cyclic loading. The specimen with higher PI required more time to reach the cyclic strain of about 9.0%, and it had a lower excess pore pressure ratio at the end of cyclic loading (Figure 8.14a). As a result, there was higher sustaining effective confining pressure at the end of cyclic loading (Figure 8.14b). Figure 8.14c shows the curve of axial strain versus excess pore pressure ratio during cyclic loading. The large axial strain of the specimen with higher PI appeared at less R_u.

Thus, the failure mode of the natural MRV silt with a PI of 5.8 was initial liquefaction under cyclic loading. Conversely, the soil mixtures with PIs of 6.0, 6.2, and 9.4 did not show initial liquefaction rather than cyclic softening, although their PI increased slightly when the added bentonite content was 1.25%. This finding comes close to supporting suggestion of Boulanger and Idriss (2006) that soil with a PI of at least 7 can be thought to have clay-like behavior. For the MRV silt tested here, the critical PI can be thought to be 6.0, which is slightly lower than the value presented by Boulanger and Idriss (2006).

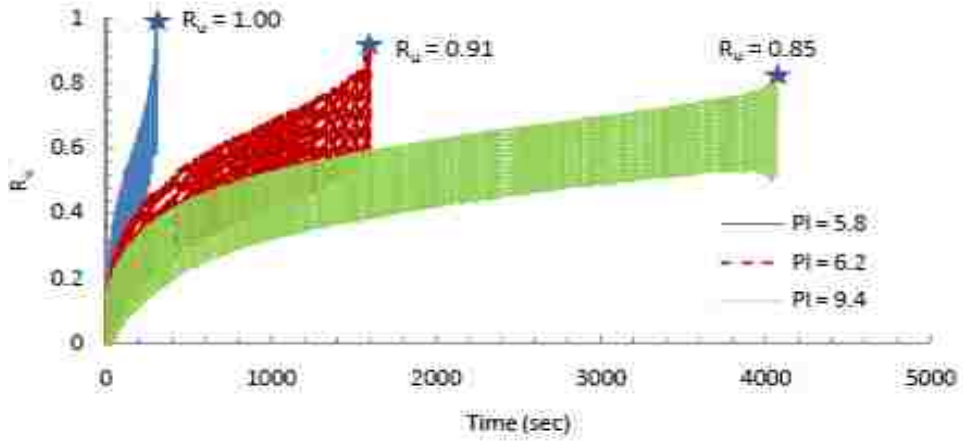

(a)

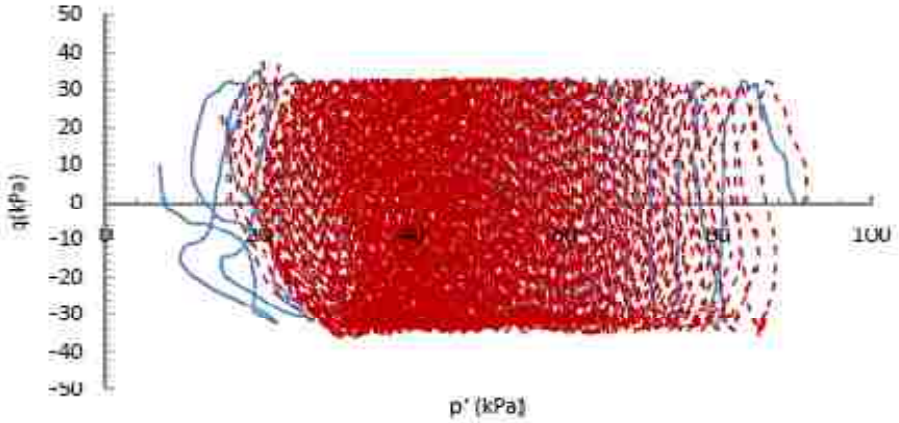

(b)

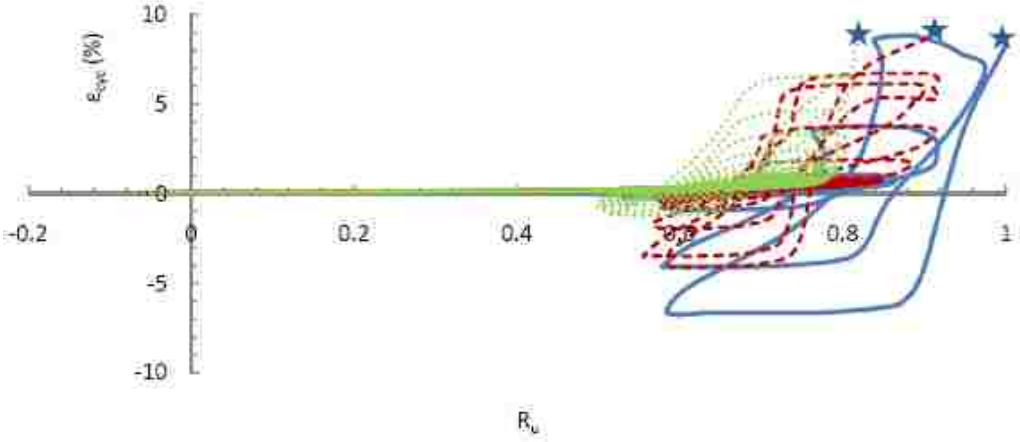

(c)

Figure 8.14. Cyclic shear behavior of MRV silt and its mixtures with various PIs at a CSR of 0.18: (a) R_u vs. Time, (b) q vs. p', (c) ε_{cyc} vs. R_u

It is noteworthy that the frequency of cyclic tests for all soils with various PIs was 0.1 Hz. As shown in Figure 8.2, the permeability of the soil decreased sharply with added bentonite content of 2.5%. As a result, the transmission of pore pressure from the specimen inside to the pore pressure transducer required more time; therefore, the pore pressure transducer, which was located outside the specimens, provided less accurate pore pressure readings for the soil with higher PI. The additional time required for the transition of pore pressure from the specimen to the transducer location could explain, in part, why the excess pore pressure shown by the transducer at the end of cyclic loading was lower with a higher CSR, as shown in Figure 8.13a. With a smaller CSR, the build-up of excess pore pressure was slower, so there was more time to transmit pore pressure from the specimen inside to the transducer during cyclic loading. Accurate measurements of pore pressure require that a miniature pore pressure transducer be placed in the specimen to measure pore pressure during dynamic loading (Muraleetharan and Granger, 1999).

8.3.2 Liquefaction Resistance. Cyclic failure was defined using the criterion of double-amplitude axial strain ($\varepsilon_{cyc,\,DA}$) of 5.0% in this section (Boulanger, 1998; Bray and Sancio, 2006; Beroya et al, 2009). Figure 8.15 shows the curves of CSR versus the number of loading cycles. Generally, at a CSR smaller than 0.35, the number of loading cycles required to induce a double-amplitude axial strain of 5.0% increased with an increase in PI from 5.8 to 9.4. This agrees with the finding by Guo and Prakash (1999), who examined the silt testing data by El Hosri et al. (1984). They presented that the liquefaction resistance increases with a decrease in PI in the low range, while the opposite is true in the high range of PI. The PI at the lowest liquefaction resistance is

around 4. When the CSR was equal 0.35, there was no significant difference in the number of loading cycles required for cyclic failures of the MRV silt regardless of PI. With larger CSRs, the curves of CSR versus the number of loading cycles were expected to be similar to the dashed lines in Figure 8.15. The fact that good liquefaction resistance curve at high CSR is probably related to the transmission of pore pressure in specimens with high PIs.

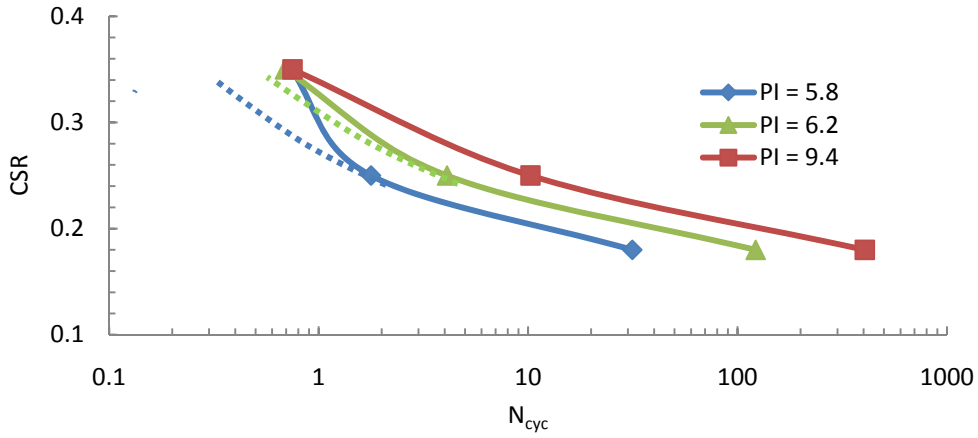

Figure 8.15. Variation in liquefaction resistance with PI of MRV silt-bentonite mixtures

8.4. EFFECT OF PLASTICITY ON POSTCYCLIC BEHAVIOR

The change of monotonic shear behavior due to cyclic loading should vary with PI because the soil with different plasticity has different resistance to be remolded during cyclic loading. Table 8.5 shows monotonic shear tests on specimens experiencing previous cyclic loading. Some of the postcyclic monotonic tests had different CSRs during cyclic loading (Table 8.5). As noted in Section 6, CSR had no significant effect on

postcyclic shear behavior, which was governed by the liquefaction level. Thus, the effect of CSR on the postcyclic shearing behavior of the MRV silt mixtures with bentonite was also assumed to be small and ignored here. The strain rates for the specimens with added bentonite contents of 2.5% and 5.0% were determined according to the respective t_{50} obtained in reconsolidation (ASTM standard D 4767 – 04), respectively.

Table 8.5. Postcyclic monotonic tests on MRV silt-bentonite mixtures

Test ID	PI	σ'_c (kPa)	CSR	ε_{cyc} (%)	U_{rc} (%)	u_e after Reconsol.	ε_v (%)	t_{50} (min)	Strain Rate (/min)
MFB2	6.2	91.3	0.25	16.1	100	0	5.36	65	0.009%
MFB3	6.2	91.9	0.18	16.9	0	87.1	NA	NA	0.009%
MFB4	6.2	91.2	0.18	9.02	100	0	3.40	40	0.009%
MFB5	6.2	90.4	0.18	8.99	0	81.3	NA	NA	0.009%
MFB6*	6.2	90.6	0.35	9.04	100	0	NA	28	NA
MFB7	9.4	91.2	0.18	8.99	100	0	2.60	110	0.004%
MFB8	9.4	91.3	0.25	9.44	0	74.1	NA	NA	0.004%
MFB9*	9.4	91.3	0.35	8.98	100	0	NA	140	NA

8.4.1 Variation in Consolidation Parameters. Figure 8.16 shows the reconsolidation curves of the MRV silt with added bentonite. As in the case of the natural MRV silt, the reconsolidation curves for the soil mixtures with PIs of 6.2 and 9.4 are more parallel to their compression lines than to their recompression lines. Thus, with a PI up to 9.4 (or perhaps higher), the soil mixture is remolded during cyclic loading and behaves more like freshly deposited soils.

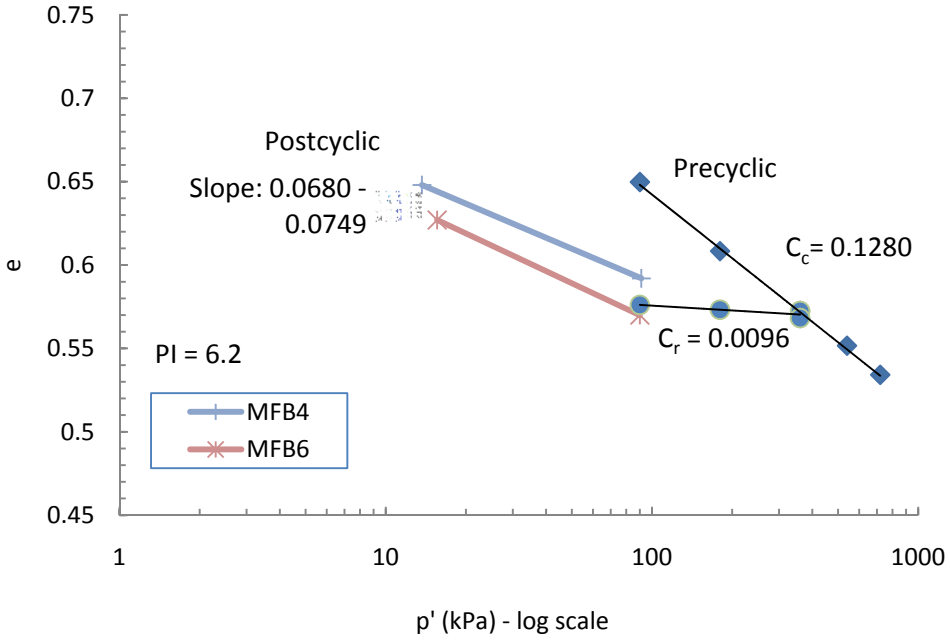

(a)

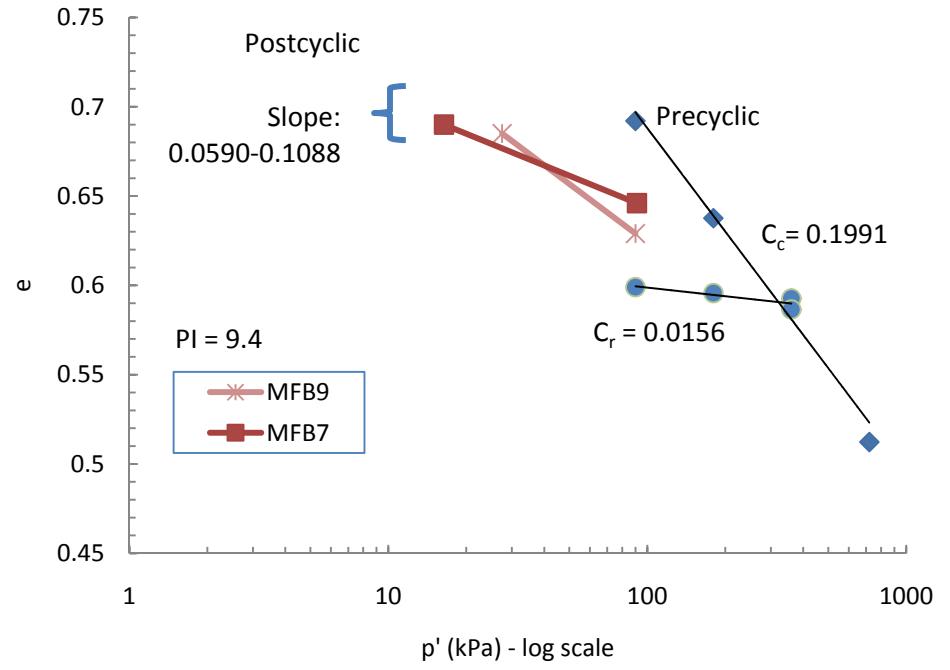

(b)

Figure 8.16. Reconsolidation curves of MRV silt with added bentonite: (a) PI = 6.2; (b) PI = 9.4

Table 8.6 shows the postcyclic permeability (k') and compression index (C'_c). As shown in Figure 8.17, they were respectively divided by precyclic permeability (k) and precyclic compression index (C_c) to obtain the permeability and compression index ratios (k'/k and C'_c/C_c), which show the changes in permeability and compressibility, respectively, due to cyclic loading. Figure 8.17 indicates that the k'/k and C'_c/C_c were lower than 1.0; therefore, the permeability and compressibility of the soils were reduced due to cyclic loading. Further, the reductions in permeability and compressibility of the soil mixtures with PIs of 6.2 and 9.4 were greater than those of the natural MRV silt with a PI of 5.8. This greater reduction may be partially attributable to the higher increase of density of the soil with added bentonite as a result of reconsolidation. The PI had no apparent effect on reduction of permeability and compressibility. More tests are required to provide more data to investigate the effect of PI on change in permeability and compressibility due to cyclic loading.

Table 8.6. Postcyclic consolidation parameters of MRV silt-bentonite mixtures

Item	**Added Bentonite Content**		
	0%	2.5%	5.0%
PI	5.8	6.2	9.4
k' (cm/s)	5.54×10^{-7}	9.30×10^{-8}	4.35×10^{-8}
C'_c	0.0589	0.0724	0.1162

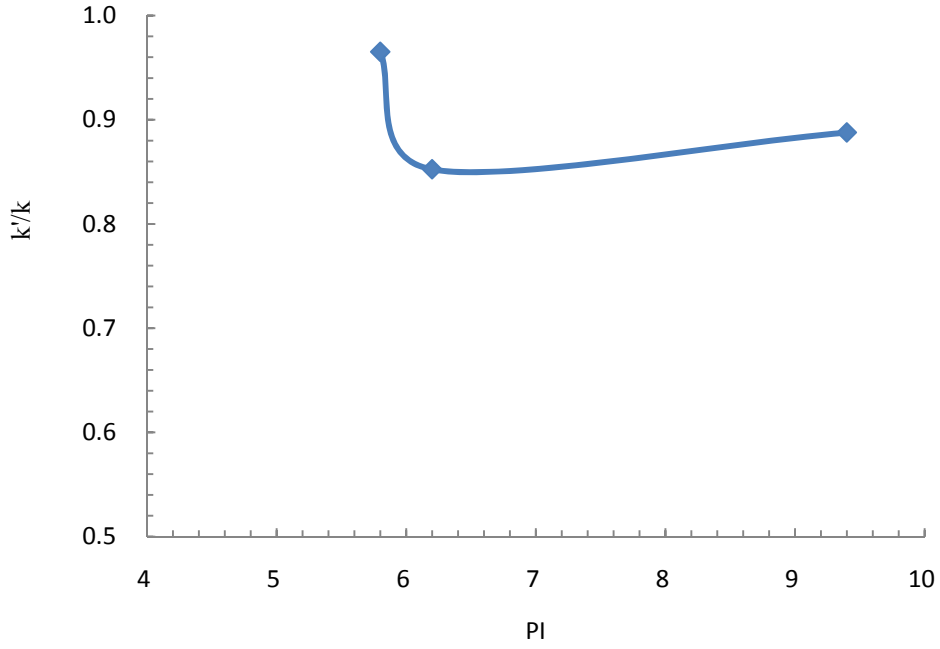

(a)

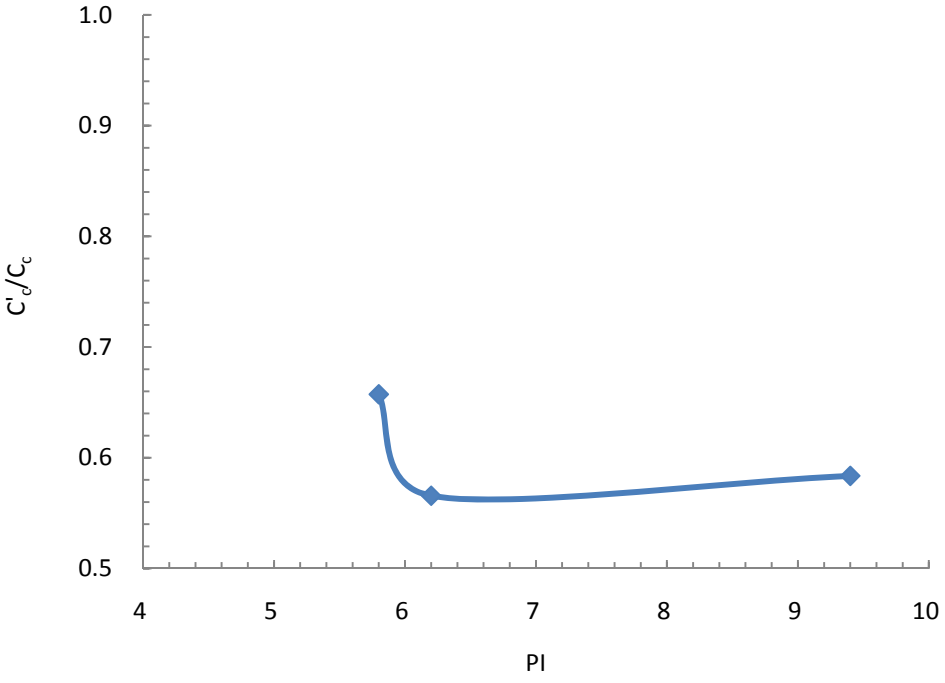

(b)

Figure 8.17. Variation of normalized permeability and compression index with PI of MRV silt-bentonite mixtures: (a) k'/k vs. PI, (b) C'_c/C_c vs. PI

8.4.2 Undrained Shear Behavior. Figure 8.18 shows the postcyclic shear behavior of the soil mixture with a PI of 6.2. For comparison, it also shows curves for static test on the mixture (MSB3) with the same added bentonite content. Specimens MFB2 and MFB4 were fully reconsolidated after cyclic axial strain (ε_{cyc}) of 16.1% and 9.02%, respectively. Since the density of the specimens increased due to reconsolidation, the reconsolidated specimens (MFB2 and MFB4) showed more strain-hardening behavior than the static specimen (MSB3) (Figure 8.18a). They also exhibited marked reductions in excess pore pressure after initial peak values (Figure 8.18b), and the specimens dilated more (Figure 8.18c). The reconsolidated specimens (MFB2 and MFB4) had significantly greater undrained shear strength at the critical state than the static specimen (MSB3). Conversely, the specimens without reconsolidation (MFB3 with a ε_{cyc} of 16.9% and MFB5 with a ε_{cyc} of 8.99%) had undrained shear strength close to that of the static specimen (MSB3), although different cyclic strains were induced by cyclic loading.

With full reconsolidation, specimen MFB2 with a ε_{cyc} of 16.1% had greater undrained shear strength than specimen MFB4 with a ε_{cyc} of 9.02%. Thus, the undrained shear strength was greater with higher cyclic strain. Without reconsolidation, specimen MFB3 with a ε_{cyc} of 16.9% had lower initial stiffness than specimen MFB5 with a ε_{cyc} of 8.99% because the former had lower effective confining pressure at the beginning of postcyclic shearing. However, the curves of deviator stress, excess pore pressure, and stress path are not significantly different for these two specimens (Figure 8.18). Especially at the large strain, the deviator stress versus axial strain curves of the postcyclic specimens MFB3 and MFB5 are close to that of static specimen MSB3. Thus,

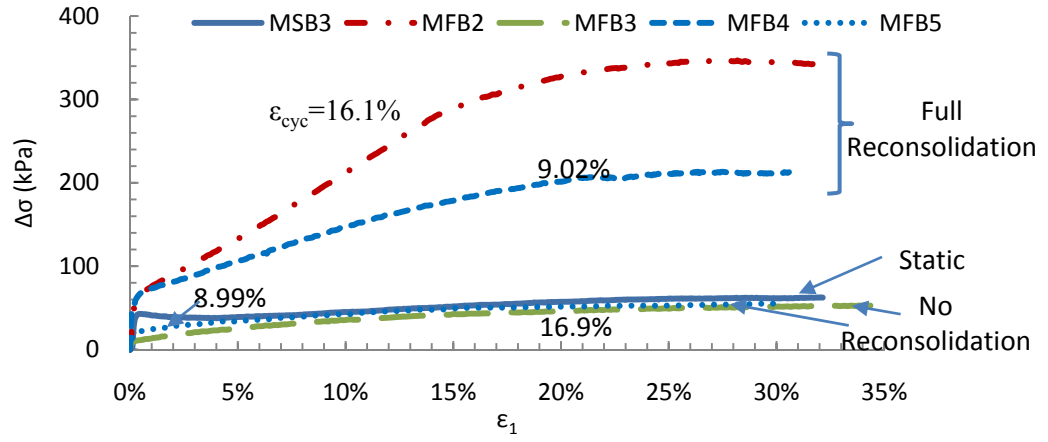

(a)

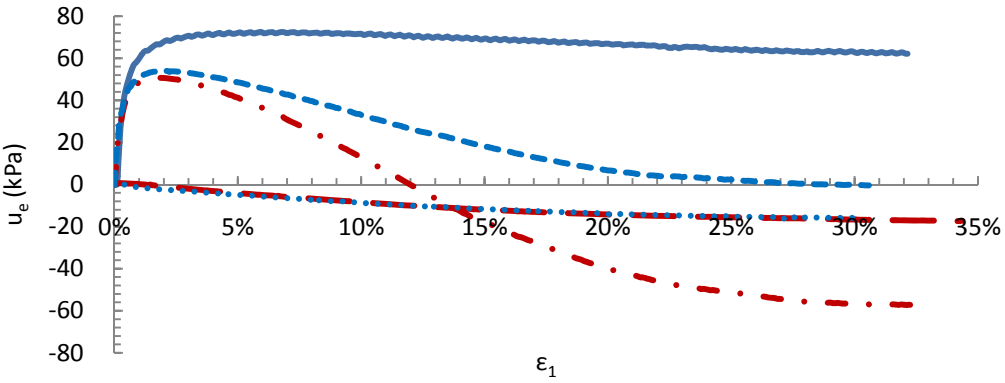

(b)

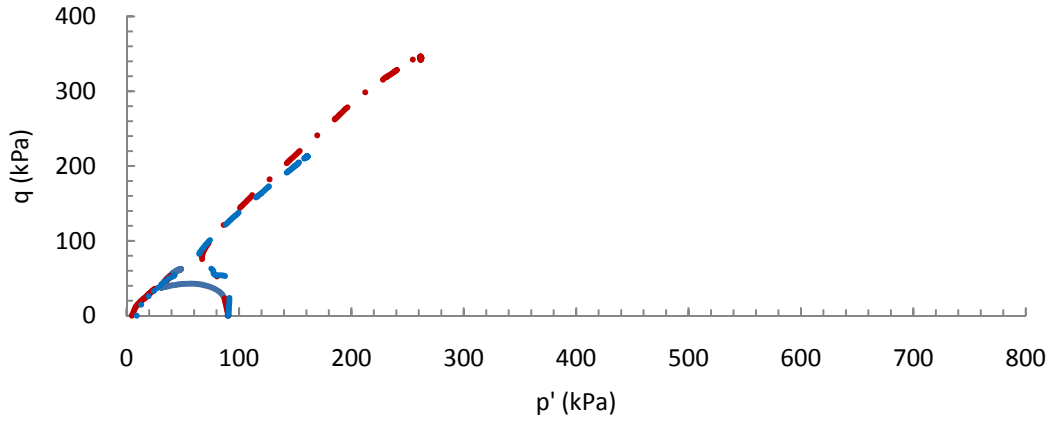

(c)

Figure 8.18. Postcyclic shear behavior of MRV silt-bentonite mixture with a PI of 6.2: (a) $\Delta\sigma$ vs. ε_1, (b) u_e vs. ε_1, (c) q vs. p'

the undrained shear strength of the soil mixture with a PI of 6.2 tends to be recovered at large deformation, regardless of the axial strain induced by cyclic loading.

Figure 8.19 shows the postcyclic monotonic shear behavior of the MRV silt-bentonite mixture with a PI of 9.4. Like the specimen with a PI of 6.2, the specimen with full reconsolidation (MFB7 with a ε_{cyc} of 8.99%) showed more strain-hardening behavior, a larger reduction in excess pore pressure after the initial peak value, and more dilative behavior than the specimen without previous cyclic loading (MSB7). On the other hand, the specimen without reconsolidation (MFB8 with a ε_{cyc} of 9.44%) had lower initial stiffness than that with no previous cyclic loading (MSB7). At large deformation, the specimen without reconsolidation (MFB8) had a deviator stress versus axial strain curve close to that of the specimen without previous cyclic loading (MSB7).

8.4.3 Shear Strength and Stiffness. This section addresses the changes in undrained shear strength and initial stiffness due to cyclic loading. By combining the testing results of the natural MRV silt (Figure 6.16), the effect of PI on changes in the strength and stiffness due to cyclic loading was addressed. Figure 8.20 shows the variations with PI in the undrained shear strength and initial stiffness of the specimens for each case. The postcyclic specimens had a residual axial strain of about 9.0% induced by previous cyclic loading. The undrained shear strength decreased sharply with an increase in PI from 5.8 to 6.2 in all cases including static tests, and postcyclic tests after no reconsolidation and full reconsolidation. With a further increase in PI, the decrease in undrained shear strength diminished; however, there was no consistent relationship between initial stiffness and PI.

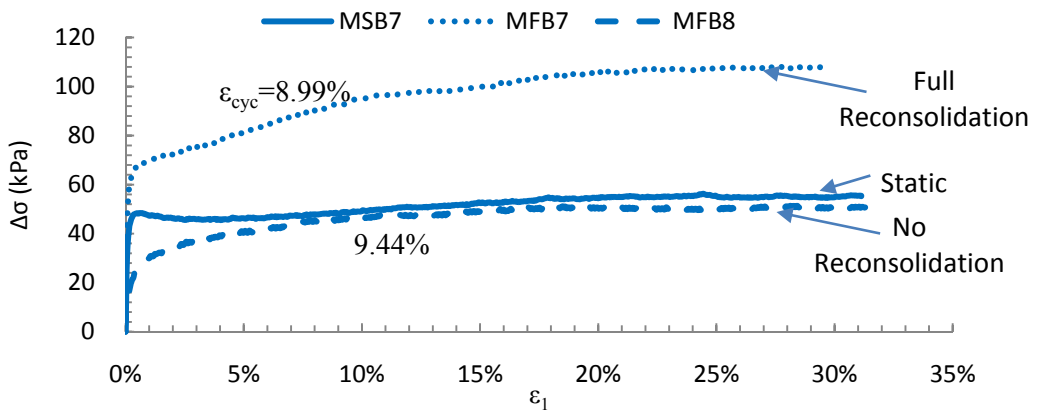

(a)

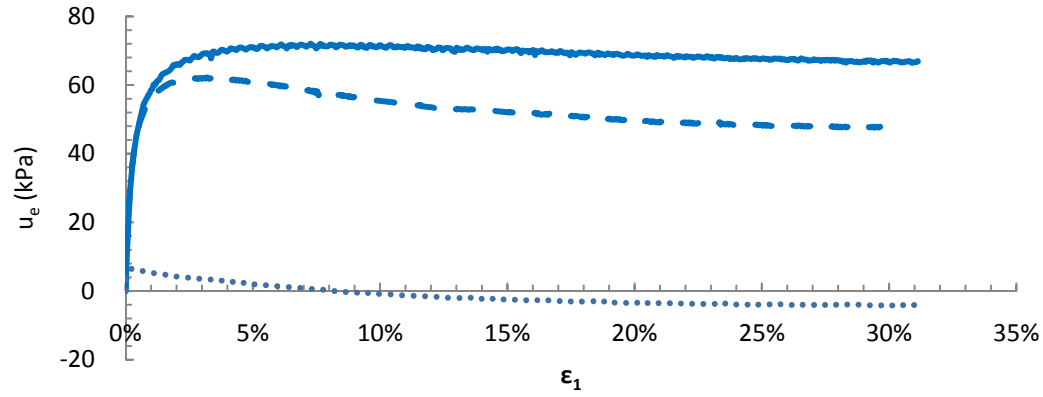

(b)

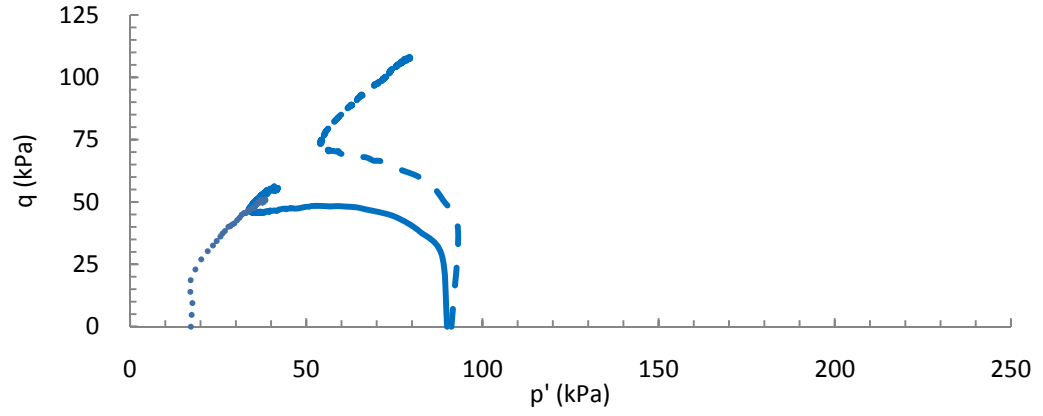

(c)

Figure 8.19. Postcyclic behavior of the MRV silt-bentonite mixture with a PI of 9.4: (a) $\Delta\sigma$ vs. ε_1, (b) u_e vs. ε_1, (c) q vs. p'

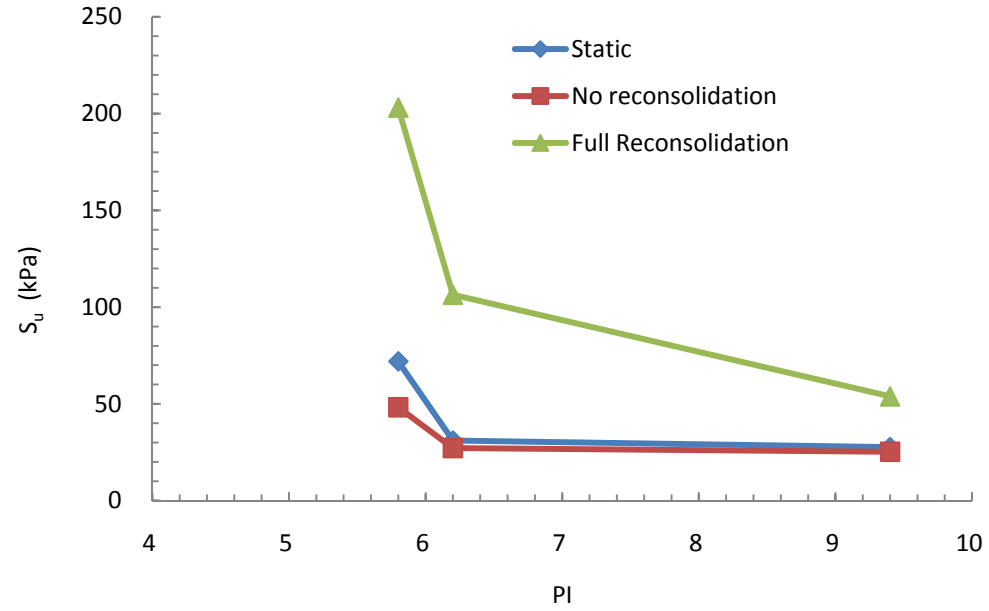

(a)

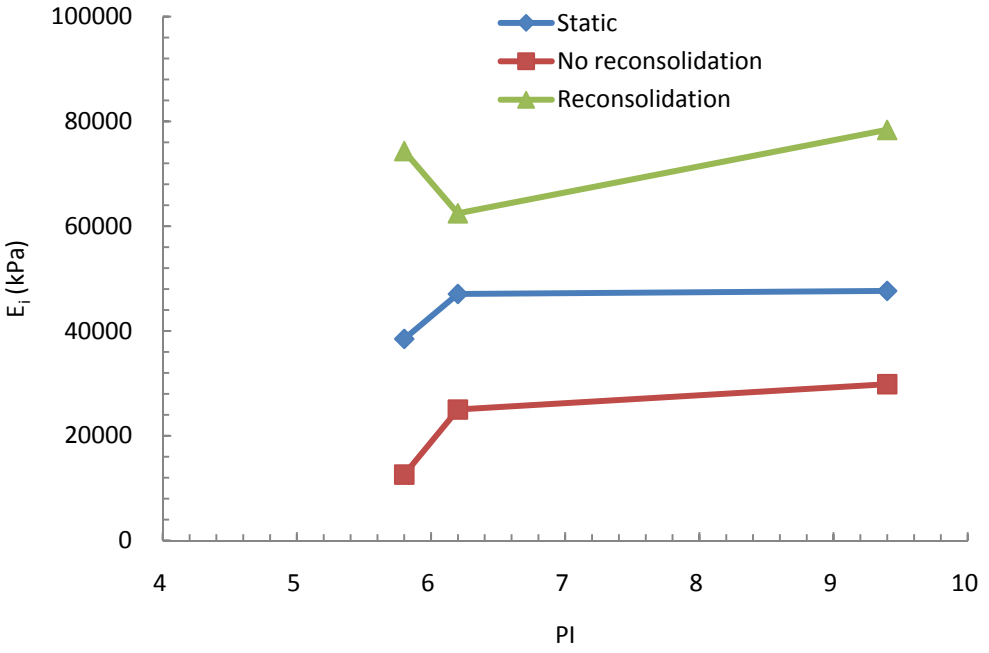

(b)

Figure 8.20. Variations in undrained shear strength and initial stiffness of the MRV silt-bentonite mixtures with plasticity index: (a) S_u vs. PI, (b) E_i vs. PI

Undrained shear strength and initial stiffness were normalized by those of the static specimen without previous cyclic loading. Figure 8.21 shows the ratios of undrained shear strength and initial stiffness of the soil after no reconsolidation and full reconsolidation to those of the soil without previous cyclic loading ($S_{u,postcyclic}/S_{u,static}$ and $E_{i,postcyclic}/E_{i,static}$) for various PIs. With full reconsolidation, the strength ratio $S_{u,postcyclic}/S_{u,static}$ is larger than unity; therefore, the undrained shear strength increased after reconsolidation. There was a slight increase in $S_{u,postcyclic}/S_{u,static}$ with a PI of 6.2 compared to the natural MRV silt. With a PI of 9.4, there was sharp reduction in $S_{u,postcyclic}/S_{u,static}$.

Without reconsolidation, the undrained shear strength decreased after cyclic loading. The strength ratio $S_{u,postcyclic}/S_{u,static}$ came closer to unity with a higher PI Thus, postcyclic undrained shear strength tended to be close to precyclic undrained shear strength for soil with a PI greater than 6.2 probably because the undrained shear strength of the soil with a PI greater than 6.2 was less affected by cyclic loading. Although there was difference in the variation in $E_{i,postcyclic}/E_{i,static}$ from that in the $S_{u,postcyclic}/S_{u,static}$, the change in initial stiffness of the soil with added bentonite due to cyclic loading was less than that of natural MRV silt, especially for soil with no reconsolidation. As noted previously, because more plastic soil is less easily remolded during cyclic loading, postcyclic soil behaves more like soil without previous cyclic loading.

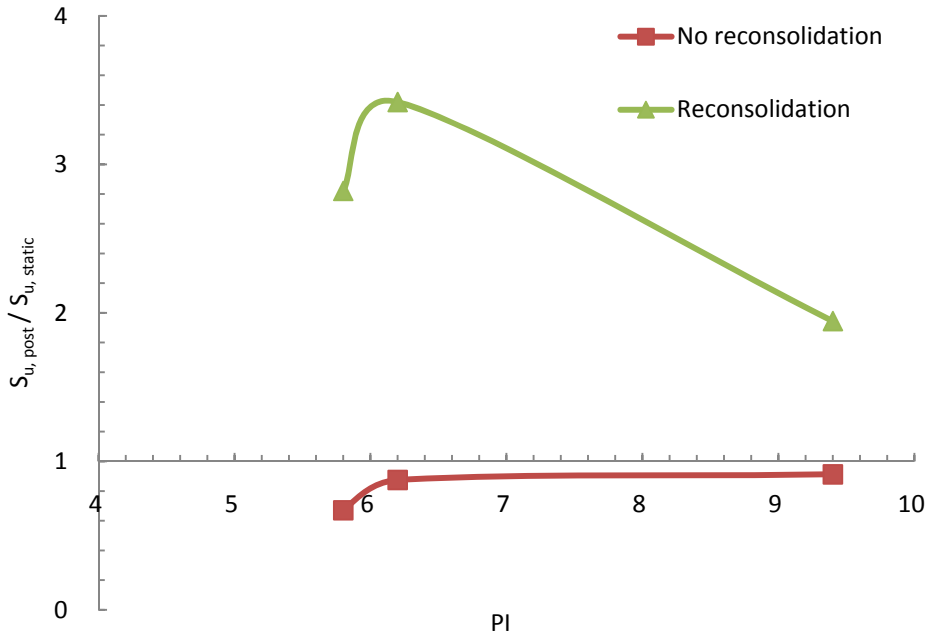

(a)

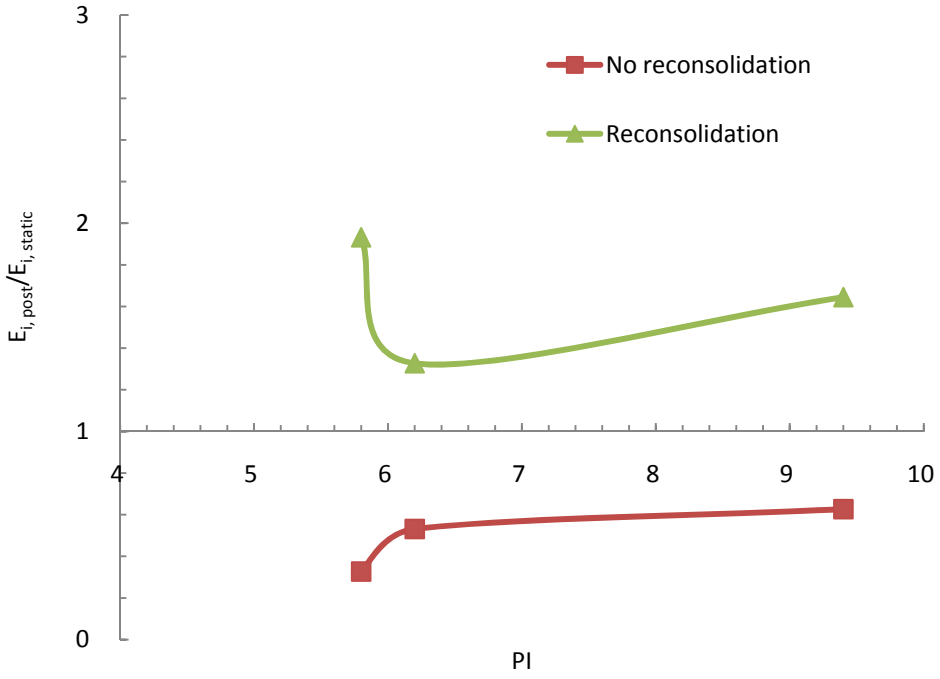

(b)

Figure 8.21. Variations in undrained shear strength and initial stiffness ratios of MRV silt-bentonite mixtures with PI: (a) $S_{u, post}/ S_{u, static}$ vs. PI, (b) $E_{i, post}/E_{i, static}$ vs. PI

8.5. DISCUSSION

8.5.1 Failure Criteria. The changes in undrained shear strength and initial stiffness of the soil after cyclic loading compared to those without previous cyclic loading became less evident with an increase in plasticity. This finding agrees with the statement by Robertson (2010), who indicated that nonplastic or low-plastic soils tend to be more susceptible to significant strength loss than more plastic soils. The difference may be attributable to the fact that that higher plasticity soils have greater cohesion, which resists remolding of soil fabric during cyclic loading. Although cyclic loading was stopped at the same cyclic strain (about 9.0%), the induced volumetric strain due to full reconsolidation after cyclic loading decreased with an increase in PI, as shown in Figure 8.22.

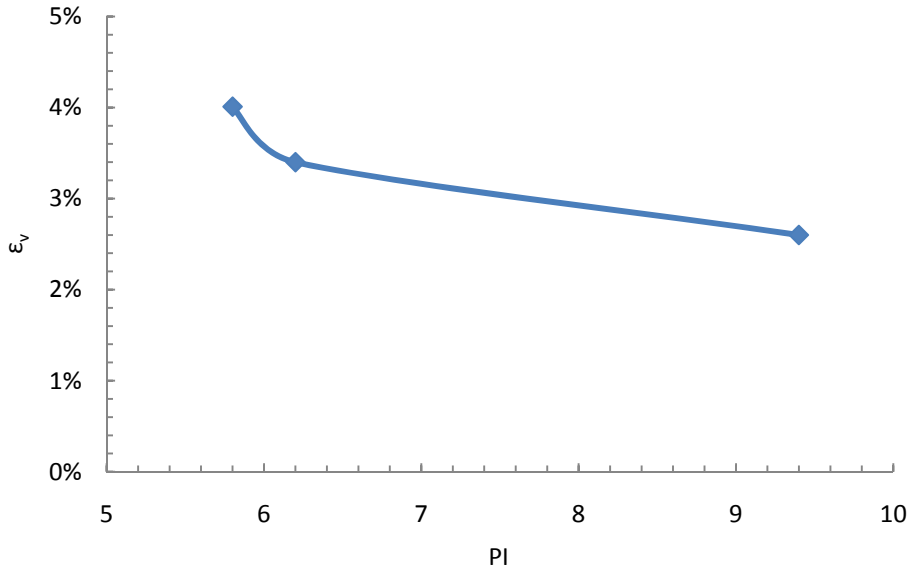

Figure 8.22. Variation in volumetric strain with PI due to full reconsolidation after nearly identical axial strain (9%) induced by cyclic loading

However, the opposite phenomenon was reported by Song et al. (2004), who conducted postcyclic shearing without reconsolidation. They indicated that stiffness tended to decrease less markedly in nonplastic silt with an increase in excess pore pressure ratio than in plastic Arakawa clay with a PI of 17.3 (Figure 2.10). Significantly, however, the frequency for all cyclic tests conducted by Song's group was 0.1 Hz, despite low permeability of the Arakawa clay compared to the nonplastic silt. Thus, the measurement of pore pressure during cyclic loading probably cannot represent the real value in the soil specimen well. Comparison of the reduction of stiffness between the soils with different PI (one nonplastic and the other 17.3) using the same level of excess pore water ratio may not be valid. Song's group report no volumetric strain, no further analysis of their results is possible.

This research on MRV silt and its mixtures with bentonite compared undrained shear strength and stiffness based on the postcyclic tests run in each case after an axial strain of about 9.0%. Figures 8.10-8.13 show that the excess pore pressure ratio at this axial strain was lower with a higher PI. For example, the measured excess pore pressure ratio was only 0.55 for the cyclic test of specimen MFB9 with a CSR of 0.35 at the end of cyclic loading. Notably, the pore pressure measured by the transducer increased until equilibrium with the drainage valves closed after cyclic loading. Thus, the pore pressure measured by the transducer cannot represent the real value during cyclic loading. For plastic soils, the effect of PI on changes in undrained shear strength and stiffness due to cyclic loading should be studied with postcyclic shear tests on specimens with the same axial strain instead of the same excess pore pressure ratio.

8.5.2 Interpretation. As noted above, the static behavior of MRV silt-bentonite mixture changed from a relatively high strain-hardening material to a plastic material as the PI increased. On the other hand, the cyclic tests indicated that the MRV silt-bentonite content changed its behavior from initial liquefaction to cyclic softening. Postcyclic tests showed that the shear strength of these mixtures decreased less due to cyclic loading than did that of the natural MRV silt. If one critical PI is required to identify clay-like soil with plastic stress-strain behavior in static tests and strain softening behavior in cyclic tests of the soil mixtures, a PI of 6 may be best option. With a PI greater than 6.0, the soil tends to show clay-like behavior. With a PI less than 6.0, the soil behaves like an intermediate material because the natural MRV silt with a PI of 5.8 has both sand-like and clay-like behavior (explained in Section 5). The critical PI to divide the sand-like and intermediate soils is not known, and additional research is required on these low PI materials. Thus, the findings on the MRV silt and its mixtures with bentonite confirm the findings presented by Boulanger and Idriss (2006) for use as criteria to identify silt behavior.

Additionally, this work evaluated soil behavior using the Plasticity Chart to classify soil according to the fine soil type using Unified Soil Classification System (USCS). Figure 8.23 shows the chart with data points for the MRV silt and its mixtures with bentonite. From left to right, the data points show Atterberg limits of the soil mixtures with added bentonite contents of 0%, 2.5%, 5.0%, and 7.5%. The soil mixture with added bentonite content of 7.5% had a PI of 13.5 and was classified as CL. This classification explains why the soil mixture showed plastic stress-strain behavior. The other three data points are located almost on the A line, so the soil mixtures can behave like both sands and clays. Thus, natural MRV silt with a PI of 5.8 behaves like an

intermediate material. The soil mixtures with PIs of 6.2 and 9.4 behaved more like clays. However, they also showed slightly sand-like behavior in that they have quasi-steady states (Figure 8.4 and 8.5), although there are no quasi-steady lines (Figure 8.9).

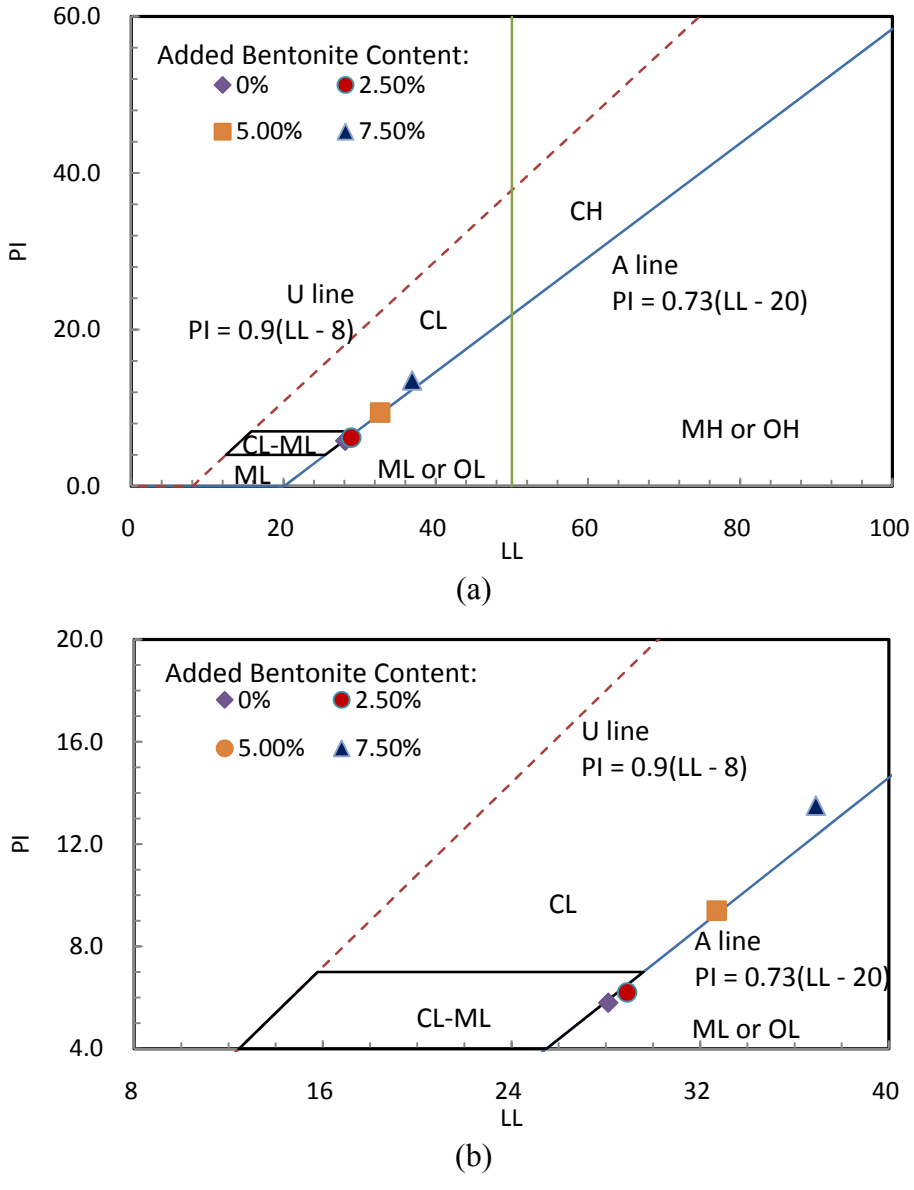

Figure 8.23. Soil types of MRV silt and its mixtures with bentonite plotted on: (a) Plasticity Chart, (b) enlarged inset

8.6. SUMMARY

This section has addressed the effect of PI on static, cyclic, and postcyclic shear behavior. The following findings are of particular interest.

With added bentonite up to 2.5%, the permeability of the MRV silt decreased significantly, but this decrease diminished when the added bentonite content was increased from 2.5% to 5.0%. However, the compressibility of the MRV silt increased more steadily with increased bentonite content.

The static triaxial compression tests indicated that the highly dilative behavior of the natural MRV silt was reduced by adding bentonite. With an increase in PI, the soil tended to lose the quasi-steady state and became more plastic. The soil mixture with a PI of 13.5 showed plastic behavior and no increase in deviator stress after yield stress. The MRV silt-bentonite mixtures with PIs equal to or greater than 6.2 had CSLs almost parallel to the NCLs, and overconsolidation affected their effective friction angle, much like the behavior of clays.

The cyclic tests indicated that the MRV silt-bentonite mixtures with PIs equal to or greater than 6.2 displayed cyclic softening behavior rather than initial liquefaction. With an increase in PI, more loading cycles were required to induce cyclic failure.

With PIs up to 9.4, the MRV silt-bentonite mixtures had reconsolidation curves more parallel to their compression lines than to their recompression lines. Thus, due to cyclic loading, the postcyclic MRV-bentonite mixtures behaved more like freshly deposited soils after they were remolded. However, cyclic loading reduced permeability and compressibility, because the specimens became denser after reconsolidation. With added bentonite, the reductions in the permeability and compressibility of the soil

mixtures were larger than those in the natural MRV silt. Thus, the soil mixture with bentonite had more "memory" of its previous stress history and was less easily remolded. Nevertheless, there was no apparent effect of PI on the changes in permeability and compressibility due to cyclic loading according to the available test data.

Up to a PI of 9.4, the undrained shear strength increased due to reconsolidation after cyclic loading. The specimens with PIs of 6.2 had a greater increase in undrained shear strength due to reconsolidation with an increase in axial strain induced by cyclic loading. With no reconsolidation, the initial stiffness of the soil was low compared to the specimen without previous loading due to high excess pore pressure induced by cyclic loading. However, the undrained shear strength was recovered at large deformation regardless of level of axial strain induced by cyclic loading. With higher PI, there was less reduction in undrained shear strength with no reconsolidation because the soil fabric was not as sensitive to cyclic loading.

On the base of the above findings, it may be concluded that the MRV silt with a PI of 5.8 behaves like intermediate material, and that with a PI > 6.0 behaves like clay. The PI to separate sand-like and intermediate materials requires further research to determine.

9. CONCLUSIONS AND RECOMMENDATIONS FOR FUTURE RESEARCH

This research conducted a comprehensive experimental program to study the postcyclic behavior of MRV silt. To understand the postcyclic behavior of this material, the static behavior of the material had to be determined. Similarly, the cyclic behavior and liquefaction curves of CSR versus number of cycles also had to be determined. Once liquefaction is reached due to the buildup of pore pressure, this excess pore pressure must dissipate. The dissipation process is referred to as a reconsolidation. On the other hand, when the buildup of pore pressure does not reach a R_u of 1, the condition is called limited liquefaction. This work investigated both postcyclic conditions using triaxial tests. Additionally, it examined the effect of added bentonite which increases plasticity at the two extreme conditions of reconsolidation. The following offers some conclusions based on this study and recommends for future research.

9.1. CONCLUSIONS

Specimen Preparation

a) A new slurry consolidation method was developed to prepare specimens for triaxial testing. The specimen uniformity was verified by water content and particle size distributions showing very little variation throughout the specimens.

b) The testing program was expedited with a special handling technique to permit simultaneous specimen preparation and triaxial testing conditions. The reliability of the specimen preparation handling technique minimized the disturbance of the specimen during the movement.

c) To further verify the specimen preparation and handling techniques, tests were repeated for both static and cyclic triaxial. Each iteration of a tests with the same conditions produced nearly identical results.

Monotonic Shear Behavior

d) The CSL of the MRV silt was not parallel to its NCL, indicating that the silt behaved like a sand. However, the OCR did play a significant role in the stress-strain behavior of the silt, as it did in that of clay. These findings indicate that the silt has both sand-like and clay-like behavior, and thus its behavior is more complex than previously thought.

e) The failure criteria of $(\sigma_1 - \sigma_3)_{max}$, $(\sigma'_1/\sigma'_3)_{max}$, $u_{e,\,max}$, stress path reaching K_f line, limiting strain, and $u_e = 0$ were examined to calculate friction angle of the silt tested here. This work suggested that limiting strain was the criterion best suited to calculate the effective friction angle because it produced a friction angle more consistently.

f) The MRV silt showed normalized shear behavior by effective consolidation pressure. An experimental expression (Equation 9) that relates normalized shear strength ratio to OCR was proposed for the low-plastic silt. The exponent *m* equal to 0.58 produces the best fit. This expression can be used to estimate the shear strength of soils if the undrained normally consolidated shear strength and OCR are known. However, Equation 10 cannot be used to relate the normalized shear strength to OCR due to the large differences between the curves for normalized shear strength versus OCR among different silts, a characteristic that makes each silt soil unique.

Postcyclic Behavior with Full Liquefaction

g) No significant difference was found in the permeability of the MRV silt before and after liquefaction. However, the specimens were remolded during cyclic loading, and they produced more consistent permeability among specimens, possibly due to the more consistent soil porosity or fabric after liquefaction. Reconsolidation due to the dissipation of excess pore pressure behaved more like compression than recompression. The MRV silt becomes less compressible after cyclic loading because the compression and recompression indices decreased below those for specimens without cyclic loading.

h) Different CSRs produced no significant differences in volumetric strain due to reconsolidation and undrained shear behavior after cyclic loading. Postcyclic volumetric strain and undrained shear behavior were governed by the level of excess pore water pressure reached, rather than by the CSR.

i) Shear strength and stiffness, at both small and large deformation, increase with an increase in the reconsolidation level. Yield strength always increases more than initial stiffness. Cyclic loading did not change the failure line developed by the locus of the stress paths.

j) Normalized shear strength was increased with an increase in OCR_{app}. The relationship of the $(S_u/\sigma'_3)_{OC}/(S_u/\sigma'_3)_{NC}$ to OCR_{app} after liquefaction was similar to that of the $(S_u/\sigma'_c)_{OC}/(S_u/\sigma'_c)_{NC}$ to OCR without previously cyclic loading.

k) The specimen without reconsolidation after liquefaction had a lower undrained shear strength than did the static specimen without previous cyclic loading. With full reconsolidation after liquefaction, the specimen gained undrained shear

strength. This postcyclic condition produced a material four times as strong as the static specimen without cyclic loading.

l) The MRV silt with cyclic loading had a CSL different from that of silt without cyclic loading. The undrained shear strength of the soil with cyclic loading was lower than that without cyclic loading at the same void ratio. At high void ratio, the difference in undrained shear strength for the silts with and without previous cyclic loading became large. When the void ratio was low enough (less than 0.57), it appears that there was no reduction in the undrained shear strength due to cyclic loading.

Postcyclic Behavior with Limited Liquefaction

m) After full reconsolidation, yield shear strength and initial stiffness increased generally with an increase in liquefaction level (R_u), and the latter increase was more pronounced. Undrained shear strength decreased slightly with a liquefaction level lower than 0.70. Conversely, with a liquefaction level greater than 0.70, it showed a marked increase. A liquefaction level greater than 0.70 is a prerequisite for significant increases in undrained shear strength. Secant modulus was apparently unrelated to the liquefaction level in silt with full reconsolidation.

n) With no reconsolidation after limited liquefaction, the undrained shear strength of silt with previous cyclic loading was lower than that of silt without cyclic loading. However, there was no apparent relationship between undrained shear strength and liquefaction level. The yield strength and initial stiffness decreased with an increase in liquefaction level. The reductions became marked when the liquefaction level was larger than 0.70.

o) This work compared the undrained shear strength of the MRV silt to test data reported by other researchers. The undrained shear strength values presented here fall in the range of those reported by Thevanayagam et al. (1996). Undrained shear strength increased significantly with a small increase in relative density, suggesting that estimation of the undrained shear strength of the MRV silt after cyclic loading is very difficult. Accurate determination of relative density is crucial to a reliable estimation of the undrained shear strength for use in the evaluation of soil structure stability during and after earthquakes.

Effect of Plasticity on Pre- and Postcyclic Behavior

p) As the bentonite was added to up to 2.5% to the MRV silt to modify its plasticity the permeability decreased. Further increase in bentonite to 5.0% did not affect its permeability significantly. However, the compressibility of the MRV increased more steadily with increased bentonite content.

q) Static triaxial compression tests indicated that the highly dilative behavior of the natural MRV silt decreased sharply at a PI of 6.0. With an increase in PI, the silt tended to lose the quasi-steady state behavior and became more plastic. The soil-bentonite mixture with a PI of 13.5 exhibited plastic behavior. Soil mixtures with a PI greater than 6.2 had CSLs almost parallel to their NCLs. As bentonite was added it appeared that the overconsolidated soil had a different effective friction angle when compared to the normally consolidated soil.

r) Unlike natural MRV silt with a PI of 5.8, the soil mixtures with PIs of 6.2 and 9.4 showed cyclic softening rather than initial liquefaction. With an increase in PI from 5.8 to 9.4, more loading cycles were required to induce cyclic failure.

s) With PIs up to 9.4 (or perhaps greater), the MRV silt-bentonite mixtures had reconsolidation curves after cyclic loading more parallel to their compression lines than to their recompression lines. Thus, the postcyclic soil mixtures behaved more like freshly deposited soils. As bentonite was added, the reduction in permeability and compressibility due to cyclic loading became obvious, suggesting that the soil mixtures with bentonite had more "memory" of previous stress history and were less remolded during cyclic loading. Nevertheless, there was no apparent relationship between the reduction in permeability or compressibility due to cyclic loading and PI, probably due to the limited testing data.

1) Up to a PI of 9.4 (or perhaps greater), the undrained shear strength increased due to reconsolidation after cyclic loading. The specimens with PIs of 6.2 had a greater increase in undrained shear strength due to reconsolidation with an increase in axial strain induced by cyclic loading. The initial stiffness of the specimen without reconsolidation was low compared to that of the specimen without previous loading. However, the undrained shear strength was recovered at large deformation regardless of level of axial strain induced by cyclic loading. Higher PI minimized the reduction in undrained shear strength of soil without reconsolidation.

In summary, the main contributions to research in the behavior of low-plasticity silt can be included as follows: A new slurry consolidation approach was developed with a special specimen movement technique to expedite testing program; The MRV silt was found to be an intermediate material, showing both sand-like and clay-like behavior; The

undrained shear strength of overconsolidated low-plasticity silt may be computed based on Ladd's equation with an *m* of 0.58 if that of normally consolidated specimen is known; The shear strength and stiffness increase steadily with an increase in reconsolidation level; The critical state line of MRV silt changes due to liquefaction, and the apparent OCR has an effect on postcyclic shear behavior as does the OCR on the static behavior; A R_u greater than 0.70 is the prerequisite of large increase in volumetric strain and undrained shear strength due to reconsolidation and significant decrease in yield shear strength and initial stiffness with no reconsolidation; The highly dilative behavior of the natural MRV silt is sharply reduced at PI equal to 6.0 by bentonite added, and the shear strength and stiffness is less reduced with plasticity if no reconsolidation.

9.2. RECOMMENDATIONS FOR FUTURE RESEARCH

a. It is necessary to investigate the change in soil fabric due to cyclic loading using some advanced tools such as SEM and X-ray. Thus, the change in soil behavior due to cyclic loading can be explained in the microscale mechanism.
b. Preparation for MRV silt specimens with added bentonite content higher than 5.0% takes too long (over one month) using the presented slurry consolidation approach; therefore, this work did not study postcyclic behavior of MRV silt with added bentonite content of more than 7.5% (PI greater than 13.5). Additional research is needed to improve specimen preparation for a more productive experimental program.
c. The specimen shape changes due to cyclic loading. This change can influence the comparability of monotonic shear behavior with and without cyclic loading.

d. Future testing programs should include tests at different effective consolidation pressures to study their effect on postcyclic monotonic shear behavior.

e. The effect of anisotropic consolidation pressure on postcyclic behavior requires further investigation.

f. Further research is required on the reliquefaction of low-plasticity silt. After liquefaction occurs, the aftershock or anther earthquake can induce liquefaction again in the same ground. The liquefaction resistance of the soil can probably decrease due to previous liquefaction.

g. More bentonite should be added to form soil mixtures with higher PI to study the effect of PI on cyclic and postcyclic monotonic shear behavior. In this research, PI was in the range of just 5.8-9.4. Sample of silt with lower PI will be necessary, however, to study postcyclic shear behavior of lower plasticity silts (i.e., those with a PI of 0–5.8).

h. The engineering strain ($\varepsilon_1 = \Delta H/H_0$) was computed here as axial strain to plot stress-strain curve. Because undrained shear strength was obtained at large axial strain (greater than 25%), errors in the computation of deviator stress occurred at large deformation. The natural strain ($\varepsilon_1 = \ln(H_0/(H_0 - \Delta H))$) may better represents the axial strain at large deformation (Popov, 1998). Thus, natural strain rather than engineering strain should be computed as axial strain.

i. This work conducted only triaxial tests. The stress path gained from the cyclic simple shear tests rather than cyclic triaxial compression tests may simulate the cyclic rotation of principal stresses during earthquake loading (Wijewickreme et al., 2005), although triaxial tests are more common in engineering practice and

easier to conduct numerous test specimen variations. Thus, the simple shear tests are more suitable for study of the liquefaction resistance of soils.

j. Additional tests should be conducted to investigate shear behavior in the triaxial extension. Soil ground can fail not only under triaxial compression but also under triaxial extension, such as the soil in the back of retaining wall or under the dam embankment.

APPENDIX

RESULTS OF CYCLIC TRIAIXAL TESTS

1. INTRODUCTION

Included with this dissertation is a CD-ROM, which contains the results of all cyclic triaxial tests inducing excess pore pressure or cyclic strain for postcyclic monotonic shearing. All documents were developed as Microsoft Excel 2007 files. As a summary, the testing conditions for cyclic triaxial tests were listed in a table in the following page. As examples, the curves of two cyclic triaxial tests (MD4 and MFB5) were shown after the table.

2. CONTENTS

The CD-ROM includes the following data files: MD1.xls, MD2.xls, MD2R.xls, MD3.xls, MD4.xls, MD4R.xls, MF1.xls, MF1R1.xls, MF1R2.xls, MF2.xls, MF3.xls, MF4.xls, MF5.xls, ML1.xls, ML2.xls, ML3.xls, ML4.xls, ML5.xls, ML6.xls, MFB1.xls, MFB2.xls, MFB3.xls, MFB4.xls, MFB5.xls, MFB6.xls, MFB7.xls, MFB8.xls, and MFB9.xls.

Testing details for cyclic triaxial tests

Test ID	Added Bentonite Content	B-Value	σ'_c (kPa)	e	CSR	N_{cyc}	R_u	ε_{cyc} (%)
MD1	--	0.948	91.1	0.669	0.10	66.17	1	0.39
MD2	--	0.944	91.2	0.661	0.18	35.2	1	10.51
MD2R	--	0.952	90.8	0.686	0.18	33.2	1	11.21
MD3	--	0.944	90.0	0.680	0.25	3.15	1	11.80
MD4	--	0.940	90.0	0.676	0.35	1.15	1	11.098
MD4R	--	0.944	89.7	0.682	0.35	1.15	1	11.42
MF1	--	0.948	90.6	0.665	<0.18	66.17	1	11.68
MF1R1	--	0.944	90.4	0.660	0.18	27.14	1	9.79
MF1R2	--	0.944	89.9	0.669	0.18	31.14	1	8.85
MF2	--	0.945	90.7	0.657	0.18	27.16	1	11.27
MF3	--	0.947	90.5	0.663	0.18	24.14	1	14.53
MF4	--	0.948	90.3	0.659	0.18	18.14	1	11.53
MF5	--	0.940	90.2	0.655	0.18	45.15	1	8.93
ML1	--	0.948	90.5	0.653	0.18	26.18	0.85	1.23
ML2	--	0.932	91.1	0.674	0.18	22.15	0.70	0.21
ML3	--	0.936	90.7	0.662	0.18	6.22	0.30	0.18
ML4	--	0.944	90.5	0.643	0.18	25.17	0.85	0.95
ML5	--	0.936	91.1	0.645	0.18	18.12	0.70	0.23
ML6	--	0.944	90.7	0.667	0.18	4.01	0.35	0.09
MFB1	1.25	0.948	90.5	0.675	0.25	5.46	0.89	20.53
MFB2	2.5	0.948	91.3	0.660	0.25	7.23	0.86	16.1
MFB3	2.5	0.940	91.9	0.667	0.18	126.17	0.89	16.9
MFB4	2.5	0.932	91.2	0.648	0.18	160.37	0.92	9.02
MFB5	2.5	0.952	90.4	0.675	0.18	89.18	0.86	8.99
MFB6	2.5	0.932	90.6	0.660	0.35	1.13	0.78	9.04
MFB7	5.0	0.948	91.2	0.690	0.18	407.29	0.82	8.99
MFB8	5.0	0.952	91.3	0.688	0.25	12.13	0.64	9.44
MFB9	5.0	0.940	91.3	0.685	0.35	1.15	0.55	8.98

Program Setup for Test MD4

Software:	C.A.T.S	Version:	1.76	
Project:	Shuying_Research			
Customer:	Shuying			
Sample:	MRV silt			
Test:	Triaxial			
Specimen:	MD4			
Number:	30			
Description:	CSR=0.35			
Container ID:	_			
Type:	Silt	Medium		
Moist Mass of Specimen:	0	(gr)		
Initial Water Content:	0	(%)		
Degree of Saturation:	0	(%)		
Specific Gravity:	0			
Initial Void Ratio:	0			
Starting Date:	6/23/2010			
Starting Time:	8:22:45			
Test Results:	Completed			
Stages:	1			
Stage Index:	1			
	Type:	Dynamic Loading		
	Specimen:			
		Height:	5.76	(inch)
		Axial Gauge Length:	5.76	(inch)
		Diameter:	2.75	(inch)
		Area:	5.95	(in^2)
		Volume:	34.2926	in^3

Testing Data for Test MD4

Time	**Δσ**	**σ_c**	**u**	**ε_{cyc}**	**u_e**	**R_u**	**p'**
sec	kPa	kPa	kPa	%	kPa		kPa
0.0000	0.35	753.17	663.25	0	0.00	0.00	90.12
0.0244	0.35	753.12	663.22	0	-0.03	0.00	90.15
0.3115	0.68	753.18	663.33	0	0.08	0.00	90.15
0.5282	3.47	753.18	663.67	-0.01	0.43	0.00	90.73
0.6239	5.94	753.09	663.97	0	0.72	0.01	91.26
0.9246	17.59	753.09	669.16	0.03	5.91	0.07	89.95
0.9363	18.21	753.14	669.42	0.02	6.18	0.07	89.89
0.9422	18.49	753.13	669.58	0.02	6.34	0.07	89.82
1.2488	38.90	753.23	679.16	0.06	15.91	0.18	87.06
1.5612	49.78	753.13	685.98	0.12	22.73	0.25	83.86
1.8717	56.75	753.16	691.70	0.21	28.45	0.32	80.47
1.8736	56.78	753.16	691.75	0.21	28.51	0.32	80.42
2.1861	59.48	753.22	695.95	0.31	32.71	0.36	77.12
2.4956	59.96	753.20	698.95	0.41	35.70	0.40	74.29
2.4985	59.97	753.23	698.97	0.41	35.73	0.40	74.26
2.8110	59.39	753.23	701.19	0.53	37.95	0.42	71.85
3.1214	58.65	753.08	702.98	0.65	39.74	0.44	69.81
3.1234	58.63	753.12	702.96	0.65	39.71	0.44	69.83
3.4358	57.66	753.22	704.56	0.77	41.32	0.46	67.90
3.7483	56.66	753.25	705.95	0.89	42.71	0.47	66.18
4.0607	50.00	753.20	705.31	0.96	42.06	0.47	64.61
4.1906	48.16	753.13	705.28	0.96	42.04	0.47	64.01
4.3731	40.63	753.12	705.02	0.96	41.77	0.46	61.77
4.6094	31.04	753.14	703.17	0.96	39.93	0.44	60.42
4.6856	27.99	753.18	702.61	0.96	39.36	0.44	59.97
4.7139	26.84	753.18	702.34	0.96	39.10	0.43	59.85
4.9980	15.77	753.14	699.83	0.94	36.58	0.41	58.68
5.2753	4.82	753.07	696.83	0.89	33.59	0.37	58.02
5.3105	3.49	753.12	696.59	0.89	33.35	0.37	57.81

Testing Data for Test MD4 (cont.)

Time	**Δσ**	**σ_c**	**u**	**ε_{cyc}**	**u_e**	**R_u**	**p'**
sec	kPa	kPa	kPa	%	kPa		kPa
7.1851	-36.89	752.91	682.66	-0.99	19.41	0.22	58.29
6.2468	-19.98	753.11	691.46	0.54	28.21	0.31	55.13
6.2478	-19.98	753.11	691.46	0.54	28.21	0.31	55.13
6.5602	-26.39	753.03	688.86	0.22	25.62	0.28	55.58
6.8726	-31.72	752.98	686.08	-0.2	22.84	0.25	56.59
7.4975	-41.77	752.62	678.68	-2.81	15.43	0.17	60.65
7.8100	-46.19	752.47	675.97	-4.69	12.73	0.14	61.87
8.1224	-49.76	752.52	671.43	-6.59	8.18	0.09	65.23
8.4348	-55.23	752.60	666.48	-8.47	3.24	0.04	68.35
8.7473	-56.01	752.65	666.00	-11	2.75	0.03	68.58
8.8713	-50.00	752.84	672.36	-11.09	9.12	0.10	64.21
9.0597	-39.03	753.05	680.23	-11.08	16.98	0.19	60.01
9.3712	-23.67	753.16	693.33	-11.02	30.08	0.33	52.03
9.3721	-23.63	753.18	693.36	-11.02	30.11	0.33	52.01
9.6846	-15.32	753.28	703.33	-10.89	40.09	0.45	44.80
9.9970	-10.71	753.25	710.26	-10.75	47.01	0.52	39.42
10.3094	-7.40	753.20	715.74	-10.55	52.49	0.58	35.04
10.6219	-4.50	753.61	722.37	-9.34	59.13	0.66	29.37
10.9343	0.17	754.61	729.73	-4.61	66.48	0.74	23.58
11.2468	20.09	755.66	745.08	2.32	81.83	0.91	14.87
11.4655	43.25	756.35	753.45	7.66	90.20	1.00	14.22

Note: σ_c – cell pressure, u – pore pressure, and D – axial deformation

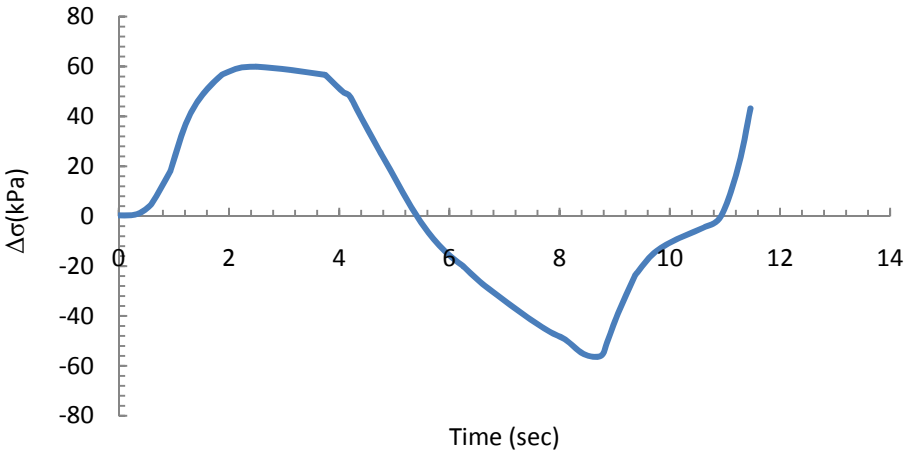

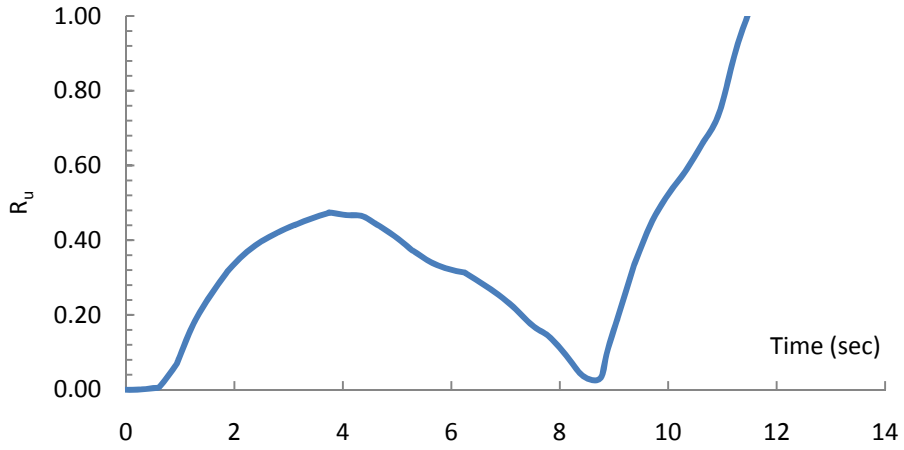

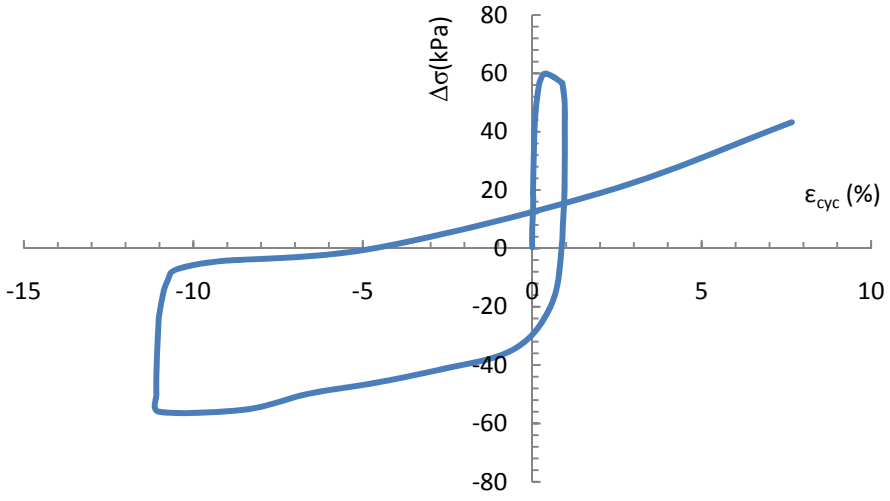

Testing Curve for Test MD4

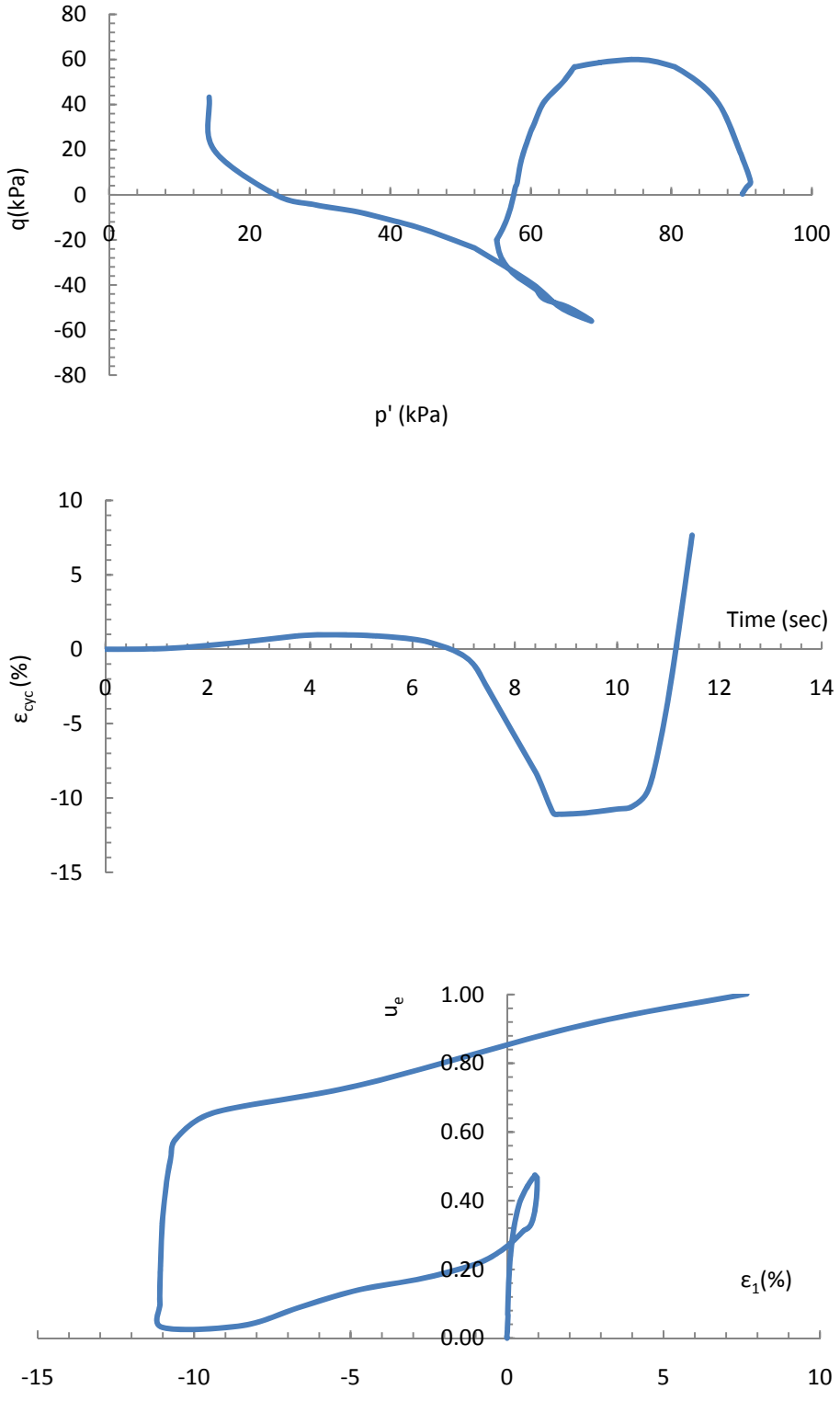

Testing Curve for Test MD4 (cont.)

Program Setup for Test MFB5

Software:	C.A.T.S	Version:	1.76	
Project:	Shuying_Research			
Customer:	Shuying			
Sample:	Oringal No2 silt			
Test:	Triaxial			
Specimen:	MFB5			
Number:	96			
Description:	_			
Container ID:	_			
Type:	Silt	Medium		
Moist Mass of Specimen:	0	(gr)		
Initial Water Content:	0	(%)		
Degree of Saturation:	0	(%)		
Specific Gravity:	0			
Initial Void Ratio:	0			
Starting Date:	12/28/2010			
Starting Time:	11:31:38			
Test Results:	Completed			
Stages:	1			
Stage Index:	1			
	Type:	Dynamic Loading		
	Specimen:			
		Height:	6.154	(inch)
		Axial Gauge Length:	6.154	(inch)
		Diameter:	2.691	(inch)
		Area:	5.69	(inch)
		Volume:	35.0005	(inch)

Testing Data for Test MFB5

Time	**Δσ**	**σ_c**	**u**	**ε_{cyc}**	**u_e**	**R_u**	**p'**
sec	kPa	kPa	kPa	%	kPa		kPa
0.0000	0.41	690.01	599.58	0.00	0.08	0.00	90.57
0.0332	0.40	690.05	599.58	0.00	0.08	0.00	90.60
0.3115	6.77	689.98	601.91	0.00	2.41	0.03	90.33
0.3242	6.95	689.95	601.98	0.00	2.48	0.03	90.29
0.6239	13.07	689.88	604.56	0.00	5.06	0.06	89.68
0.6268	13.12	689.93	604.56	0.00	5.06	0.06	89.74
0.9363	19.31	690.01	608.37	0.03	8.87	0.10	88.08
1.2419	23.75	689.96	610.30	0.04	10.80	0.12	87.58
1.2488	23.78	690.06	610.32	0.04	10.82	0.12	87.67
1.2849	23.85	689.98	610.42	0.04	10.92	0.12	87.51
1.5612	27.81	689.98	612.39	0.05	12.89	0.14	86.86
1.8160	29.17	690.03	613.17	0.05	13.67	0.15	86.58
1.8746	30.94	689.95	613.88	0.05	14.38	0.16	86.38
2.1861	33.04	689.95	615.36	0.06	15.86	0.18	85.60
2.4839	34.30	690.01	616.29	0.07	16.79	0.19	85.15
2.4985	34.37	690.03	616.30	0.07	16.80	0.19	85.19
2.8110	34.22	690.00	616.57	0.07	17.07	0.19	84.84
2.9223	33.93	690.00	616.57	0.08	17.07	0.19	84.74
3.1234	33.30	690.05	616.44	0.08	16.94	0.19	84.71
3.1263	33.29	689.96	616.46	0.07	16.96	0.19	84.60
3.4358	32.10	690.03	616.24	0.08	16.74	0.19	84.49
3.4466	32.12	690.01	616.20	0.08	16.70	0.18	84.52
3.7483	30.37	689.98	615.95	0.08	16.45	0.18	84.15
3.9172	25.80	689.93	615.61	0.08	16.11	0.18	82.92
4.0607	21.99	690.03	615.16	0.08	15.66	0.17	82.20
4.3731	14.84	689.95	613.56	0.08	14.06	0.16	81.34
4.4454	13.32	690.03	613.10	0.07	13.60	0.15	81.37

Testing Data for Test MFB5 (cont.)

Time	**Δσ**	**σ_c**	**u**	**ε_{cyc}**	**u_e**	**R_u**	**p'**
sec	kPa	kPa	kPa	%	kPa		kPa
4.6983	7.65	689.95	611.10	0.08	11.60	0.13	81.40
4.9980	0.56	689.96	608.53	0.08	9.03	0.10	81.62
5.2626	-5.73	689.95	606.16	0.07	6.66	0.07	81.88
.....							
888.2578	-31.43	687.02	648.60	-3.66	49.10	0.54	27.94
888.3320	-30.86	687.19	648.87	-3.66	49.37	0.55	28.03
888.5703	-28.21	687.41	649.49	-3.66	49.99	0.55	28.52
888.6005	-27.66	687.41	649.56	-3.66	50.06	0.55	28.63
888.8827	-23.87	687.72	650.23	-3.66	50.73	0.56	29.53
889.1287	-20.21	687.94	651.70	-3.66	52.20	0.58	29.50
889.1951	-19.09	687.99	652.09	-3.66	52.59	0.58	29.54
889.2186	-18.65	687.94	652.19	-3.66	52.69	0.58	29.53
889.5076	-13.54	688.13	653.86	-3.66	54.36	0.60	29.76
889.8200	-8.50	688.28	656.84	-3.54	57.34	0.63	28.61
890.1324	-5.77	688.55	659.18	-3.21	59.68	0.66	27.45
890.4449	-5.04	688.85	660.36	-2.64	60.86	0.67	26.81
890.7573	-3.92	689.59	662.01	-0.59	62.51	0.69	26.27
891.0698	0.99	690.69	665.76	3.37	66.26	0.73	25.26
891.3822	21.13	691.86	675.68	7.70	76.18	0.84	23.22
891.6946	25.65	691.80	676.85	8.79	77.35	0.86	23.50
891.8011	26.63	691.64	677.01	8.99	77.51	0.86	23.51

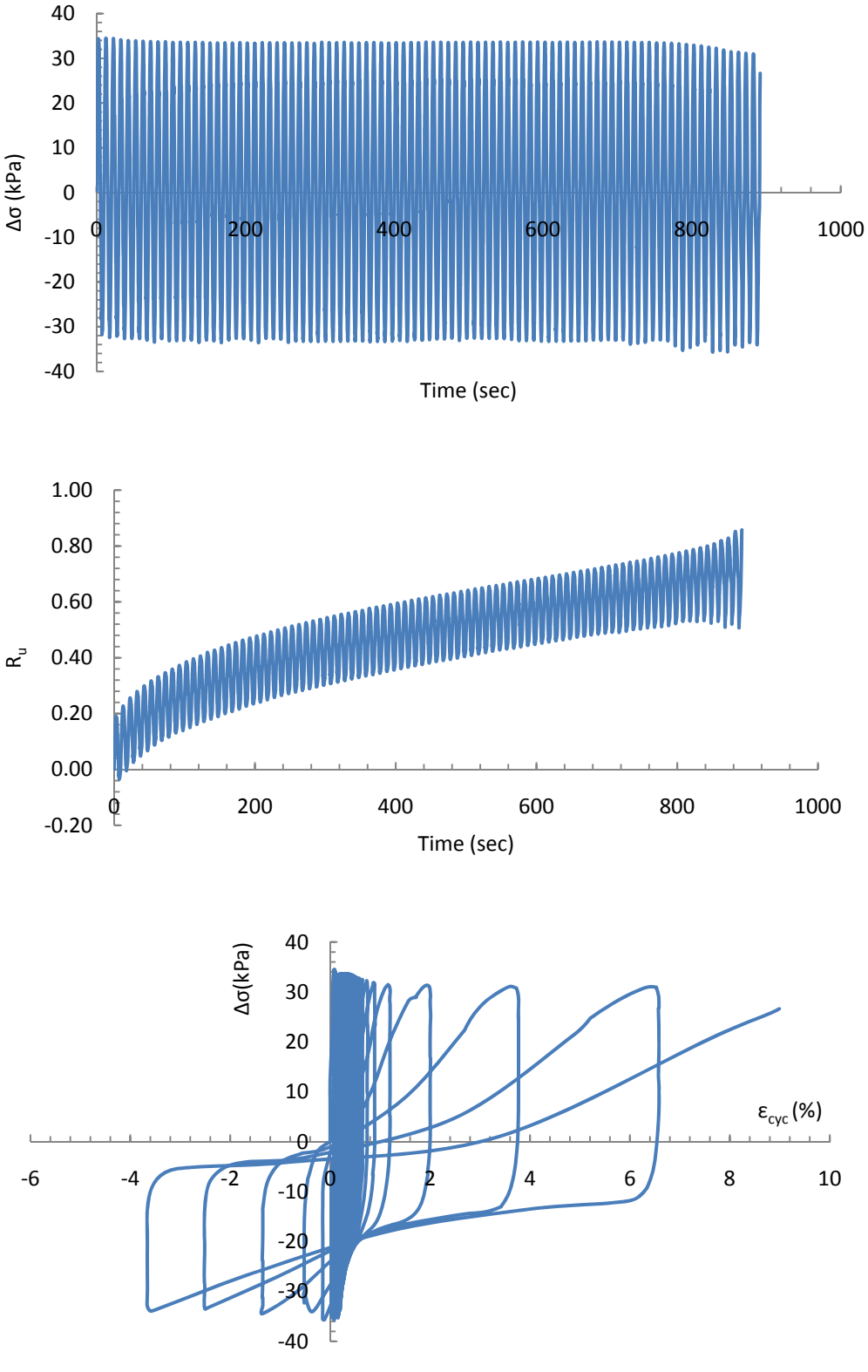

Testing Curve for Test MFB5

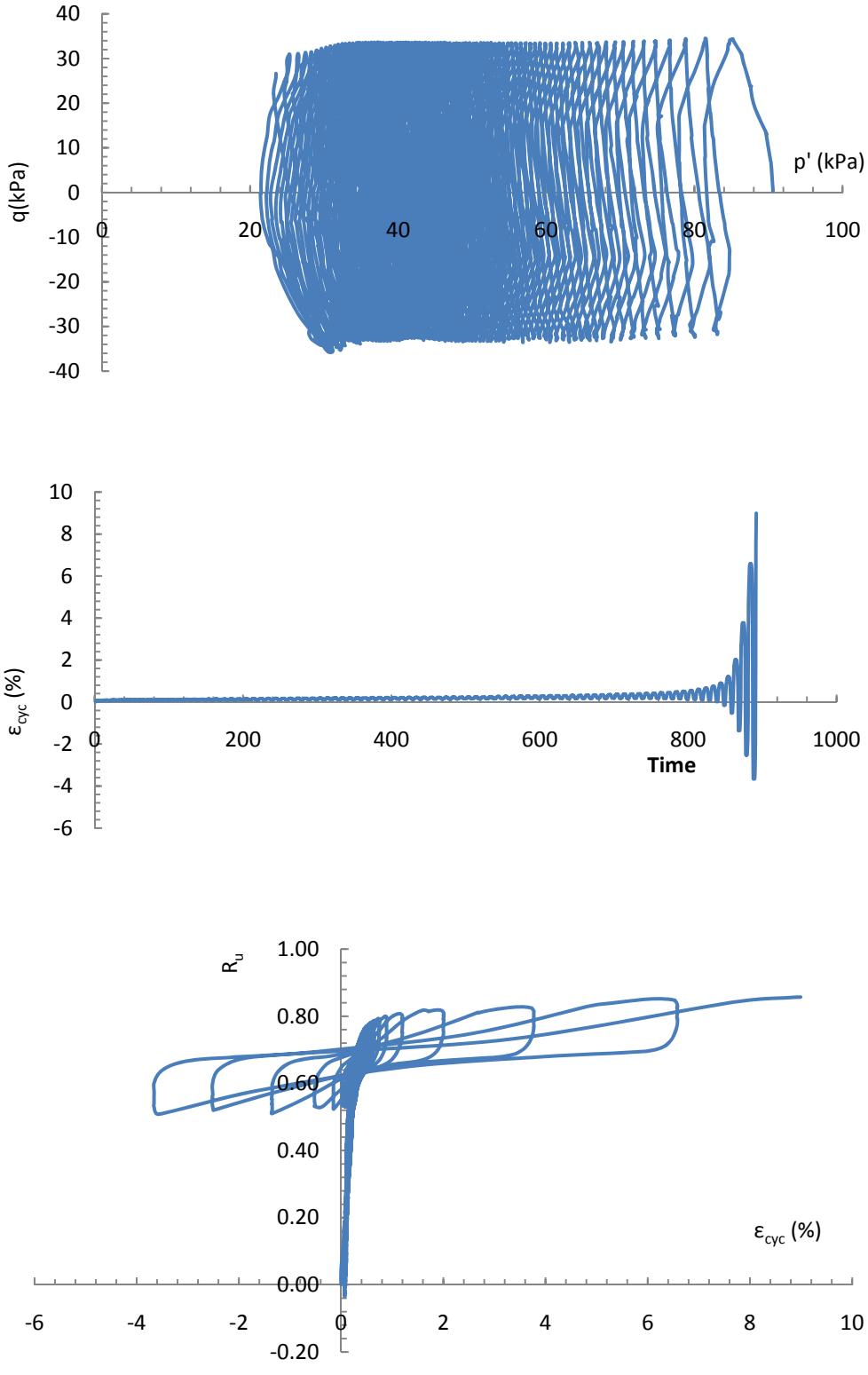

Testing Curve for Test MFB5 (cont.)

BIBLIOGRAPHY

Alba, P. D., and Ballestero, T. P. (2008). "Effect of Fines on Sand Residual Strength after Liquefaction." *Geotechnical Earthquake Engineering and Soil Dynamics, Geotechnical Special Publication*, ASCE, No. 181.

Amini, Z. A., and Trandafir, A. C. (2008). "Post-liquefaction Shear Behavior of Bonneville Silty-Sand." *Geotechnical Earthquake Engineering and Soil Dynamics, Geotechnical Special Publication*, ASCE, No. 181.

Anderson, N., Baker, H., Chen, G., Hertell, T., Hoffman, D., Luna, R., Munaf, Y., Neuner E., Prakash, S., Santi, P., Stephenson, R. (2001). "Earthquake Hazard Assessment along Designated Emergency Vehicle Access Rountes." MoDOT Report DT98-043, Missouri Department of Transportation.

Andrews, D. C. A., and Martin, G. R. (2000). "Criteria for Liquefaction of Silty Soils." *Proceeding of 12th World Conference on Earthquake Engineering*, Upper Hutt, New Zealand, NZ.

Arulmoli, K., Muraleetharan K. K., Hossain, M. M., and Fruth L. S. (1992). "Verification of Liquefaction Analysis by Centrifuge Studies Laboratory Testing Program." Soil Data Report, the Earth Technology Corporation, Irvine, CA.

Ashour, M., Norris, G., Nguyen, T. (2009). "Assessment of the Undrained Response of Sands under Limited and Complete Liquefaction." *Journal of Geotechnical and Geoenvironmental Engineering*, Vol. 135, No. 11, pp.1772-1776.

ASTM. (2000). "Standard Test Methods for Minimum Index Density and Unit Weight of Soils and Calculation of Relative Density." D 4254 - 00 (Reapproved 2006). West Conshohocken, PA.

ASTM. (2000). "Standard Test Methods for Maximum Index Density and Unit Weight of Soils Using a Vibratory Table." D 4253–00. West Conshohocken, PA.

ASTM. (2004). "Standard Test Method for Load Controlled Cyclic Triaxial Strength of Soil." D 5311-92 (Reapproved 2004). West Conshohocken, PA.

ASTM. (2004). "Standard Test Method for Consolidated Undrained Triaxial Compression Test for Cohesive Soils." D4767–4. West Conshohocken, PA.

ASTM. (2005). "Standard Test Methods for Liquid Limit, Plastic Limit, and Plasticity Index of Soils." D 4318- 05. West Conshohocken, PA.

ASTM. (2006). "Standard Test Methods for Specific Gravity of Soil Solids by Water Pycnometer." D 854 – 06. West Conshohocken, PA.

ASTM. (2007). "Standard Test Method for Particle-Size Analysis of Soils." D 422- 63 (Reapproved 2007). West Conshohocken, PA.

ASTM. (2009). "Standard Test Methods for Laboratory Compaction Characteristics of Soil Using Modified Effort (56,000 ft-lbf/ft^3 (2,700 kN-m/m^3))." D 1557-09. West Conshohocken, PA.

Beroy, M. A. A., Aydin, A., and Katzenbach, R. (2009). "Insight into the effects of Clay Mineralogy on the Cyclic Behavior of Silt-clay Mixtures." *Engineering Geology*, Vol. 106, pp. 154-162.

Boulanger, R. W., and Idriss, I. M. (2004). "Evaluating the Potential for Liquefaction or Cyclic Failure of Silts and Clays." Rep. No. UCD/CGM-04/01, Center for Geotechnical Modeling, Dept. of Civil and Environmental Engineering, Univ. of California, Davis, CA.

Boulanger, R. W. and Idriss, I. M. (2006). "Liquefaction Susceptibility Criteria for Silts and Clays." *Journal of Geotechnical and Geoenvironmental Engineering*, ASCE, Vol. 132, No. 11, pp. 1413-1426.

Boulanger, R. W. and Idriss, I. M. (2007). "Evaluation of Cyclic Softening in Silts and Clays." *Journal of Geotechnical and Geoenvironmental Engineering*, Vol. 133, No. 6, pp. 641-652.

Boulanger, R. W., Meyers, M. W., Mejia, L. H., and Idriss, I. M. (1998). "Behavior of a fine-grained soil during the Loma Prieta earthquake." *Canadian Geotechnical Journal*, Vol. 35, pp. 146 -158.

Bradshaw, A. S. and Baxter, C. D. P. (2007). "Sample Preparation of Silts for Liquefaction Testing." *Geotechnical Testing Journal*, Vol. 30, No. 4, pp. 1-9.

Brandon, T. L., Rose, A. T., Duncan, J. M. (2006). "Drained and Undrained Strength Interpretation for Low-plasticity Silts." *Journal of Geotechnical and Geoenvironmental Engineering*, Vol. 132, No.2, pp. 250-257.

Bray, J. D. and Frost, D. (2010). "Geo-engineering Reconnaissance of the 2010 Maule, Chile Earthquake." Report No. Geer-022, Geo-Engineering Extreme Events Reconnaissance (Geer) Association.

Bray, J. D. and Sancio, R. B. (2006). "Assessment of the Liquefaction Susceptibility of Fine-grained Soils." *Journal of geotechnical and geoenvironmental engineering*, Vol.132, No.9, pp. 1165-1177.

Bray, J. D., Sancio, R. B., Riemer, M. F., and Durgunoglu, T. (2004). "Liquefaction Susceptibility of Fine-grained Soils." *Proc. 11th Int. Conf. On Soil Dynamics and Earthquake Engineering and 3rd Int. Conf. On Earthquake Geotechnical Engineering*, Stallion Press, Berkeley, Calif., Vol. 1, pp. 655–662.

BS. (1990). "Methods of Test for Soils for Civil Engineering Purposes - Part 2: Classification Tests." 1377-2. British Standards Institution, UK.

Byrne, P. M., Jitno, H., and Jeremy, H. (1992). "A Procedure for Predicting the Seismic Response of Tailings impoundments." *Proc., Geotechnique and Natural Hazards: Geohazards 92*, Vancouver Geotech. Soc., Vancouver, Canada, pp. 281-289.

Carraro, J. A. H. and Prezzi, M. (2007). "A New Slurry-based Method of Preparation of Specimen of Sand Containing Fines." *Geotechnical Testing Journal*, Vol. 31, No.1, pp. 1-11.

Chern, J. C., and Lin, C. C. (1994). "Post –cyclic Consolidation Behavior of Loose Sands." *Proceeding of Settlement 94, Geotechnical Special Publication*, ASCE, No. 40.

Delage, P., Marcial, D., Cui, Y. J., and Ruiz, X. "Ageing effects in a compacted bentonite: a microstructure approach." *Geotechnique*, Vol. 56, No. 5, 291–304.

Dobry, R. and Alvarez, L. (1967). "Seismic Failures of Chilean Tailings Dams." *Jorunal of the Soil and Foundations Division*, Vol. 93, No. SM6, pp. 237-260.

Duncan, J. M. and Wright, S. G. (2005). *Soil Strength and Slope Stability,* John Wiley & Sons, Inc., Hoboken, N.J.

El Hosri, M. S., Biarez J., and Hicher P. Y. (1984). "Liquefaction Characteristics of Silty Clay." *Proceedings of the Eighth World Conference on Earthquake Engineering*, San Francisco, CA.

FEMA. (2009). "Dam Failure." http://www.fema.gov/hazard/damfailure/index.shtm, June 04, 2009.

Fleming, L. N. and Duncan, J. M. (1990). "Stress-Deformation Characteristics of Alaskan Silt." *Journal of Geotechnical Engineering*, Vol. 116, No.3, pp. 377-393.

Gratchev, I. B., Sassa, K., Osipov, V. I., and Sokolov, V. N. (2006a). "The liquefaction of clayey soils under cyclic loading." *Engineering Geology*, Vol. 86, pp. 70-84.

Gratchev, I. B., Sassa, K., and Fukuoka, H. (2006b). "How Reliable is the Plasticity Index for Estimating the Liquefaction Potential of Clayey Sands?" *Journal of Geotechnical and Geoenvironmental Engineering*, Vol. 132, No. 1, pp. 124-127.

Guo, T., and Prakash, S. (1999). "Liquefaction of Silts and Silt-Clay Mixtures." *Journal of Geotechnical and Geoenvironmental Engineering*, Vol. 132, No. 6, pp. 716-735.

Guo, Y. and Wang, Y. X. (2009), "Experimental Study about the Influence of Initial Water Content in Wet Tamping Method on Static Triaxial Test Results of Silt," *Electronic Journal of Geotechnical Engineering*, Vol. 14.

Hoeg, K., Dyvik, R., and Sandbækken, G. (2000). "Strength of Undisturbed versus Reconstituted Silt and Silty Sand Specimens." *Journal of Geotechnical and Geoenvironmental Engineering*, Vol. 126, No.7, pp: 606-617.

Holtz, R. D., and Kovacs, W. D. (2010). *An Introduction to Geotechnical Engineering*, Prentice-Hall, Inc. Englewood Cliffs, NJ.

Hyde, A. F. L., Higuchi, T., and Yasuhara, K (2006), "Liquefaction, Cyclic Mobility, and Failure of Silt," *Journal of Geotechnical and Geoenvironmental Engineering*, Vol. 132, No. 6, pp. 716-735.

Hyde A. F. L., Higuchi T., and Yasuhara T. (2007). "Postcyclic Recompression, Stiffness, and Consolidated Cyclic Strength of Silt." Journal of Geotechnical and Geoenvironmental Engineering, Vol. 133, No. 4, 416-423.

Hyde, A. F. L., Marto, A., and Yasuhara, K. (1997). "Volumetric Compression of Periodically Loaded Silt." *Proceeding of International Symp. on Deformation and Progressive Failure in Geomechanics*, Pergamon, London, 629–634.

Hyodo, M., Yamamoto, Y., and Sugiyama, M. (1994). "Undrained Cyclic Shear Behavior of Normally Consolidated Clay Subjected to Initial Static Shear Stress." *Soils and Foundations*, Vol. 34, No. 4, pp. 1–11.

Ishihara K., Sodekawa M., and Tanaka Y. (1978). "Effects of Overconsolidation on Liquefaction Characteristics of Sands Containing Fines." *Dynamic Geotechnical Testing*, ASTM, West Conshohocken, PA, pp. 246–264.

Ishihara, K., Tatsuoka, F., and Yasuda, S. (1975). "Undrained Deformation and Liquefaction of Sand under Cyclic Stresses." *Soil and Foundations*, Vol. 15, No. 1, pp. 29-44.

Ishihara, K., Yasuda, S., and Yoshida, Y. (1990). "Liquefaction-induced Flow Failure and Residual Strength of Silty Sands." *Soils and Foundations*, Vol. 30, No. 3, pp. 69-80.

Ito, H., Komine, H. (2008). "Dynamic compaction properties of bentonite-based materials." *Engineering Geology*, Vol., 98, pp. 133–143.

Izadi, A. (2006). "Static Behavior of Silts", MS Thesis, University of Missouri, Rolla, MO.

Izadi, A. (2008). "Liquefaction and Post-Liquefaction Behavior of Low Plasticity Silts using Cyclic Triaxial Tests." PhD Dissertation, Missouri University of Science and Technology, Rolla, MO.

Khalili, A and Wijewickreme, D., 2008, "New Slurry Displacement Method for Reconstitution of Highly Gap-Graded Specimens for Laboratory Element Testing," *Geotechnical Testing Journal*, Vol. 31, No. 5, pp. 1-9.

Koester, J. P. (1992). "The Influence of Test Procedure on Correlation of Atterberg Limits with Liquefaction in Fine-grained Soils." *Geotechnical Testing Journal*, Vol. 15, No.4, pp. 352–361.

Kramer, S. L. (1989). "Uncertainty in steady state liquefaction Evaluation Procedures." *Journal of Geotechnical Engineering*, Vol. 115, No. 10, pp. 1402-1419.

Kramer, S. L. (1996). *Geotechnical Earthquake Engineering*, Prentice Hall, New Jersey.

Kuerbis, R. H. and Vaid, Y. P. (1988). "Sand Sample Preparation – the Slurry Deposition Method." *Soils and foundation*, Vol. 28, No. 4, pp. 107-118.

Ladd, R. S. (1977) "Specimen Preparation and Cyclic Stability of Sands," Journal of Geotechnical Engineering Division, Vol. 103, No. 6, pp. 535–547.

Ladd, C. C. (1991). "Stability Evaluation during Staged Construction." *Journal of Geotechnical Engineering*, Vol. 117, No. 4, pp. 540-615.

Ladd, C. C. and Foott, R. (1974). "New Design Procedure for Stability of Soft Clays." *Journal of the Geotechnical Engineering Division*, Vol. 100, No. GT7, pp. 763-786.

Ladd, C. C., Foott, R., Ishihara, K., Schlosser, F., and Poulos, H. G. (1997). "Stress-Deformation and Strength Characteristics." *Proceedings of the Ninth International Conference on Soil Mechanics and Foundation Engineering*, Japanese Society of Soil Mechanics and Foundation Engineering, Vol. 2, pp. 421-494.

Lefebvre G. and LeBoeuf D. (1987). "Rate Effects and Cyclic Loading of Sensitive Clays." *Journal of Geotechnical Engineering*, Vol. 113, No. 5, 476- 489.

Liu, H. L., Zeng, C. N., and Zhou, Y. D. (2007). "Test Study on Post-liquefaction Deformation Behavior of Silt Ground." *Chinese Journal of Rock and Soil Mechanics*, Vol.28, No.9, pp. 1866-1870.

Marcuson, W. F. III, Hynes, M. E., and Franklin, A.G. (1990). "Evaluation and use of residual strength in seismic safety analysis of embankments" *Earthquake Spectra*, Vol. 6, No. 3, pp. 529-572.

Mulilis, J. P., Seed, H. B., Chan, C. K., Mitchell, J. K., and Arulanandan, K. (1977). "Effects of Sample Preparation on Sand Liquefaction." *Journal of Geotechnical Engineering Division*, Vol. 103, No. 2, pp. 91–108.

Muraleetharanl, K. K. and Granger, K. K. (1999). "The Use of Miniature Pore Pressure Transducers in Measuring Matric Suction in Unsaturated Soils." *Geotechnical Testing Journal*, Vol. 22, No. 3, pp. 226–234.

Murthy, T. G., Loukidis, D., Carraro J. A. H. (2007). "Undrained Monotonic Response of Clean and Silty Sands," *Geotechnique*, Vol. 57, No. 3, pp. 273-288.

Nagao, K., Suemasa, N., Akashi, T., and Futaki, M. (2010). "Applicability Test Of Soil Improvement Using Micro-Bubbles Against Soil Liquefaction." *Proceeding of Fifth International Conference on Recent Advances in Geotechnical Earthquake Engineering and Soil Dynamics*, San Diego, CA.

Nocilla, A., Coop, M. R., and Colleselli, F. (2006). "The Mechanics of an Italian Silt: an Example of 'Transitional' behavior." *Geotechnique*, Vol. 56, No. 4, pp. 261-271.

Olson, S. M. and Stark, T. D. (2002). "Liquefied Strength Ratio from Liquefaction Flow Failure Case Histories." *Canadian Geotechnical Journal*, Vol. 39, pp. 629-647.

Olson, S. M. and Stark, T. D. (2003). "Yield Strength Ratio and Liquefaction Analysis of Slopes and Embankments." *Journal of Geotechnical and Geoenvironmental Engineering*, Vol. 129, No. 8, pp. 727-737.

Penman, A. D. M. (1953). "Shear Characteristics of A Saturated Silt, Measured in Triaxial Compression." *Geotechnique*, Vol. 3, pp. 312-328.

Polito, C. P., and Martin, J. R. (2001). "Effects of Nonplastic Fines on the Liquefaction Resistance of Sands." *Journal of Geotechnical and Geoenvironmental Engineering*, Vol. 127, No. 5, pp. 408-415.

Popov, E. P. (1998). *Engineering Mechanics of Solids*. Prentice Hall, Upper Saddle River, New Jersey.

Porcino, D., and Caridi, G. (2007). "Pre- and Post-liquefaction Response of Sand in Cyclic Simple Shear." *Dynamic Response and Soil Properties, Geotechnical Special Publication*, No. 160.

Poulos, S.J., Castro, G., and France, J.W. (1985). "Liquefaction Evaluation Procedure," *Journal of Geotechnical Engineering*, Vol. 111, No. 6, pp. 772-792.

Prakash, K., and Sridharan, A. (2006). "Critical Appraisal of the Cone Penetration Method of Determining Soil Plasticity," *Canadian Geotechnical Journal*, Vol. 43, pp. 884-888.

Puri, V. K. (1984). "Liquefaction Behavior and Dynamic Properties of Loessial (Silty) Soils." Ph. D. Disseratation, University of Missouri - Rolla, MO.

Robertson, P. K. (2010). "Evaluation of Flow Liquefaction and Liquefied Strength Using the Cone Penetration Test." *Journal of Geotechnical and Geoenvironmental Engineering*, Vol. 136, No. 6, pp. 842-853.

Romero, S. (1995). "The behavior of silt as clay content is increased." MS thesis, University of California, Davis, CA.

Sanin, M. V. and Wijewickreme D. (2006). "Cyclic shear response of channel-fill Fraser River Delta Silt." *Soil Dynamics and Earthquake Engineering*, Vol. 26, pp. 854-869.

Seed, H. B. (1987). "Design problems in Soil Liquefaction," *Journal of Geotechnical Engineering*, Vol. 113. No. 8, pp. 827-845.

Seed, H. B., Idriss, I. M., and Arango, I. (1983). "Evaluation of liquefaction potential using field performance data." *Journal of Geotechnical Engineering*, Vol, 109, No. 3, pp. 458-482.

Seed, R. B., Cetin, K. O., Moss, R. E. S., Kammerer, A. M., Wu, J., Pestana, J. M., Riemer, M. F., Sancio, R. B., Bray, J. D., Kayen, R. E., and Faris, A. (2003). "Recent Advances in Soil Liquefaction Engineering: A unified and Consistent Framework." *26th Annual ASCE Los Angeles Geotechnical Spring Seminar*, ASCE, Long Beach, CA.

Seed, R.B. and Harder, L.F. (1990). "SPT-based analysis of Cyclic Pore Pressure generation and Undrained Residual Strength." *Proceedings of the H. Bolton seed memorial symposium*, University of California, Berkeley, Vol. 2, pp. 351-376.

Song, B.W., Yasuhara, K., and Murakami, S. (2004). "Direct Simple Shear Testing for Post-Cyclic Degradation in Stiffness of Nonplastic Silt." *Geotechnical Testing Journal*, Vol. 27, No. 6, pp.1-7.

Soroush, A. and Soltani-Jigheh, H. (2009). "Pre- and Post-cyclic behavior of mixed clayey soils." *Canadian Geotechnical Journal*, Vol. 46, pp. 115-128.

Sridharan, A. and Prakash, K. (2000). "Percussion and Cone Methods of Determining the Liquid Limit of Soils: Controlling Mechanisms," *Geotechnical Testing Journal*, Vol. 23, No. 2, pp. 242-250.

Stark, T. D., Kramer, S. L., and Youd, T. L. (1997). "Post-liquefaction Shear Strength of Granular Soils." National Science Foundation Workshop, University of Illinois-Urbana-Champaign.

Stark, T.D. and Mesri, G. (1992). "Undrained Shear Strength of Liquefied Sands for Stability Analysis," *Journal of Geotechnical Engineering*, Vol. 118, No. 11, pp. 1727-1747.

Thevanayagam, S., Martin, G. R., Shenthan, T., and Liang, J. (2001). "Post-liquefaction Pore Pressure Dissipation and Densification in Silty Soils." *Proceedings of Fourth International Conference on Recent Advances in Geotechnical Earthquake Engineering and Soil Dynamics*, San Diego, CA.

Thevanayagam, S., Wang, C. C., and Ravishankar, K. (1996). "Determination of Post-liquefaction Strength: Steady State vs Residual Strength." *Geotechnical Special Publication*, No. 58, pp. 1210-1224.

Towhata, I. (2008). *Geotechnical Earthquake Engineering*, Spring Series in Geomechanics and Geoengineering.

USGS (2005). "Assessing the Seismic Hazards of Afghanistan." http://pubs.usgs.gov/fs/2005/3038/508fs3038.html#figurecaption36651352, April 05, 2005.

Vaid, Y. P. (1994). "Liquefaction of Silty Soils," *Proceeding in Ground Failures under Seismic Conditions*, ASCE, Atlanta, GA, pp. 1-16.

Vaid, Y. P. and Chern, J.C. (1985). "Cyclic and Monotonic Undrained Response of Saturated Sands." *Proceedings of Advances in the Art of Testing Soils under Cyclic Conditions*, ASCE, New York, 120-147.

Vaid, Y. P., Sivathayalan, S., and Steaman, D. (1999). "Influence of Specimen Reconstituting Method on the Undrained Response of Sand." *Geotechnical Testing Journal*, Vol. 22, No.3, pp. 187-195.

Vaid, Y. P., and Thomas, J. (1995). "Liquefaction and Postliquefaction Behavior of Sand." *Journal of Geotechnical Engineering*, Vol. 121, No. 2, pp. 163-173.

Wang, W. S. (1979). "Some findings in soil liquefaction." Water Conservancy and Hydroelectric Power Scientific Research Institute, Beijing, China.

Wang, W. S. (1981). "Foundation problems in aseismatic design of hydraulic structures." *Proceedings of the joint U.S.-P.R.C. microzonation workshop*, Harbin, China.

Wang, J. L., Vivatrat, V., and Rusher, J. R. (1982). "Geotechnical Properties of Alaska OCS Silt." *Proceeding of 4th Annual offshore Technology Conference*, Houston, TX.

Wijewickreme, D., Sanin, M. V., and Greenaway G. R. (2005). "Cyclic Shear Response of Fine-grained Mine Tailings." *Canadian Geotechnical Journal*, Vol. 42. pp. 1408-1421.

Wood, D. M. (1990). Soil *Behavior and Critical State Soil Mechanics*, Cambridge University Press.

Yamamuro, J., and Lade, P. V. (1998). "Steady-State Concepts and Static Liquefaction of Silty Sand." *Journal of Geotechnical and Geoenvironmental Engineering*, Vol. 124, No. 9, pp. 868-877.

Yasuhara, K., and Andersen, K. H. (1991). "Recompression of Normally Consolidated Clay after Cyclic Loading." *Soils and Foundations*, Vol. 31, No. 1, pp. 83-94.

Yasuhara, K, Hirao, K., and Hyde, A. F. L. (1992). "Effects of Cyclic Loading on Undrained Strength and Compressibility of Clay." *Soil and Foundations*, Vol. 32, No. 1 pp. 100-116.

Yasuhara, K., Murakami, S., Song, B. W., Yokokawa, S., and Hyde, A. F. L. (2003). "Postcyclic Degradation of Strength and Stiffness for Low Plasticity Silt." *Journal of Geotechnical and Geoenvironmental Engineering*, Vol. 129, No. 8. pp. 756-769.

VITA

Shuying Wang was born on November 20, 1982 at Huangshan, China. He finished his primary education at Yantan, Huangshan, and middle and high school education, respectively, at Rongkou and Qimen, Huangshan. He began his studies in Civil Engineering in 2001 at Central South University, China and then earned B.S. degree in 2005 there. He pursued his Master in Civil Engineering with an emphasis on in Tunnel Engineering and earned the M.S. degree in 2007 still from Central South University.

He was awarded a Chinese scholarship under the State Scholarship Fund to study for his Ph.D. degree at Missouri University of Science and Technology, Rolla. He started his Ph.D. study in Geotechnical Engineering in January, 2008. During his studies at Missouri S&T, he participated in multiple international and national conferences. He obtained third place in the student paper competition in 2008 North American Tunneling Conference and published a paper in 2nd International Conference of Long Term Behavior of Dam, Graz, Austria. He was awarded 2010 Richard Frueh Shannon & Wilson Scholarship in recognition of his scholarly activities in research and service. He has submitted two full papers to premier journals (ASCE and ASTM), and both of them have been accepted.

He is the youngest of the three children of Qinliu Wang and Zhihui Hu and married Ke Zhang in 2009.